Glycolipid - and Lectin-Dependant Endocytosis studies by a chemical biology Approch.

Joanna Zell

▶ **To cite this version:**

Joanna Zell. Glycolipid - and Lectin-Dependant Endocytosis studies by a chemical biology Approch.. Other. Université Sorbonne Paris Cité, 2018. English. NNT : 2018USPCC239 . tel-03008821

HAL Id: tel-03008821
https://theses.hal.science/tel-03008821

Submitted on 17 Nov 2020

HAL is a multi-disciplinary open access archive for the deposit and dissemination of scientific research documents, whether they are published or not. The documents may come from teaching and research institutions in France or abroad, or from public or private research centers.

L'archive ouverte pluridisciplinaire **HAL**, est destinée au dépôt et à la diffusion de documents scientifiques de niveau recherche, publiés ou non, émanant des établissements d'enseignement et de recherche français ou étrangers, des laboratoires publics ou privés.

Université Sorbonne Paris Cité

Thèse de doctorat

de l'Université Sorbonne Paris Cité

Préparée à l'Université Paris Diderot

Ecole doctorale Frontières du Vivant, CRI, Paris

UMR3666/U1143 Chemical Biology of Membranes and Therapeutic Delivery, Institut Curie

Glycolipid- and Lectin-Dependant Endocytosis Studies by a Chemical Biology Approach

Joanna ZELL

Thèse de doctorat de chemobiologie

Dirigée par Ludger Johannes et Frédéric Schmidt

Présentée et soutenue publiquement à Paris, le 16 novembre 2018

Président du jury : Prof. Didier Dubreuil, Université de Nantes

Rapporteur : Prof. Christoph Thiele, Universität Bonn, Allemagne

Rapporteur : Dr. Boris Vauzeilles, CNRS ICSN/Université Paris Sud

Examinatrice : Dr. Lydia Danglot, Centre de Psychiatrie et Neurosciences/INSERM

Directeur de thèse : Dr. Ludger Johannes, Institut Curie/INSERM

Co-directeur de thèse : Dr. Frédéric Schmidt, Institut Curie/CNRS

Membre invité : Dr. Jean-Claude Florent, Institut Curie/CNRS

Title: Glycolipid- and Lectin-Dependant Endocytosis Studies by a Chemical Biology Approach

Abstract: Current biological techniques do not permit the functional reintroduction of long-chain glycosphingolipids (GSLs) into cells. We aim to develop molecular tools permitting cellular reconstitution of functional GSLs in a controlled manner, combining metabolic labelling of sphingolipids with copper-free *click* chemistry. Molecular tools are validated with the bacterial Shiga toxin, which gains entry to cells independently of the canonical intracellular clathrin machinery on binding to its GSL cell receptor, globotriaosylceramide (Gb3-Cer), through a recently described mechanism of endocytosis, termed GL-Lect (glycolipid-lectin). According to the GL-Lect hypothesis, cellular or pathogenic lectins drive the construction of endocytic pits by reorganising membrane lipids so as to favour the formation of narrow membrane curvature. The GSL reconstitution technique that is described here is applicable to the discovery of GSL binding partners in the study of GL-Lect-mediated endocytosis.

Keywords: Glycosphingolipid, metabolic labelling, copper-free *click* chemistry

Titre : Une approche de chemobiologie pour étudier l'endocytose dépendante des glycosphingolipides et des lectines

Résumé : Les techniques biologiques actuelles ne permettent pas la réintroduction fonctionnelle des glycosphingolipides (GSLs) à longue chaine dans les cellules. Nous proposons de développer des outils moléculaires permettant la reconstitution des GSLs fonctionnels de manière contrôlée, en combinant le marquage métabolique et la chimie *click* sans cuivre. Les outils moléculaires sont validés par la toxine de Shiga, qui pénètre dans la cellule hôte indépendamment de la machinerie clathrine intracellulaire, en se liant à son récepteur cellulaire GSL, le globotriaosylcéramide (Gb3-Cer), par un mécanisme d'endocytose récemment décrit, appelé GL-Lect (glycolipide-lectine). Selon l'hypothèse GL-Lect, les lectines cellulaires ou pathogéniques induisent la constitution de puits endocytiques en réorganisant les lipides membranaires de façon à favoriser la formation de courbures membranaires locales. La technique de reconstitution des GSLs qui est décrite ici s'applique à la découverte des partenaires d'interaction des GSL dans l'étude de l'endocytose GL-Lect.

Mots clefs : Glycosphingolipides, marquage métabolique, chimie *click* sans cuivre

Live is if you were to die tomorrow,

learn as if you were to live forever

Mahatma Gandhi

Acknowledgements

Je suis reconnaissante d'avoir fait partie de l'unité UMR3666, qui est multidisciplinaire, multiculturelle, étonnamment accueillante et ouverte à tous. À mes deux superviseurs, Ludger et Frédéric, qui ont eu tant de patience à travers les échecs et les désaccords, et les réussites toujours trop courtes ; je vous remercie de m'avoir donné cette opportunité de découvertes, défis et fascinations qui m'ont énormément motivé tous les jours. Je remercie également Jean-Claude, superviseur-ange gardien.

À mes camarades de labo, Steve, Stefan, Vesela, Haifei, Mélanie, Stéphanie, Alena, Carlos, Marco, Fabien, Antoine, Seb, Anne, Anne, Thomas, Tati, Raph, Yannick, Christine, Sylvie, Michelle, Alison, merci d'avoir travaillé avec moi et partagé ces expériences délicieuses, passionnantes et inoubliables.

À Siau, qui m'a formé en bio avec Ludger et Christian, qui m'a soutenu, m'a écouté et m'a fait sourire tous les jours.

À Raphaël G, qui m'a donné la confiance dont j'avais besoin pendant ces longues périodes de syndrome de l'imposteur.

To Julio, who has driven this project with me, feeding all the creativity, imagination and dedication, and with whom I can always share a great moment in and out of the lab.

I thank all my friends from CRI, who managed to laugh in the face of PhD stress with me, whilst nourishing overpriced pints, whenever we managed to get out of the lab.

I thank the BIOPOL Innovative Training Network (European H2020 funding) that funded the project and my international training stations, and grouped together 16 PhD students, making us spend quality-science-time together across Europe. We had never felt so different, yet so alike.

After countless hours complaining on the phone, I retain some gems from my mum, who said:
"You don't learn unless you're suffering;"
and my dad, who said
"You're doing a PhD because once you're a Dr., you never have to say if you're a bloody Miss or Mrs., because you'll be a Dr.!"
I would be nowhere without you.
Carolyn, I know one day your wisdom will come crashing down on me. I love you and M&M to the end and back.

Table of contents

Abbreviations

A.U.	Arbitrary units
Ac	Acetyl
AzCer	1-Azidoceramide
AzPhy	1-Azidophytosphingosine
AzSph	1-Azidosphingosine
BCN	Bicyclononyne
Boc	*Tert*-butyloxycarbonyl
BSA	Bovine serum albumine
Bz	Benzoyl
CAN	Ceric ammonium nitrate
Cer	Ceramide
CerS	Ceramide synthase
CES	Carboxylesterase
CHO	Chinese hamster ovary
Chol	Cholesterol
CIE	Clathrin-independent endocytosis
COP	2-Chloro[1,3,2]dioxaphospholene-2-oxide
CuAAC	Copper(I)-catalysed azide-alkyne cycloaddition
DBU	1,8-Diazabicyclo(5.4.0)undec-7-ene
DCC	*N,N'*-Dicyclohexylcarbodiimide
DIBO	Dibenzocyclooctyne
DIFO	Difluorocyclooctyne
DIPEA	Diisopropylethylamine
DMAP	4-Dimethylaminopyridine
DMF	Dimethylformamide
DMSO	Dimethyl sulfoxide
DOPC	1,2-Dioleoyl-*sn*-glycero-3-phosphocholine
DOPE	1,2-Dioleoyl-*sn*-glycero-3-phosphoethanolamine
EA	Ethanolamine

EC_{50}	Half maximal effective concentration
EDC	1-Ethyl-3-(3-dimethymainopropyl)carbodiimide
EG	Ethylene glycol
ER	Endoplasmic reticulum
ESI	Electrospray ionisation
EtOAc	Ethyl acetate
EWG	Electron-withdrawing group
FSC	Fluorescence scanning microscopy
FSL	Function-spacer-lipid
Gb3	Globotriose
Gb3-Cer	Globotriaosylceramide
GCS	Glucosylceramide synthase
GL	Glycolipid
GlcCer	Glucosylceramide
Gly	Glycine
GPI-AP	Glycosylphosphatidylinositol-anchored protein
GSL	Glycosphingolipid
GUV	Giant unilamellar vesicle
HeLa	Henrietta Lacks (cell line)
HOBt	Hydroxybenzotriazole
HPTLC	High performance thin layer chromatography
HRMS	High resolution mass spectrometry
IF	Immunofluorescence
IR	Infrared
LacCer	Lactosylceramide
L_o/L_d	Liquid ordered/disordered
LUV	Large unilamellar vesicle
MFCO	Monofluorocyclooctyne
MS	Mass spectrometry
Ms	Mesylate
NIS	*N*-Iodosuccinimide
PBS	Phosphate-buffered saline
PC	Phosphatidylcholine

PE	Phosphatidylethanolamine
PL	Phospholipid
PM	Plasma membrane
PS	Phosphatidylserine
ROS	Reactive oxygen species
rt	Room temperature
S1P	Sphingosine-1-phosphate
SIMS	Secondary ion mass spectrometry
SM	Sphingomyelin
SPAAC	Strain-promoted azide-alkyne cycloaddition
TAMRA	Tetramethyl-rhodamine
TBAF	Tetra-*n*-butylammonium fluoride
TBDPSCl	*Tert*-butyldiphenylsilyl chloride
TFA	Trifluoroacetic acid
TGN	Trans-Golgi network
THF	Tetrahydrofuran
TLC	Thin layer chromatography
TMSOTf	Trimethylsilyl trifluoromethanesulfonate
TMSSCN	Trimethylsilylisothiocyanate
UPLC-MS	Ultra performation liquid chromatography - tandem mass spectrometry
w/o	With or without

1 INTRODUCTION

1.1 Endocytosis mechanisms

Endocytosis encompasses the cellular uptake of diverse cargo, including macromolecules, membrane components, nutrients and fluids, by their encapsulation in membrane vesicles which bud inwards to be pinched off from the plasma membrane (PM). From the PM, cargoes are trafficked through endosomes, where they can be (1) recycled back to the PM, (2) sorted via the retrograde route to the Golgi apparatus and in some cases to the endoplasmic reticulum (ER), or (3) targeted to the late endosomes and lysosomes for degradation (Figure 1.1.1a). The best characterised mechanism of endocytosis is mediated by clathrin, which coats the PM on binding to its adaptor proteins, forming a concave lattice structure (Figure 1.1.1b)[1] to bend and engulf portions of the membrane containing endocytic cargoes. These clathrin-coated vesicles (70-150 nm)[2] are eventually scissionned from the PM with assistance from intracellular protein machinery including a GTPase, dynamin (Figure 1.1.2), recruited by curvature-inducing BAR domain proteins, which themselves bind to and constrict negatively charged, curved membranes.

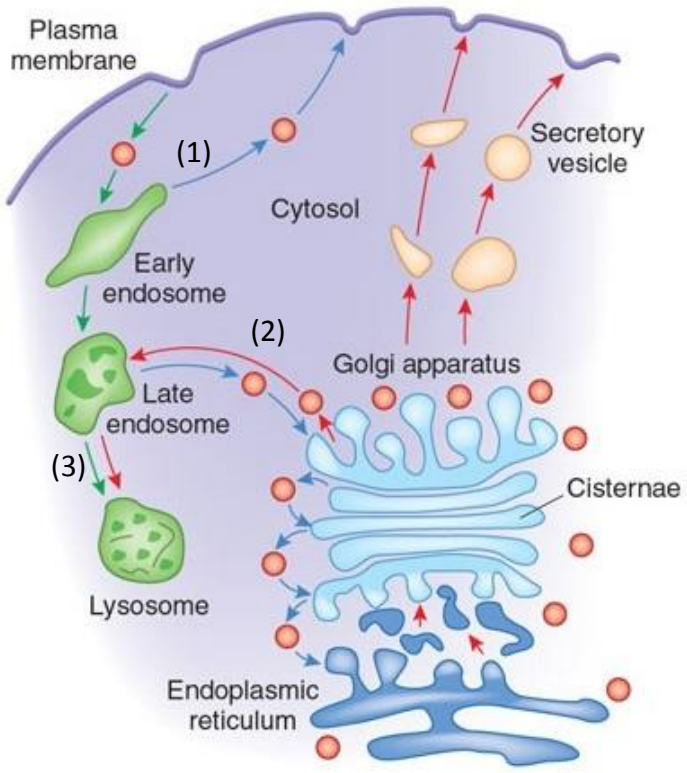

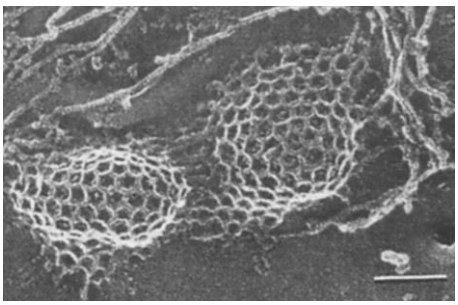

Figure 1.1.1: (a) Intracellular vesicular trafficking pathways[3] (b) Electron microscopy image of clathrin-coated pits in hypertonic fibroblasts, scale bar 100 nm[1]

Clathrin-independent endocytosis (CIE) pathways include macropinocytosis and phagocytosis (Figure 1.1.2), in which large portions of the membrane (>1 μm) are engulfed by membrane structures supported by actin filaments. In a different category of CIE, vesicles of closer size to clathrin-coated vesicles are formed by other cytosolic proteins. Caveolae are membrane invaginations formed from caveolin proteins and cavins (cavin1-4). They function as mechano-sensing domains which flatten out to buffer membrane tension. Caveolae can bend the membrane to form caveolar carriers (50-80 nm) that undergo endocytosis with the aid of dynamin, ATPase EHD2 and BAR domain protein pacsin2. Which cargoes are transported specifically by caveolae remains unclear,[4–6] and their endocytic uptake is highly dependent on cholesterol and sphingolipid content of the lipid bilayer.[7] Flotillin can localise in caveolae and itself outlines another clathrin- and caveolae-independent process.[4,5] Unlike clathrin, which is located in the cytosol and binds via membrane-bound adaptors, caveolins and flotillins are integral transmembrane proteins implicated in lipid rearrangement.[4]

Glycosylphosphatidylinositol-anchored proteins (GPI-ACs) have a high propensity to traffic through clathrin-, caveolin- and dynamin-independent endocytosis, giving the name to the clathrin-independent carrier (CLIC)/GPI-AC-enriched early endosomal compartment (GEEC) pathway.[8] The protein machinery driving endocytic uptake of these high capacity (100-200 nm)[9] carriers is complex, implicating BAR domain proteins and Rho family GTPases.[10] CIE carriers lack regular protein coats, thus are harder to image by electron microscopy compared with clathrin-coated cargos. Several other CIE mechanisms have since been characterised, including those in which lipids are redistributed to bend membranes.[8,11–13] The importance of membrane lipid content is currently studied by indirect, secondary techniques (discussed in section 1.3-4 and 1.7), since these molecular mechanisms take place below the resolution limit of light microscopy (200 nm).

CIE mechanisms can be classified by the mechanical actors in vesicle formation, such as GTPases (e.g. dynamin, RhoA and CDC42), BAR domain proteins (e.g. endophilin, pacsin2) and actin, or by their cargoes, such as GPI-APs, CD44, major histocompatibility class I (MHCI) molecules and interleukin 2 receptor.[9] Adding to this complexity in characterisation, these categories present significant interchangeability and compensatory roles in both cargo and membrane-bending machinery. Experimentally removing, manipulating or probing one factor can often be compensated by another.[14,15]

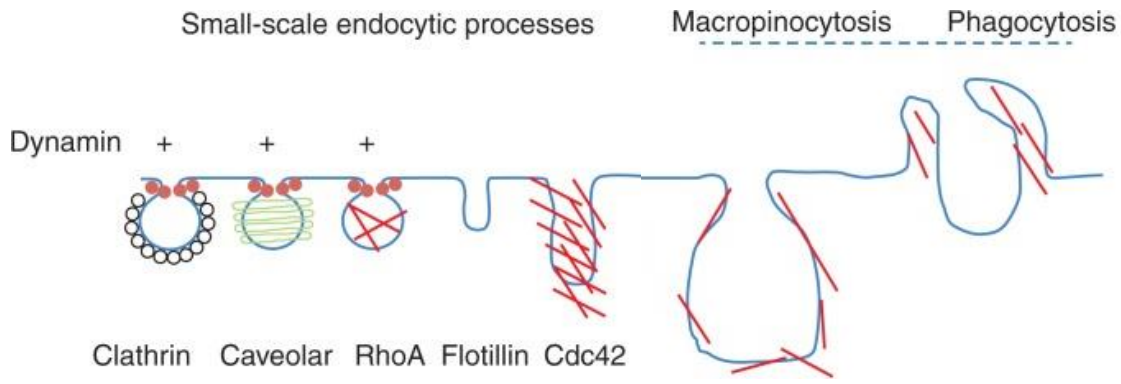

Figure 1.1.2: Mechanisms of endocytosis. Dynamin-dependent pathways (+) are typically associated with small-scale circular carriers such as clathrin- or caveolin-mediated pits.[5]

1.2 Glycolipid- and Lectin-dependent endocytosis

Lectins are proteins that bind to glycan (sugar, carbohydrate, saccharide) moieties of glycoproteins or glycolipids (GL). The GL-Lect hypothesis proposes that certain mammalian or pathological Lectins, once bound to the PM through GLs and/or glycoproteins, utilise GlycoLipids to induce nanodomain formation in the lipid bilayer, membrane curvature, and thereby, the biogenesis of endocytic pits.[16]

Clathrin-independent endocytosis (CIE) of the bacterial galactose-binding lectin, ricin, was the first CIE mechanism described.[17,18] Bacterial ricin, Shiga and cholera toxins bind via their respective B-subunits (RTB, STxB, CTxB) to their mammalian glycosyl receptors: galactosyl lipids and proteins, Gb3-Cer, or GM1-Cer, respectively (Figure 1.2.1). Once bound to the host cell and endocytosed to early sorting endosomes, the toxins bypass degradation in late endosomes and lysosomes. They are instead transported via the retrograde route (Figure 1.2.2), through the trans-Golgi network (TGN) and the Golgi stack to the endoplasmic reticulum (ER).[19] In the ER, the disulphide bond linking A- and B-subunits (orange, Figure 1.2.1) is cleaved to induce toxicity.[12,20] In the case of ricin and Shiga toxin, the A-subunit, a catalytic RNA N-glycosidase, translocates to the cytosol to induce toxicity by protein synthesis inhibition.

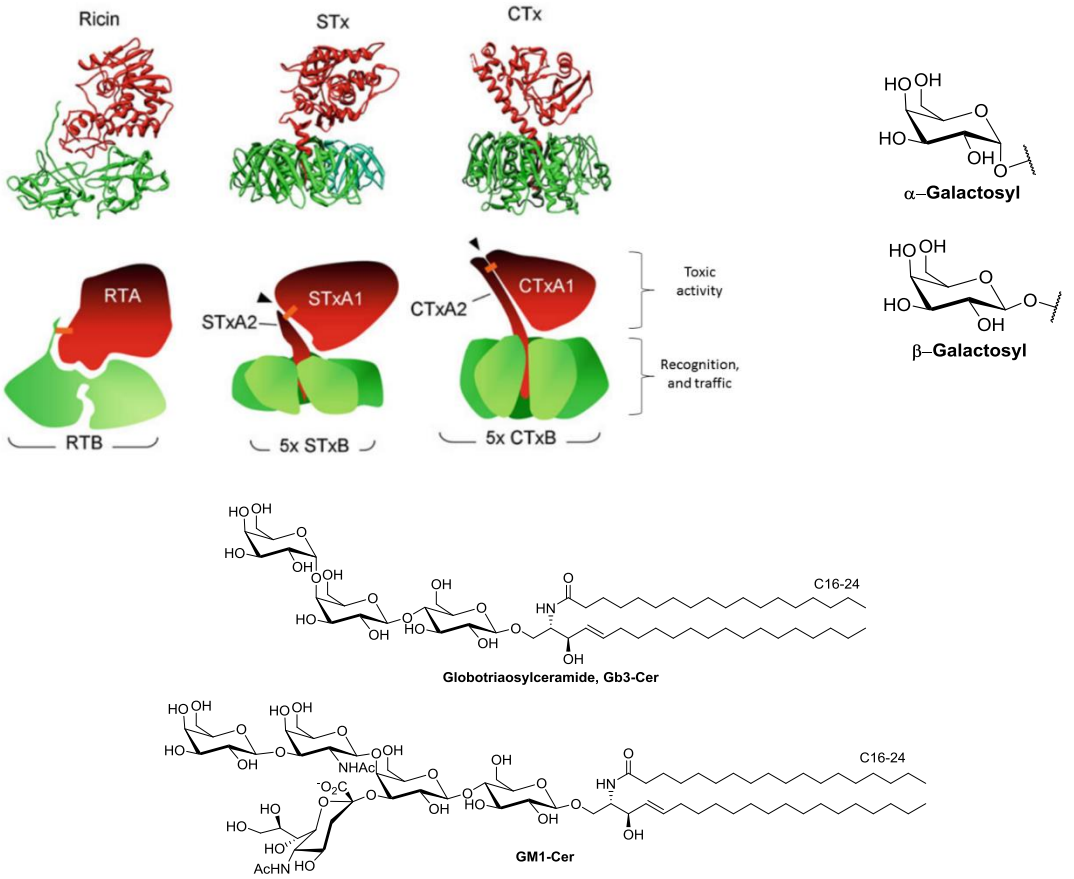

Figure 1.2.1: Crystal structures of ricin, Shiga and cholera toxins[19] with their respective receptors: galactose (presented on GLs and glycoproteins), globotriaosylceramide (Gb3-Cer), or GM1-ceramide.

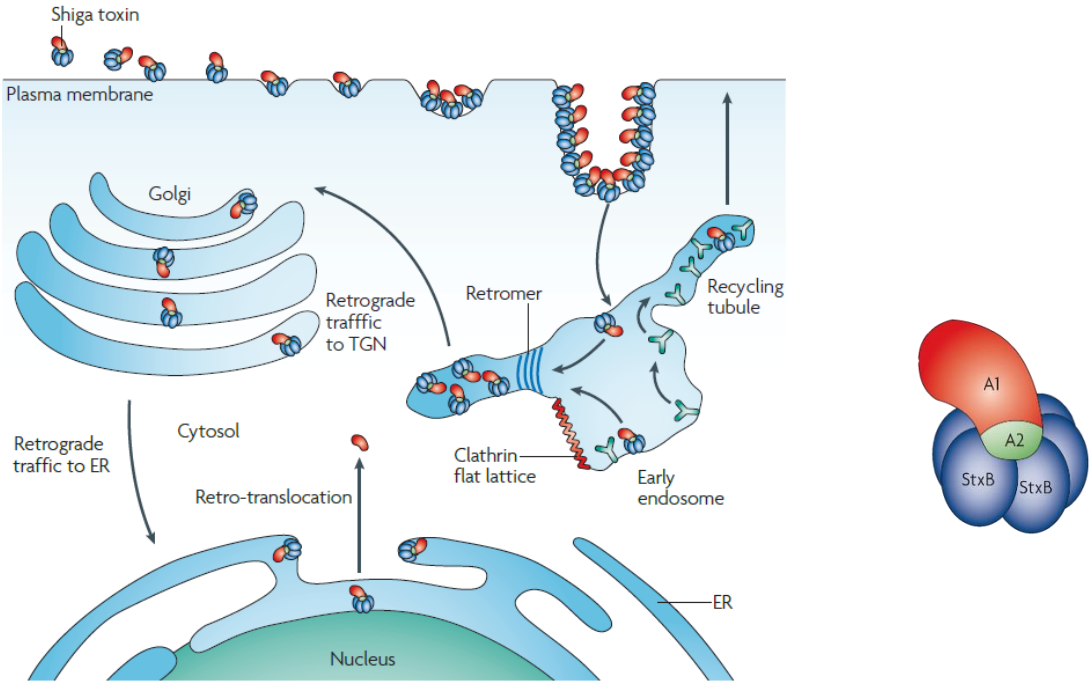

Figure 1.2.2: Retrograde trafficking of the Shiga toxin[12]

The homopentameric B-subunits of AB_5 Shiga and cholera toxin, STxB, CTxB, as well as the pentameric VP-1 capsid protein of Simian polyoma virus SV40, have flat, doughnut-like structures (Figure 1.2.3a), where they dock onto the membrane via their glycosphingolipid (GSL) receptors. The lectins' polyvalent binding is only of small individual affinity (dissociation constant $K_d \sim 10^{-3}$ M for STxB) for each GSL, but combine to a large avidity ($K_d \sim 10^{-9}$ M).[21] STxB contains three globotriose (Gb3) binding pockets per monomer, thus 15 total Gb3 binding sites. CTxB and SV40 protein have one GM1 binding pocket per monomer, totalling five GM1 binding sites.[22]

Of note, these three lectins have no sequence similarity, and yet the glycan receptors are all positioned around the edge of the protein in a seemingly overlapping geometry (Figure 1.2.3a), indicating a convergent evolution of structure. The glycan binding sites are of a geometry in which the membrane must bend up around the lectin to fit the glycan part of the GSL receptor molecules into their binding sites, thereby generating negative, inward-oriented curvature. This was recently demonstrated *in silico* for STxB-Gb3[13-15] in all-atom molecular dynamics studies (Figure 1.2.3b,d).[23] Effects on the membrane underneath the docked STxB, such as suppression of lipid fluctuations,[24] lead to membrane-mediated clustering to induce wider membrane invagination (Figure 1.2.3c). These early endocytic pits are then recognised by cytosolic machinery, dynamin, endophilin and/or actin,[15] for pit elongation and scission, before transport to endosomes.

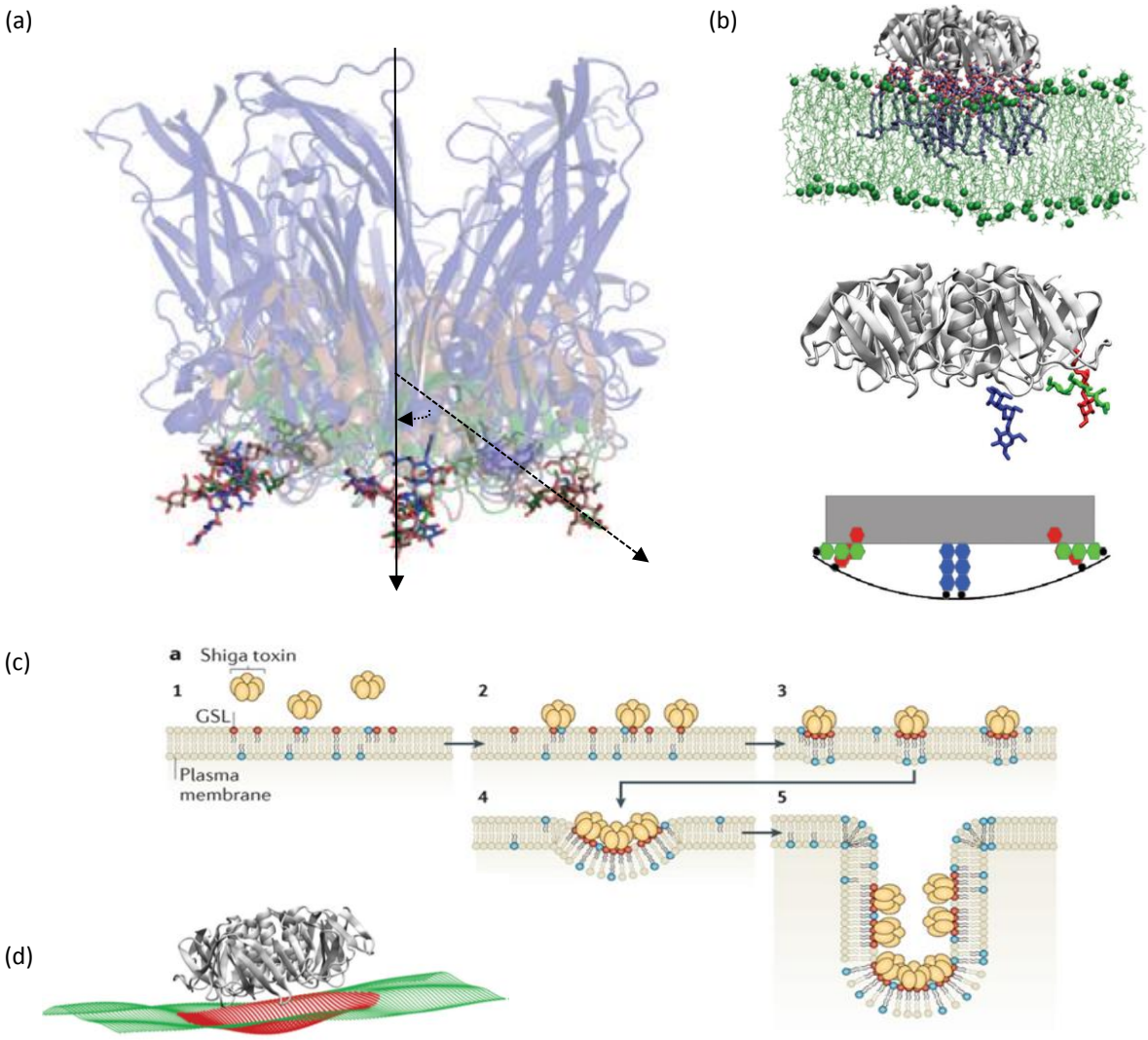

Figure 1.2.3: (a) Crystal structure overlay of STxB, (green Protein Data Bank (PDB) 1BOS), CTxB (red; PDB 1FGB), VP1 protein (blue, PDB 3BWR) bound to GSL receptors (corresponding colour)[8] (b, d) Local curvature of STxB binding to 13-15 Gb3-Cer in phospholipid bilayer[23] (c) STxB binding, inducing local curvature, clustering and membrane invagination[8]

This membrane bending phenomenon is an intrinsic property of GL-Lect complexes and can be reproduced in simple model membrane systems, liposomes. One classical experimental technique applies hydrating with an aqueous solution, a lipid mixture of phospholipid with a small molar percentage of GSL, to obtain spherical giant unilamellar vesicles (GUVs) of homogenous size similar to cells (~10 µM).[25,26] Membrane bending properties of GL-Lect drivers have been widely investigated using GUVs: Gb3 with STxB (Figure 1.2.4a)[27] or bacterial lectin LecA;[28] GM1 with SV40[29] or cholera toxin;[30] and a GSL mixture with a mammalian lectin, galectin-3 (Gal3) (Figure 1.2.4b).[31] Gal3, which undergoes GSL-

dependent endocytosis after binding to glycoproteins in cells, spontaneously forms dynamic membrane invaginations when bound to GUVs containing 5% GSL.

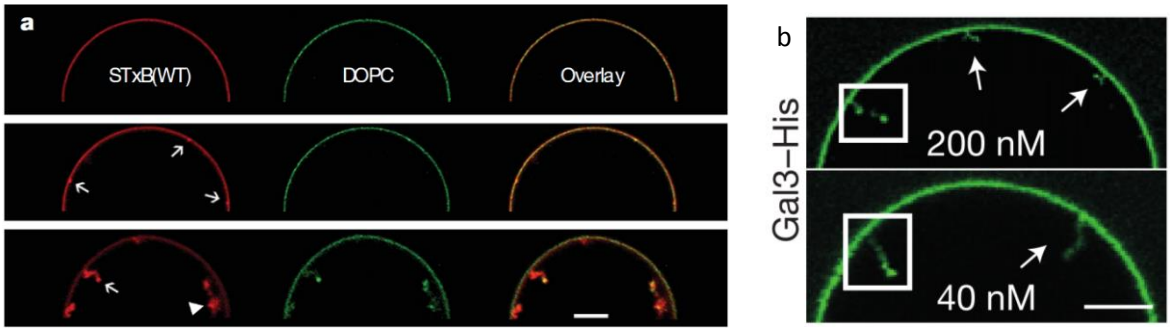

Figure 1.2.4: Giant unilamellar vesicles (GUVs) showing membrane bending induced by lectins and GSLs. (a) DOPC/cholesterol/porcine Gb3-Cer/BodipyFL-C5-HPC (green) [64:30:5:1] incubated with STxB-Cy3 (red); (b) PC/cholesterol/sphingomyelin/PS/GSL-mix/Nickel-NTA-DOGS/lissamine-rhodamine-PE (0.1mol%) [56.9:20:12:3:5:3:0.1] incubated with His-tagged galectin Gal3-His[31]

1.3 GSL function studies

Unpicking the molecular mechanism of membrane curvature formation by the STxB-Gb3 complex can give novel insight on GL-Lect endocytosis. To investigate the relative contribution of driving forces in the clustering of STxB toxins, the system was recently studied *in silico* and experimentally.[24] There are no attractive interactions between STxB proteins, so how do they cluster? A commonly cited membrane-mediated force, line tension (Gibbs free energy required to maintain domain interfaces) might contribute to clustering due to height or compositional mismatch within the lipid membrane.[32,33] Gb3-Cer and other GSLs often have longer lipid chains than bulk phospholipids, meaning the domain containing STxB-$Gb3_{x\leq15}$ (x indicates numbers of bound Gb3 molecules) should be held higher on the membrane.[34,35] When tested experimentally by varying lipid tail lengths of Gb3-Cer in GUVs, no significant difference in clustering kinetics was observed,[24] demonstrating that height mismatch line tension is not strictly required for clustering. One could also implicate line tension caused by compositional mismatch of the lipids, due to thermodynamically favourable lipid-demixing effects. Pezeshkian *et al.* suggested that Gb3-Cer domains are not required for clustering to occur, since GUVs formed from 5 or 30 mol% Gb3-Cer showed no

significant difference in binding or invagination; 30 $_{mol}$% being the Gb3 concentration that one expects to find under STxB molecules.[24] Solevyeva *et al.* showed that STxB binding induced membrane lipid domain organisation in GUVs,[36] but this reasons for the reverse causality; that STxB clustering induces compositional mismatch.

To elucidate the mechanism, synthetic Gb3-spacer-Cer analogues (Figure 1.3.1a) were synthesised in the L. Johannes laboratory and tested in GUV experiments. The longer ethylene glycol (EG) spacers between the Gb3 head and the ceramide tail increasingly inhibited STxB clustering and invaginations in GUVs (n=3 or 7, Figure 1.3.1a, b). These experiments gave birth to the fluctuation force hypothesis, proposing that a suppression of fluctuation of the membrane is required for toxins to cluster (Figure 1.3.1c). This effect is commonly alluded to being like drifting boats on the ocean, or cheerios on milk, which aggregate together. This hypothesis was studied by course-grained molecular dynamics simulations, showing that two macromolecules, with dimensions corresponding to the membrane-bound STxB-Gb3$_{x\leq15}$ complex, would randomly drift on a phospholipid bilayer. In the simulation, only the macromolecules tightly bound to the bilayer (Figure 1.3.1d) would be attracted to each other from a distance of several nanometres, whereas loosely bound macromolecules (Figure 1.3.1e) would experience no attraction force.[24] Hence, the tight binding of the toxin to the membrane via Gb3 receptors is sufficient to induce clustering. These results will in turn guide this project, in the constraints on structure of Gb3 analogues proposed and synthesised, which should retain natural lectin binding and membrane bending actively.

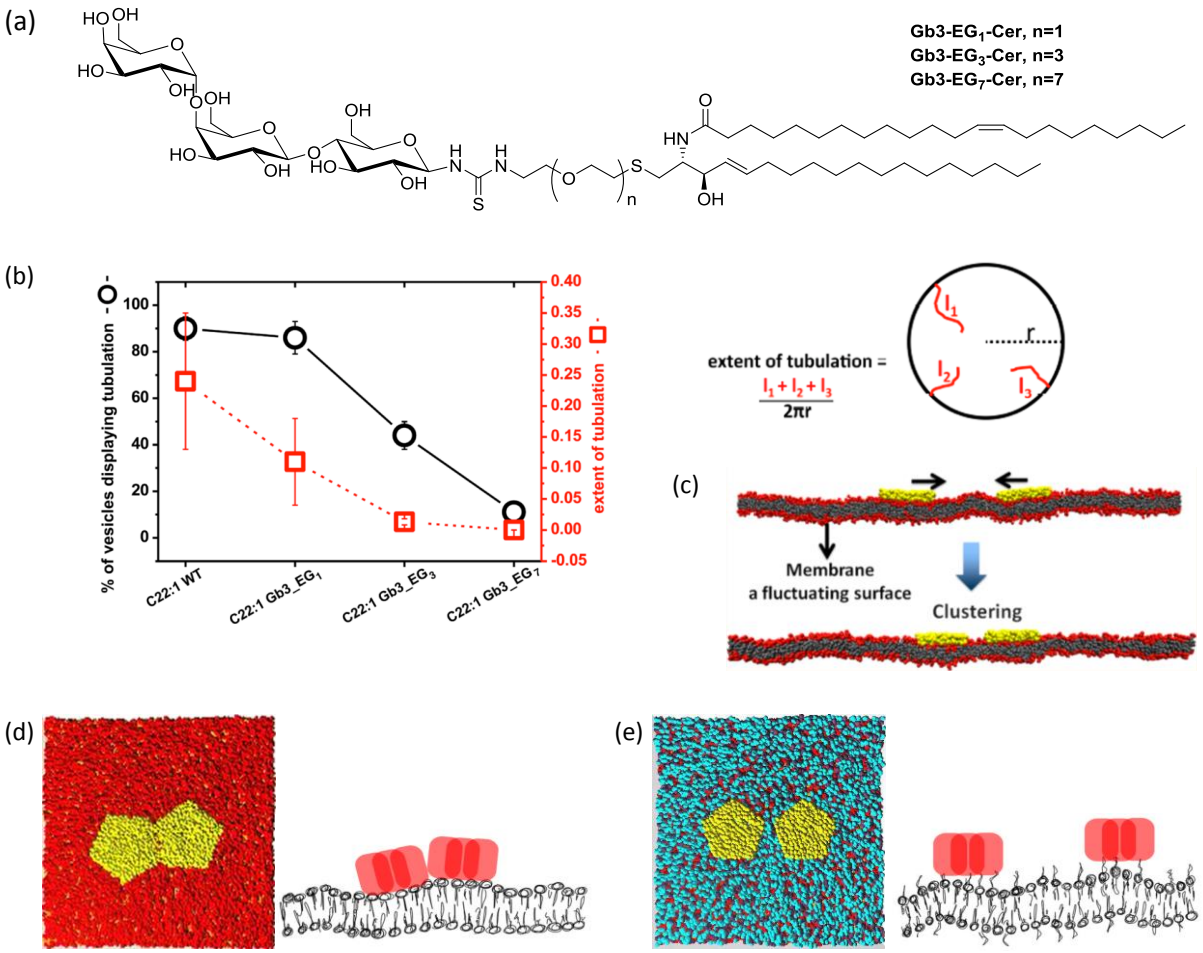

Figure 1.3.1: (a) Structures of Gb3-ethyleneglycol $(EG)_n$-Cer analogues, n=1,3,7 (b) quantification of GUV experiments showing that long, flexible spacer region inhibits tabulation (c) Suppression of membrane fluctuation induces clustering of macromolecules bound to lipid bilayer. (d,e) Course-grain simulations of pentameric toxin-like nanoparticles bound either tightly (d, no spacer) or loosely (e, flexible spacer). [24]

Despite the fact that low or high Gb3-Cer concentrations used in GUVs have little effect on STxB clustering, one must still consider that glycolipid organisation may have an effect on lectin binding and endocytosis.[33] The *lipid raft hypothesis* describes the propensity of cholesterol and sphingolipids, mostly sphingomyelin (SM) and GSLs, to phase separate into denser, more ordered regions in a lipid membrane.[37,38] The theory gained interest because of the dependence of certain biological processes on non-specific cholesterol depletion, or the easy isolation of detergent-resistant membrane domains by treating biological samples with cold detergent, justifying the binominal classification of proteins and processes as “raft” or “non-raft.” An enrichment of “raftophile” lipids, cholesterol and sphingolipids, in CIE cargos has been demonstrated in several non-direct methods.[39–41] This phenomenon of lipid organisation is observable with chemically-modified lipids, in liposomes, or using non-specific

extraction techniques, but the biological relevance is difficult to evaluate for natural, non-fluorescent lipids *in cellulo* or *in vivo*.

Lipid organisation can be driven by a multitude of factors such as actin cytoskeleton organisation,[42] ectodomain association, and membrane pits, ruffles and contact sites.[43] Specific lipid binding pockets in proteins and charge interactions also induce lipid organisation. 20-30% of the PM area is covered by proteins, and lipid solvation rings around proteins could account for the majority of the lipid area remaining.[44] Eggeling *et al*. recently used super resolution fluorescence scanning microscopy (FSC) to show that fluorescent phospholipids or cholesterol presented no significant lateral heterogeneity, whilst fluorescent SM showed transient trapping in ~80 nm domains, but hardly moved once trapped. This observation does not correspond to lipid raft criteria, but infers specific lipid interactions with membrane components.[45,46]

Another recent imaging study by Kraft *et al.* used secondary ion mass spectrometry (SIMS) with isotopically-labelled sphingolipids and cholesterol reconstituted into cells.[47,48] After fixing and imaging cells, they show ^{15}N-sphingolipids concentrated into microscale domains (Figure 1.3.2b), and ^{18}O-cholesterol evenly dispersed in the PM (Figure 1.3.2c), contesting the existence of nanoscale *lipid rafts*. These findings correlate with recent super-resolution fluorescence microscopy performed with fluorescent analogues.[49,50]

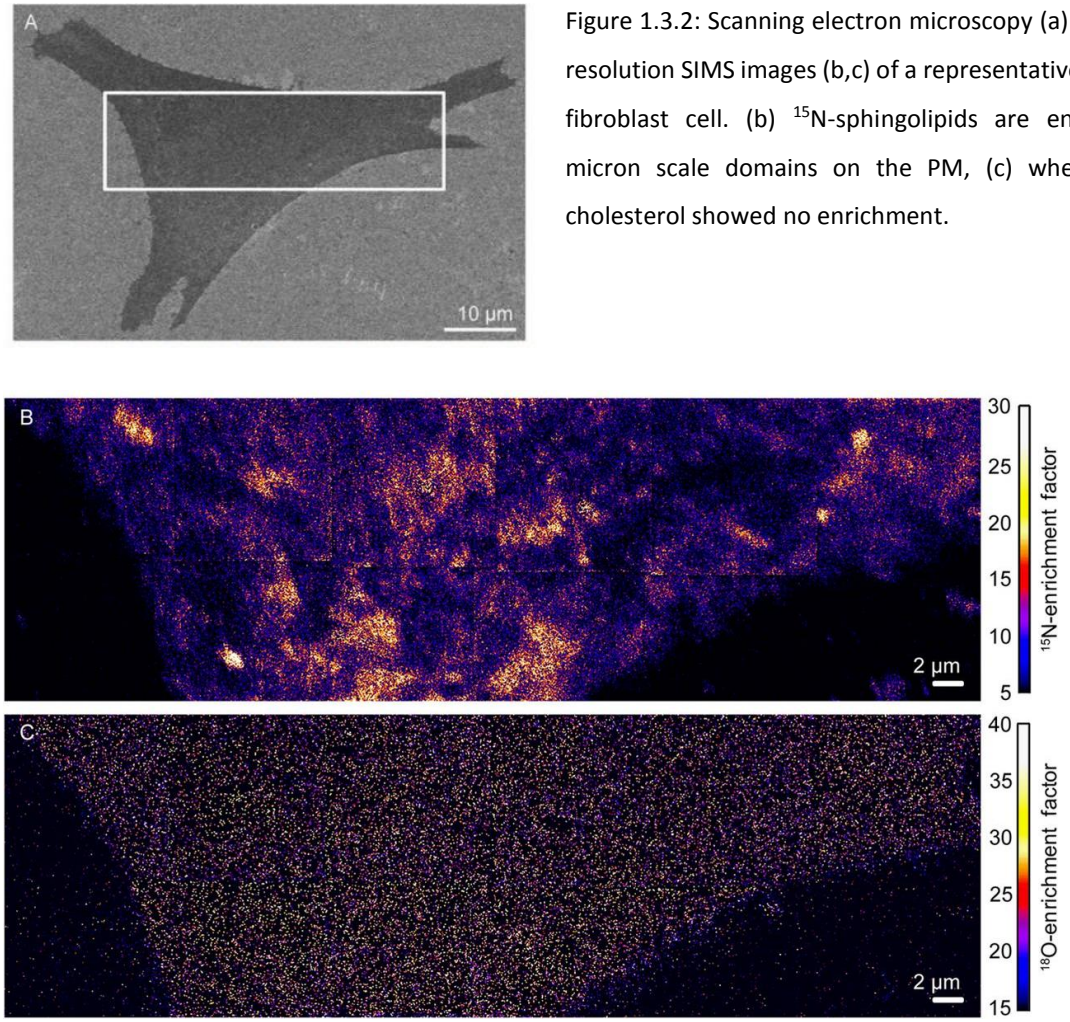

Figure 1.3.2: Scanning electron microscopy (a) and high-resolution SIMS images (b,c) of a representative clone 15 fibroblast cell. (b) ^{15}N-sphingolipids are enriched in micron scale domains on the PM, (c) whereas ^{18}O-cholesterol showed no enrichment.

The high spatiotemporal resolution of fluorescence microscopy has promoted the development of fluorescent GSLs, obtained by some complex chemical syntheses.[51–55] Despite progress in smaller fluorophores and faster imaging techniques, the study of these molecular tools in GUVs and cells has highlighted the precariousness in studying lipid properties with modified lipids. Lipids, including fluorophore-tagged lipids, can separate into ordered (L_o, e.g. saturated lipids) or disordered domains (L_d, e.g. unsaturated lipids) easily visible in GUVs by confocal fluorescence microscopy.[56,57] Patalag *et al.* recently showed that the synthetic fluorescent Gb3-Cer analogues **1** and **2** (Figure 1.3.3) separated into the lipid disordered (L_d) domains. The partitioning of natural Gb3-Cer cannot be verified or compared, but it is commonly conceived that saturated long-chain GSLs separate into L_o domains, based on the thermodynamic theory of lipid de-mixing and lipid rafts. One can directly compare Gb3-Cer analogues and wild type when bound with fluorescent STxB (red, Figure 1.3.3b,d,e). STxB

localised to the L_d domains (green) in GUVs with **1** and **2** separately, whereas with natural Gb3-Cer, STxB localised to L_o domains.[58]

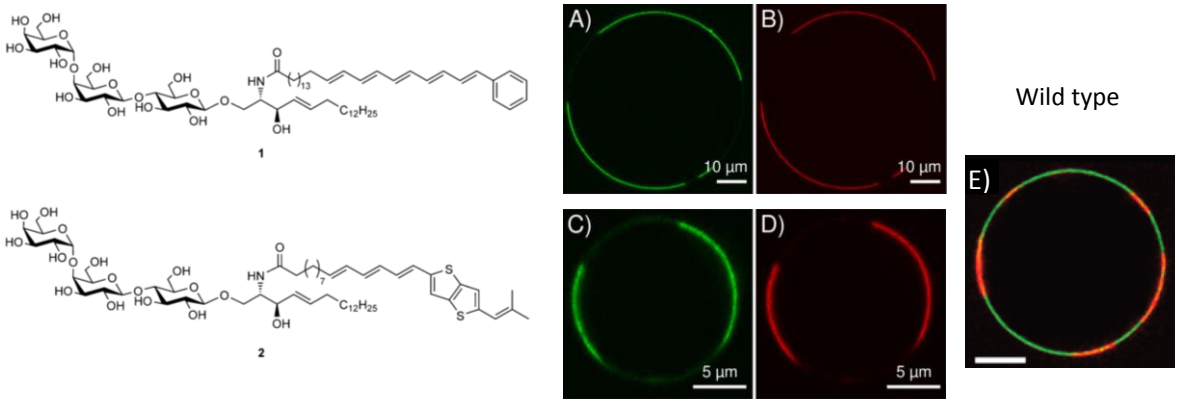

Figure 1.3.3: GUVs with 5_{mol}% Gb3 analogue **1** (a,b) or **2**[59] (c,d) or wild type Gb3-Cer (Figure 1.2.1)[58] (e) (DOPC/SM/Chol/Gb3-Cer [40:35:20:5] with <1% fluorescent phospholipid (green, L_d), incubated with STxB-Cy3 (red).

Specific study of Gb3-Cer and other long-chain GSLs in cell culture is practically unattainable since they cannot be added directly to cells in culture in a controlled manner.[60] Chinnapen *et al.*, when investigating GM1 and cholera toxin traffic in live cells, reincorporated GM1 species bearing C18 chain length or shorter, despite specifying that the natural profile contains mostly C24 and C16 acyl chains.[30] Pedrosa *et al.* showed that short C8 acyl chain GlcCer could be taken up with a yield of 20% in cancer cells, and 5% in normal cells, but do not discuss longer chains.[61] Fusogenic liposomes have been used to improve uptake,[62,63] employing neutral and positively charged phospholipids to improve fusion of lipid vesicles with the PM.

Our laboratory and others have never shown natural retrograde transport of STxB by supplementing Gb3-Cer to cells not expressing Gb3-Cer natively. Attempted reconstitution of commercial Gb3-Cer with long ceramide acyl chains (majority C22, C24 chains)[64] into GSL-negative (GSL^-) GM95 cells showed negligible STxB cell-surface binding (Figure 1.3.4a) and endocytosis. Gb3-Cer with shorter C18 acyl chain could allow STxB binding to cells, at 4°C, before endocytosis (Figure 1. 3.4c), but its traffic is misdirected away from the Golgi (Figure 1. 3.4d). An example by Haicheur *et al.* shows the canonical retrograde transport of STxB to the Golgi in Gb3-expressing D1 murine dendritic cells (Figure 3. 3.4e),[65] which is reproducible in most Gb3-expressing ($Gb3^+$) cell lines.[40] Even when two strains of bacterial STx, verotoxin 1 and 2, bind to distinct PM domains, they coalesce into retrograde traffic to the Golgi.[66]

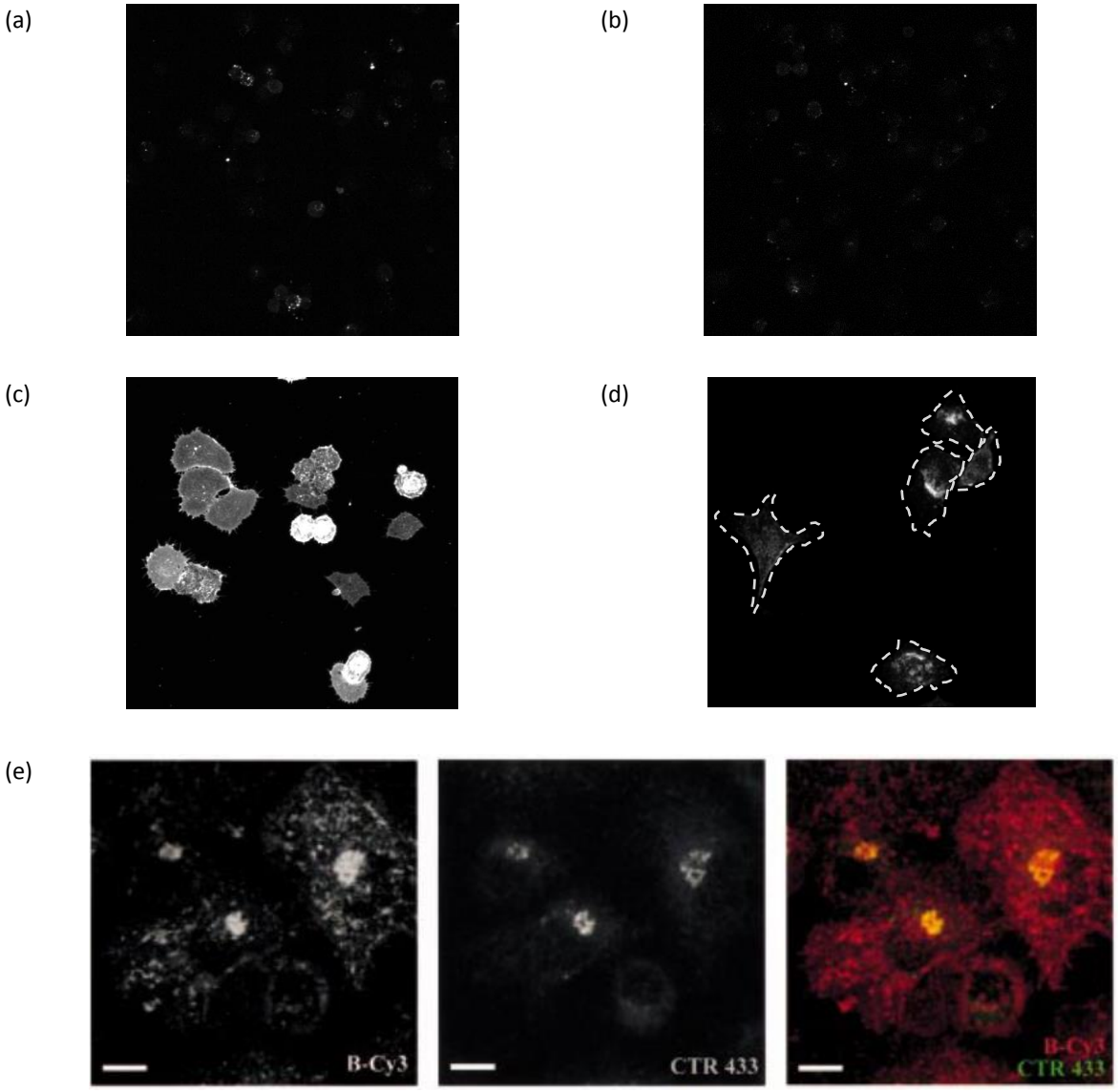

Figure 1.3.4: GM95 cells incubated with Gb3 commercial mix (Matreya) with bovine serum albumin (BSA) (20 µM) (a) or without (b), then incubated with STxB-Alexa488 to observe surface binding (4°C, 30 min). Short chain Gb3 C18:1 shows binding at 4°C (c) and uptake but misdirected traffic at 37°C (d). (e) When internalised on natural Gb3, STxB is transported to the Golgi and colocalises with CTR433, a Golgi marker.

1.4 GSL function and biosynthesis

The biosynthesis of glycosphingolipids (GSLs) is well documented. However, GSL function and their interactions is still mystifying scientists, apt to the etymology of the word "sphingolipids" – named by J. L. W. Thudichum in 1884 after the enigmatic sphinx.[34] Over 400 unique oligosaccharide head groups make up the enigmatic "glycolipidome" in mammals.[67] GSLs constitute 2-10% of total lipids in membranes,[68] where sphingomyelin (SM) is estimated at 15-20% of the plasma membranes (PM).[69] GSLs are found at higher concentrations at the apical side of epithelial cells, and in certain cell types including oligodendrocytes and neurons. Their fingerprint expression levels vary throughout development and pathogenesis, amongst cell and tissue type.

Functions of groups of GSLs have been studied by genetic suppressions. Mice deficient in all GSLs, obtained with a glucosylceramide synthase (GCS) gene knockout, do not survive beyond gastrulation,[70] similar to lactosylceramide synthase knockout mice.[71] Genetic suppression of the gala- and ganglio-series GSLs in mice shows phenotypes in nervous system or neuronal functions respectively (Figure 1.4.1).[72,73] GSLs have classically been used as differentiation markers, especially the stage-specific embryonic antigens (SSEA1-4).[74,75] GSLs are implicated in cell migration, adhesion and signal transduction,[76] as well as clathrin-independent endocytosis.[13,31] Many GSL-protein interactions are implicated in signal transduction,[77] such as the activation of epidermal growth factor receptor (EGFR).[78] GLSs undergo individual and polyvalent interactions with proteins, as proposed in the lipid raft hypothesis, where they play a direct role in membrane organisation and activation of raft-localised proteins.[79] Such polyvalent interactions means that GSLs have low individual affinity for protein interaction partners, making GSL-protein interactions difficult to identify by standard immunopurification techniques. High resolution mass spectrometry (HRMS) techniques are improving rapidly in GSL analysis, particularly shot-gun lipidomics.[80,81] In spite of this, a topological and temporal interaction map of GSL function and interactions is still far from reach.

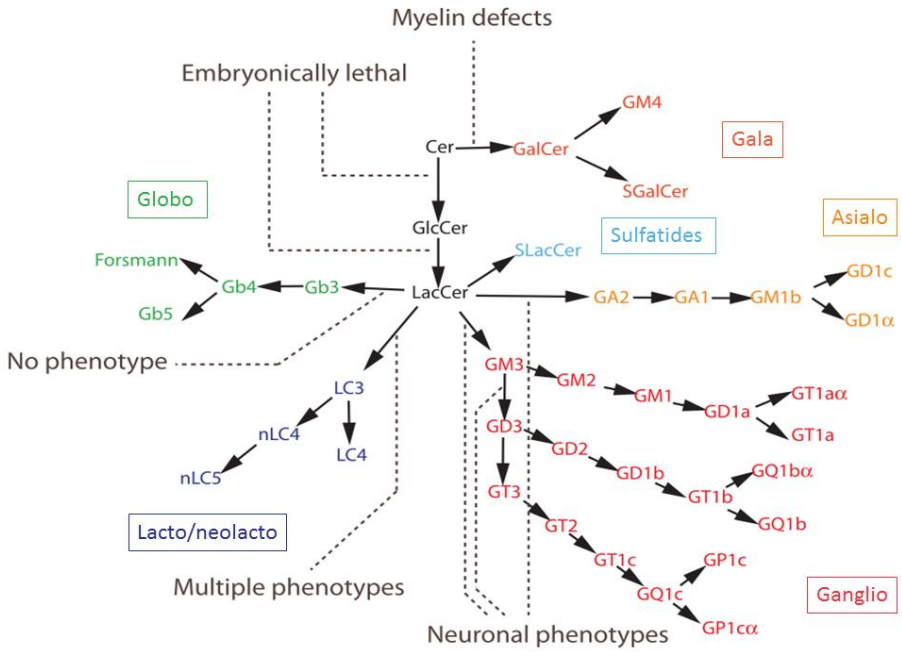

Figure 1.4.1: Stepwise synthesis of GSLs from ceramide (Cer). Knockout of pathways shows phenotypes in early development, myelin (nervous system) or neuronal function. Modified from D'Angelo *et al.*[82]

Ceramide, the central building block for sphingolipids (Figure 1.4.2), is synthesised in the *de novo* pathway at the cytosolic leaflet of the endoplasmic reticulum (ER) (Figure 1.4.3a). First, L-serine and palmitoyl-CoA are condensed by serine palmitoyl transferase (SPT) to form 3-ketodihydrosphinganine, which is reduced by 3-ketosphinganine reductase (3-KSR) to sphinganine. Sphinganine is *N*-acylated to dihydroceramide by the ceramide synthases (CerS1-6) to produce dihydroceramide. Each CesS has a specificity for CoA-fatty acid precursor(s) and catalyse formation of the corresponding *N*-acyl C14-26 products (Figure 1.4.3b).[83] Dihydroceramides (C16-24) are dehydrogenated by dihydroceramide desaturase (DES) to ceramide (C16-24). In the ER, ceramide can be galactosylated to galactosylceramide by galactosylceramide synthase (GalCS), going on to form sulfatide GSLs in the Golgi.[69] This represents a small but pathologically important family of GSLs.[67,84]

Ceramide is transported from the ER to the Golgi to form the two major families of sphingolipids, SM and GSLs. Sphingomyelin synthase (SMS) transfers the phosphocholine head group from the cell's most abundant glycerophospholipid, phosphatidylcholine (PC),[69] to ceramide, forming SM and diacylglycerol (DAG), in the trans-Golgi and PM.[85,86] Glucosylceramide (GlcCer), the precursor of most GSLs, is synthesised in the cytosolic leaflet of the Golgi by glucosylceramide synthase (GCS), a.k.a. UDP-glucose ceramide glucosyltransferase (UGCG). The stable *UGCG* gene knockout cell line, GM95, is a useful tool

in the study of GSL function.[87] In lesser part, ceramide is phosphorylated to ceramide-1-phosphate (C1P) by ceramide kinase (CK).[88,89]

The only irreversible degradation route leaving the sphingolipid network is the catabolic pathway. Ceramide is reversibly hydrolysed to sphingosine by ceramidases (CDase), which are organelle specific, pathway specific and substrate specific.[85] Sphingosine is phosphorylated to sphingosine-1-phosphate (S1P) by sphingosine kinase (SK), while the reverse reaction is catalysed by S1P phosphatase (S1PP). S1P can then be irreversibly degraded to ethanolamine-1-phosphate and C16 fatty acid by S1P lyase in the ER.

Ceramide is (re)formed in the salvage pathway, by reacylation of sphingosine, predominantly by the CerS5 enzyme.[83,90] This pool cycles back to form 50-90% of total sphingolipid content.[91] Ceramide is also reformed by the degradation of GSLs by glycosylceramidase (GCS) or galactosylceramidase (Gal-CDase) in lysosomes, the degradation of SM by sphingomyelinase (SMase), and of C1P by ceramide-1-phosphate phosphatase (C1PPase).

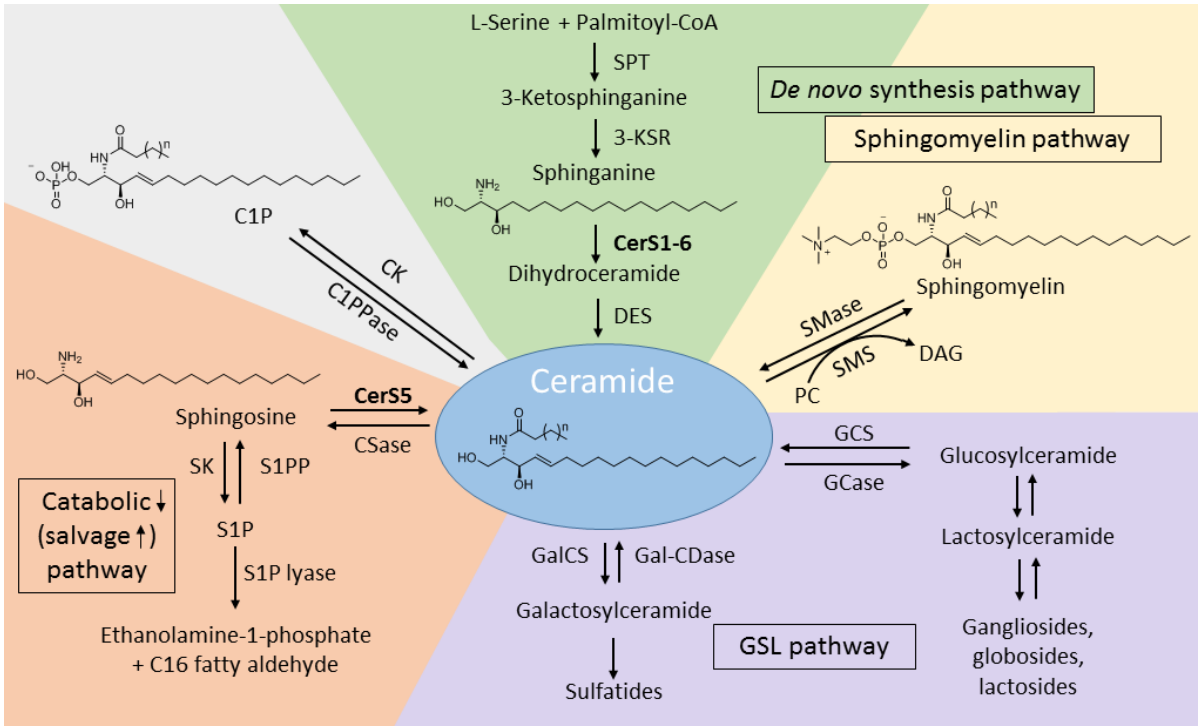

Figure 1.4.2: Sphingolipid biosynthesis, modified from S Merscher *et al*.[86]

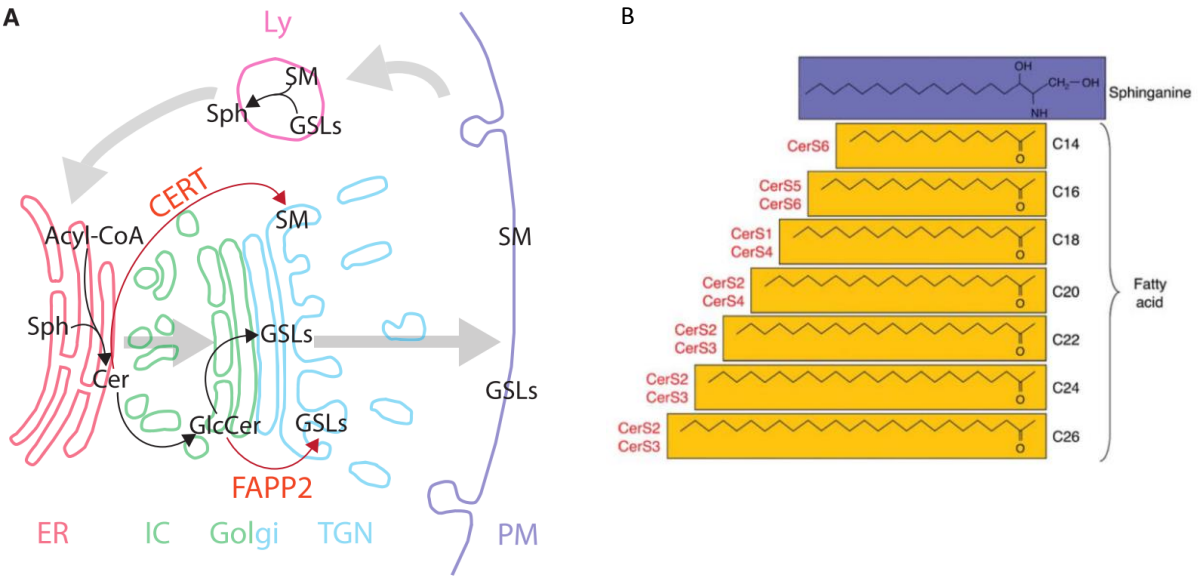

Figure 1.4.3: (a) GSL synthesis and transport through cellular compartments.[72] (b) Ceramide synthase (CerS) specificities.[83]

The stepwise biosynthesis of complex GSLs (Figure 1.4.4a) is fed by two distinct pools of lactosylceramide (LacCer), both formed by LacCer synthase from GlcCer, differing in localisation and glycosylation fate. The pool of GlcCer transported through the Golgi cisternae by vesicular transport forms LacCer to be sialylated to GM3 and ensuing gangliosides (sialosides, sialic acid-containing GSLs) (Figure 1.4.4b). Alternatively, GlcCer transported by the FAPP2 transfer protein to the trans-Golgi network (TGN) feeds the pool of LacCer which is galactosylated by Gb3 synthase to form Gb3 and the globo- and asialo-series.[82] The biosynthesis of GSLs is mediated by glycosylation enzymes in the Golgi, which can act on multiple GSL substrates. However, the glycosylations are not random. Twelve glycans are used in the GSL "alphabet," with sulfatation adding further complexity. However, only 400 different head groups have been characterised. D'Angelo *et al.* commented that, of the 144 linkages possible from 12 glycans, only 29 unique covalent bonds are observed.[72] SphinGOMAP, an open source website compiled by the GSL research community (www.sphingomap.org), contains over 500 sphingolipid and GSL species arranged according to their biosynthesis, displaying nomenclature and stereochemistry.

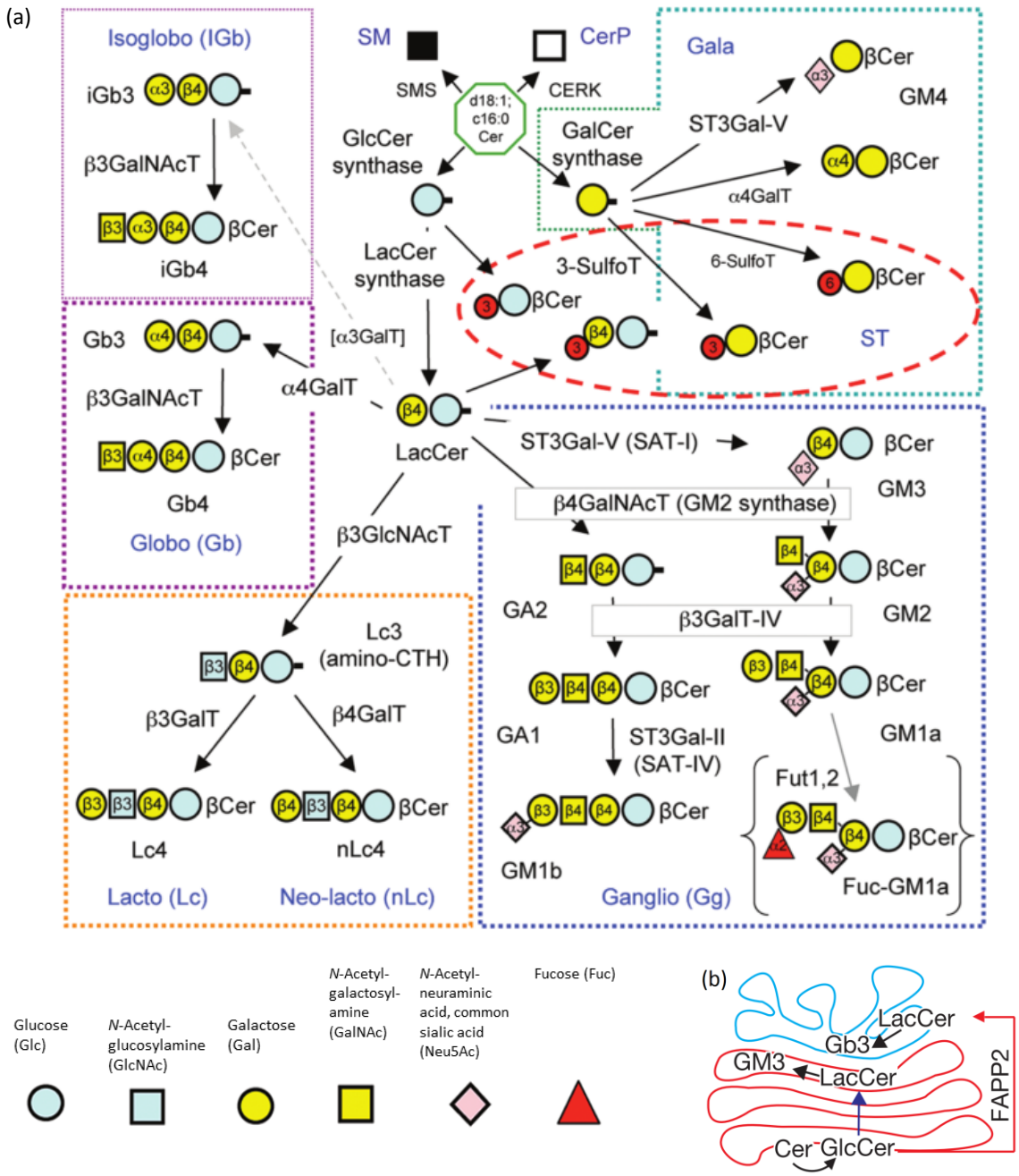

Scheme 1.4.4: (a) Initial roots of GSL families in branched, stepwise biosynthesis.[34] (b) Two distinct pools feed the biosynthesis of complex GSLs.[82]

GSLs are localised between the Golgi, where they are synthesised, and the PM, where they are recognised by antibodies and lectins.[92] Localising GSLs in cellular compartments is challenging since functionalisation with a fluorophore can change considerably their localisation and traffic. Antibodies can be used to recognise GSLs as antigens. However, antibodies cannot cross the PM without disrupting the localisation of the GSL in question.[93,94] Reports differ on GSLs' actual localisation.[34,89,95]

1.5 Biomedical relevance

In this project, we develop tools for the investigation of GSLs in GL-Lect endocytosis. GSLs are of medical interest for the investigation of GSL lysosomal storage diseases, caused by mutations in sphingolipid degradation genes. Major examples include Gaucher disease, (GlcCer accumulation), Fabry (Gb3-Cer), Tay–Sachs and Sandhoff (GM2) diseases.[86,96] These can be treated with substrate reduction therapy, such as the glucosyl-ceramide synthase inhibitor N-butyldeoxyno-jirimycin,[84] and enzyme replacement therapy at high cost.

Moreover, better comprehension of the molecular mechanism of toxins, which hijack mammalian GSLs for cellular uptake via GL-Lect endocytosis, will aid the development of treatment. Shiga toxin, the major virulence factor of *Shigella dysenteriae*, and Shiga-like toxins, also known as verotoxins, secreted by enterohemorrhagic strains of *Escherichia coli* bacteria, have a highly conserved structure.[97] All bind specifically to Gb3-Cer, which is expressed on kidneys and brain tissues,[98] and some strains bind to Gb4-Cer with lower affinity. Infection induces diarrhoea, and eventually haemolytic uremic syndrome (HUS) and acute renal failure, with high infant fatality rate across the world, and complex cases can have neurological symptons.[20] Cholera toxin, secreted by *Vibrio cholerae,* causes cholera, a lethal disease with high fatalities in the developing world, and outbreaks of disease in conflict zones is regularly reported in standard news media around the world.[99] Currently no curative treatment is known for disease caused by the Shiga and cholera toxin-producing bacteria.[20]

Gb3 is expressed in several cell types of interest to cancer research: cancer cells and cancer stem cells themselves,[100,101] and antigen-presenting dendritic cells, which stimulate the immune system. The interest in GSLs spans the development of cancer chemotherapeutics, in which it is paramount that effective drug targets are cell-specific to reduce non-specific toxicity. GSLs as cell biomarkers is under-explored territory in the state of chemotherapeutic research, and yet their expression levels are known to change drastically with pathogenesis.[101,102] Furthermore, study of the GL-Lect mechanism will inform the development of lectin- or STxB-conjugated drug-vectors; the rational for which aims at following the non-degradative retrograde pathway, from which STxB benefits, to target and invade host cells (Figure 1.5.1).[98] This route is complementary to the standard pathway followed by large antibody-drug conjugates (ADCs),[103] which are normally taken up by

clathrin-mediated endocytosis and sorted to lysosomes to be degraded. STxB-drug conjugates have shown promise in targeting Gb3-overexpressing cancer cells.[104–110]

Endogenous lectins and their GL-Lect interactions with GSLs are coming to light.[2,16] For example, galectin-3, which is deregulated in human cancers, is endocytosed with CD44 and β1-integrin in a clathrin-independent mechanism dependent on GSLs and *N*-glycosylation.[31] Gb3-Cer is the cell receptor for the Shiga toxin, but no endogenous functions are currently known. Although GSLs are not classically "druggable" compounds due to their undesirable pharmacokinetic properties, research into their function and therapeutic role requires methods to manipulate their expression in cells. Hence a robust and versatile reconstitution method and related syntheses of these products are of great interest.

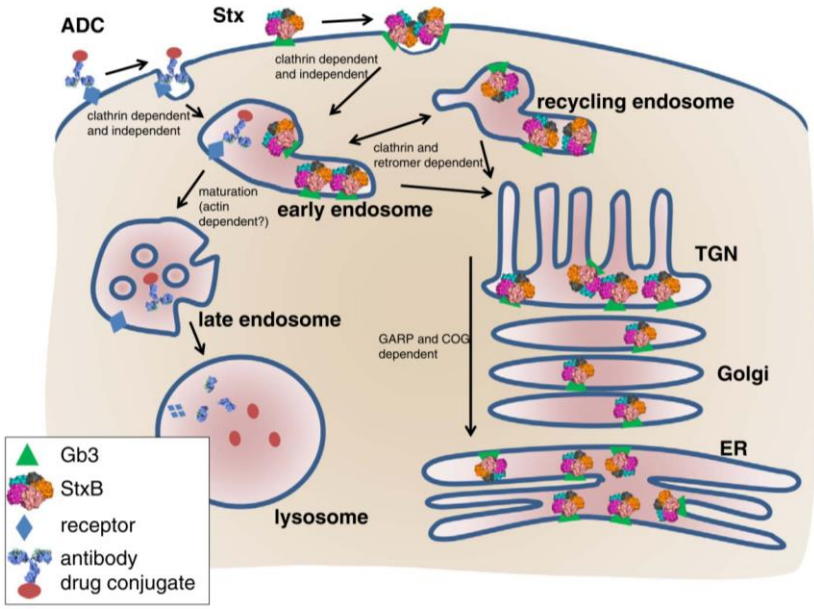

Figure 1.5.1: Cellular incorporation and traffic of antibody-drug conjugates (ADCs) and STx and its conjugates

In this project, we endeavour to reconstitute GSLs by conjugating *in situ* the two parts of a GSL (glycan and lipid) with a spacer group of the smallest possible size. We employ specific bioorthogonal chemistry, known as *click* chemistry, to achieve this in cell culture.

1.6 Bioorthogonal conjugations and *click* chemistry

Chemical biology uses chemical techniques to effect or probe biological systems at the molecular level. This includes the development of fluorophores, small-molecule protein inhibitors/activators, non-natural amino acids and any other synthetically modified biomolecule. Genetic tagging of proteins, for example, with green fluorescent protein (GFP), has significantly promoted research in molecular biology. However, smaller chemical modifications are needed for smaller metabolites, lipids, carbohydrates and post-translational modifications. Although chemical synthesis may never attain the complexity of nature's highly regulated protein factory, progress is constantly being made in establishing better, subtler and more specific manipulation and higher-resolution study of the cellular system.

Current techniques for the study of lipids and GSLs are limited. Stable isotope labelling should not disrupt the biochemical interactions of the molecule under study, but incorporation is often low yielding, requiring technically complicated protocols for low sensitivity and high costs, and topological imaging techniques able to localise stable isotopes are still developmental (secondary ion mass spectrometry, SIMS, section 1.3). Radioisotope labelling can be localised but is innately hazardous. Mass spectrometry (MS) coupled to liquid chromatography (LC-MS) has traditionally been used for exact identification for the brute structure of the *lipidome*, all of the lipids present in a biological sample. Liquid chromatography separation of analyte species allows higher signal to noise ratio, but is not quantifiable. Now, shotgun lipidomics is coming to dominate the field, and is applied in this project. This rapidly developing technology permits identification and quantification of the lipidome using high resolution mass spectrometry (HRMS) to access exact masses at a parts-per-million (ppm, 10^{-6}) mass unit accuracy, coupled with high-throughput data handling. Highly adapted lipid extraction protocols are employed with direct infusion, without chromatographic separation. Direct infusion allows exact quantification since a constant flow of lipid sample of known concentration is analysed, with the use of appropriate internal standards.[111,112]

To investiage biomolecule localisation and function, small chemical reporter groups, such as fluorophores for fluorescence imaging, or affinity tags like biotin for purification, can be incorporated *in vitro*, before their incorporation and study in cells or organisms. For *in vitro*

tagging, selective or *orthogonal* chemical conjugations are required for specific tagging in a non-perturbing site on the biomolecule. For small biomolecules such as lipids and carbohydrates, where even the smallest fluorophores can perturb lipid function,[57] the reporter group can be added *in cellulo* by means of a minute, latently reactive *tag* or *labelling* group. After cellular incorporation and biological function, the *tag* can be specifically conjugated to a *reporter* group (e.g. fluorophore or biotin) for visualisation or isolation (Figure 1.6.1).[113] Such chemical conjugation (or scission) reactions must occur specifically in a complex biological environment, and are termed *bioorthogonal*. The bioorthogonal reactant partners must be specifically, mutually reactive whilst being inert to their environment, and as small as possible. Since applications are often in live cell culture, the reaction must occur at a similar timescale to standard cellular processes.[114]

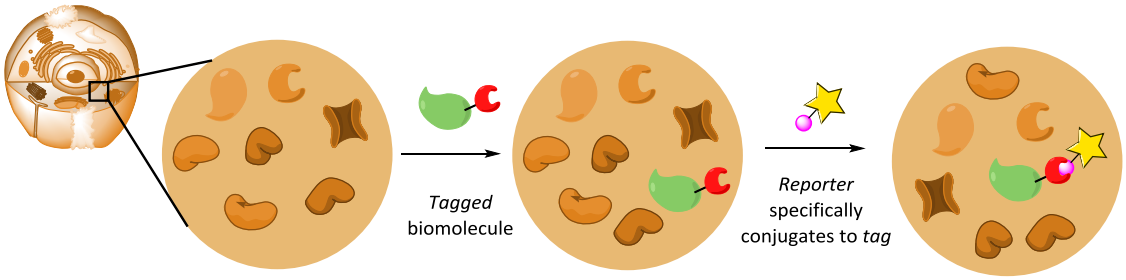

Figure 1.6.1: Tagging a biomolecule and analysing its cellular localisation or metabolism products using a reporter molecule, often fluorophore or biotin affinity tag.

Early specific, orthogonal chemical reactions were used to chemically modify proteins *in vitro*. Reactions include disulfide exchange or maleimides for cysteine residues, and *N*-hydroxysuccinimides and iso(thio)cyanates for lysine residues (Figure 1.6.2a).[115] However, for complete regiospecificity, these reactions require that only one active thiol or amine is present in the conjugation environment. Ketones and aldehydes can be condensed with aminooxy and hydrazide forming oxime or hydrazine conjugations respectively (Figure 1.6.2b). These were among the first specific chemical conjugations applied to the surface of whole, live cells. Bertozzi *et al.* described the *metabolic labelling* of cell surface glycans using a ketone-labelled analogue of N-acetylmannosamine (ManNAc), N-levulinoylmannosamine (ManLev, Figure 1.6.3), which is metabolised into sialic acid-containing glycolipids and glycoproteins and presented at the cell surface, where they selectively conjugated with a hydrazide-biotin reporter.[116–118] These aminooxy and hydrazide conjugations require high

concentrations of reactants, and fall prey to high cross-reactivity with natural ketones and aldehydes.

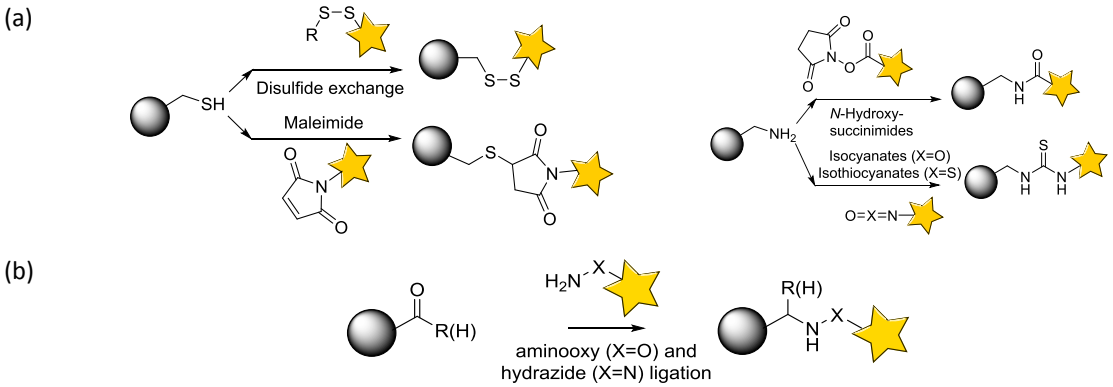

Figure 1.6.2: (Bio)orthogonal chemical conjugations. (a) Disulfide exchange and maleimide conjugations for cysteine residues and *N*-hydroxysuccinimides and iso(thio)cyanate and iso(thio)cyanates for lysine residues. (b) Oxime/hydrazine with aldehyde/ketones.

The Staudinger ligation uses azide- and arylphosphine-functionalised partners and has been applied to bioorthogonal live cell labelling[119–121] and prodrug release,[122] since bonds are formed and broken in the reaction mechanism (Figure 1.6.3a). Azides are ideally small, non-perturbing and stable in cells and organisms.[123] For example, an azide group is present in the well-known anti-AIDS drug, 3'-azidothymidine (AZT).[124] The bioorthogonal Staudinger ligation derives from the classic reduction of azides with phosphines,[125] using a functionalised aromatic phosphine which traps the aza-ylide intermediate, forming a stable conjugation. The traceless Staudinger reaction (Figure 1.6.3b) leaves a perfectly small amide bond after the conjugation and intramolecular elimination of the arylphosphine. These variants are less applied in live cell studies due to poor kinetics, selectivity and solubility.[126]

Saxon and Bertozzi showed live cell *metabolic labelling* with an azide-labelled analogue of ManNAc, Ac_4ManNAz (Figure 1.6.3c).[119,127] The hydrophobic, peracetylated glycan is used to increase cell permeability, and is deacetylated by non-specific cytosolic esterases to ManNAz in the cell.[128] ManNAz then follows the endogenous anabolic sialic acid pathway to SiaNAz, and is incorporated into sialic acid-containing proteins and glycolipids.[129] The azide-functionalised sialosides were then conjugated specifically with an arylphosphine-biotin for quantification. Unfortunately, Staudinger ligations suffer from impractically slow kinetics ($k_2 \approx 3\times10^{-3}\ M^{-1}s^{-1}$), require high concentrations (>250 µM triarylphosphine),[127] and phosphines are prone to enzymatic or atmospheric oxidation.

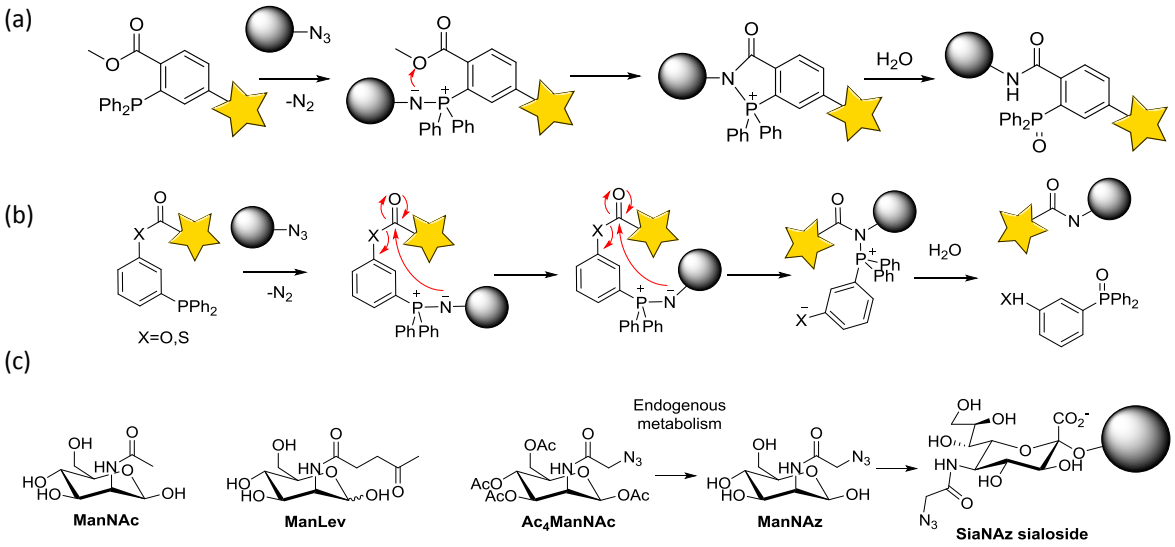

Figure 1.6.3: Bioorthogonal chemical conjugations (a) Staudinger and (b) traceless Staudinger ligations. (c) ManNAc, Natural sialic acid precursor. Synthetic analogues ManLev and Ac_4ManNAc, used for metabolic labelling of sialic acid-containing glycoproteins and glycolipids.[117,130]

The term *click* chemistry was coined to describe reactions which are fast, specific, high yielding, occur in mild (aqueous, aerobic, biological) conditions, and produce inert or no byproducts.[131] Reactions coming close to meeting these criteria are now so popular they are used by chemists and non-chemists, in common, commercial laboratory kits. The heat-driven 1,3-cycloaddition between alkyne and azide was described by Huisgen in the the 1960s.[132] The copper(I)-catalysed azide-alkyne 1,3-dipolar cycloaddition (CuAAC) variation (Figure 1.6.4a), first described in 2002,[133,134] is still an extremely useful orthogonal conjugation in organic synthesis,[132,135] allowing complex molecules to be coupled specifically, in the presence of diverse functional groups, without need for protecting groups. CuAAC reactions came to dominate *click* chemistry for its extremely fast reaction times and specificity (10-200 $M^{-1}s^{-1}$ in the presence of 20–500 mM Cu(I)). Sadly, the copper, solubilised in a ligand complex, is abundantly taken up into cells and causes rapid toxicity by the formation of reactive oxygen species (ROS).[136] This is augmented by ascorbate, the standard reductant used to form Cu(I) from Cu(II), which also promotes ROS formation.[136,137] Copper is also reported to chelate to amino acids, impeding protein structure and function.

To combat this, ligands have been developed promising to reduce toxicity whilst retaining copper catalysis and solubility (Figure 1.6.2b).[138] These have been successfully applied in cell surface labelling.[139] For example, Cairo *et al*. showed that they could induce cell adhesion-like properties in alkyne-lipid labelled Jurkat (a human T lymphocyte line) cells when

clicked with azide-coated beads and L-histidine ligand.[140] Besanceney-Webley *et al.* developed BTTAA (Figure 1.6.4b), which they showed chelates copper to catalyse the cell surface *click* reaction with azide-labelled sialic acids (SiaNAz) in 3 minutes. This is fast enough that copper could be used without significant cell death in Jurkat and HEK cells. They cite the use of 30 µM Cu(I), [ligand]/[Cu]=6:1, where 30 µM Cu(I) and no ligand shows no significant cell death, and yet 50 µM killed 90% of cells in the same time.[141]

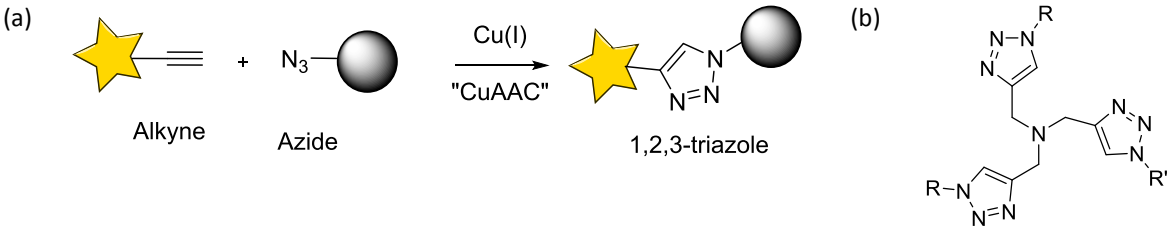

Figure 1.6.4: (a) Copper-catalysed azide-alkyne cycloaddition (CuAAC). (b) Cu-chelating ligands for CuAAC; TBTA: R, R'=CH_2Ph; THPTA: R, R'=$(CH_2)_3OH$; BTTAA: R=^tBu; R'=CH_2CO_2H.

Cyclooctynes can react with azides without copper catalysis (Figure 1.6.5a). They have higher reactivity due to their strained cyclic structure, in a reaction termed the strain-promoted azide-alkyne cycloaddition (SPAAC).[113] In 1961, Witting and Krebs reported that a stable cyclooctyne reacted "like an explosion" with phenylazide, but it was not until 2004 that Agard, Prescher and Bertozzi synthesised OCT (Figure 1.6.5b) and showed its specific reaction on cells labelled with SiaNAz, without copper catalysis.[142]

The standard 1,3-dipolar SPAAC occurs between the $LUMO_{\pi\,,\,alkyne}$-$HOMO_{\pi,azide}$ (Figure 1.6.5c).[143] The electronic properties of the alkyne have been fine-tuned by adding electron-withdrawing groups (EWGs, Figure 1.6.5c) to lower LUMO energy of the electron-rich alkyne.[144,145] Difluorocyclooctyne (DIFO, Figure 1.6.5b) bares two small, biologically inert fluorine atoms, with an inductive electron-withdrawing effect. Monofluorocyclooctyne (MFCO, Figure 1.6.5b) is less reactive – more stable – with one inductive EWG, fluorine, and a carbonyl or amide, slightly poorer, mesomeric EWGs. Dibenzocyclooctyne (DIBO) bares planar aromatic groups which increase reactivity by increasing ring strain.[143] Unfortunately, π-conjugated cyclooctynes can undergo side reactions with endogenous nucleophiles as Michael acceptors (electrophile prone to 1,4-addition),[114,142] as well as reducing DIBO-conjugates aqueous solubility. Bicyclononyne (BCN), alternatively, has greater reactivity due to ring strain caused by a fused cyclopropane ring. Many reported studies display impressive application of specific labelling in cells and *in vivo* with cyclooctynes (Introduction 1.7).[146]

When choosing a *click* reagent, one must consider that increasing reactivity is often detrimental to specificity and stability.

(a)

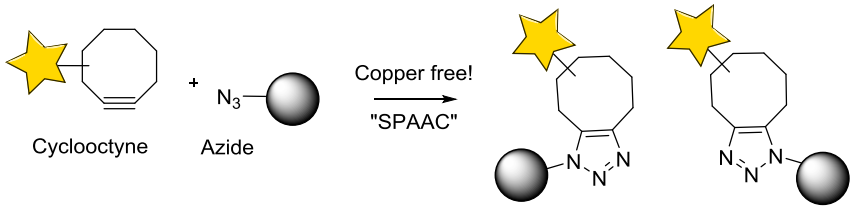

(b)

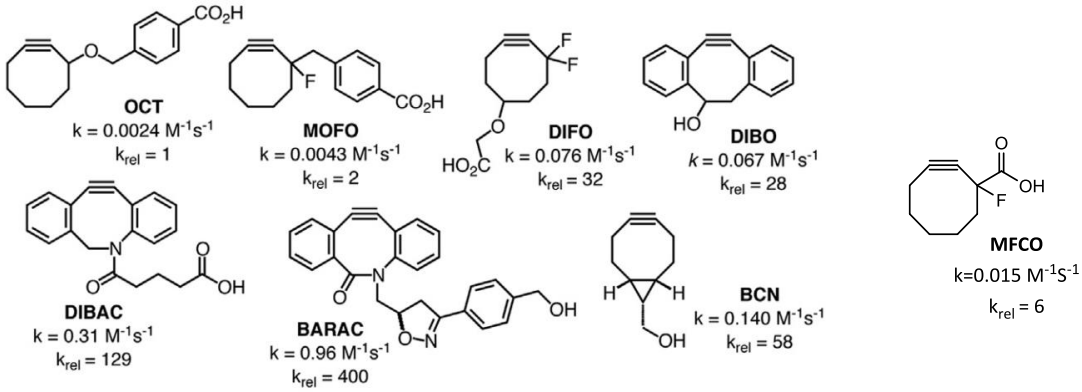

(c)

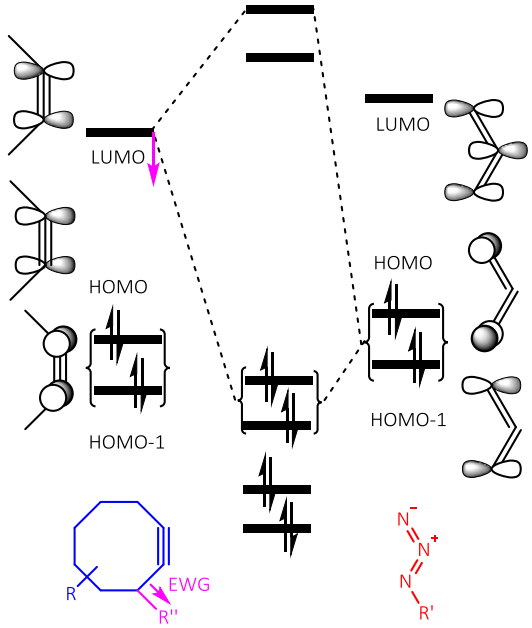

Figure 1.6.5: (a) SPAAC *click* reactions. (b) Derivatised cyclooctynes, rate constants for benzyl azides, relative to parent compound OCT.[147,148] (c) SPAAC forming triazole. Orbital diagram of bonding interactions between cyclooctyne LUMO and azide HOMO, activated by adding electron-withdrawing groups (EWG) to the cyclooctyne.[144]

Chemical evolution of *click* reagents has led to studies on nitrones, nitrile oxides and sydnones, which react quicker than azides with cyclooctynes (Figure 1.6.6 a-c). For example, strain-promoted alkyne-nitrone cycloaddition (SPANC) reactions demonstrate rate constants up to 60 $M^{-1}s^{-1}$.[147] However, their syntheses are not commonly mastered and their use as tags in biomolecules can prove more cumbersome than the classic azide. Nitrones were stable enough to efficiently label large proteins in live cells without degradation.[149] However,

nitrone-labelled glycans fared less well, as the nitrone modification was not accepted into the biosynthetic pathway.[150] Inverse electron demand Diels-Alder (IEDDA, Figure 1.6.6d, e) conjugations come out ahead as the quickest bioorthogonal reactions, but leave a remarkably large scar in the structures of modified biomolecules.

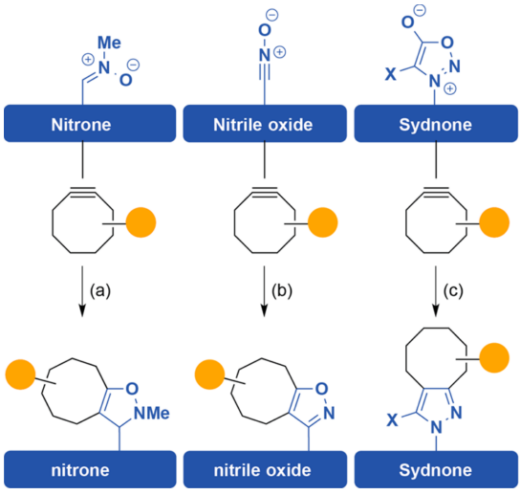

(d)

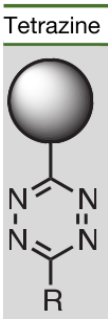

Figure 1.6.6: (a-c) 1,3 dipoles which react with cyclooctynes via SPAAC. Rate constants with BCN: (a) k<60 $M^{-1}s^{-1}$ (b) k=0.054 $M^{-1}s^{-1}$. (c) k=1.6 $M^{-1}s^{-1}$.[147,151] Tetrazines (d) react specifically with strained alkenes (dienophile, e) via the inverse-electron demand Diels-Alder Reactions (IEDDA).[147]

(e)

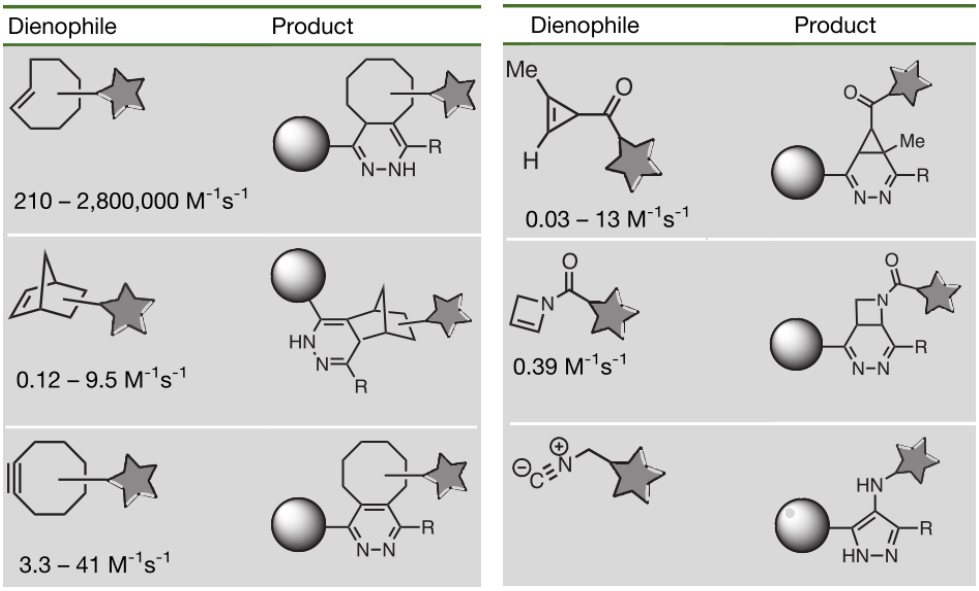

1.7 Metabolic labelling of glycans and lipids

Click chemistry's application in metabolic labelling has had great influence on several advanced biological techniques. Genetic code expansion, using synthetically evolved derivatives of tRNA synthetases, now allows site-specific genetic encoding of *clickable* amino acids.[152] With *click* chemistry, radiolabels can be added to proteins regioselectively under mild conditions, for techniques such as positron emission tomography (PET) and radiotherapy, and which show potential in animal models.[153] This project has been inspired and guided by recent innovations in *metabolic labelling* to study lipid and glycan interactions, briefly outlined in this chapter.

Azide-modified glycans such as Ac_4ManNAz (Figure 1.6.3),[119] an analogue of the sialic acid precursor, ManNAc, are popular substrates for labelling the cell surface, and have been applied to many high-tech labelling techniques. Laughlin *et al.* demonstrated the use of Ac_4GalNAz for spatiotemporal labelling of zebrafish embryo morphology (Figure 1.7.1), displaying early (red) and late (green) gestational post-translational glycosylation, using a fluorophore functionalised with difluorocyclooctyne (DIFO, Figure 1.6.5b). Wang *et al.* showed that Ac_3ManNAz could be coupled with a tumour-selective self-immolative linker in the anomeric (C1) position to specifically label tumour tissue in mice.[154]

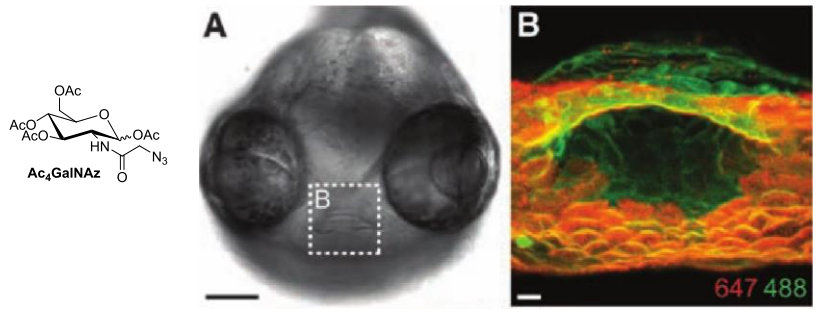

Figure 1.7.1: Zebrafish embryo labeled with Ac_4GalNAc. DIFO-647 (red) *click* 60 hours post-fertilisation (hpf), then DIFO-488 *click* 62 hpf after an additional 1h pulse of Ac_4GalNAc labelling. Scale bars 100 µm (A), 10 µm (B).

Click chemistry has been used to probe lipid localisation and metabolism in a myriad of substrates. Jao *et al.* showed that incorporating *clickable* propargylcholine (Figure 1.7.2a),[155] and later the azide analogue (Figure 1.7.2b)[156] at high concentrations was non-toxic, and could give dose-dependent labelling up to 44% phosphatidylcholine (PC), transferring to sphingomyelin labelling (SM, <15%) at later time points, with a similar profile to natural choline-containing lipids (Figure 1.7.2c). Labelling fixed cells with an azide-fluorophore and copper catalysis labelled all cellular membranes (Figure 1.7.2c).

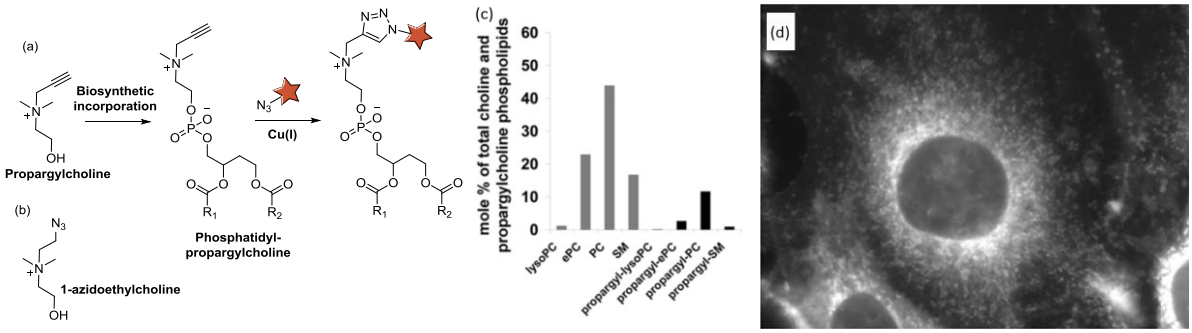

Figure 1.7.2: *Clickable* choline analogues, (a) propargylcholine[155] and (b) 1-azidoethylcholine,[156] are metabolised into phosphatidylcholine (PC), ether phospholipids (ePC) and sphingomyelin (SM). (c) Propargylcholine treatment (100 µM) shows similar profile of choline-containing lipids by ESI-MS/MS analysis. (d) Alkyne-lipids undergo CuAAC *click* reaction with alkyne-fluorophore (fluorescence microscopy image).

Lipids with terminal ω-alkyne or ω-azide groups (Figure 1.7.3a,b) have been widely used to study fatty acylated-protein localisation.[157] Hang *et al.* first investigated the metabolism of *clickable* fatty acids in proteins by Western blotting,[158] whereas Thiele *et al.* developed a lipid extraction technique which would permit the analysis of *clickable* lipid metabolism by thin layer chromatography (TLC).[159,160] *Clickable* ω-alkyne-oleoyl-lysophosphatidic acid, ω-alkynesphinganine and palmitoyl-lyso-propargyl-phosphatidyl-choline (Figure 1.7.3c-e) displayed canonical metabolism in cells.[161] Enzyme affinity (K_m) measurements of such substrates showed no significant difference in binding affinities with native biosynthesis enzymes compared with natural lipids.[161] Localisation of *clickable* lipids, *clicked* to a fluorophore with copper-catalysed or copper-free[162,163] protocols, seem to reliably demonstrate, with negative controls, that fluorescent labelling is specific to the lipid analogue.[164] Most often the *clicked* lipid is lodged non-specifically in plasma membrane and intracellular membranes, as is conceptualised for natural lipids. One less subtle modification in a ceramide analogue with trans-cyclooctene in the lipid tail (Figure 1.7.3f) provides the lipid strong Golgi specificity.[165]

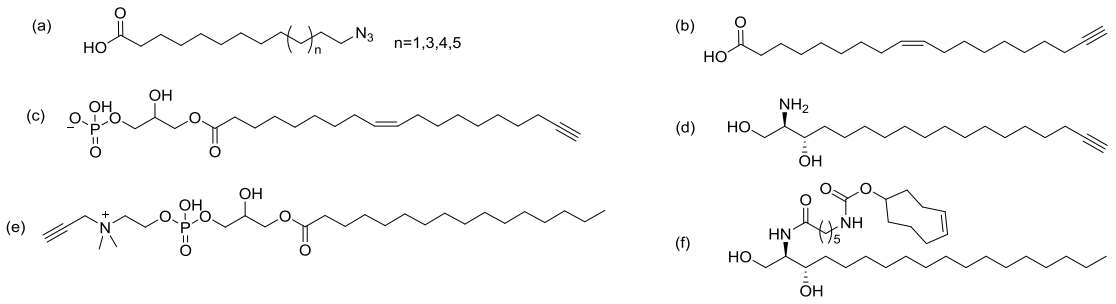

Figure 1.7.3: *Clickable* lipids. (a,b) Fatty acids,[158,159] (c) alkyne-oleoyl-lysophosphatidic acid (d) ω-alkynesphinganine (e) palmitoyl-lyso-propargyl-phosphatidyl-choline.[161] (f) Golgi-specific transcyclooctene ceramide.[165]

Clickable glucosylceramide (GlcCer) with short ω-alkyne C8 acyl chain gave intracellular membrane staining on alkyne-fluorophore *click* reaction (**1**, Figure 1.7.4a). This localisation is in agreement with Pedrosa *et al*., who used a ω-azide C8 acyl chain on GlcCer.[61] Inversely, an azide in the glycan head group or C4 acyl chain (**2**, Figure 1.7.4b) gave PM labelling. Long C14 GlcCer (**3**) and lactosylceramide (LacCer) analogues with an azide in the 6''-OH position and short chain C4 or C8 acyl chain (**47**, **48**, Figure 1.7.4) stained the PM, and required fusogenic liposomes to be incorporated.[62]

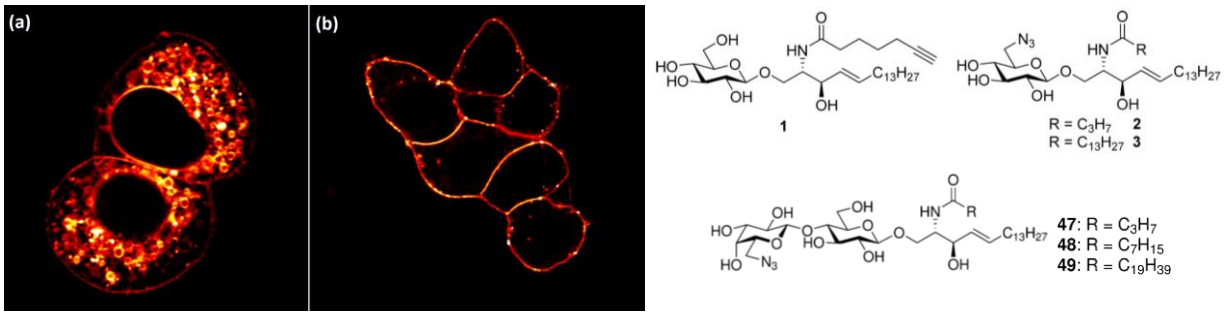

Figure 1.7.4: *Clickable* glycolipids localise in intracellular cellular membranes (a, analogue **1**) and PM (b, analogue **2**). Short chain LacCer analogues **47** and **48** localised to the PM. Analogues **3** and **49** were incorporated using fusogenic liposomes, localising in the PM.

Discernibly from these examples and others, visualising modified lipids can indicate properties of that lipid with a large margin of error. So what can we learn from them about the natural system? Isolating lipid-protein interactions is of great interest, but non-covalent affinities are too weak to be used with standard immunoprecipitation techniques (Introduction 1.3-1.4). *Photoactivable crosslinkers* have been incorporated into lipids to study their interactions.[166] This strategy, often known as affinity-based probes, is commonly used to identify protein targets of small biomolecules in the field of drug discovery.[167] The most

common groups are benzophenone, diazirine and aryl azide (Figure 1.7.5a-c). These small chemical groups are activated by a flash of UV light, forming a reactive, radical species which bonds covalently to any molecule (often heteroatoms) close to the tagged molecule of interest. Their standard usage involves cellular incorporation of the photoactivatable small molecule, UV activation, cell lysis, and visualisation or isolation of the lipid-protein partners by *clicking* to a fluorophore or solid support respectively (Figure 1.7.5e). The use of photoactivatable crosslinking groups has led to the identification of interaction partners of plant glycoglycerolipids,[168] phospholipids,[169] sphingosine,[170] cholesterol.[171] A photoactivatable, *clickable* GlcCer analogue was recently described, but no new interaction partners have yet been reported.[172]

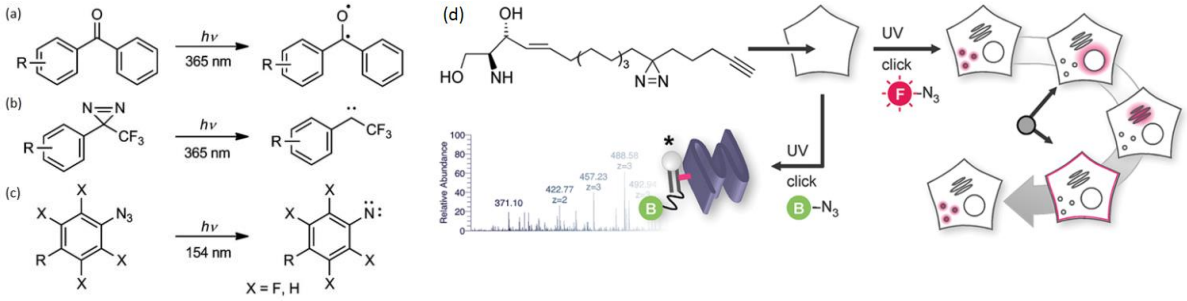

Figure 1.7.5: Photocrosslinkable groups, benzophenone (a), 3-phenyl-3-(trifluoromethyl)diazirine (b), and aryl azide (c) with their reactive radical forms.[167] (d) Confirmed photoactivatable sphingosine probe; protocol involves live cell incubation, UV light activation, extraction and *click* with a fluorophore for visualisation, or biotin-streptavidin beads for purification and mass spectrometry characterisation.[170]

1.8 Project aims

Biosynthesis of GSLs (Figure 1.4.4) is stepwise and likely under equilibrium, and one gene does not code for one GSL but several. This makes genetic manipulation of a single GSL impossible without offsetting the expression of other GSLs. Current methods to supplement cells with pure long chain GSL species, a process here termed cellular reconstitution, are extremely inefficient (Introduction 1.3).[60–62] The study of GSL function is thus challenging and new molecular tools are highly desirable. We aim to synthesise biomolecule analogues able

to reconstitute the biological and mechanochemical properties of GSLs. Tools must be reconstituted in an easy protocol, whilst retaining biological function.

We aim to develop a biorthogonal, *clickable* kit of GSL precursors from proof-of-concept studies on GSL globotriaosylceramide (Gb3-Cer) and the Shiga toxin (STxB). To reconstitute a functional Gb3-Cer analogue, we attempt to commandeer the native GSL biosynthesis and traffic; supplementing cells with a *clickable* 1-azidosphingosine (AzSph, Figure 1.8.1), which is natively metabolised to 1-azidoceramide (AzCer) and presented at the plasma membrane (PM), to which we *click* the functionalised oligosaccharide head group of choice by a highly selective, copper-free *bioorthogonal click* reaction.

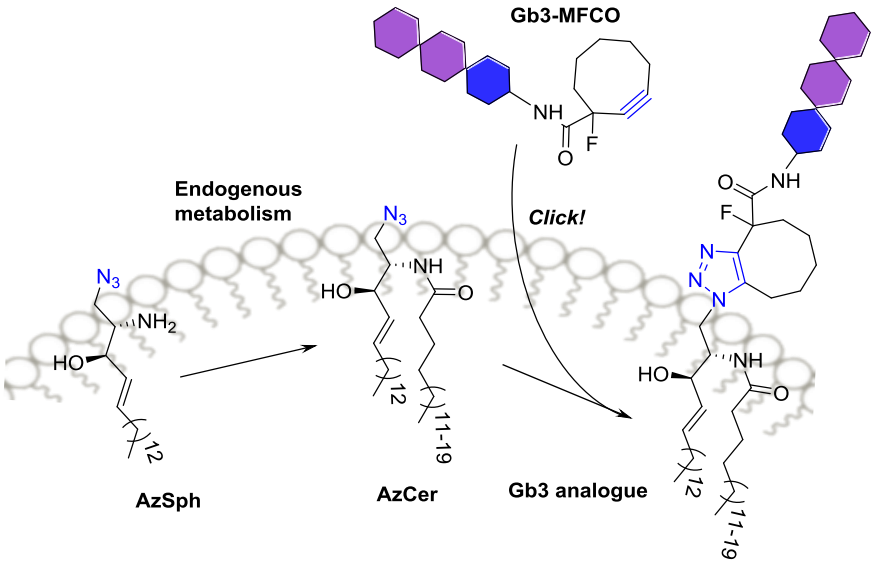

Figure 1.8.1: GSL *click* reconstitution. Sphingolipid precursor, 1-azidosphingosine (AzSph) is natively metabolised to 1-azidoceramide (AzCer), ideally presented at the PM to be *clicked* with the prepared *clickable* oligosaccharide (Gb3-MFCO) to form the final Gb3 analogue. (Lipid membrane not to scale)

The maintaining biological activity, by using the smallest least perturbing chemical groups possible is constantly balanced with having a fast and specific *click* reaction (Figure 1.8.2a). We base our design on previous studies showing that clustering of STxB was greatly inhibited with long, flexible linkers, but a small linker in the central region (n=1, 10Å) permitted native function (Figure 1.8.2b, Introduction 1.3).[173] We design our final *click* analogue with dimensions of this size or smaller. Previously a GM1-phospholipid analogue retained its native function in binding and trafficking with the cholera toxin and simian virus 40.[29] We consider the use of a Gb3-phospholipid, proposed to be soluble enough to permit efficient cellular reconstitution (Discussion 3.1).

If these neo-glycolipids are functional and reconstituted with a feasible yield, this strategy could potentially tolerate further chemical modifications, allowing further probing of native GSL interactions. One long-term goal is to reconstitute photoactivatable, traceable GSLs, for example containing a diazirine group (Figure 1.8.2c), to identify GSL interaction partners (cf. Perspectives).

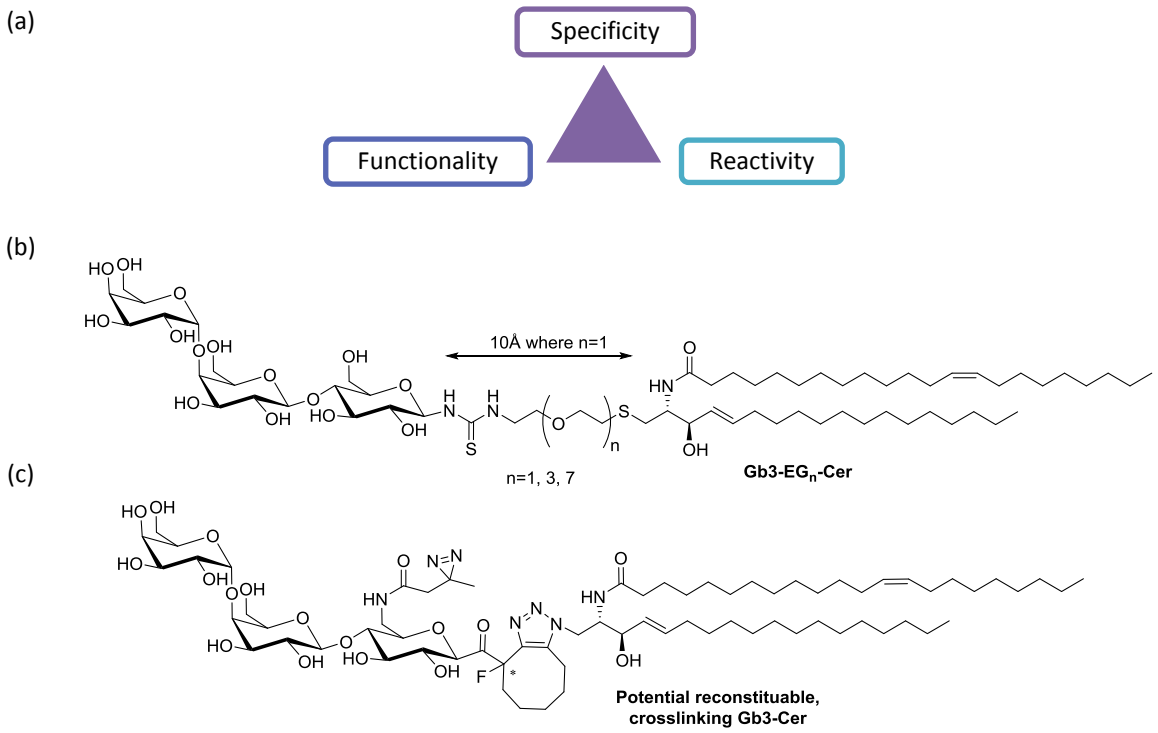

Figure 1.8.2: (a) Balance between reactivity and specificity of *click* partners, with the biological functionality of final *clicked* product. (b) Gb3-EG_n-Cer analogues able to bind Shiga toxin in liposome models, whilst only Gb3-EG_1-Cer is able to induce membrane bending.[24] (c) Potential photoactivatable and reconstituable Gb3.

2 RESULTS

2.1 Synthesis of biomolecule analogues

2.1.1 Reconstitutable globotriose phospholipid

We aim to synthesise a Gb3 with retained native function that can be reintroduced into cells in culture. Gb3-phospholipid analogues, or function-spacer-lipid (FSL) constructs, have shown to retain similar biological activity as the natural Gb3-Cer with known binding lectins: Shiga toxin (verotoxin1) and HIV-1.[29,174,175] Crucially, phospholipids (PLs) are more efficiently incorporated into cells in culture than GSLs (Introduction 1.3).[60,62] Hence, we proposed that a Gb3-PL would be a valuable tool. The spacer between glycan functional head and lipid tail of the FSL must be biostable, meaning it must not be recognised and digested by cellular clearance machinery. We require the spacer between the Gb3 head group and phospholipid tail to be short to retain membrane bending properties (Introduction 1.3).[24] This contributes to the originality of this endeavour, since only long Gb3-phospholipids have been synthesised in the literature.[29,174,175]

Synthetic routes to install isothiocyanate and azide functions at the anomeric position of glycans are well documented.[176] Isothiocyanates conjugate specifically with amines to form a thiourea (Scheme 2.1.1.1). The classic bioorthogonal copper-catalysed azide-alkyne cycloaddition (CuAAC, Introduction 1.6) forms a triazole. Both thiourea and triazole are stable in cells.

Our project is applied to the Gb3 triose, synthesised in a four-step synthesis (Section 2.1.3). We began testing syntheses on a lactose model for matters of cost and scale. Lactose (Scheme 2.1.1.2) was peracetylated with acetic anhydride in pyridine, to which the isothiourea (SCN) group was installed with the use of trimethylsilyl thiocyanic acid (TMSSCN) and $SnCl_4$ as a Lewis acid catalyst to form peracetate lactosyl isothiocyanate **1**.[24,177] This was conjugated to 1,2-dioleoyl-*sn*-glycero-3-phosphoethanolamine (DOPE, **15**) under basic conditions to form thiourea conjugate **2**. Despite an orthogonal deprotection of four acetyl groups being described,[178] this hydrazine-mediated deprotection was unfeasible in our hands without simultaneous breakdown of phospholipid ester groups, and conjugate **3** was not fully characterised. Alternatively, deprotection of isothiocyanate **1** was tested prior to conjugation

with DOPE, but isothiocyanate was unstable to methoxide conditions. It proved equally impossible to install the isothiocyanate group without hydroxyl protecting groups.

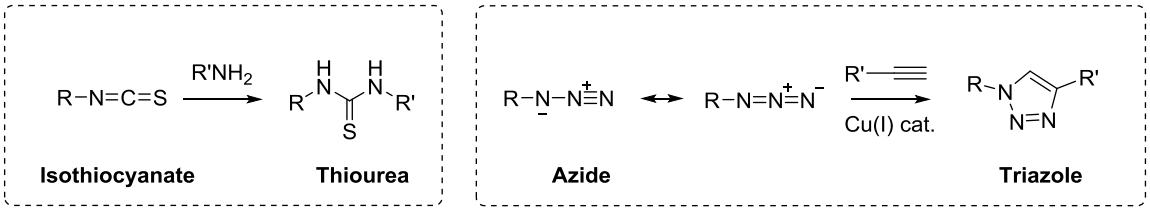

Scheme 2.1.1.1: Biostable chemical conjugations

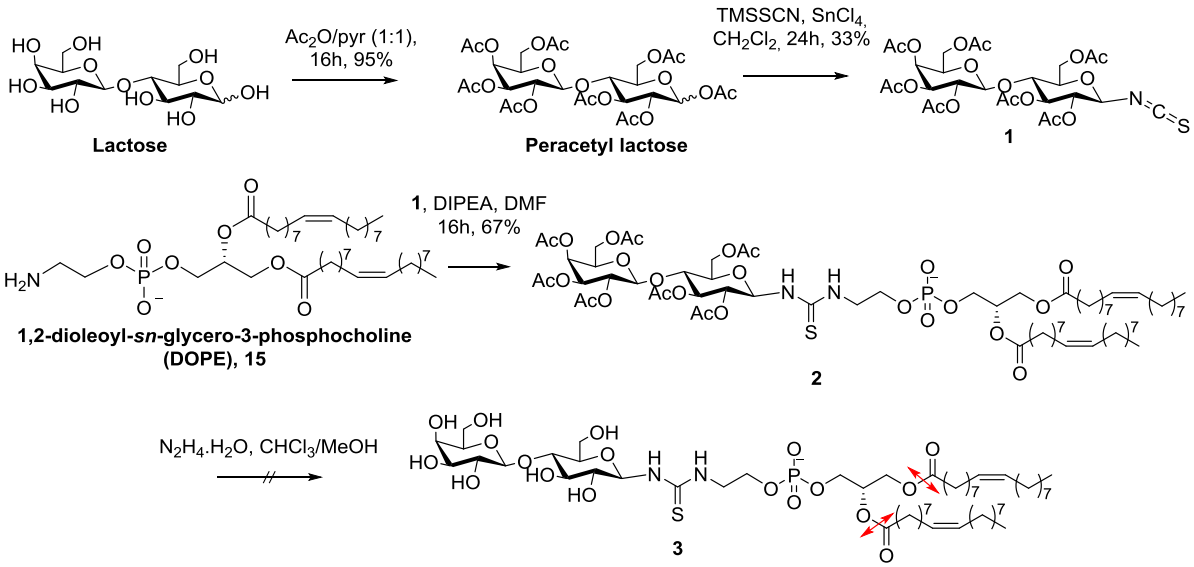

Scheme 2.1.1.2: Attempted synthesis of lactose-phospholipid analogue with isothiocyanate linkage.

We wanted to avoid the use of protecting groups on the glycan part, which are difficult to remove once the phosphodiester tail is installed. A highly orthogonal CuAAC *click* was thus envisaged. The synthesis is here proposed with 1-azidoglobotriose, **4** (Scheme 2.1.1.3) since the high yielding *click* reaction would not require optimisation with a lactose model. Azide-functionalised glycan **4** could *click* with alkyne-functionalised phospholipid **5** to form a Gb3-PL **6**.

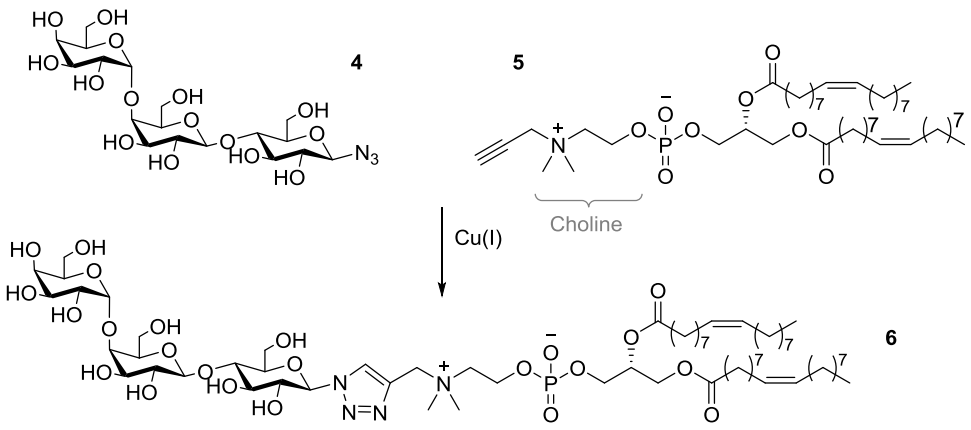

Scheme 2.1.1.3: Proposed globotriose-phospholipid formed from *click* conjugation.

Installation of an alkyne on the phospholipid to obtain **5** was described by Sandbhor *et al.*[179] 1-Octanol was first used in synthesis to model the desired glycerolipid starting material, reacting with 2-chloro-2-oxo-1,2,3-dioxaphospholane (COP, **7**, Scheme 2.1.1.4) in the presence of trimethylamine (Et_3N) to form the highly sensitive cyclic phosphate intermediate **8**, which is quickly reacted with *N*,*N*-dimethylpropargylamine and trimethylsilyl trifluoromethanesulfonate (TMSOTf) to form **9**. 1,2-dioleoyl-*sn*-glycerol, **10** formed the analogous glycerolipid cyclic intermediate **11**. This glycerolipid starting material is also unstable, undergoing fast 1,2-1,3 isomerisation. Ring-opening of **11** with *N*,*N*-dimethylpropargylamine to form functionalised phospholipid **5** was minor compared with formation of the hydrolysis side product **12**. Ring-opening of **11** with propargylamine, a primary amine with higher nucleophilicity, was equally poor yielding.

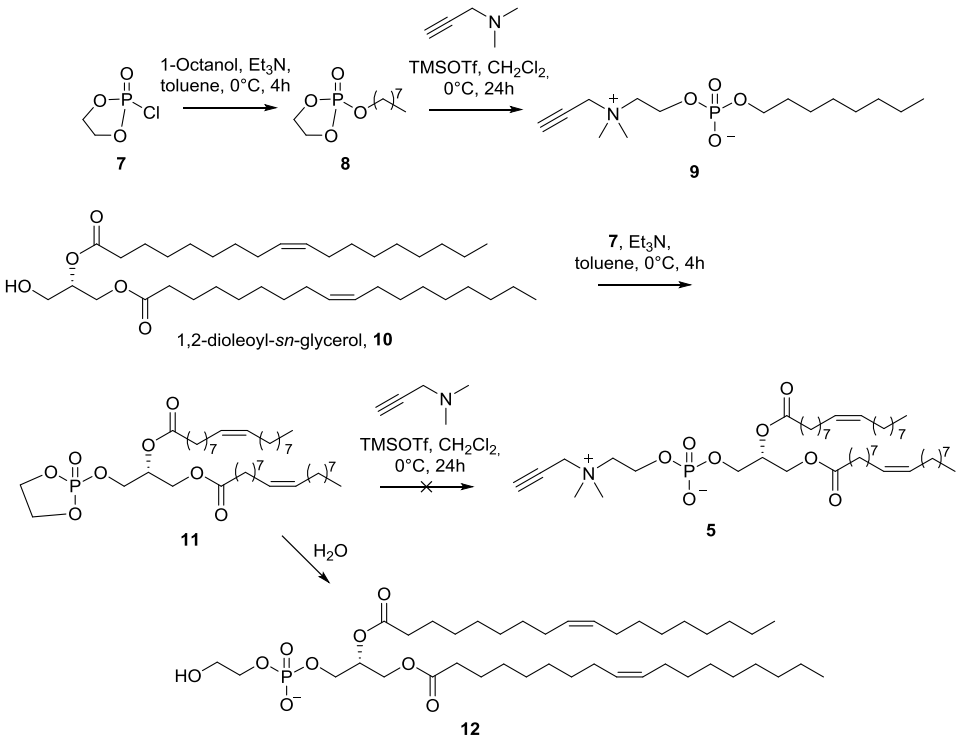

Scheme 2.1.1.4: Attempted synthesis of alkyne-functionalised phospholipid and major hydrolysis side product.

Installation of an azide with sodium azide in DMF via the cyclic intermediate **11** to form azidophopholipid **13**, confirmed by MS (Scheme 2.1.1.5). However, constant atmospheric hydrogenation of the unsaturated lipid tails became problematic during the lengthy purification from the ever-present hydrolysis product **12**, and full characterisation was not completed. This reaction was initially tested on 1-decaoctanol to obtain alkyne-phosphate **14**.

We trialled a peptidic conjugation of an alkyne-carboxlic acid, as described,[180] to form alkyne-phospholipid **16** from DOPE **15**. However, the small scale and poor acid reactivity of propiolic acid impeded isolation. In the face of the difficulties of purification of such unstable and amphiphilic phospholipid products, and the small scale nature of synthesis, the strategy was discontinued and we transferred our attention to a sphingolipid-based strategy.

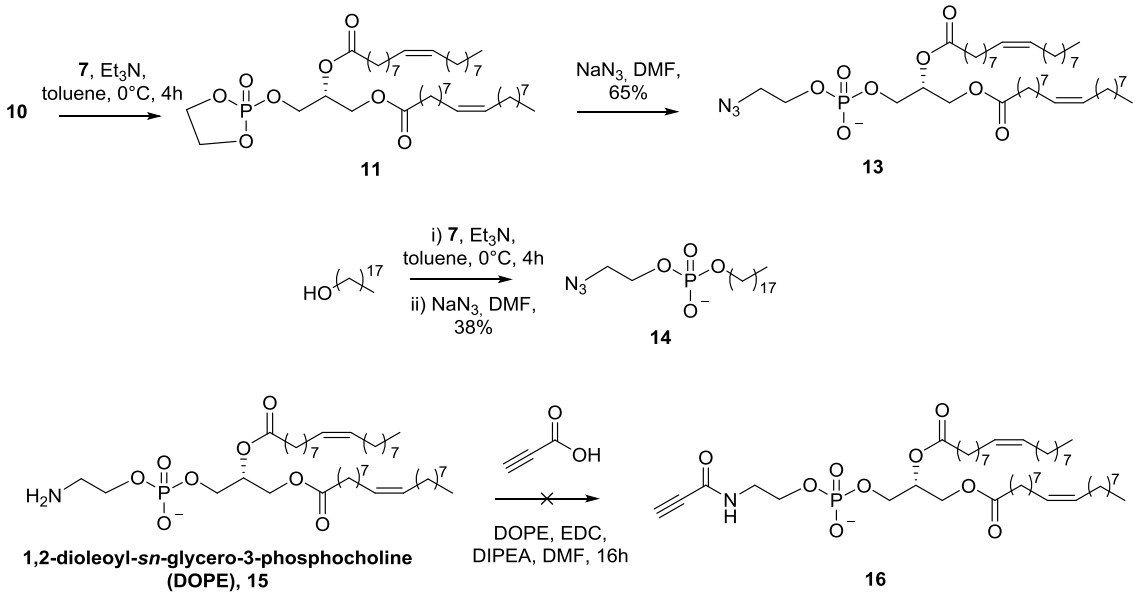

Scheme 2.1.1.5: Further syntheses of alkyne and azide phospholipids.

2.1.2 Clickable sphingolipid and globotriose

According to the scheme proposed (Figure 1.8.1, Introduction 1.8), we aim to reconstitute a Gb3 lipid analogue by first incorporating a *clickable* lipid precursor into cells, to be conjugated *in situ* with the mutually *clickable* glycan head group. *Clickable* 1-azidosphingosine (AzSph) and peracetyl Gb3-MFCO **47** had been previously synthesised in the laboratory. We optimised syntheses of AzSph and 1-azidoceramide (AzCer), fully characterising products and side products.

Synthesis of the AzSph **17** (Scheme 2.1.2.1) from commercial phytosphingosine began with a described 4-step synthesis to protected sphingosine **21**.[181,182] Briefly, phytosphingosine underwent N^2-azido protection to **18**, followed by selective O^1-silyl protection with TBDPSCl to form **19**. The vicinal diol is cyclised with $SOCl_2$ to a sulfoxide intermediate which is oxidised by $RuCl_3/NaIO_4$ to cyclic sulfate **20.**[183] Ring-opening with iodide from Bu_4NI, β-elimination by treatment with a strong base, and acid hydrolysis of the sulfate ester selectively forms the *E*-allylic alcohol at the C-4 position in **21**. This route is ideal for its selective stereo- and regiochemistry. From protected sphingosine **21,** O^3-hydroxyl is benzoylated to **22**, the azide at C-2 is reduced to amine **23** by PPh_3-mediated Staudinger reduction, which is immediately

protected with dichloroacetamide (N^2-$COCHCl_2$) to form **24**. This allowed deprotection of the O^1-silyl group in **25** and sequential activation of the C-1 position with mesylate to form **26**, then iodide to form **27**, for installation of the azide in **13**. Final deprotection with potassium hydroxide afforded AzSph **17** with structural analysis identical to the product previously described.[184]

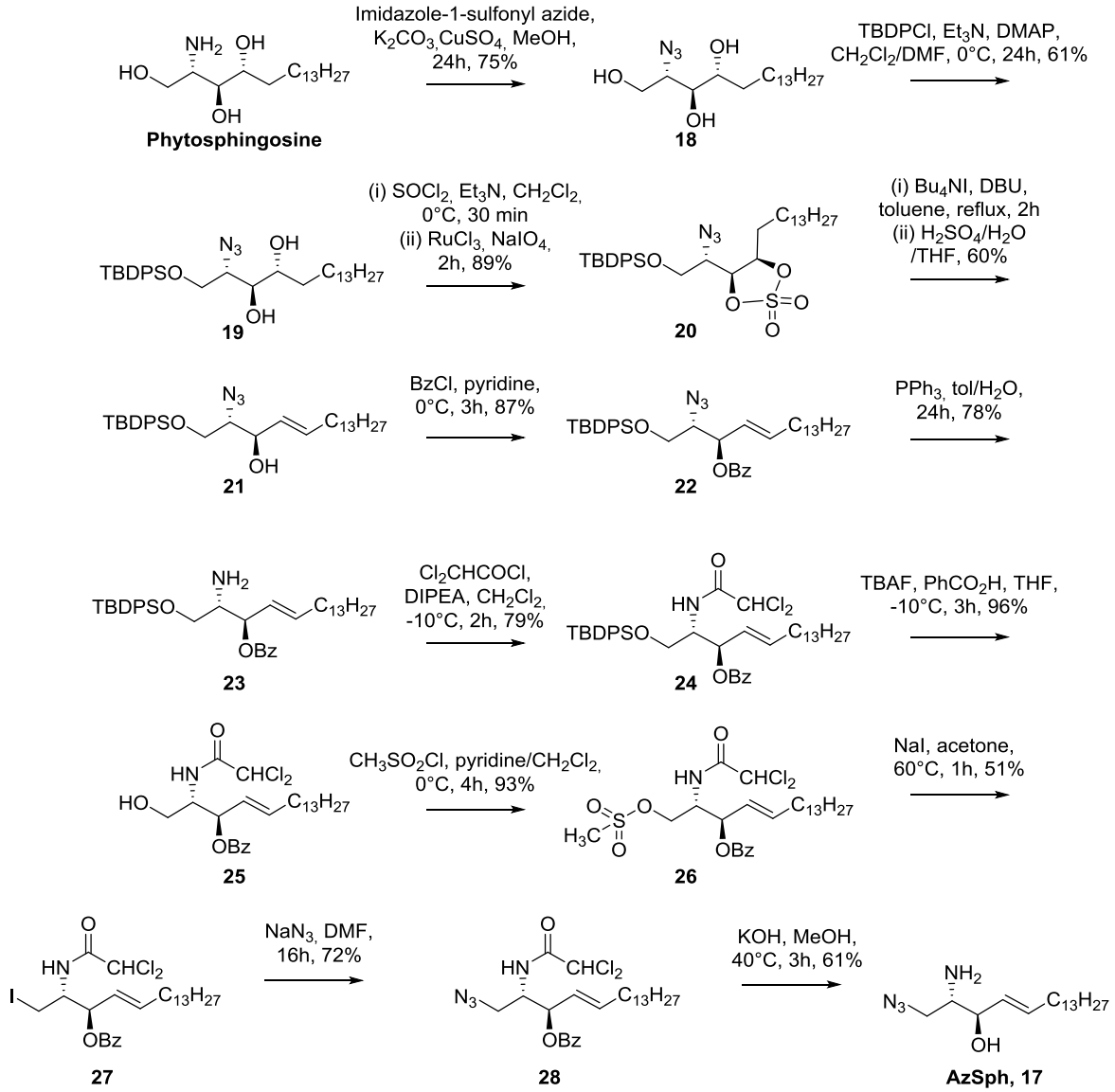

Scheme 2.1.2.1: 1-Azidosphingosine (AzSph) synthesis.

It is worth noting that attempts to form the azide directly from the mesylate **26** resulted in an oxazaline side product **28b** (Scheme 2.1.2.2). This oxazoline side product dominated when using a N^2-tert-butyloxycarbonyl (Boc) protecting group during azide formation. This obliged us to use the electron-withdrawing dichloroacetamide protecting group.[185]

From a previous synthesis in the laboratory, we characterised another cyclisation side product, a cyclic carbamate (oxazoline) **29**, formed from the iodide **27** with NaN_3 and ensuing deprotection with KOH (Scheme 2.1.2.2). This cyclic carbamate was unhelpfully similar to AzSph in R_f, molar mass, ^1H and ^{13}C NMR, and is likely formed from the hydrolysis of the dichlorooxazoline side product **28b**. We confirmed its structure by a weak staining in ninhydrin on TLC, a lack of azide bands in IR, and a strong C^{19}-$H^{1a,b}$ coupling in NOESY NMR.

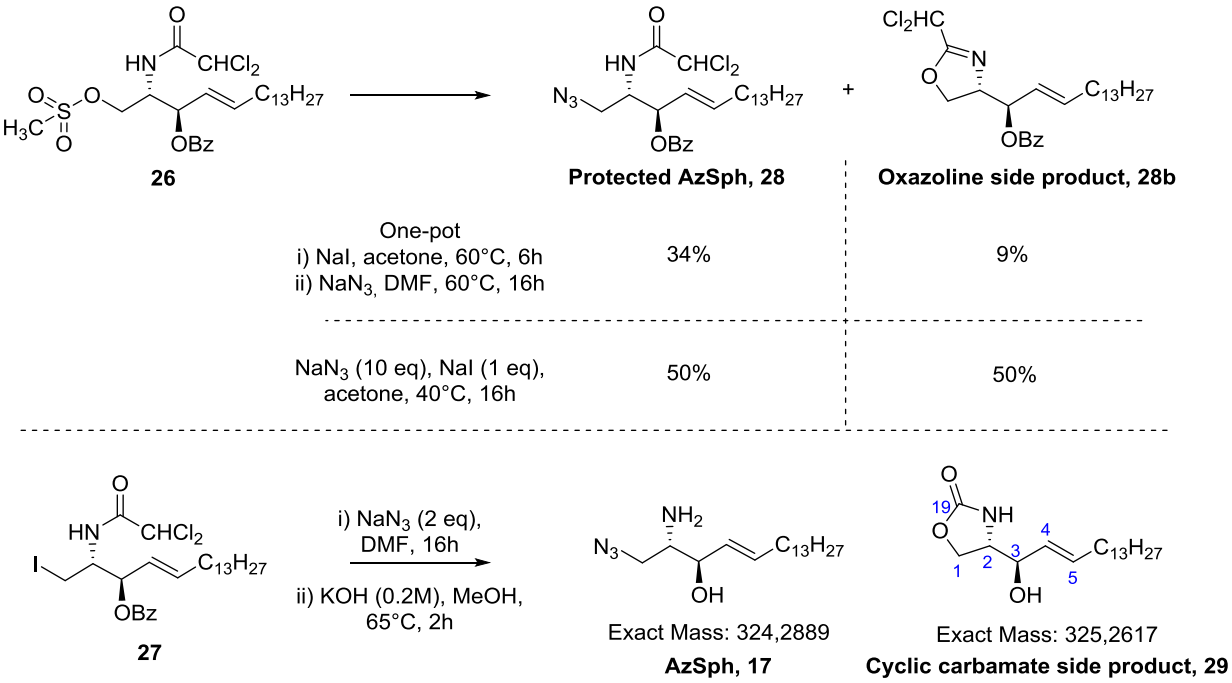

Scheme 2.1.2.2: Side reactions observed in synthesis of AzSph.

Chemical and enzymatic acylation of AzSph **17** with erucic acid (C22:1) to form AzCer **30** (Scheme 2.1.2.3) were trialled. Standard peptidic coupling conditions: EDC and pentafluorophenyl-trifluoroacetic acid (PFP-TFA) with DIPEA in CH_2Cl_2 and DMF respectively proved effective but lengthier to purify from hydrophobic EDC-urea and PFP side products. The most efficient acylation proved to be the enzymatic activity of SCDase, a commercial transacylation enzyme which can be tuned to acylate or deacylate sphingosine analogues based on the reaction buffer pH.[186,187] SCDase and 0.4% TritonX detergent are mixed in phosphate buffer with the sphingolipid and fatty acid, shaken in an Eppendorf overnight, lyophilised, and purified by silica column with no highly lipophilic impurities. AzCer **30** was used to form final *clicked* GSL analogues (Scheme 2.1.3.1) for model membrane testing, and as a mass spectrometry (MS) internal standard, permitting precise quantification of the

cellular metabolism of AzSph. The 12-step synthesis from phytosphingosine to AzCer **30** was completed with a 3% overall yield.

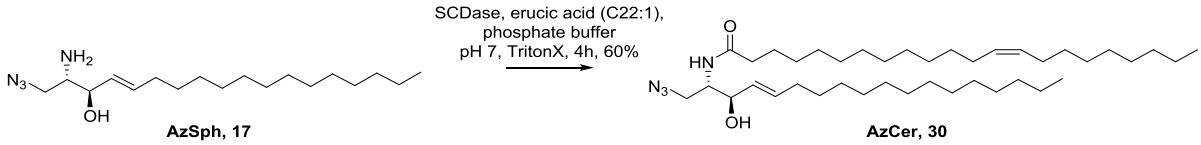

Scheme 2.1.2.3: 1-Azidoceramide (AzCer) chemoenzymatic synthesis.

We investigated the unusually slow Staudinger reduction (deprotection) of azide **22** to amine **23** (Scheme 2.1.2.4) via the stable phosphazene intermediate, (MH^+ 902, $\delta^{NMR}(H^2)$=3.54 ppm), which breaks down overnight to **23** ($\delta^{NMR}(H^2)$=3.16 ppm) and the NHBz side product. This phosphazene intermediate may be stabilised by the neighbouring *O*-benzoyl group, and is stable for over 24h in THF/H_2O. We simultaneously observe epimerisation at the C-2 position, which becomes separable after the following protection with dichloroacetyl chloride to form **24** (Scheme 2.1.2.1), confirmed by ^{1}H-NMR and MS.

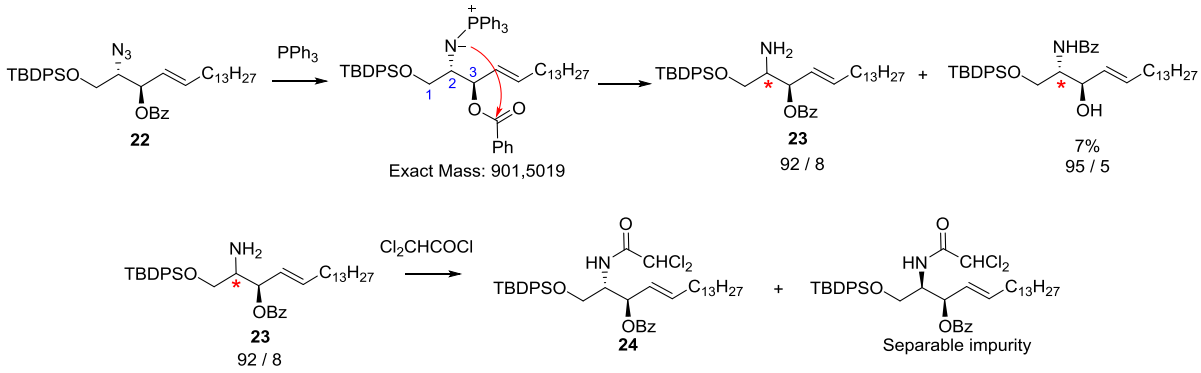

Scheme 2.1.2.4: Staudinger reduction (N^2-azide deprotection).

Other azide-functionalised sphingolipids and their cellular metabolism are also of interest. We expected their metabolism profile to be slightly different to that of AzSph due to the high specificity of ceramide synthase (CerS) enzymes (Discussion 3.5). From the biosynthesis described in the Introduction 1.4, **sphinganine** (Scheme 2.1.2.5) is metabolised to dihydroceramide by all ceramide synthase (CerS) enzymes 1-6, which install C16-24 acyl chains, whereas **sphingosine** is converted to ceramide by CerS5, which has a specificity for C16 chains. We wished to investigate the metabolism of another azidolipid closer in structure to sphinganine. The phytosphingosine analogue has no double bond, like in sphinganine.

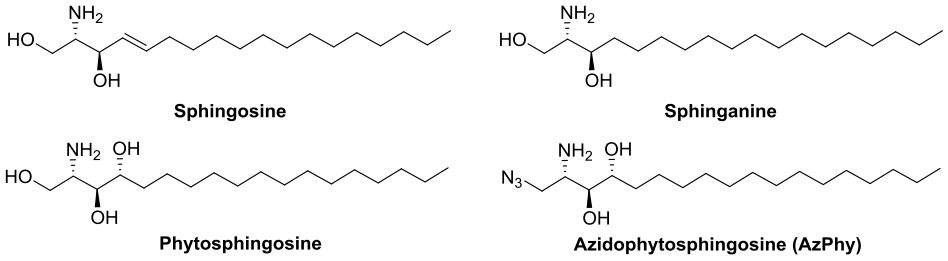

Scheme 2.1.2.5: Ceramide precursors: sphingosine (CerS5 substrate) and sphinganine (CerS1-6 substrate); plant-derived phytosphingosine, and its azide-functionalised analogue.

Phytosphingosine was converted into 1-azidophytosphingosine (AzPhy, **31**) in a three-step synthesis with a 13% overall yield (Scheme 2.1.2.6). The amine is initially protected with the dichloroacetamide protecting group to form **32**. Then, unlike the previous synthesis, the azide group was installed with a selective, Mitsunobu-like azidolysis, using NaN_3 and PPh_3/CBr_4, forming **33**, along with the cyclisation side product **34**.[188,189] N^2-dichloroacetamide group is then removed under standard basic conditions to yield 1-azidophytosphingosine (AzPhy, **31**). The cyclisation side product **34** presumably forms after the activation of the primary alcohol with PPh_3^+/Br^-, via an attack of the alcohol in the C-3 position (Scheme 2.1.2.7). These reaction conditions gave varying results of 1:1 (product/side) at a 50 mg scale, but 1:4 at a 200 mg scale. In contrast to AzSph, the synthesis of 1-azidophytosphingosine (AzPhy) was much shorter and thus lower-yielding steps were possible. To confirm the structure of side product **34**, the N^2-dichloroacetamide group was removed in standard deprotection conditions after separation and the resulting spectra corresponded to the described 2-epi-Jaspine B.[190]

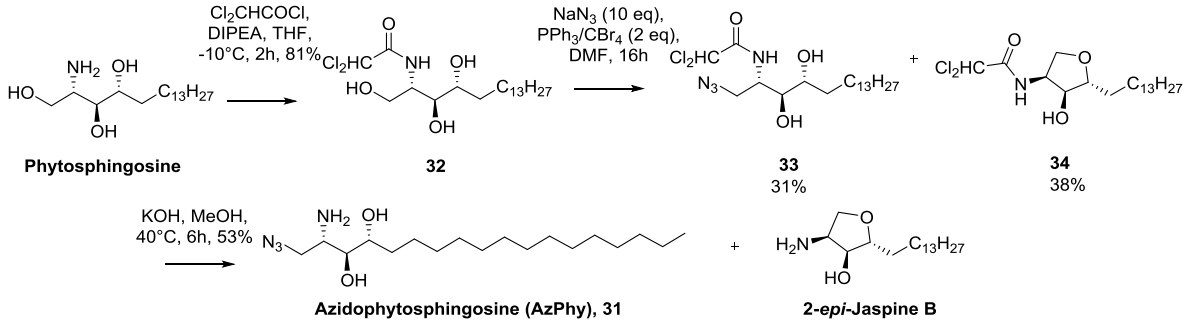

Scheme 2.1.2.6: Azidophytosphingosine synthesis with major cyclisation side product.

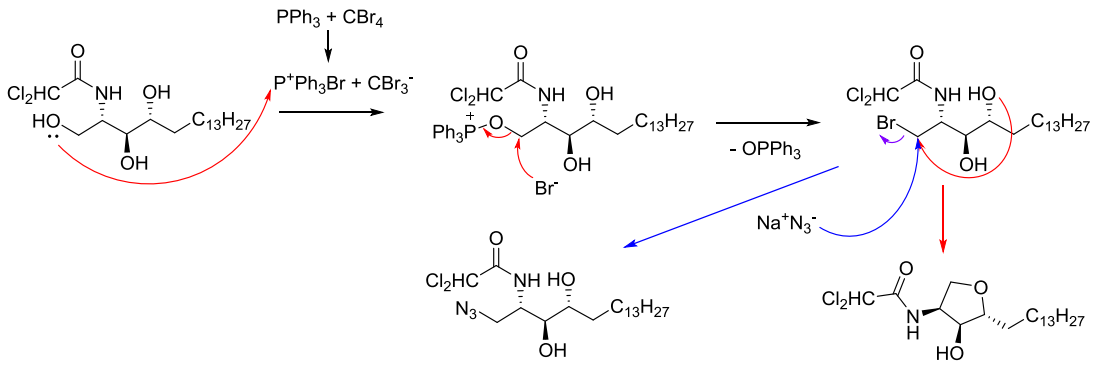

Scheme 2.1.2.7: Proposed selective azidolysis mechanism and cyclisation side reaction.

The *N*-dichloroacetamide protecting group was installed since cyclisation could hinder the synthesis in an analogous way (Scheme 2.1.2.8). An N^2-Boc group was also tested, however no product nor the known cyclised derivatives were observed.

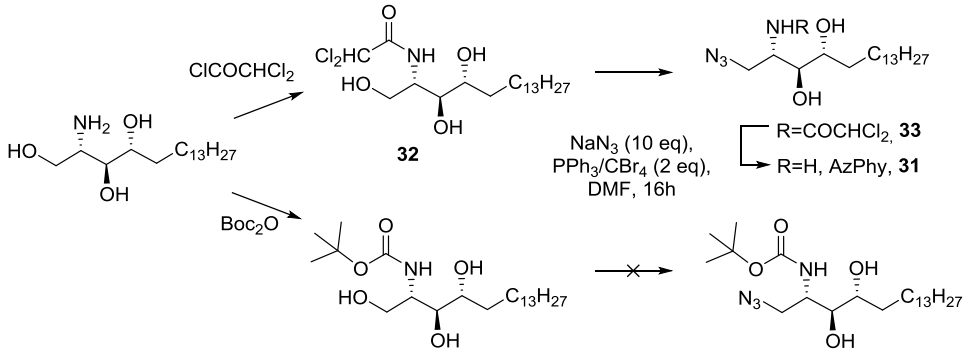

Scheme 2.1.2.8: Selective azidolysis reaction with different *N*-protecting groups.

2.1.3 Cyclooctyne-functionalised glycans

According to the constraints of our reconstitution strategy (Introduction 1.8), the *clickable* Gb3 head group must *click* with AzCer specifically in cell culture to form a Gb3-Cer analogue with a short, straight, biostable spacer. Cyclooctynes react quickly with azides without copper catalysis. The monofluorocyclooctyne (MFCO) was chosen for its small size and high specificity. Its synthesis had already been completed in the laboratory.[148,191,192] In this chapter I will describe the various *clickable* glycans synthesised. We suspected that the bent angle within the final reconstituted Gb3-MFCO-AzCer **35** (Scheme 2.1.3.1), could hinder

its function, so we additionally synthesised an analogue with a flexible linker region between the triose and MFCO, which would relieve this angle strain. We tested the syntheses of two flexible linkers, ethanolamine (EA) and glycine (Gly) (Scheme 2.1.3.7). We worked on the model lactose-MFCO **49** and lactose-Gly-MFCO **50** for larger scale synthesis. Lactose species can be used to test initial cellular *click* kinetics, since they should present similar cellular uptake and *in cellulo click* kinetics, which we follow by HRMS, without the need for STxB-Gb3 recognition. Later in this chapter I will present the synthesis of another lactose-cyclooctyne conjugate functionalised with the commercial (1*R*,8*S*,9*S*)-bicyclo[6.1.0]non-4-yn-9-ylmethanol (BCN) (Scheme 2.1.3.8), and the synthesis of final *clicked* Gb3 lipid analogues from the functionalised glycans and 1-azidoceramide (AzCer) (Scheme 2.1.3.9).

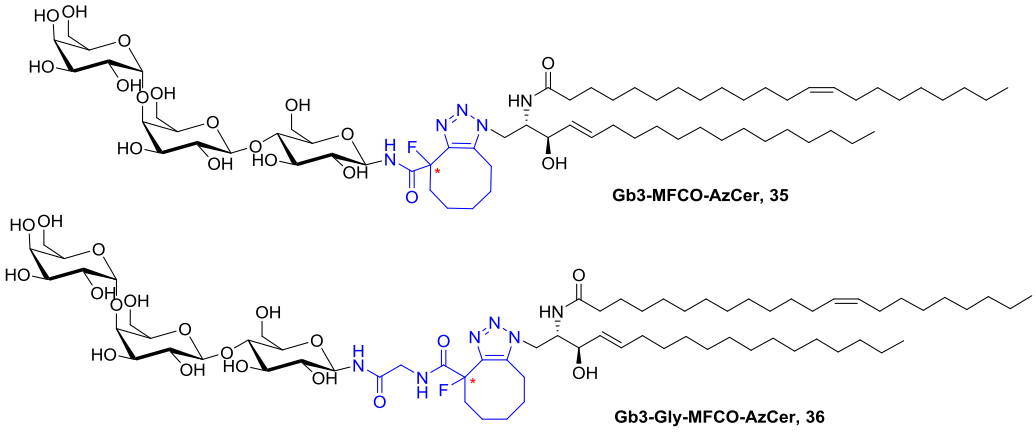

Scheme 2.1.3.1: Final *clicked* Gb3-AzCer analogues.

Gb3-MFCO **37** synthesis (Scheme 2.1.3.2) was developed by a former PhD student, Haifei Gao. The glycine linker was incorporated in a similar synthesis to afford Gb3-Gly-MFCO **38**. Synthesis of globotriose was as published by the laboratory,[24] beginning from commercial reagents protected thiophenylgalactose **39** and partially-protected lactose **40**. The triose **41** is formed from the glycosyl donor **40** and the glycosyl acceptor **39** in the glycosylation reaction, where the kinetically favoured α-triose product **41** is best formed at -55°C. The benzyl protecting groups are then switched to acetyl protecting groups to obtain **42a**, which is orthogonally deprotected in oxidative conditions to hemiacetal **42b**, and acetylated with acetic anhydride and pyridine to obtain peracetylated triose **42c**. **42c** is converted to the β-anomeric azide **43** by a glycosylation-type reaction with $TMSN_3$ and Lewis acid $SnCl_4$, in which the neighbouring acetyl group in the C-2 position aids in the formation of the desired β-stereochemistry.[176] The stable azidoglycoside **43** is easily reduced to the aminoglycoside

(decaacetyl-Gb3-β-NH_2) **44**. This aminoglycoside **44** is sensitive to hydrolysis back to hemiacetal **42b**, visible by ninhydrin TLC staining, and α/β isomerisation, thus is formed and immediately coupled with MFCO **45** or MFCO-glycine **46** to form the peracetyl-Gb3-MFCO **47** and peracetyl Gb3-Gly-MFCO **48** respectively. These were deprotected under basic methoxide conditions to afford Gb3-MFCO **37** and Gb3-Gly-MFCO **38**.

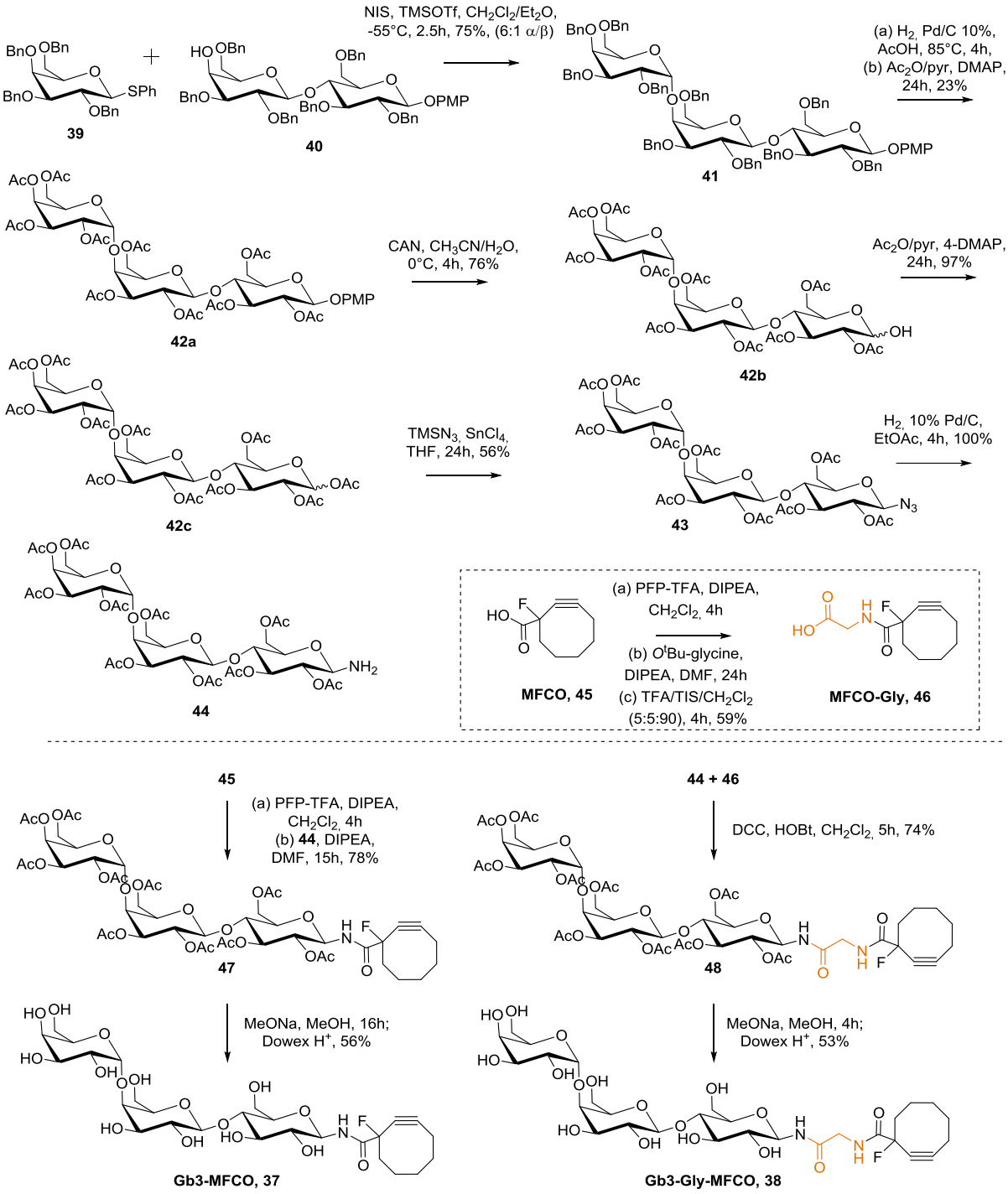

Scheme 2.1.3.2: Functionalised triose Gb3-MFCO and Gb3-Gly-MFCO synthesis.

MFCO-Gly **46** was synthesised by activating MFCO carboxylic acid **45** with PFP-TFA and coupling with *O*-^{t}Bu-glycine (Scheme 2.1.3.3). Although the *tert*-butyl protecting group should remain stable in basic conditions, approximately half is lost during the base-catalysed coupling reaction. Thus, when the coupling is complete, the remaining *O*-^{t}Bu-glycine-MFCO is deprotected *in situ* (one-pot, without purification) with TFA/TIS/CH_2Cl_2 (5:5:90). By mass spectrometry (MS), we observe trace formation of the doubly conjugated MFCO-Gly-Gly, which is easily separated. Synthesis was complicated by the instability of MFCO, which would break down to various highly polar compounds that were not characterised.

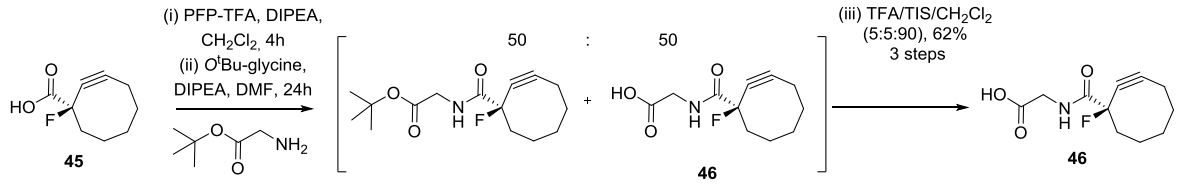

Scheme 2.1.3.3: One-pot peptidic coupling and deprotection to form MFCO-Gly.

Lactose-MFCO **49** and lactose-Gly-MFCO **50** (Scheme 2.1.3.4) were synthesised, analogous to Gb3, from peracetyl lactose, converted to 1-β-azido-hexaacetyl-lactose **51**. The azide **51** is reduced to the unstable 1-β-aminohexaacetyl-lactose **52**, which is coupled immediately to MFCO **45** or MFCO-Gly **46** to afford **53** and **54** respectively. These are deprotected to free *clickable* glycosides **49** and **50** under standard basic conditions.

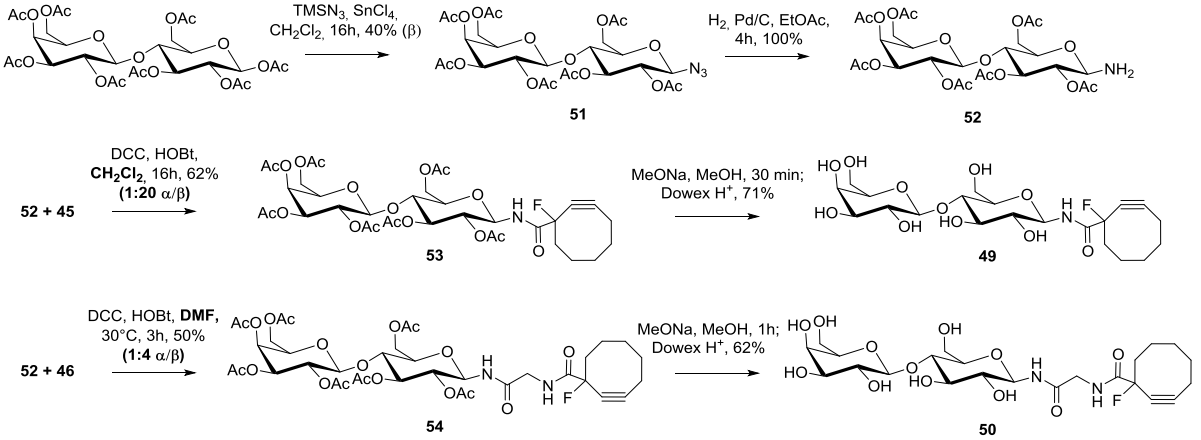

Scheme 2.1.3.4: *Clickable* lactose model synthesis.

The peptidic coupling of described heptaacetyl-lactose-β-NH_2 **52** or decaacetyl-Gb3-β-NH_2 **44** with MFCO-Gly **46** was tested with PFP-TFA (condition A, Scheme 2.1.3.5) which showed extremely poor reactivity, unlike what had previously been described in the laboratory to form decaacetyl-Gb3-β-NH_2 **44** from similar starting materials. The

aminoglycosides **44** and **52** were poorly nucleophilic, and unstable, often resulting in decomposition of both glycoside and cyclooctyne starting materials. On reaction with DCC and HOBt (condition B), we obtained product and were able to characterise a host of side products (Scheme 2.1.3.5): the hemiacetal glycoside **55**, N-acetyl lactose **56**, and the N-trifluoroacetate **57**. This latter is likely formed from trace TFA remaining from the purification of MFCO-Gly **46**.

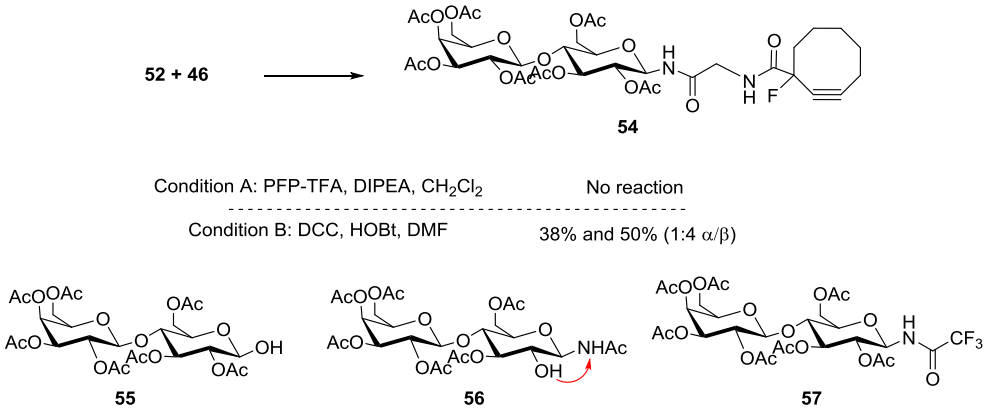

Scheme 2.1.3.5: MFCO-Gly coupling with aminoglycoside and side products formed.

In the case of the lactose syntheses, the α/β isomers are not separated, since the applications of these model molecules are to test the cellular kinetics of an MFCO-glycoside, followed by MS, for which the stereochemistry has no affect. Gb3 analogues must be of β-stereochemistry for their biological interaction with STxB. We tested the DCC coupling reaction in CH_2Cl_2 (condition C, Scheme 2.1.3.6) and obtained greater β-stereoselectivity; 1:20 α/β ratio, rather than 1:2 with DMF (condition B). This higher selectivity was reproducible in the synthesis of heptaacetyl-lactose-β-MFCO **53** from corresponding starting materials. When first forming **53**, we tested the coupling with PFP-TFA (condition A), expecting these products to have a similar reactivity to the reaction forming peracetyl-Gb3-MFCO **47**, however no reaction was observed.

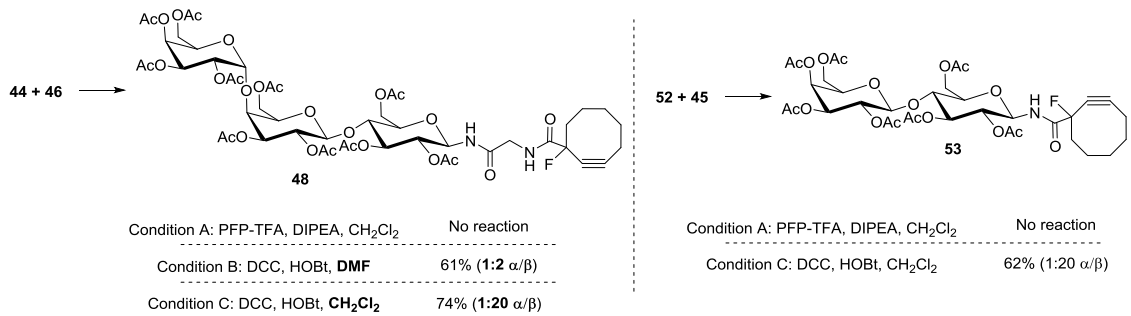

Scheme 2.1.3.6: MFCO-Gly coupling reaction conditions.

In parallel to the glycine linker, we tested the synthesis of the ethanolamine (EA) linked Gb3 analogue (Scheme 2.1.3.7) which could be used for the same purposes as the Gly analogue. We isolated MFCO-EA **59** by aminolysis of MFCO intermediate **58** with freshly distilled ethanolamine (EA) in THF. The glycosylation of protected Gb3 **60** with MFCO-EA was undertaken, via the activated trichloroacetimidate glycoside **61** in the presence of a Lewis acid. Low yield was due to poorly anhydrous conditions, often inevitable on small scale, reforming **60** from **61**. **62** formation was confirmed by MS but was isolated on a scale too small to continue to the deprotection step.

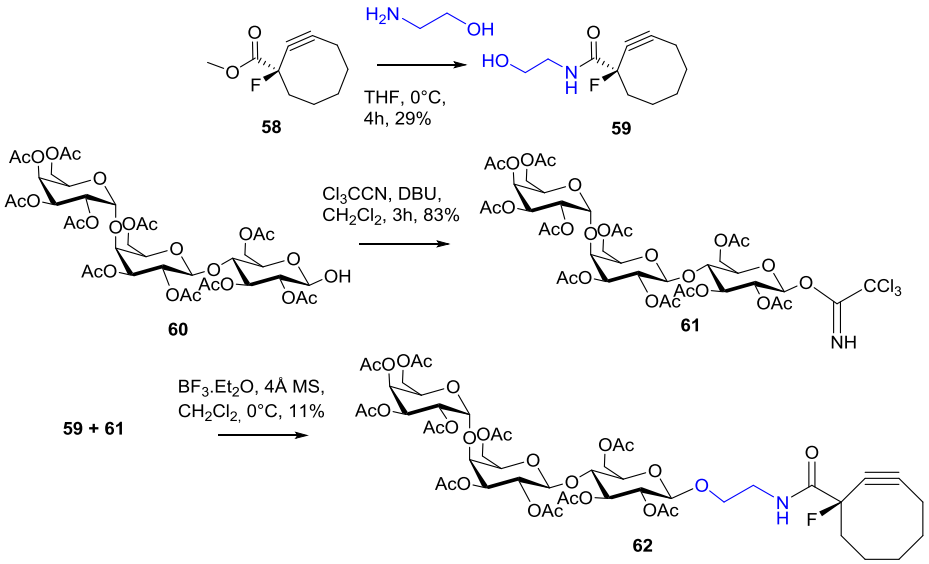

Scheme 2.1.3.7: Synthesis of ethanolamine-MFCO and glycosylation.

We briefly visited the synthesis of cyclooctyne-glycoside **63** with the commercial (1*R*,8*S*,9*S*)-bicyclo[6.1.0]non-4-yn-9-ylmethanol (BCN). As for the previous glycosylation reaction (Scheme 2.1.3.7), we activate the anomeric position of the protected lactose **64** to form the trichloroacatamidate **65**, which is glycosylated with the BCN alcohol (Scheme 2.1.3.8). Poor yields were due to hydrolysis of **65** back to **64**, and formation of the stable trichloroacetamide **67**, as before (Scheme 2.1.3.5).[176]

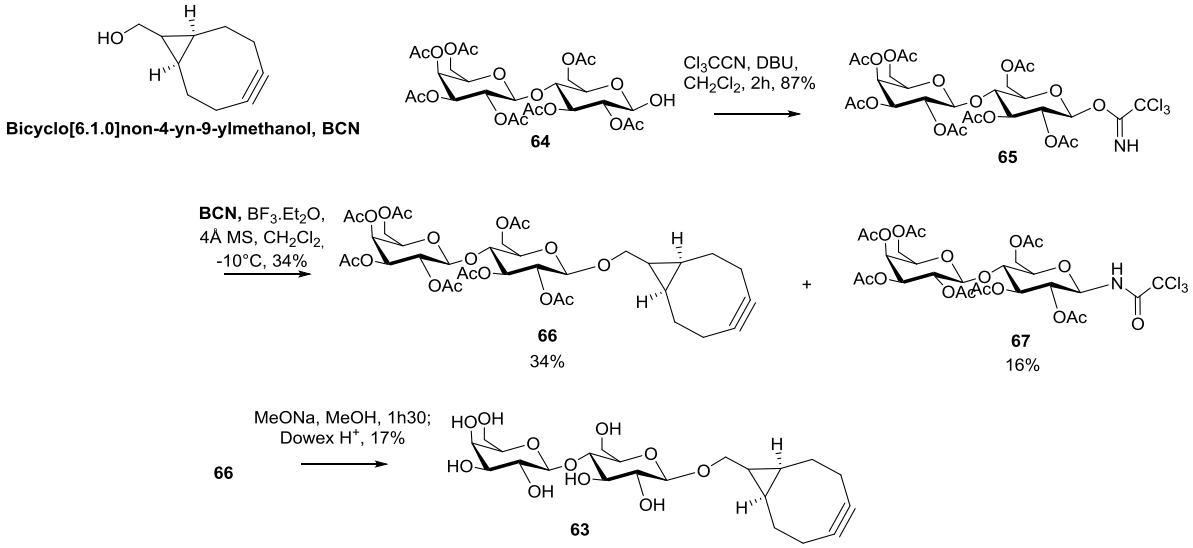

Scheme 2.1.3.8: Synthesis of glycoside-conjugated bicyclo[6.1.0]non-4-yn-9-ylmethanol (BCN).

Functionalised trioses, Gb3-MFCO **37** and Gb3-Gly-MFCO **38,** were clicked *in vitro* with AzCer, and the products (Scheme 2.1.3.9), a mixture of regio- and stereoisomers (Discussion 3.2), were purified for use as internal mass spectrometry standards, and in model membrane experiments to test their recognition by and membrane-bending with STxB.

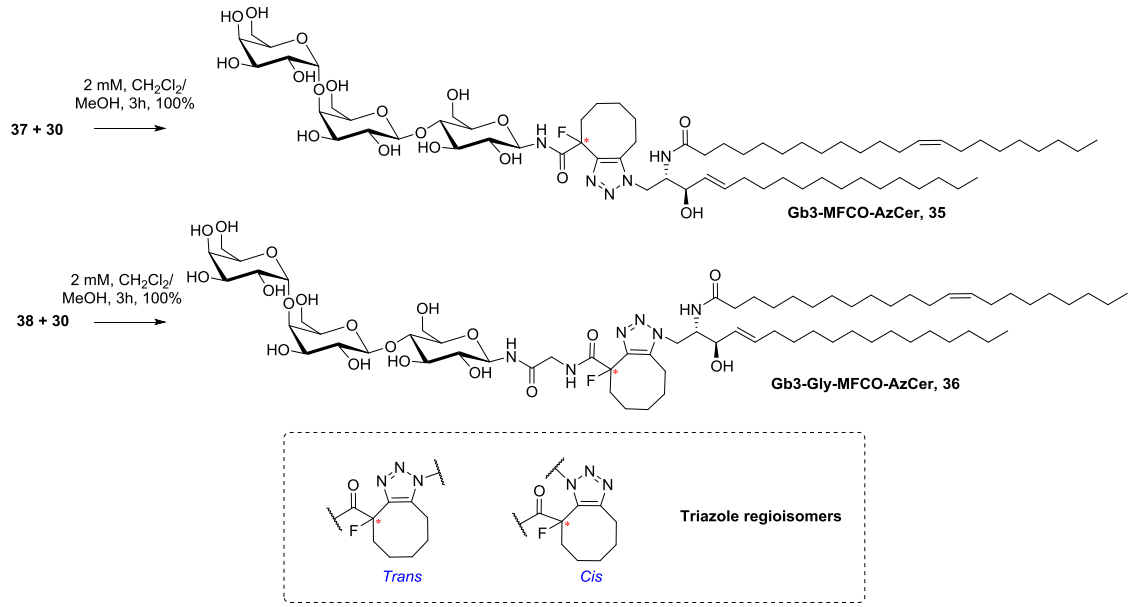

Scheme 2.1.3.9: Clicked Gb3-Cer analogues, from Gb3 head groups and AzCer **30.**

2.2 Biological validation of analogues

2.2.1 Model membrane validation

We conducted preliminary validation of the biological function of final *clicked* Gb3 analogues by testing their binding and membrane bending properties with the B-subunit of the Shiga toxin (STxB) (Introduction 1.2). These mechanochemical properties of the GSL analogues are traditionally tested in model membrane systems called giant unilamellar vesicles (GUVs), or liposomes. This robust technique shows spontaneous, dynamic tubule formation of STxB bound to the natural Gb3 in the liposome bilayer, indicating that GL-Lect dependant endocytic interactions could occur in a cellular environment. We use this technique to test each final synthetic product. To follow the process by fluorescence microscopy, we use STxB-Alexa488, where the green fluorophore (Alexa488) is conjugated via a lysine-specific sulfodicholorphenol (SDP) functionality. A red fluorescent phospholipid, Rhod-SDP-PE, is used to stain the liposome (Figure 2.2.1.1).

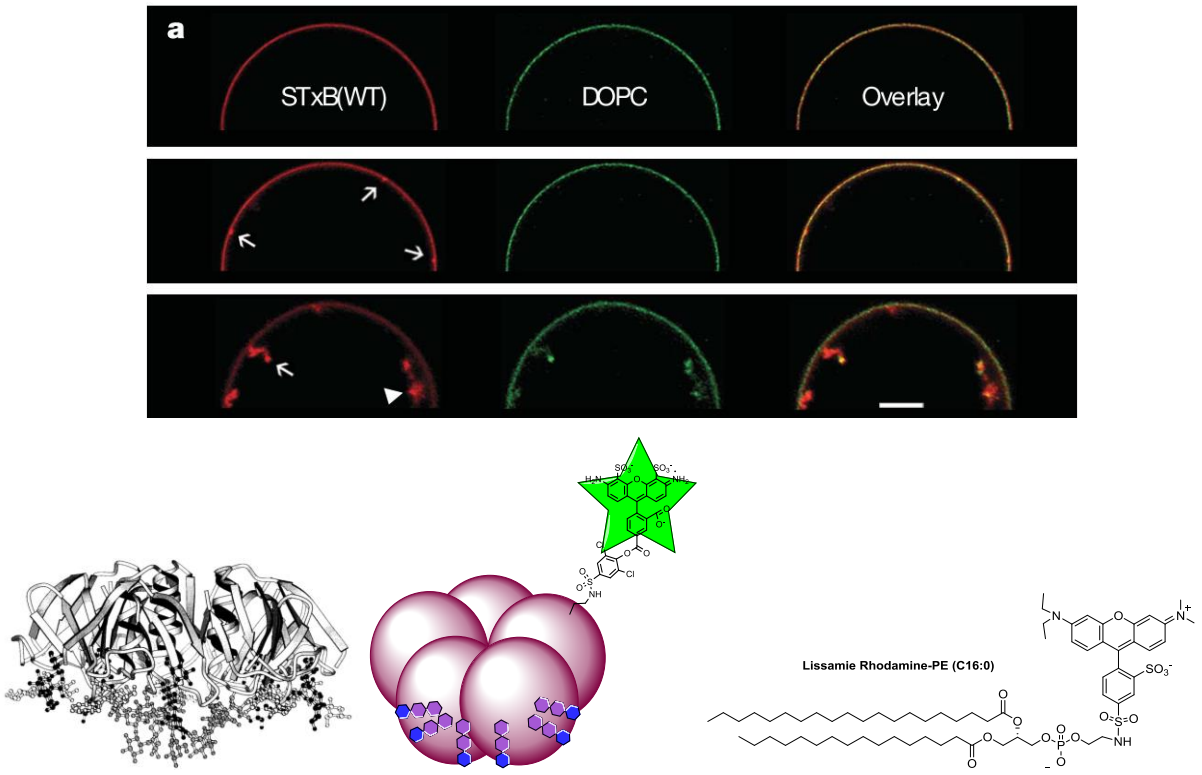

Figure 2.2.1.1: Canonical STxB-Cy3(wild type, red) binding and invagination of membrane in GUVs (64 $_{mol}$% DOPC; 30$_{mol}$% chol; 5$_{mol}$% porcine Gb3; 1$_{mol}$% BodipyFL-C5-HPC (green)).[27] Schematic structures of STxB bound with 15 Gb3,[193] STxB-Alexa488 with Gb3 binding sites, and Lissamine Rhodamine phosphoethanolamine (Rhod-SDP-PE).

GUVs are formed by mixing the cocktail of desired lipids in chloroform, allowing a lipid film to dry under vacuum and rehydrating in a sucrose solution of known osmolarity under a constant alternating current (10 Hz, 1.1 V, Experimental 6.2.1). Each experiment included a negative control (no GSL) and a positive control (natural Gb3-Cer). Molar ratio of lipids in GUVs was used as described previously by Römer *et al*.: 64.9% DOPC, 30% cholesterol, 5% Gb3 species, 0.1% Rhodamine-PE.[27]

Highly dynamic invaginations of GUVs are observed after 5-10 min of incubation with STxB-Alexa488 with the two Gb3 analogues: Gb3-MFCO-AzCer **35** and Gb3-Gly-MFCO-AzCer **36**, similar to that observed on wild type Gb3 (Figure 2.2.1.2-3). We were thus happy to use these substrates in ensuing cellular experiments. As mentioned in Results section 2.1.3, the *cis/trans* regioisomers formed from the *click* cycloaddition were not separated since this will not be controllable in cells, and this test is to evaluate the function of our synthetic analogues in cells.

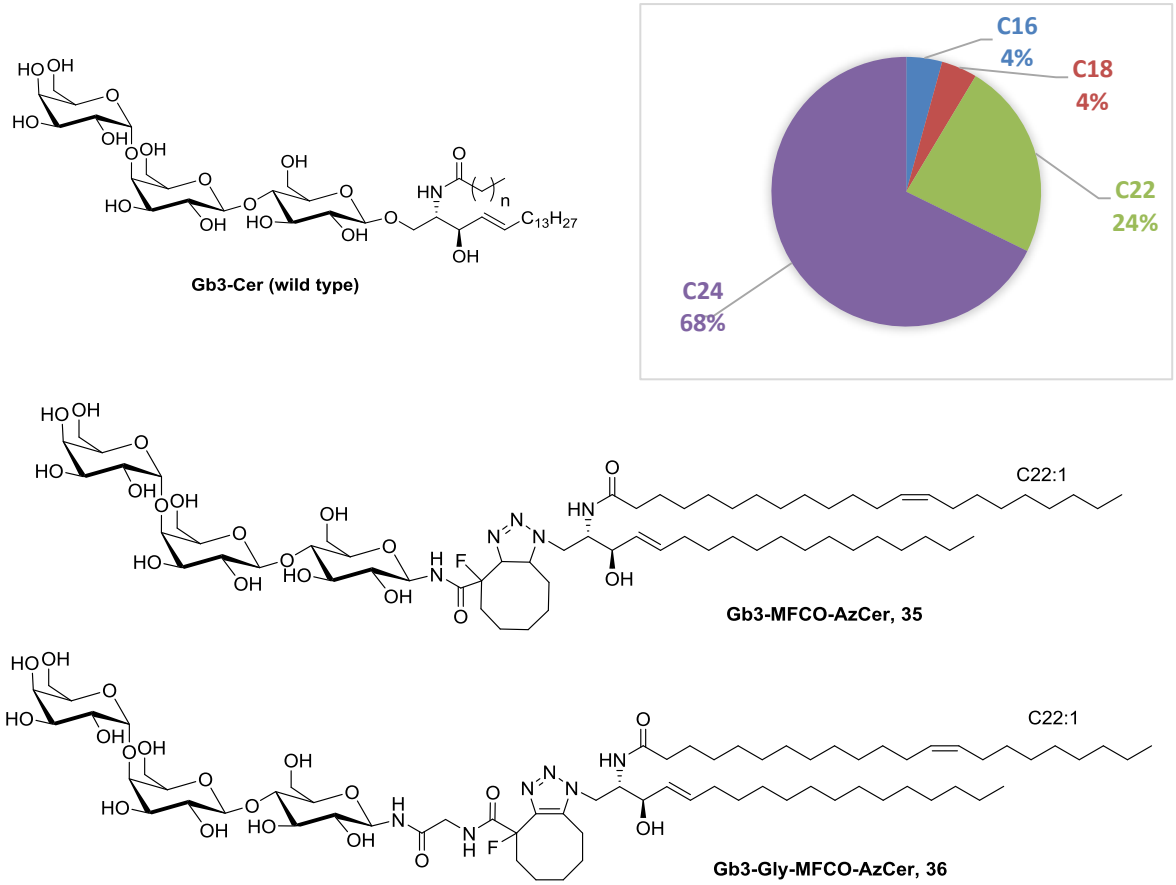

Figure 2.2.1.2: Natural porcine Gb3-Cer with acyl chain profile,[64] with Gb3 analogues tested in GUVs

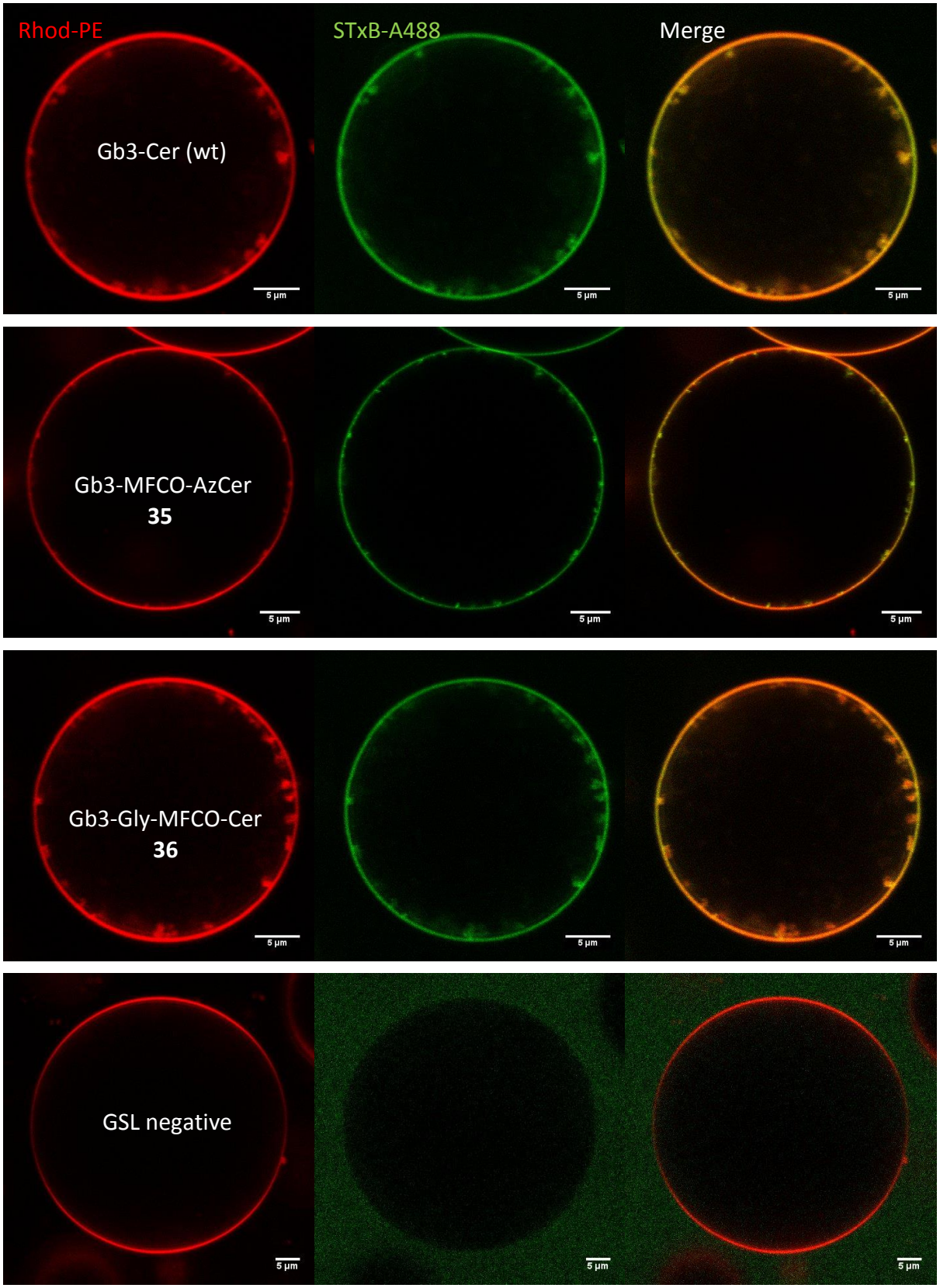

Figure 2.2.1.3. Dynamic membrane invaginations observed on GUVs containing 5% Gb3 species or w/o, and incubated with STxB (green). (64.9$_{mol}$% DOPC, 30$_{mol}$% cholesterol, 5$_{mol}$% Gb3 species, 0.1$_{mol}$% Rhodamine-PE (red)) Images taken on a Leica SP8 confocal microscope.

To test the *click* reaction on a liposome model, we formed large unilamellar vesicles (LUVs, 200 nm) containing AzCer and incubated with equimolar amounts of Gb3-MFCO (5_{mol}% AzCer, 65_{mol}% DOPC, 30_{mol}% cholesterol in liposomes; 4 nmol cyclooctyne, 1 eq; Experimental 6.2.2). LUVs are simpler to form and are less uniformly aesthetic than GUVs, so not ideal for microscopy experiments, but have the same chemical properties for the scale of our interest. The mass spectrometry (MS) results showed product forming with time, but only a very small proportion of AzCer reacted.

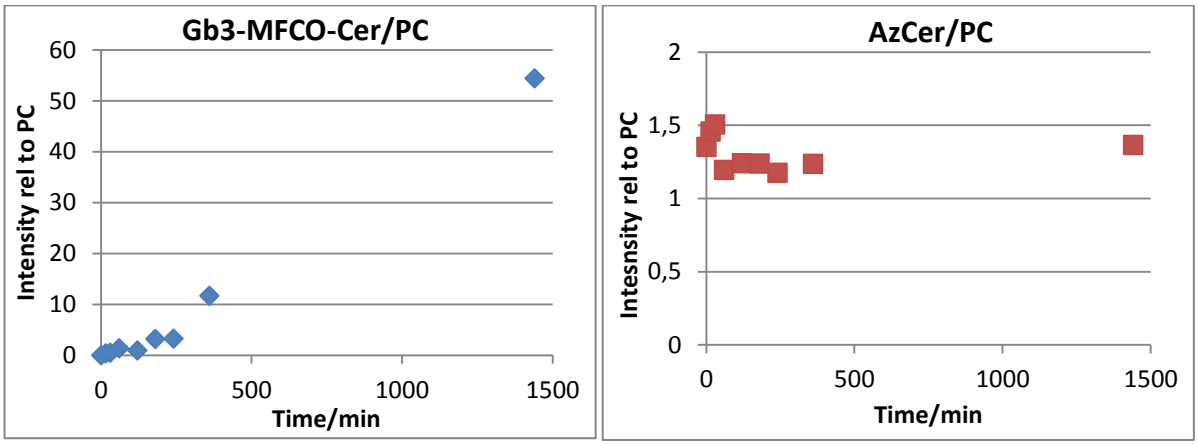

Graph 2.2.1.1: Formation of Gb3-MFCO-Cer and consumption of AzCer on LUV *click* reaction.

2.2.2 Cellular metabolism and localisation of AzSph

GSL-deficient GM95 cells and Gb3-deficient Chinese hamster ovary (CHO) cells were incubated with AzSph to study its cellular metabolism. Cells were incubated with AzSph (10 µM) in media for various lengths of time. The cells were then lysed, the lipids extracted, and the azide-metabolites *clicked* with a fluorophore (Alexa488-alkyne and copper catalyst, or tetramethyl-rhodamine (TAMRA)-dibenzocyclooctyne (DIBO), Experimental 6.2.3). This reaction mixture was spotted and migrated on high performance thin layer chromatography (HPTLC) plates, and visualised with a fluorescent plate reader. When possible, samples were compared with pure reference AzSph and AzCer previously *clicked in vitro* with the fluorophore (Alexa488-AzSph and -AzCer, or TAMRA-AzSph and -AzCer).

AzCer from cell lysate samples was often below detection limit on the fluorescent plate reader after HPTLC migration. We obtained better results with the more lipophilic (fast migrating) *clickable* fluorophore TAMRA-DIBO. In one experiment (Figure 2.2.2.1), the

fluorescent band of reference compounds AzSph and AzCer are visible. However, no band is observable in the treated cells that could correspond to *clicked* AzCer. Figure 2.2.2.2 shows bands which would specifically correspond to TAMRA-AzCer in treated cells. After scanning the plate, the fluorescent bands were scratched off to isolate silica. Lipid species were extracted from the silica in a dichloromethane/methanol mixture and analysed by MALDI-MS. By this method, exact masses of the AzSph and AzCer synthetic reference compounds were observed, thus confirming their migration properties. In MALDI-MS, we were able to see the TAMRA-AzCer (C16:0) formed (Figure 2.2.2.3), showing that the C16:0 chain is enzymatically added to AzSph in cells with high preference (Discussion 3.4).

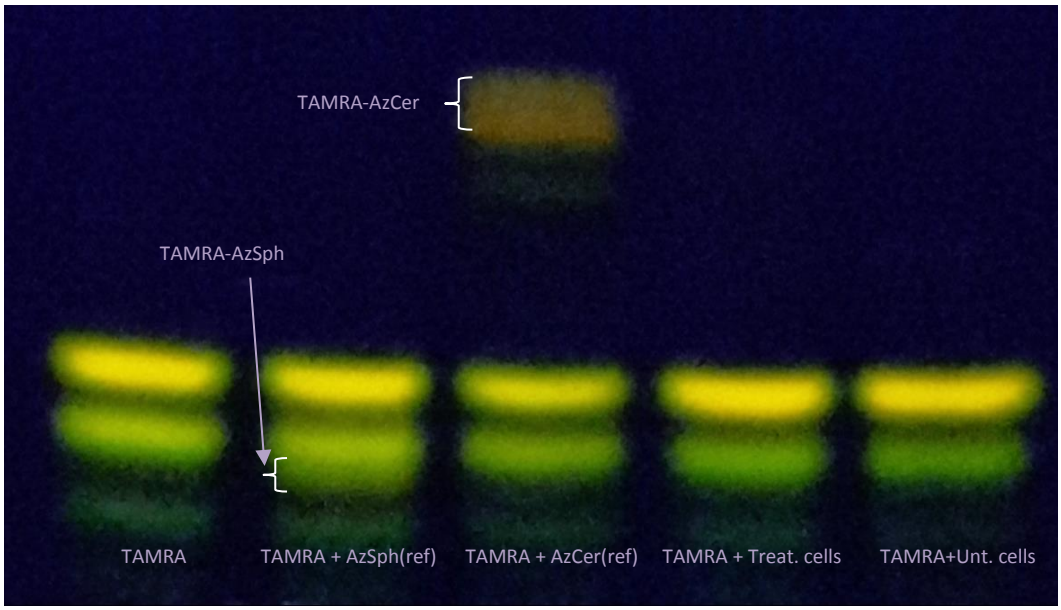

Figure 2.2.2.1. Incubation of AzSph (10 µM, 3h) in GM95 cells, allowing cellular AzCer synthesis. Reference compounds indicate migration properties. Cannot observe AzCer in treated cell lysate.

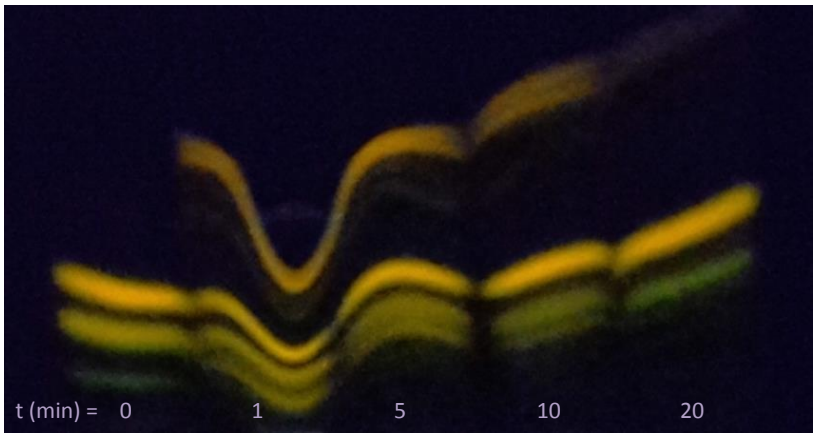

Figure 2.2.2.2: Time course of AzSph treated cells. We observe TAMRA-AzCer in a specific manner in AzSph treated cells.

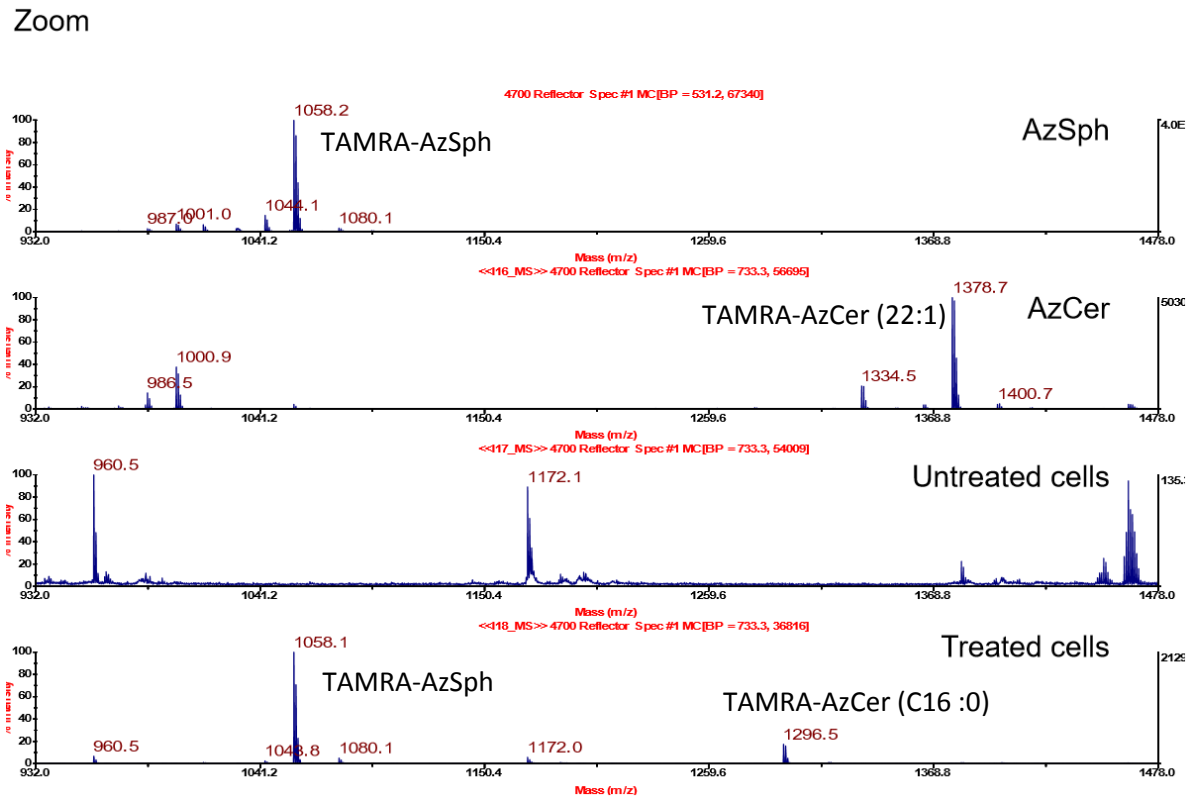

Figure 2.2.2.3: First MALDI-MS results showing AzCer formed in AzSph treated cells.

During these experiments we observed cell death at 10 µM of AzSph beyond 6h of incubation. We measured the half maximal effective concentration (EC_{50}), concentration for 50% cell survival, using a colorimetric MTT assay, which indicates cell viability with 3-(4,5-dimethylthiazol-2-yl)-2,5-diphenyl tetrazolium bromide (Figure 2.2.2.4), a compound which after action of oxidoreductase enzymes in living cells only, produces the strong purple compound, formazan. We measured cell survival after 24h incubation (Experimental 6.2.4). Despite slight variability for different cell densities, we obtained reproducible results with an average EC_{50} value of 3.5 µM in GM95 cells and 1.8 µM in CHO cells. EC_{90} values (concentration for 90% cell survival) were measured at 0.4 µM and 0.3 µM (Discussion 3.4).

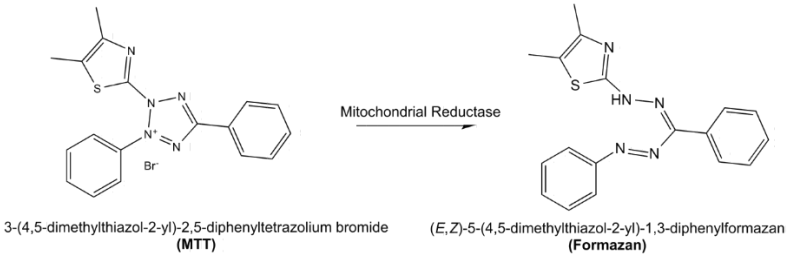

Figure 2.2.2.4: MTT reaction occurring in living cells producing strong purple formazan.

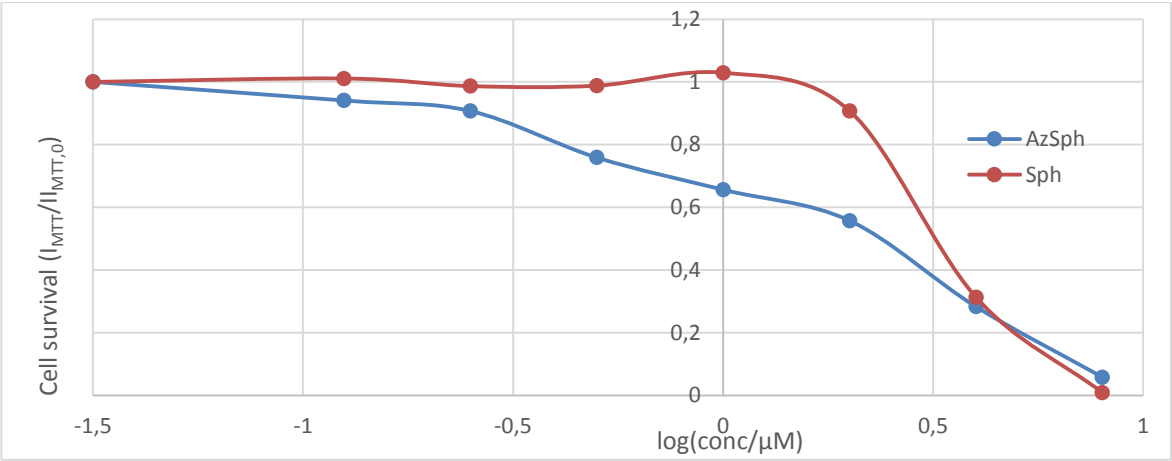

Graph 2.2.2.1: Cytotoxicity of AzSph and sphingosine on GM95 cells.

With the arrival of a HRMS facility at our institute, we were able to obtain much greater detail in our lipid metabolism analysis. We improved MS resolution by performing a simplified Folch lipid extraction best adapted to sphingolipids (Experimental 6.2.5).[194] By washing with ammonium bicarbonate we reduced background noise from salts compared with PBS, ideal for MS analysis. Crucially, this washing must be performed quickly since GM95 cells are poorly adherent and will detach after prolonged incubation in PBS or ammonium bicarbonate. After washing treated cells twice only with ammonium bicarbonate, we scratch the cells off the plate and collect in ammonium bicarbonate solution, concentrate cell suspension by centrifugation, and homogenise by passing the solution through a needle. The biological sample is spiked with a known concentration of internal standards (AzCer 22:1 and Cer 12:0), allowing for exact quantification of the sample. All samples are further normalised to ceramide. Protein quantification, analysed by a MicroBCA kit, was also used as a proxy for the number of recuperated cells. This protein (cell) quantification gives an early, crude indication of cell death and proliferation induced by the *click* treatment. Priliminary protein quantification of biological samples allows us to carry out lipid extraction on an equal quantity of cells from each condition for HRMS, thus making each condition quantifiable relative to each other. The cell lysate (200 µl containing equal quantity of cells per condition) is extracted by shaking vigorously with chloroform/methanol. The organic phase is recuperated for concentration and HRMS direct infusion.

The AzCer profile, i.e. the variety of different acyl chains enzymatically added to AzSph, was similar in GM95 and CHO cells (Graph 2.2.2.2). This AzCer profile is equally

dissimilar to the natural ceramide profile (Graph 2.2.2.3) in both cells lines, which contain more long chain C24 ceramides. AzCer profile remains constant over 24h (Graph 2.2.2.4). At low AzSph concentration (0.5 µM) we show a stable ratio of approximately 2-3 molecules of AzCer to ceramide (Graph 2.2.2.6), with the aid of internal standards. Natural ceramide levels (Graph 2.2.2.5-6) also remains constant under these non-toxic AzSph treatment conditions.

To prevent the dilution of AzCer in cells over several days, which would be important to ensuing experiments, we tested incorporation of AzSph in DMEM media with and without (w/o) serum, to inhibit cell proliferation. We observed that a 3:1 AzCer/Cer ratio was maintained for 48h in serum-free conditions on GM95 cells (Graph 2.2.2.7), with analogous results obtained in CHO cells.

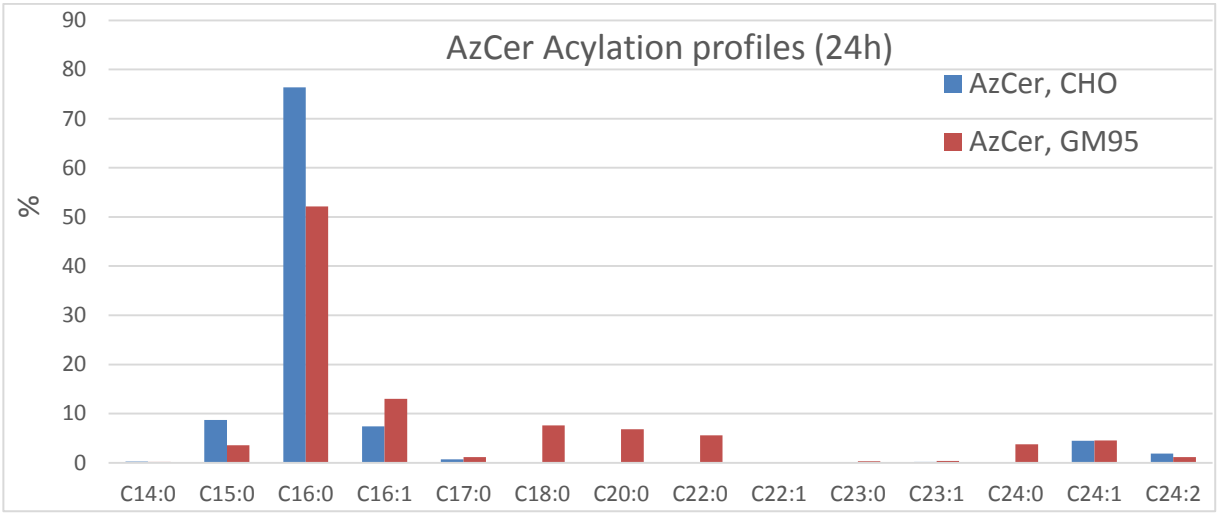

Graph 2.2.2.2: AzCer profile in GM95 and CHO cells after AzSph treatment (0.5 µM, 24h).

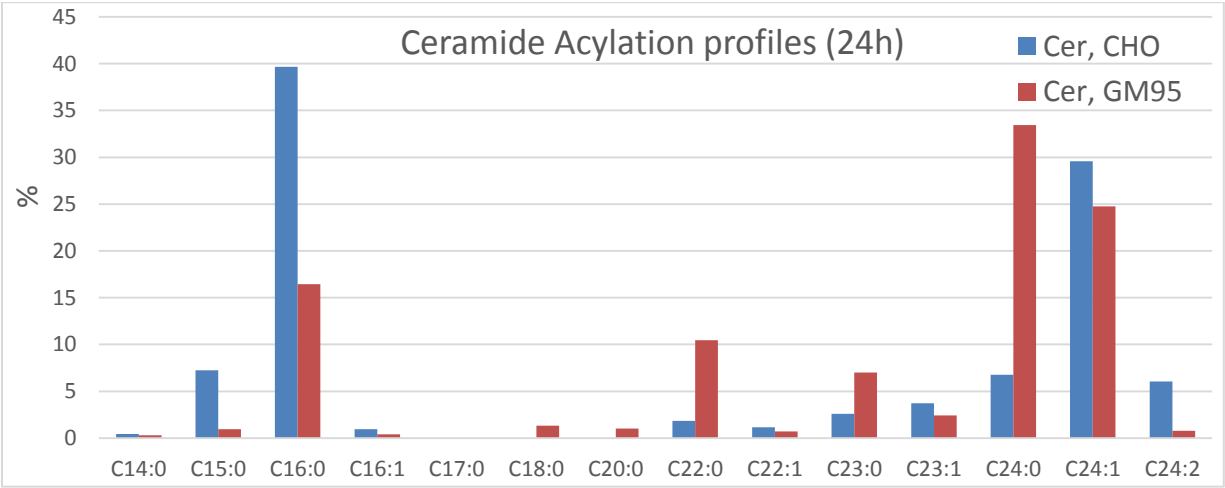

Graph 2.2.2.3: Ceramide profile in GM95 and CHO cells after AzSph treatment (0.5 µM, 24h).

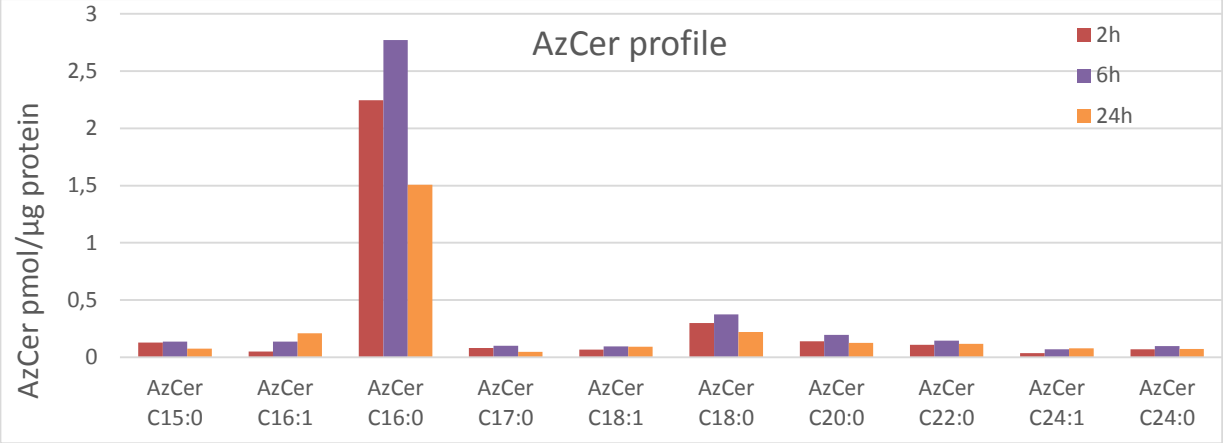

Graph 2.2.2.4: AzCer profile over 24h in GM95 after AzSph treatment (0.5 µM).

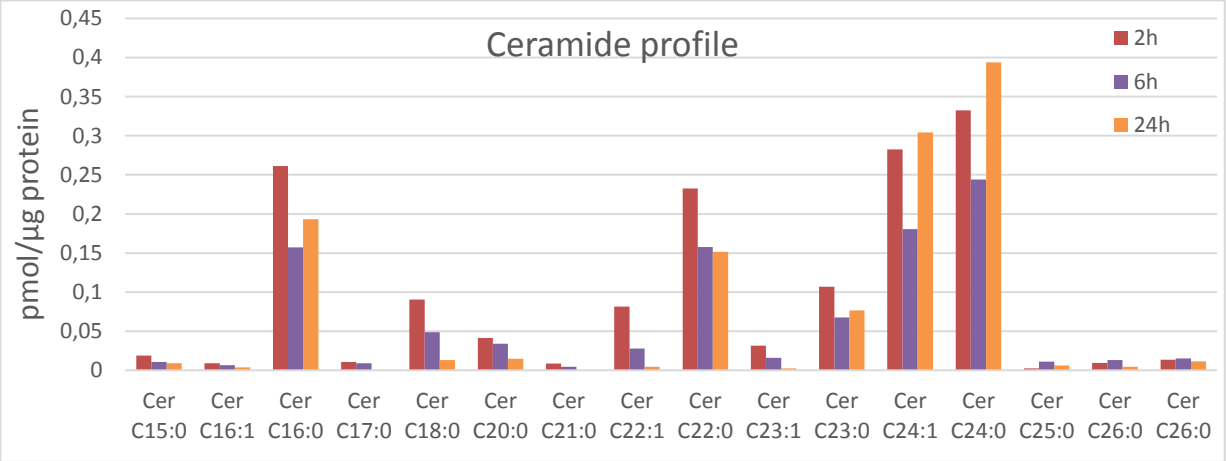

Graph 2.2.2.5: Ceramide profile over 24h in GM95 after AzSph treatment (0.5 µM).

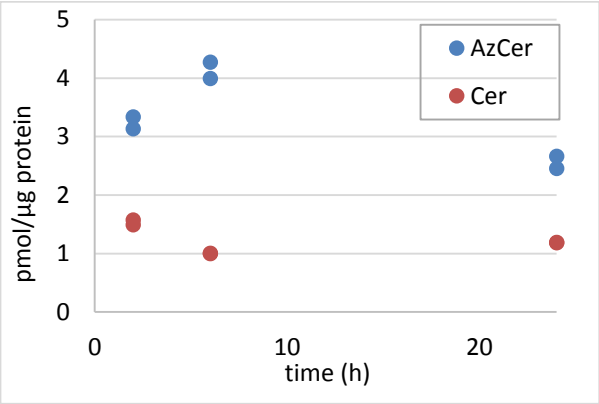

Graph 2.2.2.6: AzCer and ceramide quantification in cells after AzSph treatment (0.5 µM).

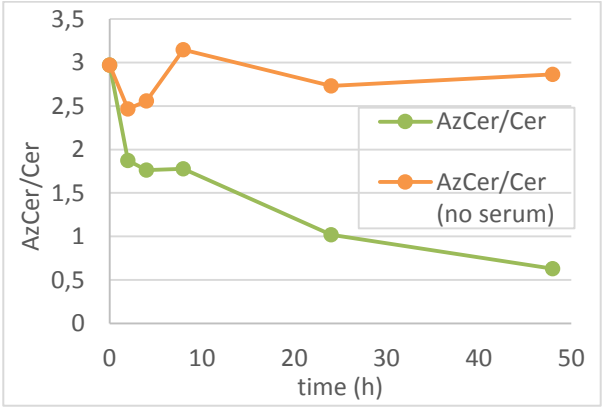

Graph 2.2.2.7 : No serum conditions to prevent AzCer dilution in GM95 cells.

To study the intracellular localisation of AzCer in cells, we conjugate azide metabolites with a *clickable* fluorophore. Copper-catalysed *click* reagents are commonly considered to give less background signal than copper-free, cyclooctyne *click* reagents, so we began with a copper-catalysed *click* on fixed cells (Experimental 6.2.6). Due to the poor adherence of GM95

cells, immunofluorescence (IF) experiments were also performed on HeLa cells (Figure 2.2.2.5) and CHO cells, and all three cell types showed a similar staining in all intracellular membranes, in the ER and Golgi. Live cell imaging showed similar co-localisation with ER- and Golgi-labelling by transfection of CHO cells with Golgi and ER markers, galactosyltransferase-GFP and RDEL-HALO. The staining was relatively weak at the plasma membrane (PM) where the *click* reaction would ideally occur, but we considered that constant recycling of membranes by vesicular transport would allow temporary presentation of AzCer at the PM, which could undergo *click* reaction.

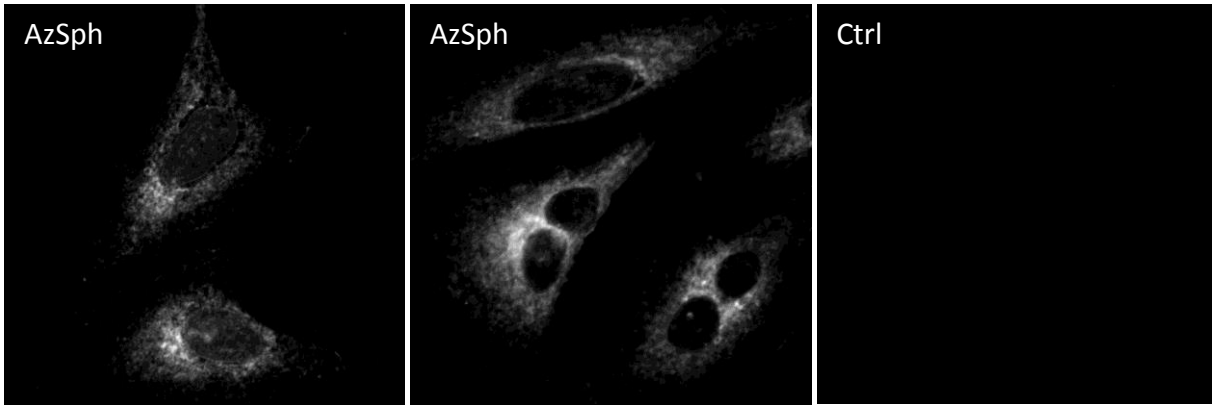

Figure 2.2.2.5: AzSph treated HeLa cells (5 µM, 1h), fixation, Alexa488-alkyne (2.5 µM) and copper (0.4 µM), imaging by confocal microscopy.

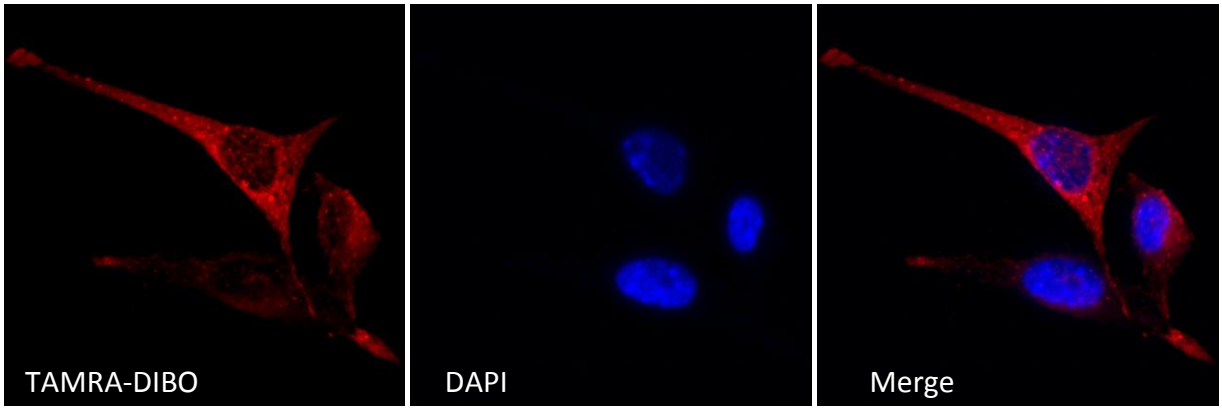

Figure 2.2.2.6: GM95 cells, AzSph (0.5 µM, 8h), *click* with TAMRA-DIBO (0.5 µM), fixation, confocal imaging.

2.2.3 Glycan *click*

To test the *click* reaction *in cellulo*, we incubated cells with AzSph in cell medium, in conditions optimised to have stable, non-toxic levels of AzCer (0.5 µM, 6-16h), then replaced this with medium containing the cyclooctyne (Scheme 2.2.3.1, Experimental 6.2.5). Commercial Alexa488-DIBO or TAMRA-DIBO were first tested (Figure 2.2.3.1). After overnight incubation, we scratch the cells and extract the lipids as before. We follow the consumption of AzCer, normalised to ceramide (Cer), which remains constant throughout treatment, and is present at approximately 2:1 (AzCer/Cer). We observe a highly efficient *click* reaction of AzCer with TAMRA-DIBO by a major depletion of AzCer (Graph 2.2.3.3) and a strong signal from TAMRA-DIBO-AzCer *click* product by HRMS (Graph 2.2.3.4). Inversely, Alexa488-DIBO and lactose-MFCO show no indication of *click* product forming. Either the *click* reaction does not occur at all, or the product is formed on a small scale and is not extracted for analysis. We considered that the bioavailability of the reagent, as well as the reactivity of the cyclooctyne, has an important effect. Neutral TAMRA is more lipophilic than Alexa488, with an overall 2-charge; thus TAMRA should permeate cell membranes much better than Alexa488. Mass spectra of fluorophore-*click* products, for which no internal standard was used, are shown in arbitrary units (A.U.).

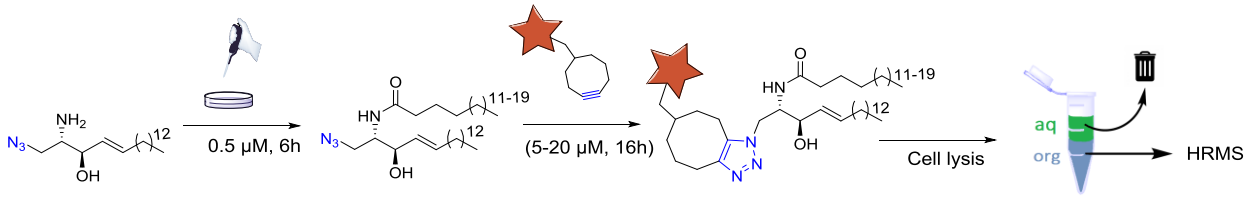

Scheme 2.2.3.1: *In cellulo click* protocol. Cells incubated with AzSph, followed by cyclooctyne, lysed, extracted and analysed by HRMS (Experimental 6.2.5).

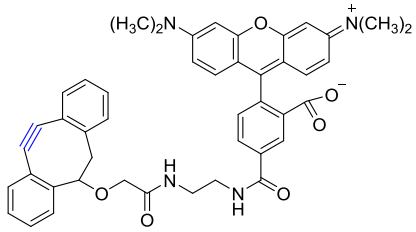

TAMRA-DIBO

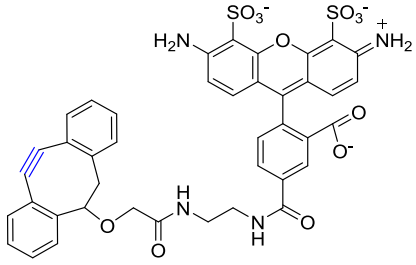

Alexa488-DIBO

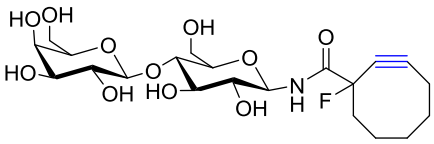

Lactose-MFCO, **49**

Figure 2.2.3.1: Cyclooctyne structures.

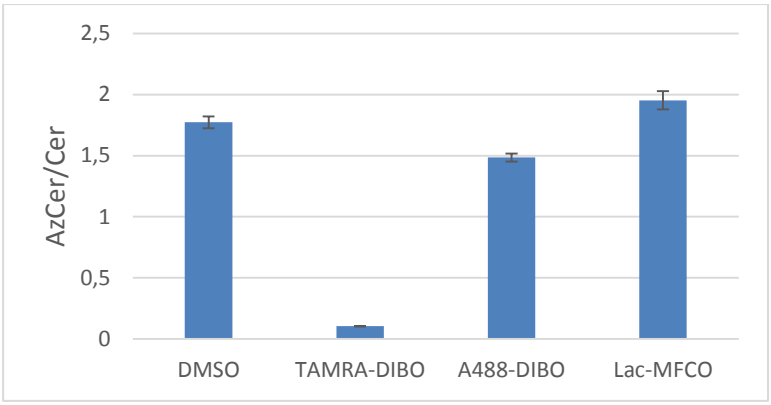

Graph 2.2.3.3: AzCer in cells treated with AzSph (0.5 µM), then cyclooctyne (5 µM), normalised to ceramide.

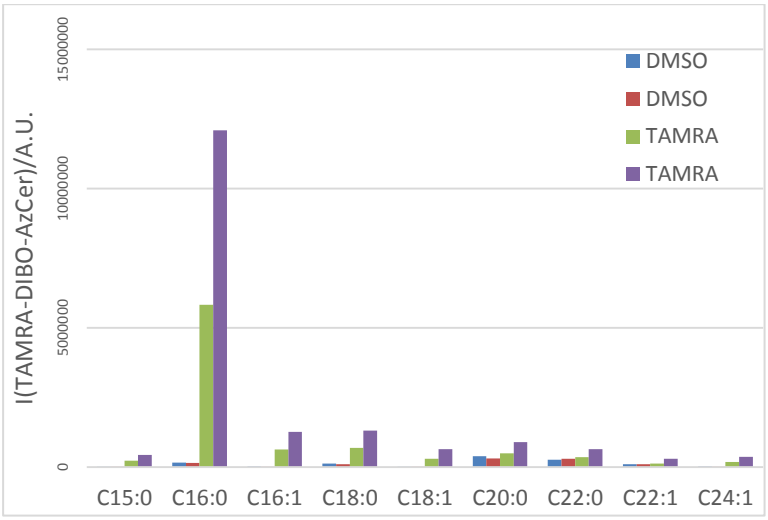

Graph 2.2.3.4 : TAMRA-DIBO cellular *click* product with AzCer (C15-24).

By this logic, the *click* reaction was more efficient with hydrophobic, membrane-permeating peracetylated glycans: peracetyl lactose-MFCO (Ac-Lac-MFCO **53**), peracetyl lactose-bicyclononyne (Ac-Lac-BCN **66**), peracetyl Gb3-MFCO (Ac-Gb3-MFCO **47**) and peracetyl Gb3-Gly-MFCO (Ac-Gb3-Gly-MFCO **48**); compared to hydrophilic free glycans: Lac-MFCO **49**, Lac-BCN **63**, Gb3-MFCO **37** and Gb3-Gly-MFCO **38**, which showed no reaction at 5 µM of glycosyl-cyclooctyne (Figure 2.2.3.2, Graph 2.2.3.5).

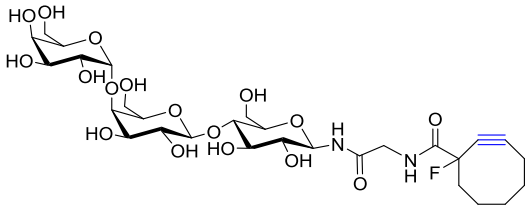

Gb3-Gly-MFCO, **38**

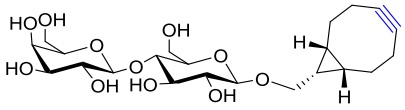

Lactose-bicyclononyne (BCN), **63**

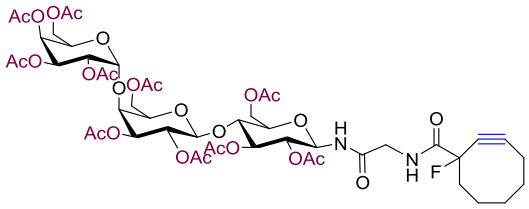

Ac-Gb3-Gly-MFCO, **48**

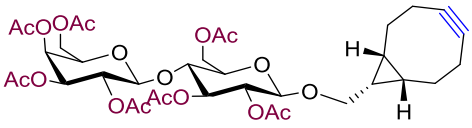

Ac-lactose-BCN, **66**

Figure 2.2.3.2 : Structures of *clickable* cyclooctynes.

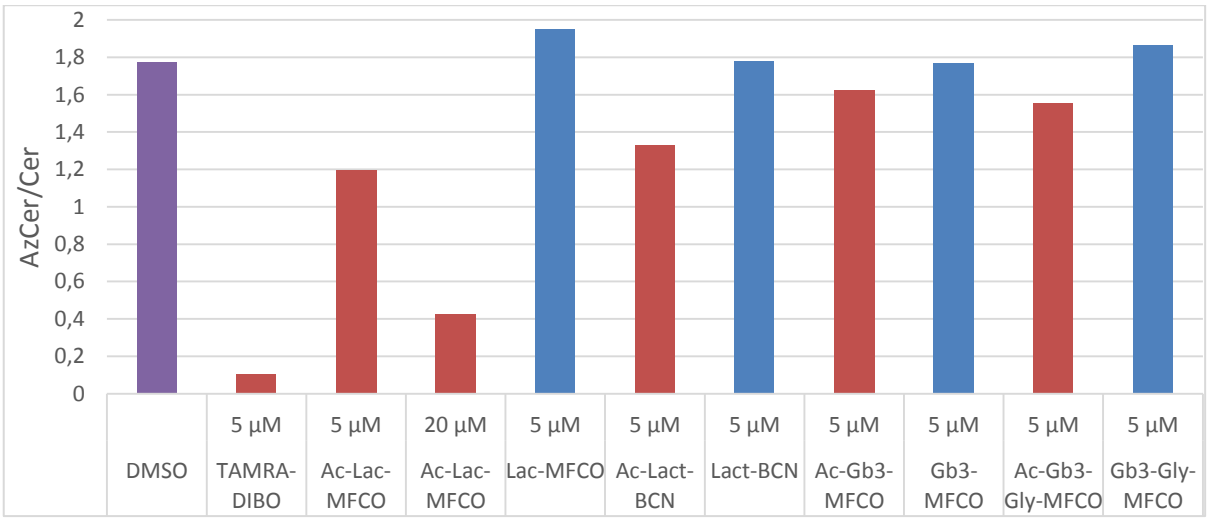

Graph 2.2.3.5: AzCer/Cer levels in cells treated with AzSph (0.5 µM), and then with hydrophobic (orange) or hydrophilic (blue) cyclooctyne (5/20 µM).

Hydrophobic peracetylated glycans are commonly used to increase cellular uptake of glycans since they diffuse passively through membranes, and are deacetylated by non-specific esterases (Introduction 1.6).[118,128] We observe efficient formation of Ac-Lac-MFCO-AzCer *click* product **68** (Figure 2.2.3.3, Graph 2.2.3.6) on incubation with Ac-Lac-MFCO, with initial enzymatic deacetylation occurring after 16h. Lac-MFCO-AzCer, the fully deacetylated product (-7Ac), is present only at noise levels. Acetylated Gb3 *click* product **69** forms (Graph 2.2.3.7), but is deacetylated even less than lactose **68**, and did not undergo much more deacetylation after 48h (Graph 2.2.3.8). Peracetylated Gb3 *click* product **69** was synthesised *in vitro* from Ac-Gb3-MFCO **37** and AzCer **30** for use as an internal standard in HRMS analysis. Ac-Lac-BCN-AzCer, product of *click* reaction with an alternative cyclooctyne BCN, is detected in cells

(Figure 2.2.3.4, Graph 2.2.3.9), but no deacetylation is observed. Conversely, the *click* product of peracetylated Gb3-Gly-MFCO **48** was not observed. Potentially **48** is too large to permeate the cell membrane, despite being hydrophobic.

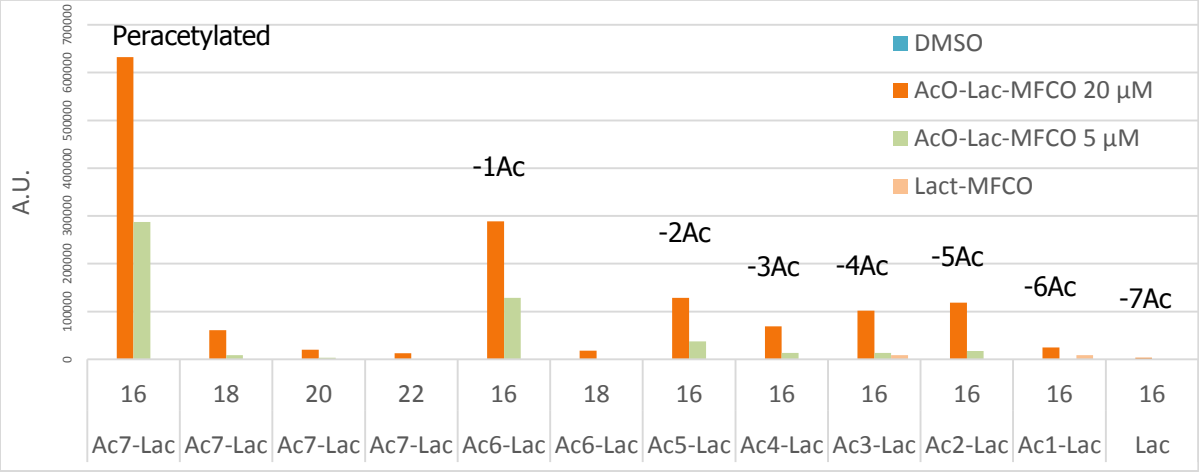

Graph 2.2.3.6: Deacetylation profile of Ac-Lac-MFCO-AzCer product in GM95 cells treated consecutively with AzSph (0.5 µM, 8h) and (Ac)-Gb3-MFCO (5 or 20 µM).

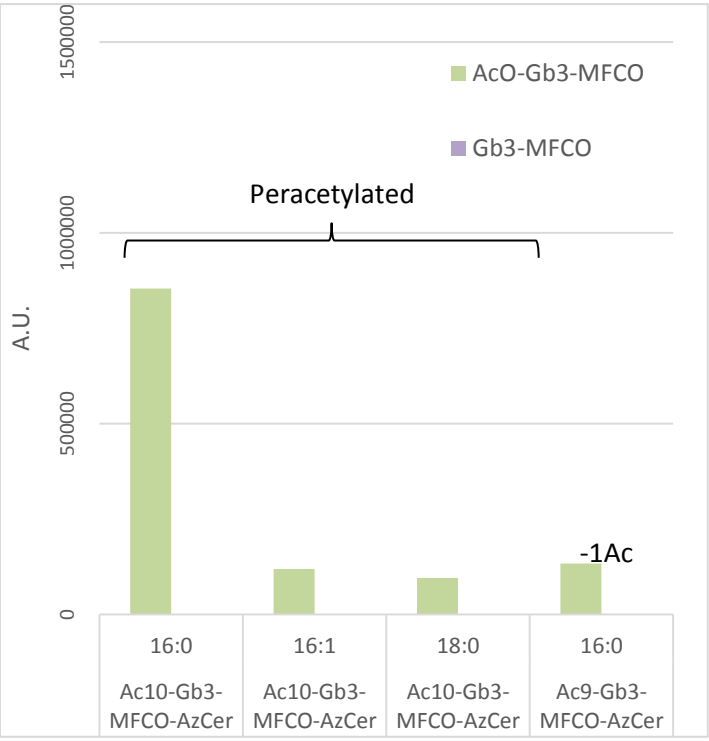

Graph 2.2.3.7: Ac-Gb3-MFCO-AzCer **69** deacetylation in GM95 cells treated with AzSph (0.5 µM, 8h), then with (Ac)-Gb3-MFCO (5 µM).

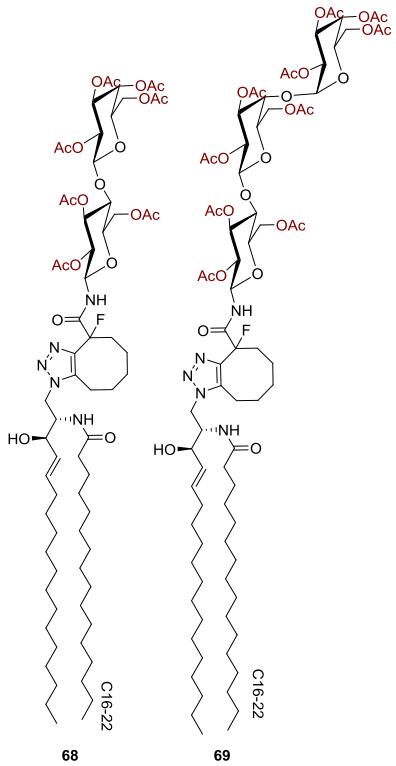

Figure 2.2.3.3: Ac-Lac-MFCO-AzCer **68** and Ac-Gb3-MFCO-AzCer **69.**

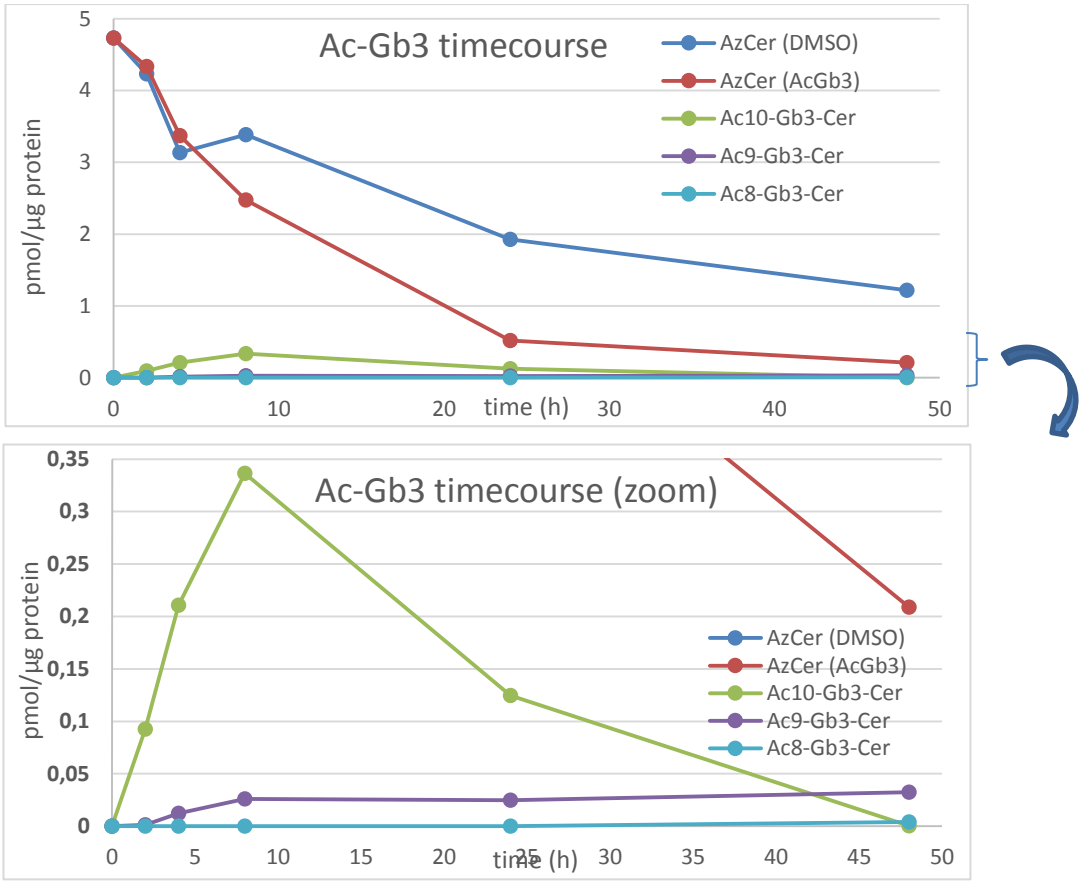

Graph 2.2.3.8: Time course of deacetylation of Ac-Gb3-MFCO-AzCer.

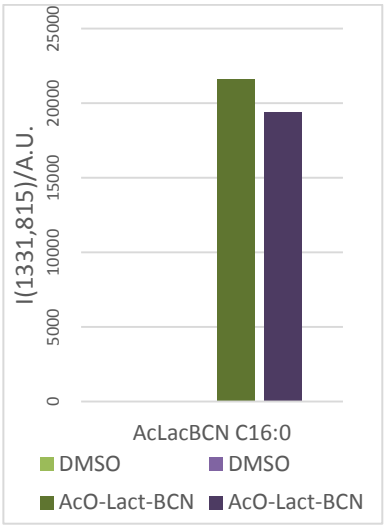

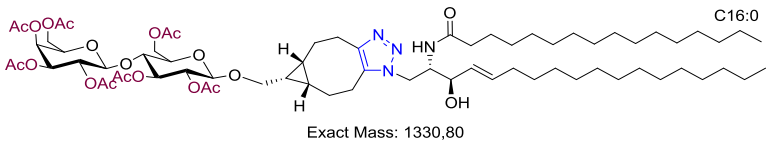

Figure 2.2.3.4: Ac-Lac-BCN-AzCer (C16:0)

< Graph 2.2.3.9: Ac-Lac-BCN *click* product with AzCer

To improve deacetylation we carried out fluid-phase uptake of a commercial esterase, pig liver esterase, which has been shown to increase drug metabolism.[195,196] We incubated cells with AzSph (0.5 µM, 8h), followed by either sequential treatment with Ac-Lac-MFCO (15 µM, 16h), then esterase (50 or 500 mU, 8h), or co-treatment with Ac-Lac-MFCO (15 µM) and esterase (50 or 500 mU) for 24h. No significant difference in the acetylation profile of esterase-treated cells was observed (Graph 2.2.3.10). When peracetylated glycan-

cyclooctynes where tested *in vitro* with commercial pig liver esterase, only minor deacetylation of 1 or 2 groups was observed, even at high enzyme concentrations in PBS buffer. Deacetylation could not be improved by first incubating cells with the peractylated glycan, followed by AzSph. In fact, no *click* product was formed (data not shown).

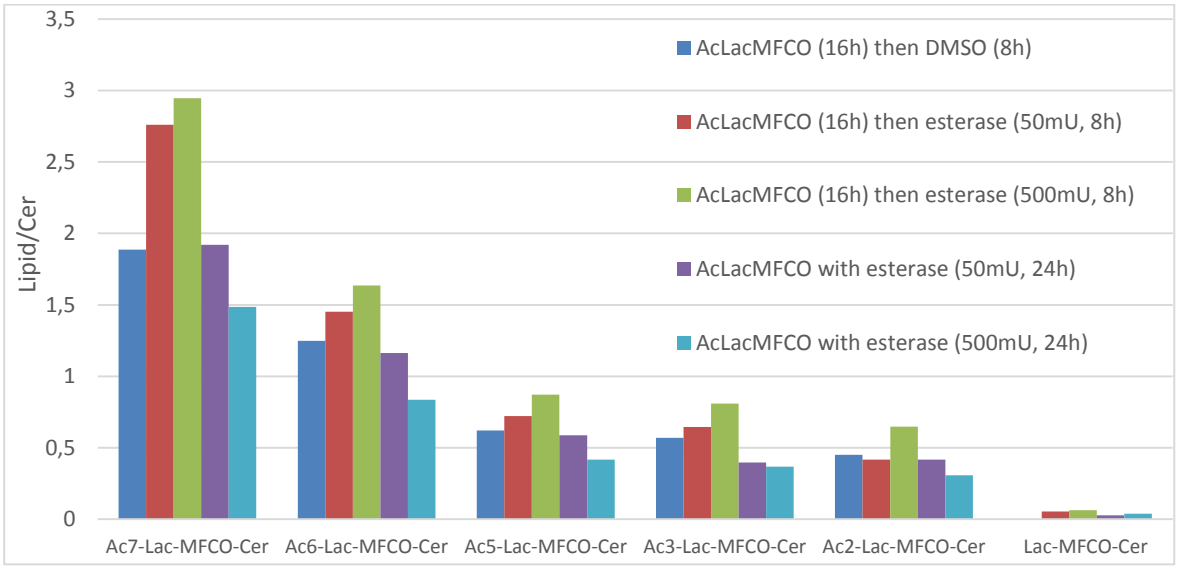

Graph 2.2.3.10: Ac-Lac-MFCO-AzCer lipid profile of cells treated with AzSph (0.5 µM, 8h), then sequential or co-treatment with Ac-Lac-MFCO (15 µM) and pig liver esterase.

Sarkar *et al.* described a bioactive disaccharide must be used at concentrations exponentially higher than the concentration of the same peracetylated disaccharide to show activity.[128] We must avoid using cytotoxic levels of our *clickable* glycan, since cytotoxicity levels of lactose-MFCO (tested by MTT assay as before (section 2.2.2)) were non-negligible. EC_{90} concentration was 10 µM, compared to lactose (EC_{90}=27 µM). Over 50% of cells were viable in conditions tested (EC_{50}>100 µM) over 24h (Graph 2.2.3.11).

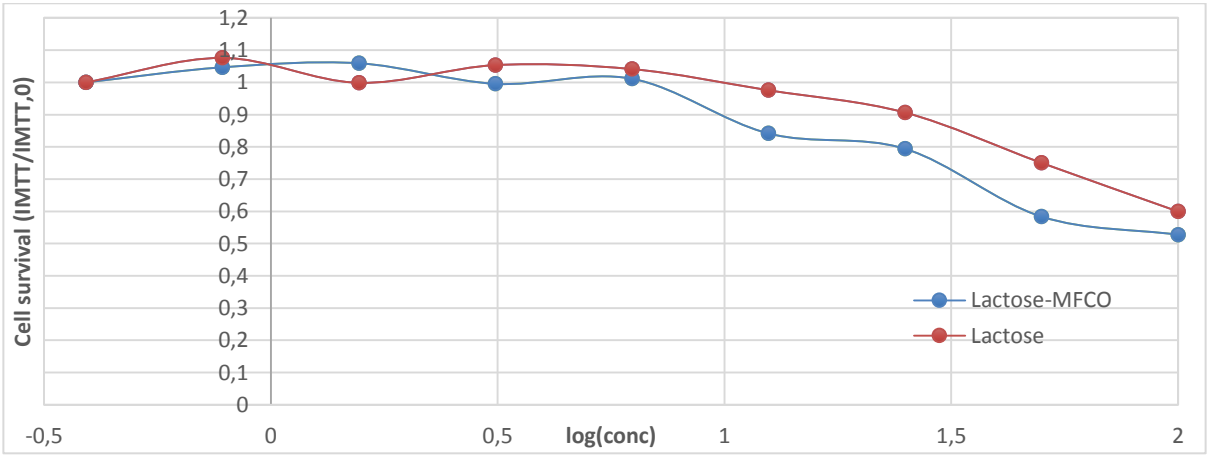

Graph 2.2.3.11: Lactose-MFCO cytotoxicity on GM95 cells over 24h.

We showed that incubating cells with higher concentrations of lactose-MFCO **49** and Gb3-MFCO **37** (20 µM) permits cellular *click* reaction with AzCer detectable by lipidomics. Approximately 2% of AzCer is *clicked* with lactose-MFCO **49** after 24h, and 4% after 48h (Graph 2.2.3.12). 10% of AzCer appears to be *clicked* after 48h with no serum, where cell proliferation is halted. However, over 50% cell death is observed under serum starvation conditions after 48h for CHO cells. Gb3-MFCO **37** showed similar extent of *click*, forming up to 0.1$_{mol}$% of all lipids extracted (Graph 2.2.3.13). In spite of these encouraging results, the levels of surface Gb3 is not high enough to observe STxB binding in immunofluorescence (IF) experiments.

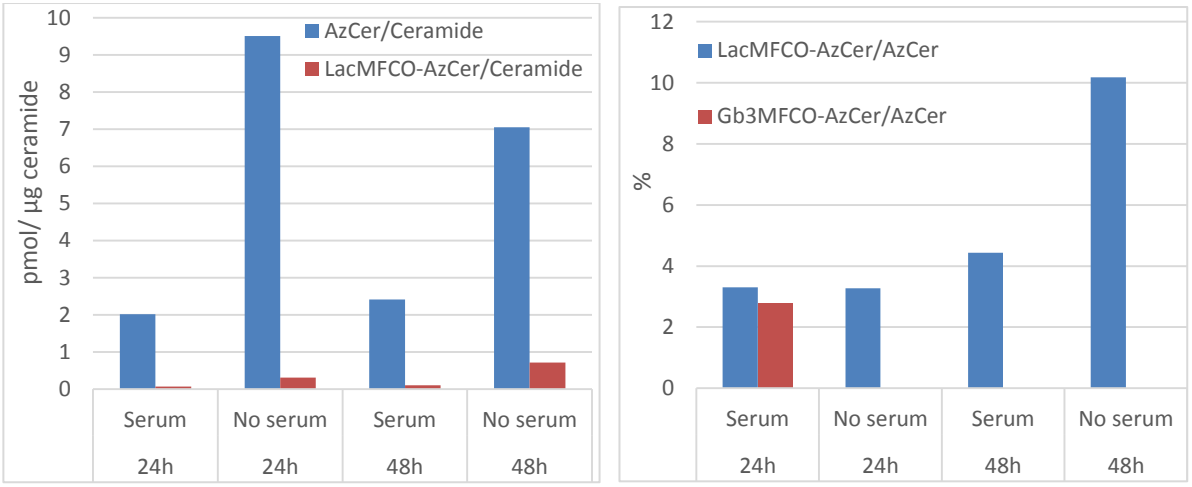

Graph 2.2.3.12: AzCer formed from AzSph (0.5 µM, 6h) in CHO cells and *clicked* product with Lac-MFCO **49** or Gb3-MFCO **37** (20 µM, 24/48h) w/o serum, normalise to ceramide and AzCer.

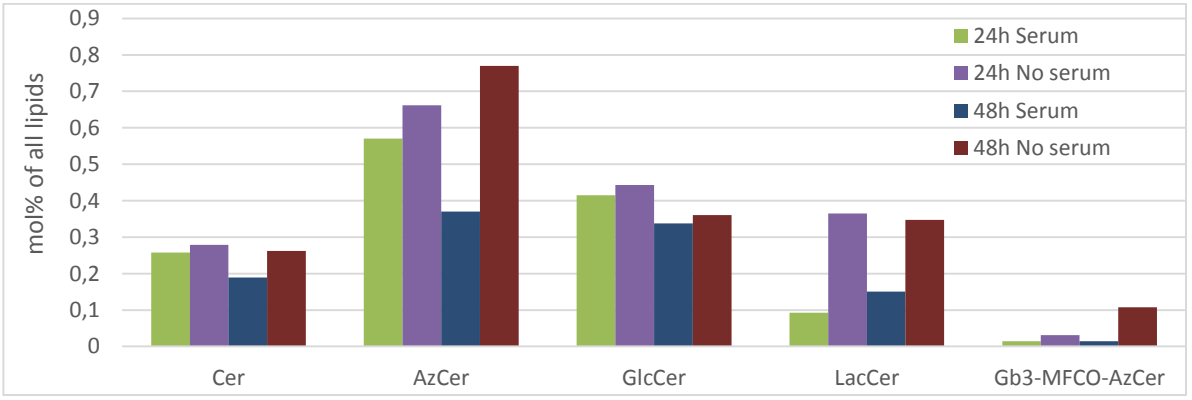

Graph 2.2.3.13: Sphingolipids and GSLs present, as a molar % of all lipids in cells treated with AzSph (6h, 0.5 µM) then Gb3-MFCO (20 µM).

2.2.4 Changing the lipid precursor to change localisation

To circumvent the necessity of using peracetylated *clickable* glycans, we would ideally have our azide group present in high amounts at the plasma membrane (PM). The current dogma suggests that the PM houses longer lipids, and transmembrane proteins with longer transmembrane domains, whereas the Golgi and ER membranes are thinner.[197] To increase presence of a *clickable* azidolipid at the PM, we would install a longer lipid chain.

According to the natural biosynthesis (Introduction 1.5, Figure 1.4.3b), **sphinganine** (Scheme 2.2.4.1) is acylated to dihydroceramide by all ceramide synthase (CerS) enzymes 1-6 with various acyl chains C16-24. Whereas, **sphingosine** is acylated to ceramide by CerS5, which has a specificity for C16 chains. Like plant-derived phytosphingosine is accepted in mammalian cells for cosmetic and biomedical studies, 1-azidophytosphingosine (AzPhy, **31**) showed similar cytotoxicity to that of 1-azidosphingosine (AzSph); EC_{50} = 2 µM and 3 µM respectively, in GM95 cells.

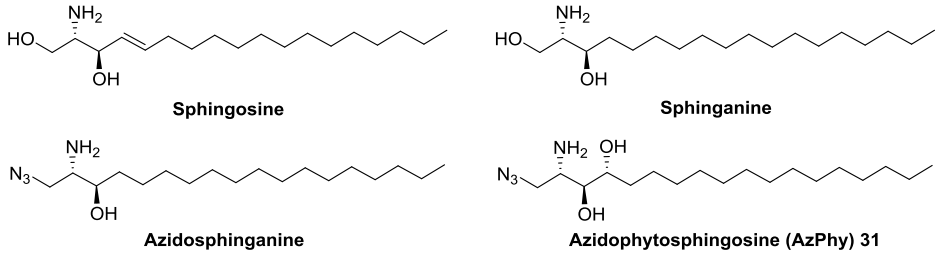

Scheme 2.2.4.1: Ceramide precursors: sphingosine (CerS5 substrate in salvage pathway) and sphinganine (CerS1-6 substrate in *de novo* pathway), with possible azidolipid analogues.

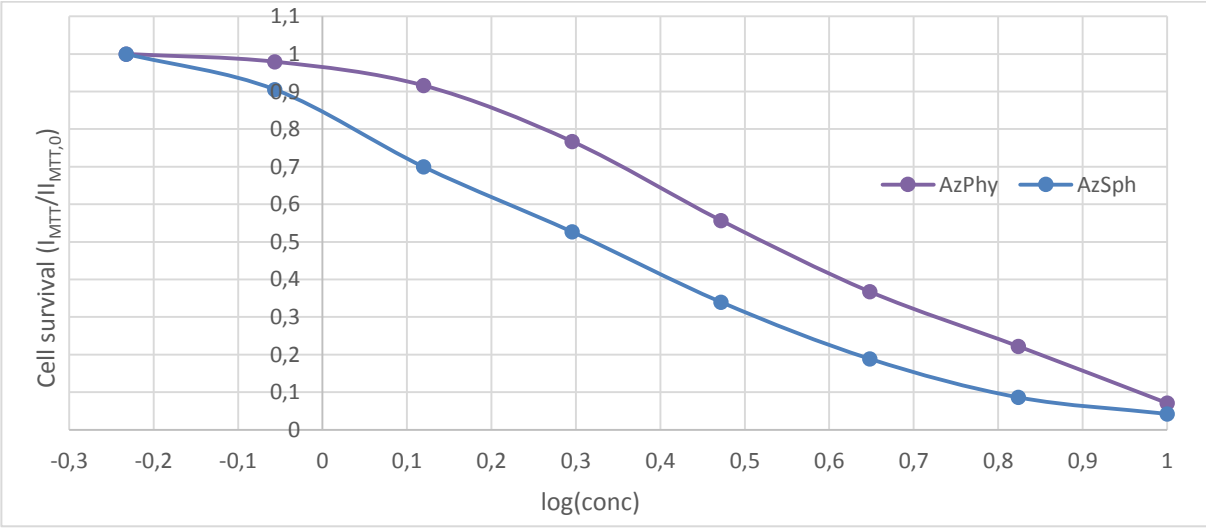

Graph 2.2.4.1: Cytotoxicity of AzPhy and AzSph in GM95 cells over 24h.

To compare AzPhy **31** metabolism with that of AzSph **17** (Results 2.2.2), we incubated cells with AzPhy (0.5 µM) for various time points, lysed the cells, extracted lipid membranes as before (Experimental 6.2.5), and analysed their metabolism profile by HRMS. As expected, we observe acylation to 1-azidophytoceramide (AzPhyCer) (Graph 2.2.4.2) with an acyl chain profile comprising a higher percentage of long acyl chains (C18, C22, C24) than short C16 chains. In GM95 cells, the acyl chain length profile is intermediate to that of AzCer formed from AzSph and native ceramide (Cer). In CHO cells, the profile is almost identical to that of native ceramide, which has fewer long chain ceramides compared to GM95 cells anyway (Graph 2.2.4.3). In both cell types, at 0.5 µM of AzPhy we observe steady acyl chain profiles of natural ceramide over 72h, with approximately 2:1 AzPhyCer/Cer, as observed for AzSph. The quantity of AzPhyCer stabilises in GM95 cells throughout 72h incubation (Graph 2.2.4.4), whereas cellular levels increase continuously in CHO cells (Graph 2.2.4.5).

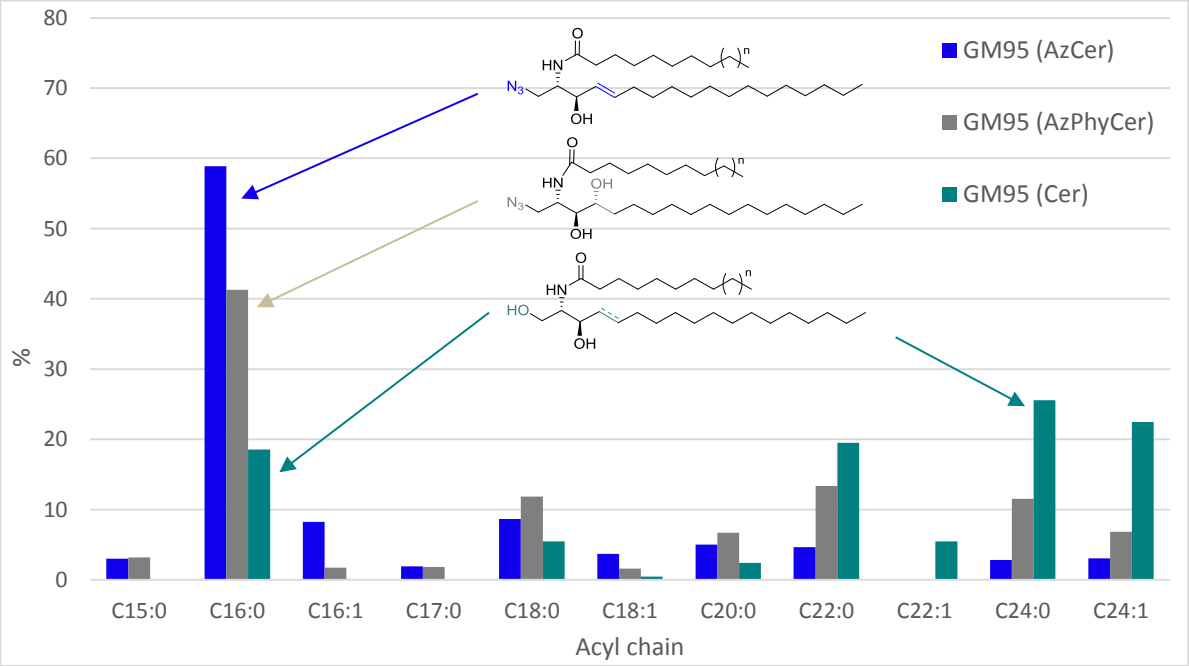

Graph 2.2.4.2: Acylation profile of sphingolipid analogues AzSph (forming AzCer, blue) and AzPhy (forming AzPhyCer, grey), compared with native ceramide (Cer, green), in GM95 cells after 24h incubation.

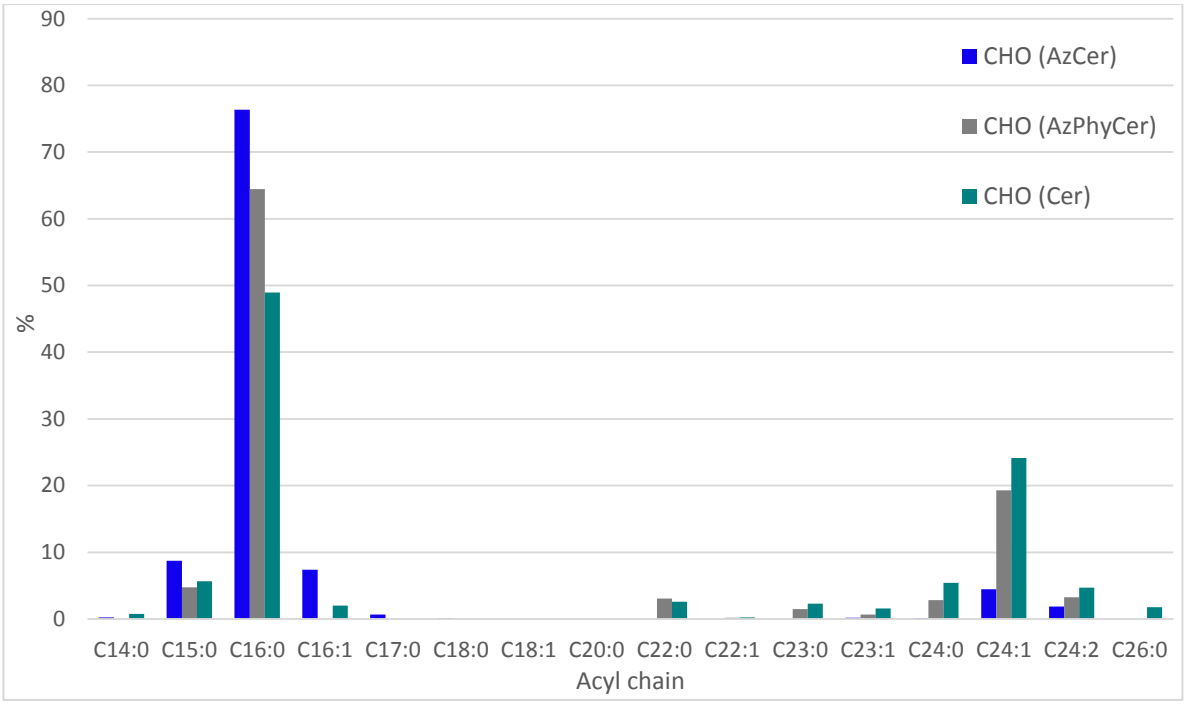

Graph 2.2.4.3: Acylation profile of sphingolipid analogues after 24h incubation.

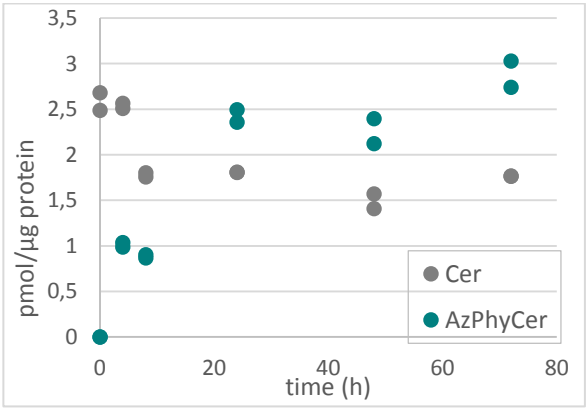

Graph 2.2.4.4: GM95 cells, accumulation of AzPhyCer on AzPhy incubation, and native ceramide (Cer). Data points from two MS injections of each condition.

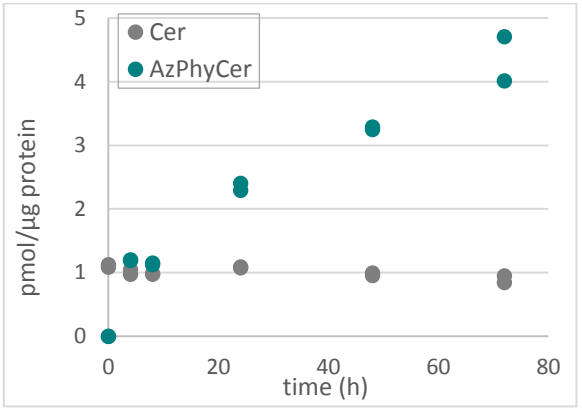

Graph 2.2.4.5: CHO cells, accumulation of AzPhyCer on AzPhy incubation, and native ceramide (Cer). Data points from two MS injections of each condition.

The localisation of AzPhy metabolites, i.e. AzPhyCer, was probed with hydrophilic Alexa488-DIBO and hydrophobic, permeable TAMRA-DIBO. Specific staining was observed with both fluorophores in live CHO cells overnight. Both AzPhyCer and AzCer show similar intracellular staining. The *click* reaction with hydrophilic Lac-MFCO **49** was not more efficient on the surface – AzPhy metabolites appear to be no more accessible than AzSph metabolites.

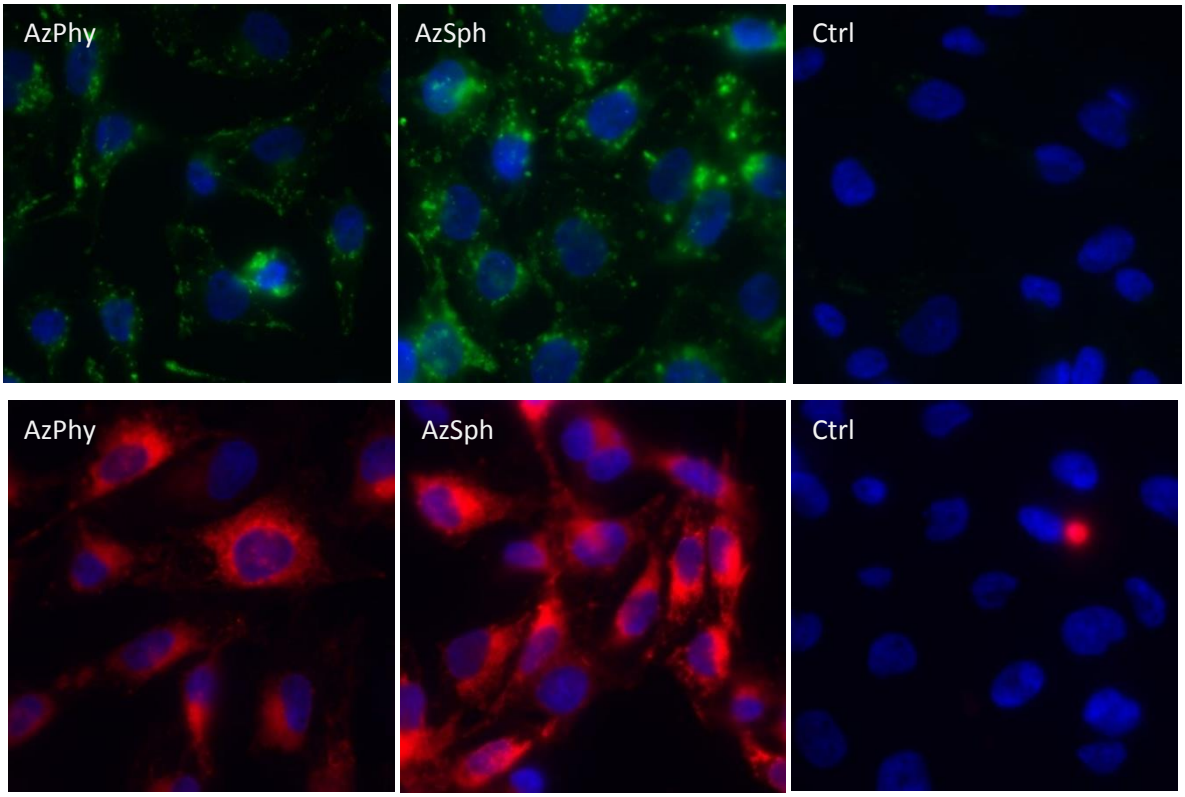

Figure 2.2.4.1: CHO cells treated +/-AzPhy or AzSph (1 µM, 6h), followed by Alexa488-DIBO (1 µM, 16h, green) or TAMRA-DIBO (1 µM, 16h, red), fixed, permeabilised and imaged by epifluorescence.

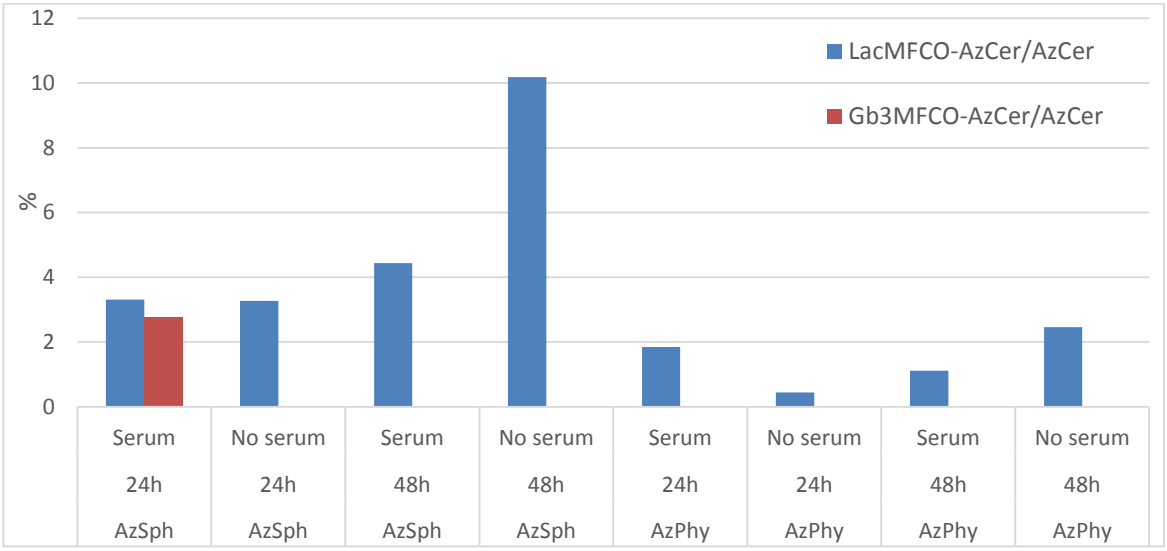

Graph 2.2.4.6: AzCer formed from AzSph (0.5 µM, 6h) in CHO cells, and *clicked* product with Lac-MFCO **49**or Gb3-MFCO **37** (20 µM, 24/48h) w/o serum.

3 DISCUSSION

3.1 Phospholipid strategy

The lack of methods for efficient reconstitution of natural, long-chain GSLs has thus far hindered their study. Phospholipids are more easily taken up into cell culture, to the extent that they are used to make liposomes for transfection and drug delivery agents.[63,198] Synthetic glyco-phospholipids, with enhanced cellular uptake, could constitute a valuable tool in studying the "glycocode" represented by GSL head groups.[199,200] Previously, phospholipid analogues of GSLs, or function-spacer-lipid (FSL) constructs, have been used to study GSL binding and antigen properties.[175] The Gb3-phospholipid analogue (Scheme 3.1.1), showed verotoxin (STxB) binding on TLC and could protect cells in culture against HIV-1 virus infection, similar to natural Gb3-Cer.[174] Ewers *et al.* showed that a GM1 analogue with a phosphatidylethanolamine (PE) lipid tail could be recognised by Simian virus 40 (SV40) which induced membrane curvature on giant unilamellar vesicles (GUVs), and allowed for SV40 trafficking into cells.[29] We set out to form a FSL construct of Gb3 with a short spacer region between the phospholipid tail and triose head group. The length of the spacer is imperative to the receptor function, as shown by Pezeshkian *et al.*, where Gb3-spacer-Cer analogues with spacer lengths >1 nm inhibited STxB clustering, curvature generation and trafficking into cells (Introduction 1.3).[24]

The lipid raft theory proposes that sphingolipids and cholesterol separate into ordered domains in a lipid membrane,[38,201] whereas common phospholipids such as 1,2-dioleoyl-*sn*-glycero-3-phosphocholine (DOPC) and 1,2-dioleoyl-*sn*-glycero-3-phosphocholine (DOPE, Scheme 3.1.1) occupy less ordered regions of the lipid bilayer. Despite theoretical reasoning that phase separation of phospholipids and sphingolipids in the biological membrane may inhibit receptor function of an FSL construct, the above-mentioned study by Ewers *et al.* on a GM1-phospholipid analogues demonstrates otherwise.[29] Furthermore, Shiga toxin binding on Gb3-Cer-presenting liposomes can induce lipid organisation in basic membrane models,[36,202] indicating that initial Gb3-Cer domain organisation is not necessary for toxin binding and clustering. STxB-induced membrane invagination is not affected when liposome models are constituted of 5 or 30_{mol}% Gb3-Cer, indicating that dense clusters of GSL are not necessary for

membrane bending (Introduction 1.2).[24] We can thus propose that preliminary sphingolipid organisation is not necessary for STxB binding, clustering and membrane bending.

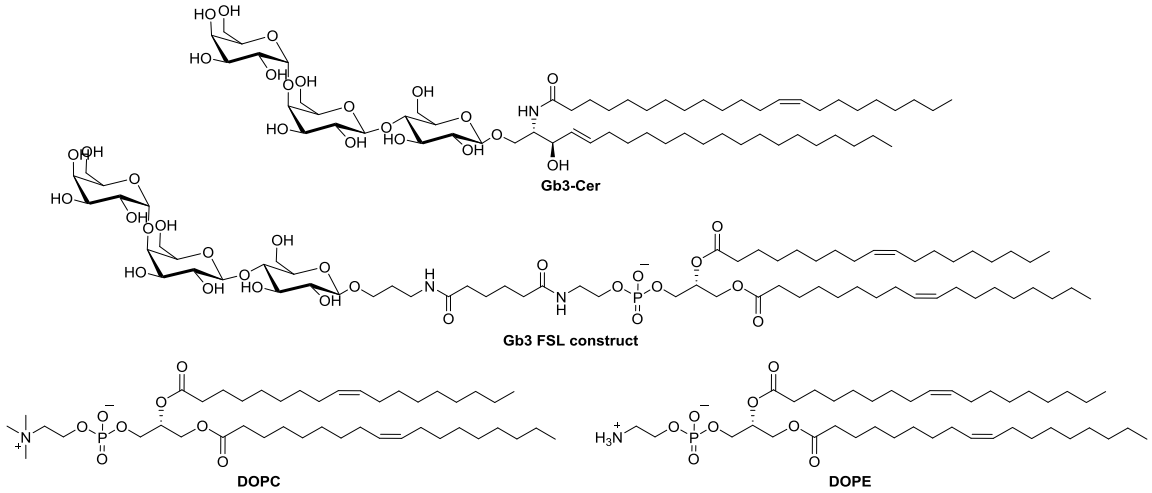

Scheme 3.1.1: Natural Gb3-Cer; synthetic Gb3-phospholipid analogue, FSL construct; common phospholipids DOPC and DOPE.

To synthesise the Gb3-phospholipid analogue we must consider the chemical conjugations available to link the two opposing parts, Gb3 triose and a phospholipid, which each present distinct compatibility and stabilities in synthetic reaction conditions. The strategy in this endeavour must account for two major challenges: the high cost of glycan and lipid starting materials, thus necessitating a short synthesis (few steps); and the various functional groups present. Eleven hydroxyl groups on the triose and unstable esters and phosphoester groups in the lipid require specific conjugation reactions and no cross-reactivity. Throughout these synthetic considerations, one must always consider the biological functionality and biocompatibility of the final target molecule.

One popular bioorthogonal conjugation between a glycan's anomeric hemiacetal and a primary amine (e.g. DOPE) is a reductive amination. This results in the opening of the first glycan (Scheme 3.1.2), and was used by Ewers *et al.* at the reducing end of GM1 pentasaccharide.[29,203] All three glycans in Gb3 are held within the binding pocket of STxB, therefore modifying the structure of one of these glycans could be detrimental to STxB recognition. Additionally, opening the first glycan could risk that the Gb3 analogue becomes too flexible to permit native biological properties.

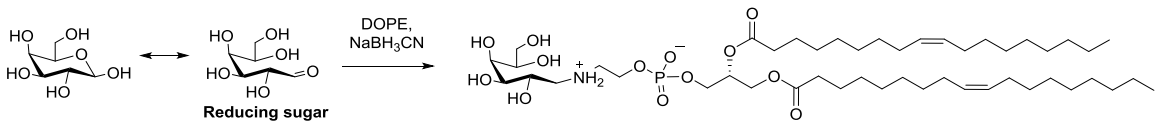

Scheme 3.1.2: Reductive amination of aliphatic amines with reducing sugar.[203]

We tested syntheses with and without hydroxyl protecting groups on the triose (Results 2.1.1). Those syntheses for which protecting groups were installed, including the isothiocyanate conjugation (Fig 3.1.3), proved infeasible since deprotection was impossible without simultaneously removing the ester-bound lipid tails.

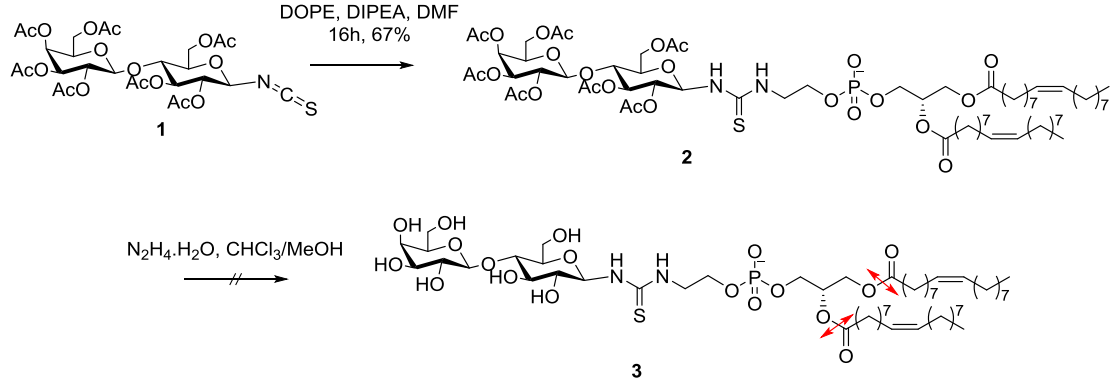

Scheme 3.1.3: Attempted thiourea synthesis from isothiocyanate-functionalised glycan.

In order to avoid using protecting groups, we sought to use specific conjugation conditions between small chemical moieties that are easily installed onto the two starting materials: triose and phospholipid. Because of the instability of ester and phosphoester bonds in phospholipids, this specific conjugation must take place in mild conditions. *Click* chemistry reactions became popular for their fast kinetics, high yields and mild conditions. The copper-catalysed alkyne-azide cycloaddition (CuAAC) is perhaps the most well-known and presents the smallest spacer group, a triazole (Scheme 2.1.1.1). The triazole is also considered to be highly biostable.[204]

The attempted syntheses of alkyne- or azide-functionalised *clickable* phospholipids are described (Results 2.1.1). However, a *clickable* phospholipid was not isolated to *click* with the Gb3 head group due to the small scale, lack of sufficiently anhydrous conditions, and the instability of the cyclic phosphate intermediate **11** central to the synthesis. Reactions were successful on 1-octanol and 1-decaoctanol models, forming phosphates **9** and **14** (Scheme 3.1.4). If the synthesis were to be revisited, one must take all precautions possible to obtain the driest possible conditions and timely purify products.

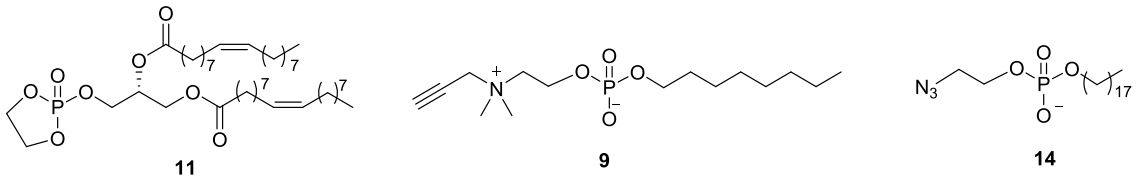

Scheme 3.1.4: Clickable phospholipid analogue models successfully isolated and characterised.

Kolb, Finn and Sharpless coined the term *click* chemistry in a review published in 2001,[131] in which they describe the need for protecting groups as "the most insidious problem" of synthesis in its growing complexity, and hail chemistry's liberation from organic solvents. Using protecting groups innately requires two extra steps: protection and deprotection, and an overall poorer atom economy.[205] As hydrophobic groups, they simultaneously necessitate the use of unecological organic solvents over aqueous solvents. The draw of protecting group-free chemistry is manifold, reducing costs in time and resources. They were probably not considering phospholipid synthesis when they imagined a straightforward water-soluble synthesis. However, one can still try to apply these principles to lipids.

3.2 Clickable sphingolipid synthetic strategy

We diverted our efforts to another *click*-based strategy: to reconstitute Gb3 by metabolically labelling sphingolipids with an azide moiety, onto which we could *click* the functionalised oligosaccharide head group of choice. The choice of chemical *click* groups, azide and cyclooctyne, was primarily based on their small size and biocompatibility, since the length and flexibility of the final Gb3 analogue was of highest importance.

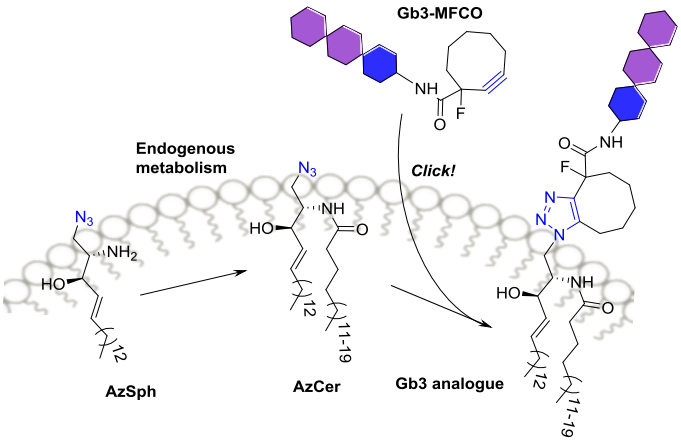

Scheme 3.2.1: GSL reconstitution via *click* chemistry.

Most *click* studies apply a standard format: cellular incorporation and native metabolism of a biomolecule analogue labelled with a small *clickable* moiety, followed by *click* with a reporter (fluorophore or biotin) (Introduction 1.6, Figure 1.6.1). In this project, we attempt to introduce biological activity using a *click* conjugation. Few reports attempt to recreate lost or supressed native downstream signalling interactions, despite most papers agreeing that lipids and glycans are important signalling molecules. Prescher *et al.* even suggest that azide-labelled sialic acids should not interfere with signalling, since they are present at approximately 3% of the sialic acids.[127] Our conjugation is performed before the desired biological activity, thus we must have the smallest possible *click* groups. Simultaneously, the *click* partners must be selective enough to react on the complex cellular environment, on live cells.

We sought the smallest possible spacer region between lipid and glycan, which conjugates specifically and quickly, ideally within 24h.[192,206,207] The toolbox of azide *click* partners includes the Staudinger phosphine reagents, alkynes for copper-catalysed cycloaddition, and cyclooctynes for strain-promoted copper-free alkyne-azide *click.* A cyclooctyne appeared to be most adapted to our system due to the range of size and reactivity available, relatively simple formation, and their stability in storage and *in cellulo* compared with phosphines, which are highly sensitive to oxidation. Amongst the variety of cyclooctynes, monofluorocyclooctyne (MFCO) was chosen for its ideal balance between small size and fast reactivity with azides (Introduction 1.6).[114,145] The reactivity is not as high as some popular dibenzocyclooctyne derivatives (DIBO, DIBAC, etc, Figure 3.2.2) but the small size of MFCO is highly desirable in our project. It is easily accessible via a four step synthesis (Scheme 3.2.3),[148] and had been previously used in the laboratory.[191] The major drawback we found was that the free carboxylic acid MFCO **22** was unstable and could not be stored for more than 6 months.

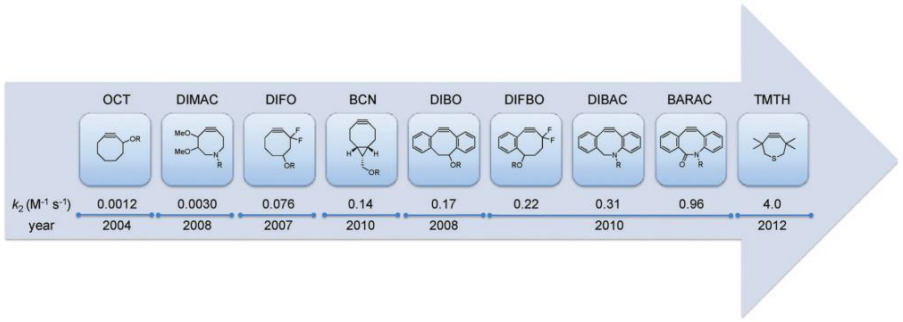

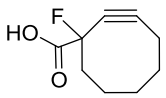

MFCO, 45

Figure 3.2.2: Evolution of alkyne reagents for strain-promoted azide-alkyne cycloaddition.[150]

Azides are ideally small and stable in cells (Introduction 1.6).[147] An azide was installed at the head position (C-1) in the place of the natural hydroxyl group of sphingosine, since this would form the most linear GSL analogue. The azide group is less hydrophilic than the hydroxyl group, and may or may not be held within the hydrophobic layer of the lipid bilayer when in a biological environment. Despite this, we were confident it would retain its reactivity with a hydrophobic cyclcooctyne partner, as many literature reports suggest that *click* reaction *in cellulo* and in liposomes can occur with lipids functionalised with a hydrophobic moiety held within the membrane.[170,208] Garrido *et al.* showed that 1-azidoceramide incorporated into liposomes could undergo efficient copper-catalysed *click* reaction with an alkyne-fluorophore.[209]

Even before the rise in *click* chemistry, the azide was a common functional group on the synthetic route to amines, to which azides are easily reduced.[210] The azide group is so stable and convenient it is used as an amine protecting group,[181] the latter being sensitive to oxidation and carboxylation in long term storage. Phytosphingosine (Scheme 2.1.2.4) is an ideal inexpensive starting material, with stereochemistry in the 2,3-positions identical to that of sphingosine, and multiple syntheses to sphingosine have been reported.[182,211,212] Synthesis of sphingosine was mastered in the laboratory, to obtain natural Gb3-Cer for various structure-function studies.[24,27,35,54] We follow the synthesis described by Kim *et al.*[181] to sphingosine **6** (Scheme 3.2.2), installing an azide protecting group in the N-2 position for two major advantages: the azide is non-nucleophilic, thus avoids possible cyclisation side reactions (Scheme 2.1.2.2), and the azide cannot form a hydrogen bond with the terminal hydroxyl group and the N-2 position, thus facilitating the ensuing functionalisation, in this case the selective O^1-silyl protection.[182]

After protection and installation of the double bond selectively at the C-4 position in **6** (Scheme 3.2.3), we protected the C-3 hydroxyl with a benzoyl (Bz) group as in **7**, as has been performed in the past for the natural Gb3-Cer synthesis, and because we considered this was the most stable form for long-term storage of a large-scale synthesis. Once we obtained sphingosine **22**, we swapped the N^2-azide for dichloroacetamide in **24** in order to eventually install the N^1-azide. One disadvantage in this route is that on deprotection of the azide, the benzoyl can transfer to the amine, forming the thermodynamically more stable amide product (NHBz) (Scheme 3.2.3). In hindsight, we could have avoided the parasitic NHBz rearrangement by deprotecting the azide earlier, from compound **21** (Scheme 3.2.1),

installing the dichloroacetamide and then performing benzoyl protection. Instead we managed this drawback by simply protecting the free amine with the dichloroacetamide immediately after purification. Alternatively, we could have tried another orthogonal amine protecting group from the beginning, for example the tetrachlorophthalimide (TCP) used by Panza *et al*.[182] (Scheme 3.2.1), which presents the same advantages as the azide protecting group and can be deprotected orthogonally, although harsher installation conditions are required. This would have avoided needing to change the protecting group.

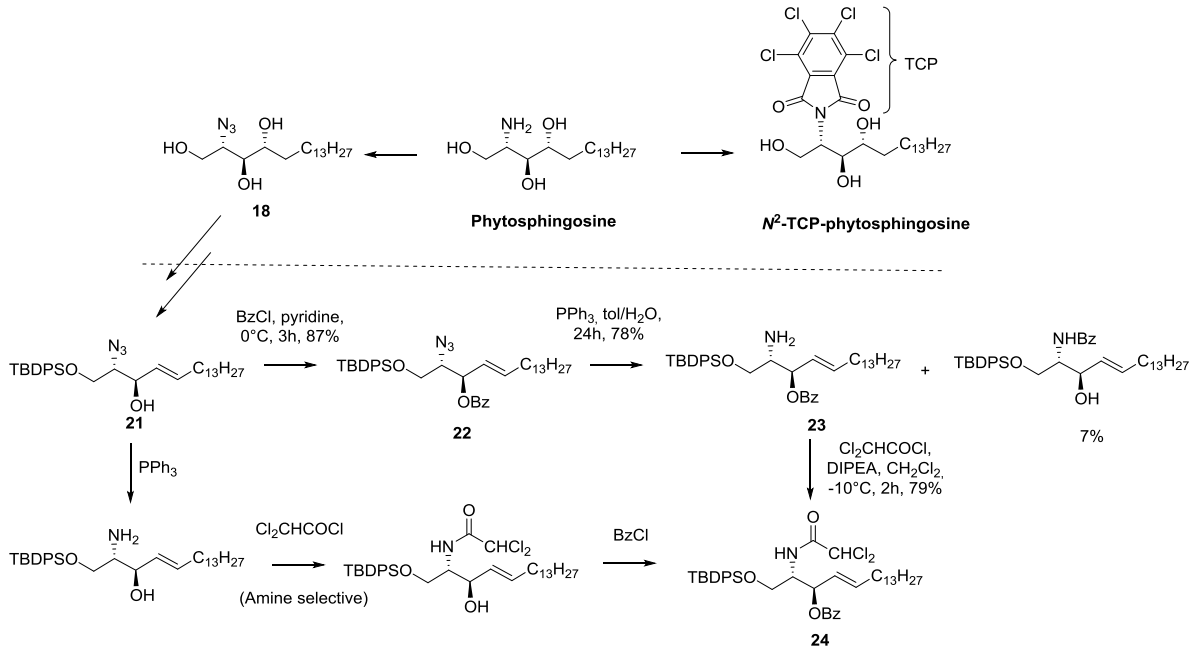

Scheme 3.2.3: Envisageable alternatives to our AzSph synthesis.

We chose the *N*-dichloroacetamide protecting group following the investigations by Haifei Gao, a previous PhD student, who tested first the *N*-Boc group and characterised the oxazoline cyclisation product (Results 2.1.2, Scheme 2.1.2.2), and showed its formation was less important when an electron-withdrawing protecting group was used. This cyclisation continued to hamper the synthesis during the installation of a leaving group at the C-1 position even with the dichloroacetamide group. We observed that a stepwise transformation from mesylate (Ms), to iodide, to azide gave the highest yield with less cyclisation product. Converting directly from mesylate to azide, for example, produced the cyclisation product in majority. Although lengthy, one must accept in multistep synthesis that the highest overall yield may be obtained from a strategy with more steps.[212] As is often the case in chemical biology project, we did not further optimise the synthesis, but continued to cellular testing of AzSph after the final deprotection step.

The synthesis of 1-azidosphingosine (AzSph) has been reported in the thesis of M. Garrido Martínez (Scheme 3.2.4).[184] The synthesis begins with an amino acid starting block and uses a bridging protecting group on the C2 and C3 position. Thus they could not observe the same cyclisation as ours. However, they were confronted with the formation of a pyrroline side product and an extremely low-yielding deprotection step.

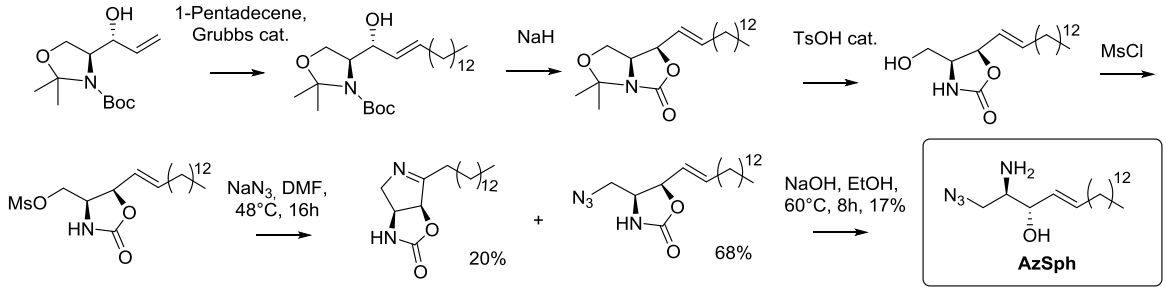

Scheme 3.2.4: Garrido Martinez synthesis to 1-azidosphingosine.[184]

Alongside AzSph, used for cellular labelling, we synthesised AzCer. This would be used for two purposes: (1) as an internal standard in mass spectrometry (MS) experiments to quantify the cellular acylation of AzSph to AzCer, synthetic standard in HPTLC migration studies, and (2) for the synthesis of *clicked* glycolipid analogues and the testing of their membrane-bending properties in liposomes.

Enzymatic acylation of AzSph to AzCer proved to be the most efficient synthesis on a small scale (Results 2.1.2). The enzyme used, SCDase, is a common chemoenzymatic reagent used to form modified sphingosines and ceramides, and is highly adaptable to acylation or deacetylation dependant on buffer pH.[213,214] Since AzCer was used to form the *clicked* GSL analogues (Scheme 2.1.3.1) for model membrane testing, we installed the erucic acid (C22:1) chain which shows function in liposomes with STxB in one literature report, where the C22:0 chain does not.[27]

MFCO **45** was synthesised by Mélanie Le Hénaff according to the synthesis shown (Schme 3.2.5). **45** and MFCO-Gly **46** are conjugated to Gb3 triose **44** as a racemic mixture (Results 2.1.3). Once conjugated to a glycoside, with a proximate stereogenic centre at the anomeric position, the two diastereoisomers are formed, faintly visible by TLC (different R_f). TLC indicated approximately a 50:50 ratio. We did not attempt to purify the R/S isomers since we considered that the right-left tilt in the plane of the length of the Gb3 analogue would not have much effect on Shiga toxin binding and membrane bending.

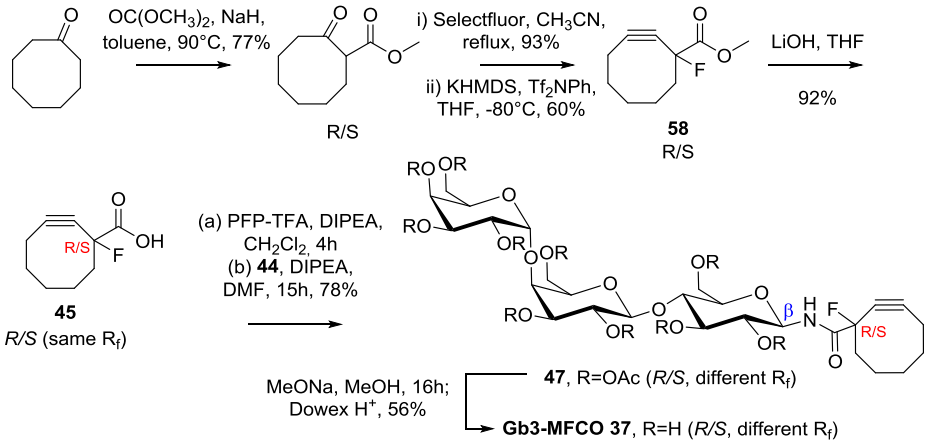

Scheme 3.2.5: Standard non-enantioselective MFCO synthesis[148] and formation of diasteriomeric mixture of MFCO-functionalised triose. Click reaction with AzCer gives cis/trans regioisomers.

We synthesised two *clickable* glycan head groups, Gb3-MFCO **37** (Scheme 3.2.3) and Gb3-Gly-MFCO **38** (Scheme 3.2.6), in consideration of the strained angle at which the AzCer is held once *clicked* to the Gb3-MFCO **37**, where the flexible glycine linker would alleviate the angle constraint. Two flexible linkers were considered, glycine and ethanolamine (EA). Following the principles of convergent synthesis, we decided to conjugate the linker first to MFCO **45**, a product formed in a four step synthesis from cheap starting materials, rather than Ac-Gb3-NH_2 **44** or Ac-Gb3-OH **42b**, synthesised from seven or four steps from expensive glycoside starting materials. During the syntheses, the glycine route drew ahead as the most feasible, and will be applicable in later projects incorporating a photoactivable group (Perspectives 4).

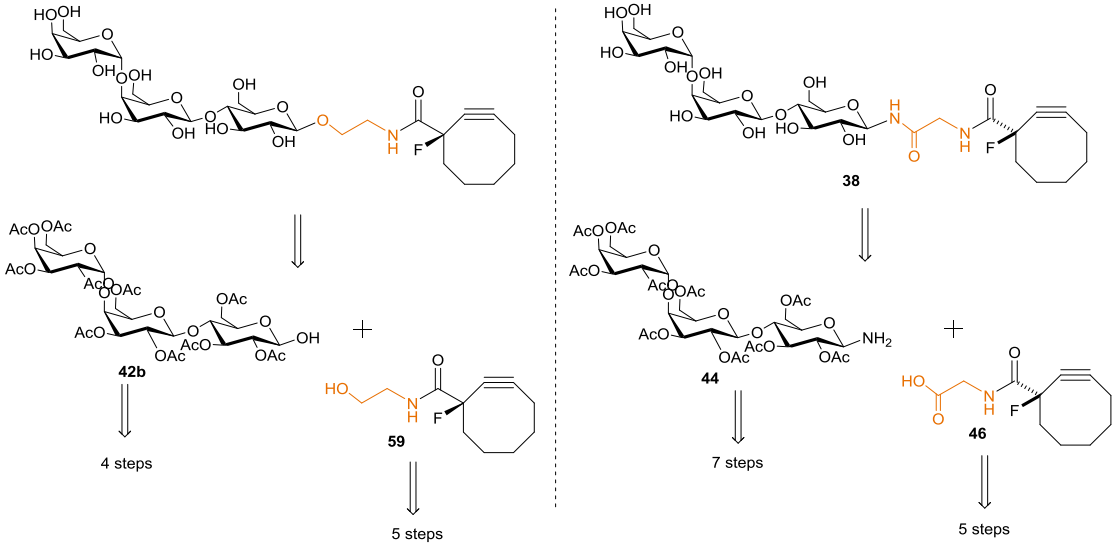

Scheme 3.2.6: Retrosynthetic analysis of Gb3-linker-MFCO.

Other linkers could have been envisaged, for example an ethylenediamine linker (Scheme 3.2.7), which can easily be installed on MFCO **45** and coupled with the reducing sugar **42b**. However, this strategy requires an excess of amine-MFCO reagent, and, for the amine linkage to be stable to hydrolysis, it must be "capped" with an acetate group.[215] This would add extra bulk to our linker, which may hinder biological activity.

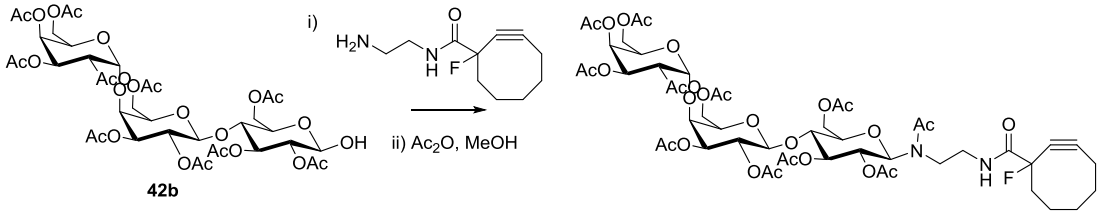

Scheme 3.2.7: Potential amine functionalisation of reducing sugar.

Unlike the copper-catalysed *click* cycloaddition, the copper-free *click* is not regioselective, thus the *cis* and *trans* regioisomers are typically formed in an approximately 50:50 ratio (Scheme 3.2.8), described in the supporting information of first literature report by Pigge *et al.*, and observed by TLC.[148] NMR and UPLC-MS analyses are insufficiently resolved to quantify further. We did not attempt to purify regioisomers to test their activity. In cells, we cannot prevent the two isomers from forming, so the molecule of interest is the *cis/trans* mixture. Commercially available bicyclo[6.1.0]non-4-yne (BCN) could also hold potential in this project. Is it slightly longer than MFCO, but its functional groups, alcohol and alkyne, are at opposite ends of the cyclooctyne, creating a straighter molecule when *clicked* (Scheme 3.2.6), in which the *cis/trans* diastereoisomers are more symmetrical.

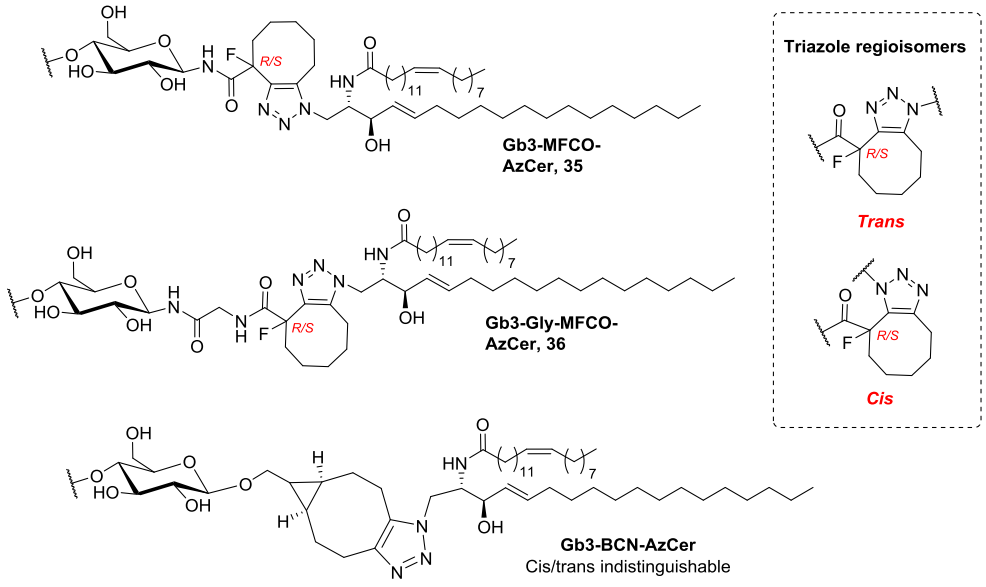

Scheme 3.2.8: Final *clicked* Gb3 analogues.

3.3 Model membrane testing

Giant unilamellar vesicles (GUVs) provide a single bilayer of homogeneous size similar to that of a cell (typically diameters of 10-30 µm). GUV testing is the classical method for investigating membrane bending properties, as they can be observed under the microscope. We followed the protocol of the pioneering report of membrane tubulation induced by Shiga toxin on GUVs containing Gb3-Cer.[27] Although membrane invaginations can differ with the tension and osmolarity of GUVs, the results are a robust indication of basic mechanochemical properties of the glycolipid-lectin interaction.

The two *clickable* glycan head groups, Gb3-MFCO **37** and Gb3-Gly-MFCO **38**, were tested in order to compare the importance of the strained angle at which the AzCer is held once *clicked* to the Gb3-MFCO **37**. The flexible glycine linker would alleviate the angle constraint. We remained within the constraints set out in the structure-activity study of Gb3-EG_n-Cer analogues (Introduction 1.3), which concluded that 10Å constituted an important guideline for the maximum length spacer region, as in Gb3-EG_1-Cer. Gb3-Cer analogues **35** and **36** were within this constraint, and both GSL analogues retained membrane bending properties in complexation with STxB in GUVs.

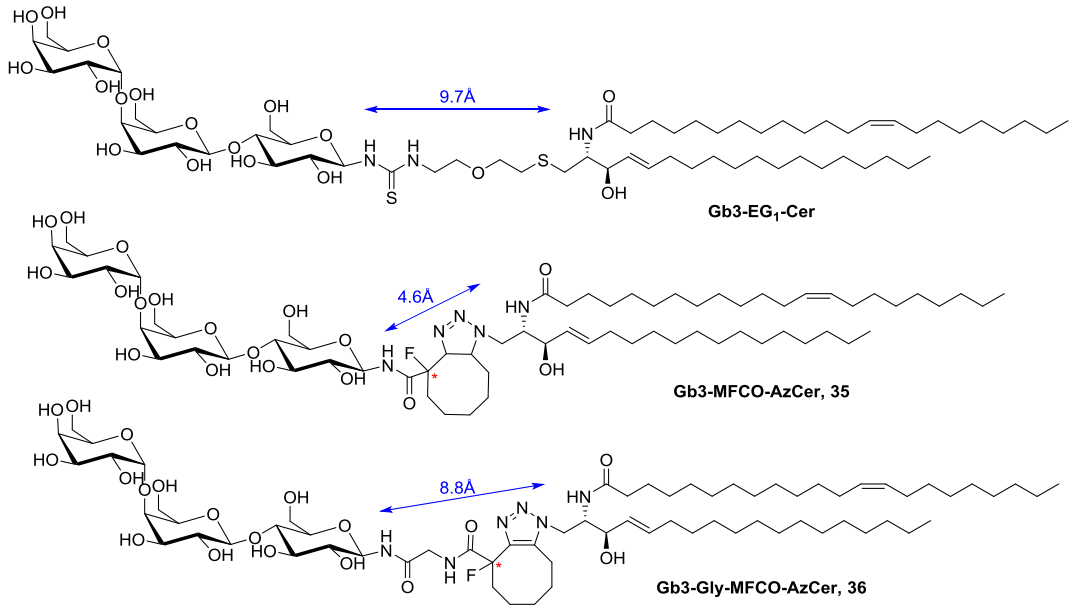

Scheme 3.3.1: Final Gb3 analogues spacer regions compared with confirmed functional Gb3 analogue.[24]

GUVs are extremely simplified systems compared to the cell membrane, which contains much more heterogeneity in lipid and protein composition. We considered this indication of

membrane curvature on GUVs sufficient to test the molecules in cells, despite the fact that the cellular system is so chemically different.

We tested the *click* reaction on LUVs constituting 5% AzCer, since LUVs are simpler to prepare and have similar chemical reactivity to GUVs, and are often used in the literature.[216,217] GUVs are typically used for microscopy observations, while LUVs can be obtained in high quantities for biochemical studies. We observed very slow *click* kinetics. This could be explained by the concentrations used, since *click* cycloadditions are extremely dependent on concentration. Salomé *et al.* use similar LUV concentration (100 nM of lipid) and observed 37% conversion after 24h with the solution phase reagent in large excess, whereas we used 1 equivalent.[218] Since this experiment required a large quantity of *click* reagents, we did not optimise the experiment, but preferred to use the material for cellular studies.

3.4 Sphingolipid metabolism

We began cellular testing on GM95 cells, a stable mutant cell line derived from mouse melanoma MEB-4 cells, which are deficient in GSLs due to a lack of glucosylceramide synthase (GCS) activity. Since we can envisage our reconstitution technique being applied to any glycoside head group, for the functional reconstitution of any GSL analogue, not only Gb3, we chose a system in which we could validate efficient reconstitution of any GSL. This cell line has been used in many previous studies on GSL function.[11,31,82] Chinese hamster ovary (CHO) cells were used to validate our results further in a second cell line, since they express some GSLs but lack the Gb3 synthase enzyme.

We followed the metabolism of 1-azidosphingosine (AzSph) into 1-azidoceramide (AzCer) in cells via acylation by ceramide synthase (CesS) enzymes. We first analysed azide metabolites by *clicking* with an alkyne-functionalised fluorophore *in vitro,* after cell treatment and lysis. This method, pioneered by Thiele *et al.*, involves separating the *clicked* biological sample, based on their polarity, on high performance thin layer chromatography (HPTLC) plates. This normally involves a purification step on the cell lysate; either protein precipitation[159] or lipid extraction,[219] to purify lipid components from aqueous metabolites, proteins and genetic molecules present in cells. We observe a specific band for AzCer *clicked*

with a fluorophore (Fig 3.4.1) without carrying out an extraction or purification step, but by simply resuspending cell lysate in methanol. Only once we began performing a lipid extraction step (Experimental 6.2.3), were we able to observe cellular AzCer by mass spectrometry (MS) from extracted silica of HPTLC plates or directly after extraction. Testing began with the hydrophilic fluorophore Alexa488-alkyne, and a specific, fast-migrating band which corresponded to AzCer-Alexa488 *click* product were observed by HPTLC (Figure 3.4.1). The migration properties of *click* product AzSph-Alexa488 was very similar to *unclicked* fluorophore and difficult to distinguish. With hydrophobic, copper-free *clickable* TAMRA-DIBO, we could distinguish AzCer and AzSph metabolites (Figure 2.2.2.1). Many reports use a hydrophobic *clickable* coumarin.

We performed all HPTLC experiments with high concentrations of AzSph (10 µM) due to the extremely poor resolution of HPTLC plates. To analyse the molar mass of azide-lipid species, silica from HPTLC plates was scratched off in specific regions, extracted in chloroform/methanol and analysed by MALDI-MS. Large quantities were required likely due to the poor ionisability of the amphiphilic, zwitterionic fluorophore-*clicked* lipid.

Cellular testing at 10 µM of AzSph induced remarkable cell death after 6h (Fig 3.4.1). Most reports describing the cellular incorporation of modified sphingolipids use a low concentration[165,208,220] compared with concentrations of modified fatty acids or phospholipids described, and for short incubation times.[140,155,159,161,221] However, Collenburg *et al.* showed that ceramides modified in the lipid chains were non-toxic in T cells, up to 25 µM for 2h.[162] Haberkant *et al.* tested the bifunctional sphingolipid, photoSph (Fig 3.4.2), at 0.1 µM, mentioning that no loss in cell viability is observed from 0.1 to 5 µM.[220] They cite the role of ceramide in apoptosis signalling as a reason for this toxicity.

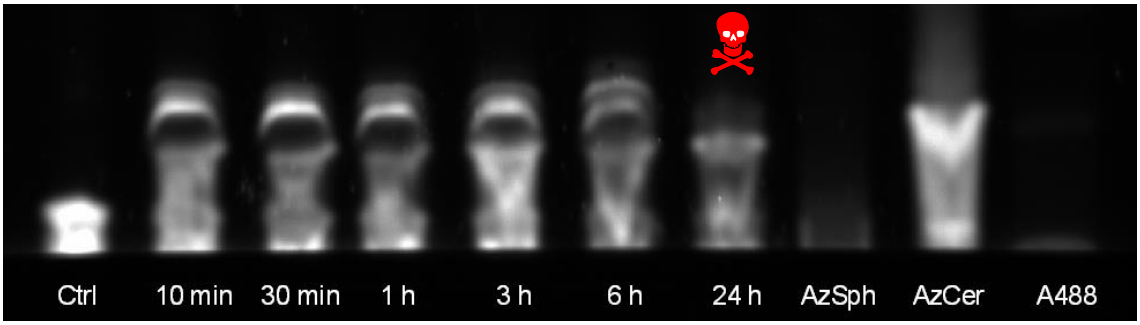

Figure 3.4.1: Incubation of AzSph (10 µM) on GM95 cells shows formation of AzCer. Cytotoxicity beyond 6 h. HPTLC separation of azido-metabolites clicked with alkyne-fluorophore (Cu(I), 3 mM) following lipid extraction.

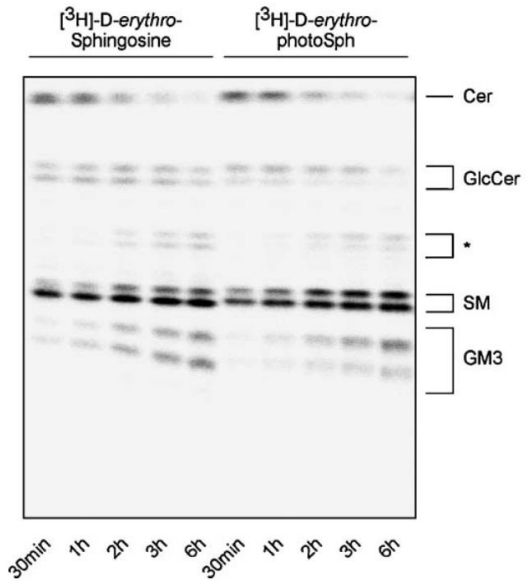

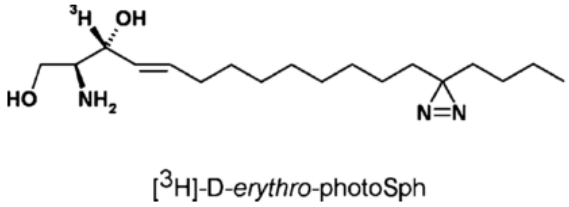

[3H]-D-*erythro*-photoSph

Figure 3.4.2. Photoactivatable sphingosine, photoSph, investigated by P. Haberkant *et al.,* is converted into photoCeramide within 5 min, and photoSphingomyelin (SM) and trisaccharide glycosphingolipid GM3 at longer incubation times.[220] Visualised by spraying with ^{3}H-specific Amplify Fluorographic Reagent.

Sphingolipids, particularly ceramide, are well-known modulators in apoptosis. Under stress, ceramide is produced from SM and GSLs, inducing apoptosis signalling.[88,222–224] Ceramide analogues which inhibit CerS, have been shown to inhibit proliferation or induce apoptosis.[225–227] Standard lipid membranes have a low concentration of ceramide (Cer <1%) compared with sphingomyelin (SM, 5-8%) and GSLs (2-8%), and even lower sphingosine (Figure 3.4.3).[80] Our sphingolipid analogue may affect such signalling pathways. We tested the cytotoxicity of AzSph using the MTT assay, measuring EC_{50} and EC_{90} values (concentrations at which 50% and 90% of cells are viable) for two cell lines (Table 3.4.1).

We observe a higher cytotoxicity of AzSph (and sphingosine) in GM95 than CHO cells. GM95 cells are deficient in the GlcCer synthase (GCS) gene (*UGCG*) which catalyses the first step on the pathway to all major GSLs (Scheme 3.4.5), and thus GM95 cells have a 1.5 times higher SM content compared to the parent cell line.[87] Thus, one of the two pathways to reduce sphingolipid stress signalling, via conversion of ceramide to GSLs/SM, is absent in GM95 cells. This ill-balanced sphingolipid equilibrium may explain why they may be more sensitive to AzSph cytotoxicity.

Table 3.4.1: EC_{50} and EC_{90} values of AzSph in two cell lines

	GM95 cells		CHO cells	
	AzSph (n=9)	Sphingosine (n=6)	AzSph (n=3)	Sphingosine (n=3)
EC_{50}/µM	3.5	6.2	1.8	>>10
EC_{90}/µM	0.4	1.8	0.34	2.7

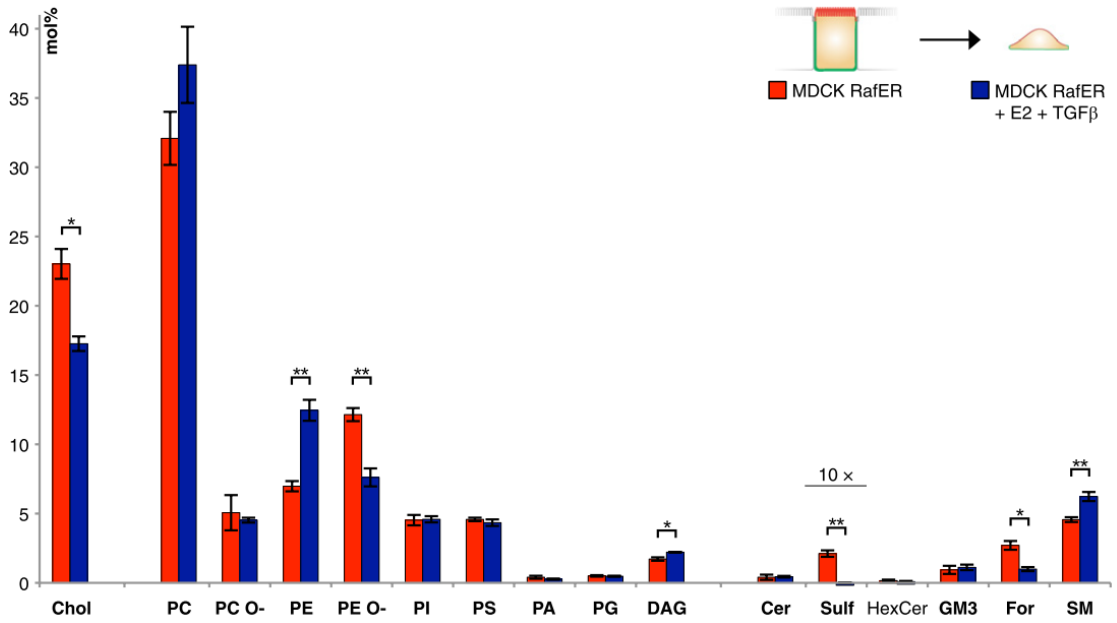

Figure 3.4.3: Lipidome of MDCK cells in the endothelial (red) and mesenchymal (blue) states.[80]

In AzSph, the hydroxyl group in sphingosine in the C1 position is replaced with an azide group, since this forms a linear GSL analogue on *click* reaction with a functionalised glycan. This is simultaneously advantageous because phosphorylation at this position is blocked, thus blocking the only sphingolipid degradation pathway via sphingosine-1-phosphate (S1P) (Introduction 1.5). Sphingolipid degradation is funnelled through the phosphorylation of sphingosine to S1P, catalysed by sphingosine kinase (SphK), which is then degraded into ethanolamine-1-phosphate (EA1P) and C16 fatty acid by S1P lyase (Scheme 3.4.4). Haberkant *et al.* described the breakdown of one modified sphingolipid via phosphorylation and S1P lyase metabolism, leading them to employ SIP lyase-deficient cells to obtain high levels of cell labelling.[219,228] Additionally, we do not observe 1-aminoceramide, which could potentially be formed from nonspecific reductases. The build-up of AzCer necessarily contributes to its toxicity, as it accumulates indefinitely throughout incubation.

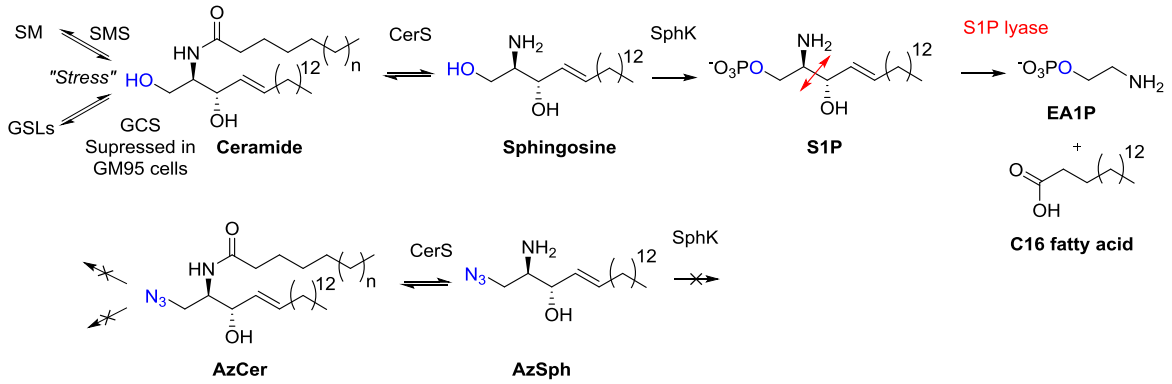

Scheme 3.4.4: Sphingolipid degradation pathway via S1P is blocked for AzSph.

Cellular uptake of AzSph is fast due to its small size and hydrophobicity. We observe no significant signal of AzSph in cells, meaning it is immediately acylated. This corresponds with the above-described report of photoSph (Figure 3.4.2), which describes photoCer formation within 5 minutes.[220] Haberkant *et al*. here observed major formation of photoSM ensuing photoCer formation, with C16:0 and C24:1 acyl chains, reflecting the native SM and ceramide profile. Although our AzSph cannot be modified at the head position to SM like photoSM, we observe equally fast fatty acid acylation to AzCer. Other sphingosine analogues modified in the lipid tail are reported to give a native acyl chain profile.[208,219] However, our AzCer acyl chain profile is not analogous to the native ceramide profile – the C16:0 chain in AzCer is significantly more abundant, whereas ceramides have C16-24 chain lengths (Graph 2.2.2.3).

CerS enzymes are described to be highly selective enzymes (Introduction 1.5), and it appears that one CerS acts on AzSph preferentially, resulting in a more abundant C16:0 fatty acid chain in AzCer. CerS5 is specific for the palmitoyl (C16) chain, and CerS6 for the palmitoyl (C16) and myristyl (C14) chain.[83] Furthermore, CerS5 has highest preference for the acylation of sphingosine via the salvage pathway, whereas all other CerSs act on dihydrosphingosine to form dihydroceramide in the de novo pathway.[90,91] Since our AzSph more closely resembles sphingosine in its double bond, it is likely that AzSph is acylated by CerS5.

This in turn could justify the induced cytotoxicity, since C16:0 chains have been implicated in apoptosis signalling. C16 ceramide has indeed been described as proapoptotic in different published reports.[229–233] This may depend on cell and tissue type, and will be involved in a complex signalling cascade. The cause of cytotoxicity and the identity of acylation enzymes could be studied further with small molecule inhibitors, e.g. CerS inhibitor

fumonisin B, manipulation of CerS enzyme expression, interference with apoptotic cascades such as those depending on caspases, or broadening experiments to a further cell types.

Since each GSL is often present at a very small molar percentage of the PM (Figure 3.4.3), we considered that even a low concentration of our modified lipid at the PM should be sufficient to observe lectin binding, this being our final validation. To avoid cytotoxic effects of ceramide analogues, we incubated cells with a low AzSph concentration (0.5 µM) to obtain a stable ratio of approximately 2-3 molecules of total AzCer to total ceramide (Graph 2.2.2.6), and a stable amount of ceramide over 24h, indicating that cells are not under ceramide-signalling stress.

Attempts to halt cell proliferation, to thus reduce the dilution of AzCer labelling, serum starvation conditions were tested. The presence of natural sphingolipids in serum should also be noted. No serum conditions induced a higher AzCer/Cer ratio over 48h compared to serum conditions. Eto *et al.* described an increase in cellular C16 ceramide in serum-free culture conditions due to an onset of apoptosis.[230] Despite this, we do not observe reduction in cell viability at low AzSph concentration.

The lateral localisation of Gb3-Cer on the cell surface appears to be important to its receptor activity (Introduction 1.3). In the natural system, Gb3-Cer is transported from the Golgi to its functional position as a lectin receptor on the cell surface. Gb3-Cer negative ($Gb3^-$) cells incubated with external Gb3-Cer/BSA can permit low levels of binding of STxB at the cell surface. However, the lectin's traffic is always dysregulated from the natural retrograde route (Figure 1.3.4). Externally supplemented Gb3-Cer with short acyl chains (natural long chain species fail to be reconstituted) may function non-canonically because it does not organise correctly within biological membranes. We hypothesised that AzCer with the natural complement of acyl chains would be incorporated into native lipid transport of the cell, allowing it to be recycled through a native pathway, to the PM, although temporarily, to undergo *click* reaction and present Gb3-Cer at the surface.

We studied the intracellular localisation of AzCer by immunofluoresence (IF) experiments. When cells were treated with AzSph, then stained with alkyne or cyclooctyne fluorophores, AzSph metabolites (AzCer) appear to be localised in intracellular membranes, possibly the ER, where CerS enzymes are known to be localised.[83] One must consider a margin of error in lipid localisation, since performing *click* reactions on AzSph with a fluorophore may change its localisation. In general, fixation is poorly effective on lipids, which contain few

nucleophilic, fixable groups, even after the most robust fixation techniques.[93] A permeabilisation step with Saponin was the cleanest method to wash cells of nonspecific *unclicked* fluorophore. However, this treatment destabilises the membrane and adds even greater possible error. Despite this, we see repeatedly specific staining compared to negative controls, and similar staining in live cell imaging. AzCer localisation in all intracellular membranes is rational since the substrate closely resembles ceramide, which is synthesised in the ER and should have little intracellular specificity. Furthermore, short chain lipids are considered to preferentially localise in the Golgi and ER, whereas long chain lipids would preferentially localise in the PM, observed by differences in the thickness of transmembrane domains of PM/Golgi/ER proteins.[197]

GM95 cells were too poorly adhesive to undertake lengthy IF experiments to study the intracellular localisation of AzCer metabolites. GSLs have long been known as modulators of cell adhesion.[87,234,235] Jwa Hidari *et al.* showed that GM95 cells lost the ability to adhere to standard extra-cellular matrix proteins when treated with sphingomyelinase, which removes SM from the cell surface, whereas GSL-expressing MEB-4 cells, from which GM95 cells were mutated, showed no loss in adhesion.[87] An inhibitor GCS and major GSL synthesis, PDMP, blocked adherence of macrophages during differentiation, further indicating GSLs are implicated in cell adhesion.[225] In the same way, PPMP treatment of naïve E14 mouse stem cells sporadically reduced adhesion during differentiation (unpublished). *Click* protocols for imaging the localisation of *clickable* lipids were optimised on CHO and HeLa cells (Experimental 6.2.6).

3.5 In cellulo click

We synthesised Gb3-MFCO **37**, Gb3-Gly-MFCO **38** (Scheme 2.1.3.2), lactose-MFCO **49**, lactose-Gly-MFCO **50** and lactose-BCN **63** (Scheme 2.1.3.4, Results 2.1.3). Our final validation of a functional GSL analogue would be via the recognition of the Gb3 head group with its specific lectin binder, the Shiga toxin. However, to first study the *click* reaction via high resolution mass spectrometry (HRMS) we tested the protocol with lactose-MFCO **49**, obtained on larger scale.

We observed that the reaction with lactose-MFCO **49** was poorly efficient, since there is no significant drop in cellular AzCer levels even when using an excess of cyclooctyne reagent. In comparison, *click* reaction was efficient with hydrophobic *clickable* fluorophore TAMRA-DIBO. This was observed by a major consumption of cellular AzCer and appearance of the *clicked* product TAMRA-DIBO-AzCer. To confirm the lipid extraction of the *clicked* glycolipid, we synthesised *in vitro* purified Gb3- and lactose-MFCO-AzCer (C22:1). These were used as internal standards, spiked into biological samples before the lipid extraction, to ensure that the *click* product is extracted and analysed by HRMS by our protocol. Since we observe the Gb3- and lactose-MFCO-AzCer (C22:1) internal standards after extraction, we can confirm that our extraction protocol is adapted to the desired glycolipid products, and that cellular *click* reaction forming lactose-MFCO-AzCer is inefficient since no cellular product is observed.

We had hypothesised that, although AzCer may be predominantly present in intracellular membranes, it would cycle to the plasma membrane (PM) by vesicular trafficking in order to undergo *click* reaction at the cell surface (Fig 3.5.1a). Since we observed no *click* reaction with hydrophilic, non-permeating cyclooctynes (lactose-MFCO, Alexa488-DIBO), we suggested that very little AzCer is present at the PM. This corresponds with the commonly accepted localisation of natural ceramide, synthesised in the ER, glycosylated in the Golgi and thus depleted at the PM.

Alexa488-DIBO is a commonly-used reagent for live-cell staining[62,162,163], and is able to specifically stain AzSph and AzPhy in IF experiments on live CHO cells (Fig 3.5.1b). Such experiments were performed with overnight incubation of fluorophore, indicating that the AzCer recycles to the PM overnight to *click* with extracellular fluorophore. Alternatively the fluorophore could penetrate to the intracellular AzCer. Alexa488-DIBO *click* product was not observed in HRMS experiments because it is too hydrophilic to be extracted in our lipid extraction protocol, not because it was not taken up or *clicked*. After *click* at the surface, the *click* product is endocytosed to intracellular membranes, as likely occurs to the small percentage of the Gb3-MFCO-AzCer product. This would explain why no STxB binding is observed.

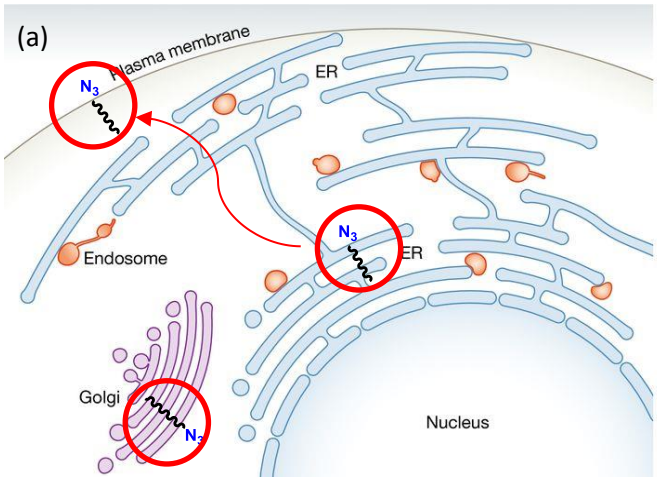

Figure 3.5.1: (a) Recycling of azide-lipid to the PM (b) IF experiment of ±AzSph (6h), Alexa488-DIBO (16h) (Results Figure 2.2.4.1).

We used higher concentrations of glycan-MFCO (20 µM), and observed a small percentage of *click* reaction occurring by lipidomics (Results, Graph 2.2.3.12-13). The percentage *click* is similar for the di- and the trisaccharide, indicating that *click* is occurring at the surface and not after permeation of the glycan, since the kinetics of permeation would be different for di- and trisaccharides. *Clicked* Gb3-MFCO-AzCer does not appear to be recognised by fluorescent STxB in IF experiments. One can speculate that more *clicked* Gb3 is required, potentially more than the natural Gb3 for efficient STxB binding, and/or that the Gb3-MFCO-AzCer formed does not remain at the PM. Although molar percentages of natural GSLs can be analysed (Figure 3.4.3), their surface presentation is difficult to quantify.

To increase the permeability of the glycan-cyclooctynes, which would allow them to react with intracellular AzCer, we incubated AzCer-labelled cells with the peracetylated substrates, obtained from the second-to-last step of the glycan-cyclooctyne synthesis (Results 2.1.3). The acetyl group is used in chemistry to protect chemically reactive functional groups, but is also a common signalling adduct in biology, regulating the genetic expression in the cell nucleus, for example. Non-specific carboxylesterases (CES) are known to remove acetyl groups from small molecules in the cytosol.[236]

Acetyl groups (CH_3CO-) are hydrophobic groups that have historically been used to mask more polar, hydrophilic hydroxyl groups, augmenting the permeability of drugs in *prodrugs*. A drug is a substance with a non-nutritive effect on the body. A prodrug is a compound that, after administration, is metabolised in the body into a pharmacologically active drug. Prodrugs are designed to aid delivery or bioavailability. Examples include aspirin (acetylsalicylic acid) which is metabolised to active salicylic acid (Fig 3.5.1a), and heroin

(diacetylmorphine), metabolised to morphine after permeating the blood brain barrier. The technique has been widely used in for the metabolic labelling of cells with azidoglycans (Introduction 1.7).[127] The concept was first proved for disaccharide uptake by Sarkar *et al.*,[128] and made famous by Bertozzi *et al.* for metabolic labelling of *clickable* glycans (Figure 3.5.1b).[237,238] All chemical biology papers cite the action of non-specific, intracellular (carboxy)esterases.[127] Such esterases acting on glycans are likely to be the CES enzymes, CES1 and CES2, responsible for the metabolism of common prodrugs, localised in the cytosol and endoplasmic reticulum (ER).[236]

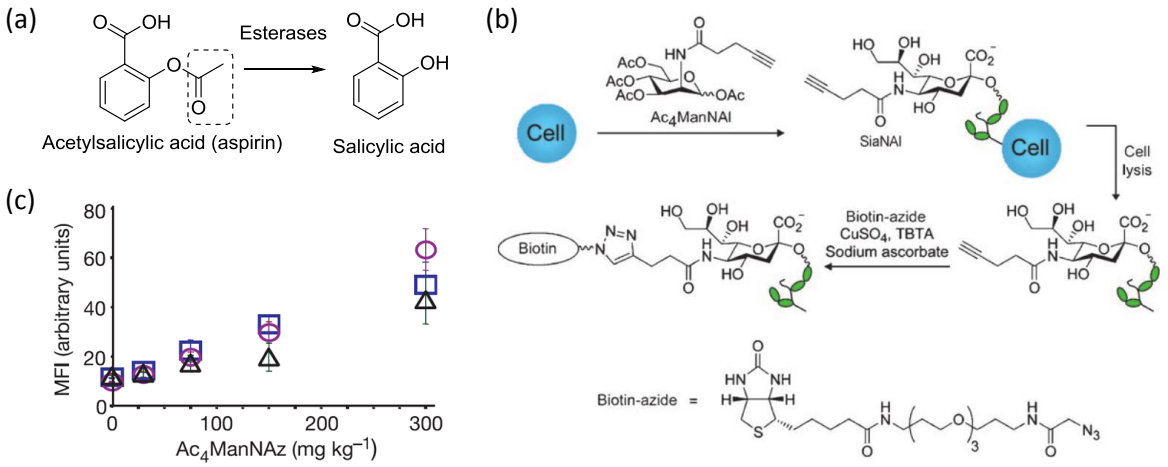

Figure 3.5.1: (a) Conversion of aspirin to salicylic acid. (b) Metabolic labelling of *clickable* peracetylated alkyne-derivatived glycan, incorporated into the native glycoprotein biosynthesis and *clicked* to be isolated via biotinylated azide.[238] (c) Quantification of surface azides by mean fluorescence intensity (MFI) of splenocytes from mice deficient in plasma Ces1 (triangles) or wild-type B6D2F1 mice (circles, males; squares, females) treated with Ac_4ManNAz.[127]

Disappointingly, the deacetylation of functionalised di- and trisaccharides was poor and incomplete after 48h. This project aims to reconstitute functional GSL analogues with which one can further test their biological activity in cells. Therefore, reconstitution protocols must be practical for standard laboratory research work, where >48h incubation times are unfeasible. We are currently pursuing the upregulation of one of these genes, *Ces2*, to increase deacetylation of our incorporated product. *Ces2* is reported to preferentially mediate the metabolism of permeating drugs corresponding to our substrate's size – a large hydroxyl and small acetyl group.[236,239] One recent paper has shown that such an upregulation can increase esterase activity by three times,[240] which – in our case – may be sufficient to catalyse the full metabolism. Prescher *et al.* suspected that plasma CESs could reduce the bioavailability of ManNAz in mice treated with Ac_4ManNAz, with the objective of labelling all

mouse tissues.[127] They trialled the use of plasma *Ces1*-deficient mice to reduce deacetylation in the plasma, but saw no difference in labelling of splenocyte (cells rich in sialiosides) (Figure 3.5.1c) and tissues compared with control mice. This indicates some compensatory effect of multiple CES enzymes.

3.6 Optimisation of lipid localisation

To obtain an azide labelling at the plasma membrane (PM), we envisaged different azide-lipid precursors, which might prove to have a different metabolite profile, and thus a different cellular localisation. Longer chain lipids are thought to be preferentially housed in the PM, whereas shorter lipids localise to the Golgi or ER. Although this theory is difficult to verify, a study of protein transmembrane domains showed that longer hydrophobic domains exist in PM-localised proteins than the ER- and Golgi-localised proteins.[197]

AzSph is acylated to AzCer (C16:0) by the CerS5 enzyme, which has high specificity for sphingosine formed in the salvage pathway.[91] Sphinganine, formed in the *de novo* synthesis pathway, is metabolised by other CerSs, which have individual specificities for longer fatty acid chains (Graph 3.6.1, Introduction 1.5). An azide analogue of sphinganine holds promise as it may be metabolised like sphinganine, via the *de novo* pathway to long chain ceramides, which should have a higher propensity to localise to the PM. Phytosphingosine is structurally more similar to sphinganine than sphingosine as it has no double bond in the C4 position. Phytosphingosine is a plant-derived starting material from which we begin the AzSph synthesis. 1-azidophytosphingosine (AzPhy) was easily obtained synthetically (Results 2.1.2).

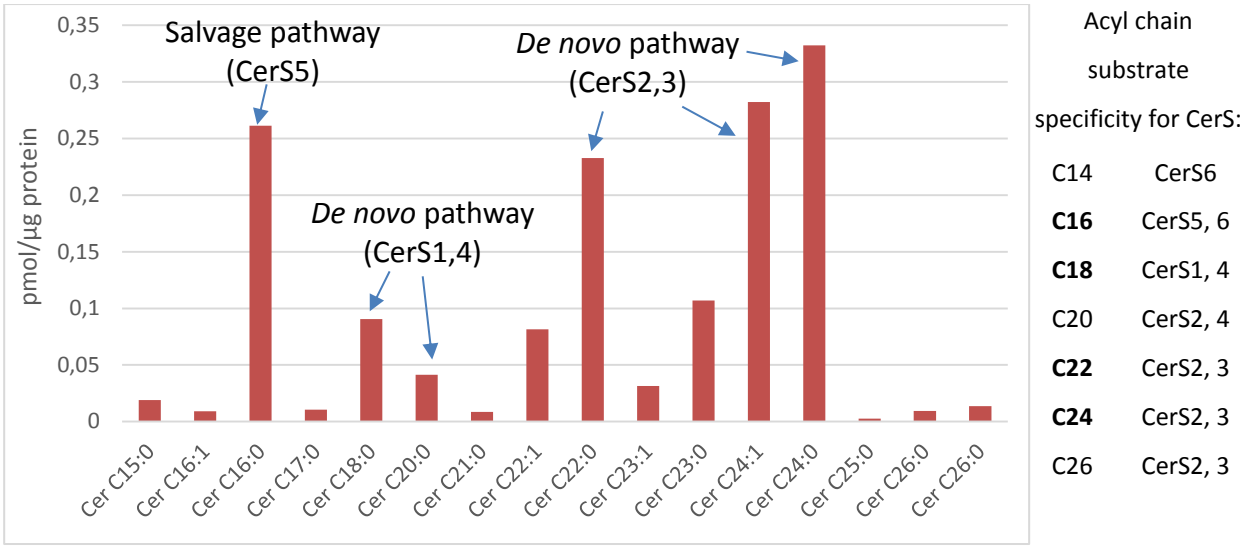

Graph 3.6.1: Native ceramide chain length and the specificity of ceramide synthase (CerS) enzymes.

Garrido *et al.* studied the metabolism of three ω-alkyne sphingolipids **1-3** (Figure 3.6.2),[208] analogues of sphingosine, sphinganine and ketosphinganine. In the natural biosysnthesis, ketosphinganine is reduced to sphinganine by 3-ketosphinganine reductase (3-KSR) (Introduction 1.4). ω-Azidosphinganine **2** and ω-azidoketosphinganine **3** show a slighter higher percentage of long C24:1 chains compared with ω-azidosphingosine **1**, indicating they are better substrates for CerS enzymes using longer CoA-acyl chains. Likewise, Gaebler *et al.* described major transformation of ω-alkyne-sphinganine (Figure 1.7.3) to C24:1 dihydroceramide in liver microsomes, highly expressing *CerS2*, and moderate to weak acylation with other acyl chains in *CerS2*-suppressed tissue samples.[161]

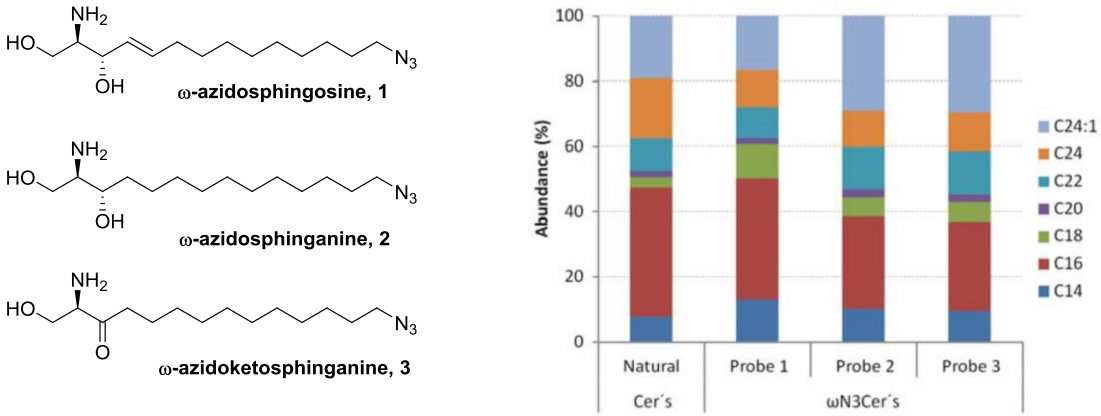

Figure 3.6.2: ω-Azidosphingolipid probes and their acyl chain profiles (6h, 5 µM), later converted to 1-phosphated and SM analogues.[208]

Phytosphingosine is a popular cosmetic product and literature suggests that it is widely accepted by mammalian cells.[241] Indeed, AzPhy showed cytotoxicity similar to that of AzSph; EC_{50} = 2 μM and 10 μM in GM95 and CHO respectively, compared with 3 μM and 2 μM for AzSph. As hoped, the profile of AzPhy metabolites is closer to the profile of native ceramide than that of AzSph, comprising a higher percentage of long chain lipids. We suggest that this is due to the metabolism of AzPhy by some other CerS enzyme(s), CerS1-6, which have other fatty acid chain specificities (Graph 3.6.1). There were no traces of dehydroxylation of azidophytoceramides into mammalian azidoceramides.

In immunofluorescence experiments, no difference in localisation was observable compared with AzSph. Furthermore, AzPhyCer did not show improved reactivity in cellular *click* experiments. HRMS-detectable levels of *click* product are formed from surface *click* with Lac-MFCO **49**, yet their levels are not significantly different from that observed with AzSph (Graph 2.2.4.6). One can suggest that the change in lipid length of AzPhyCer does not significantly change its localisation.

4 PERSPECTIVES

Our primary aim to reconstitute functional Gb3 analogues in cells using *click* chemistry could be attained by optimising our protocol or our *clickable* reagents. The upregulation of a major non-specific esterase, *Ces2*, is envisaged to increase deacetylation (Discussion 3.5). Alternatively, because permeable, acetylated glycosides are much better *clicked* than free glycosides, one could consider using partially acetylated glycosides. These products could be taken up by cells and more easily deacetylated. Sarkar *et al.* describe that mono-, di- and trimethylation of disaccharides (Figure 4.1, lanes 3-5) greatly increases their cellular uptake compared with hydrophilic glycan (lane 2). We can envisage the partial acetylation of Gb3-MFCO **37** or partial deprotection of peracetyl Gb3MFCO **47.** Enzymatic deacetylation of **47** using pig liver esterase was very poor. Chemical acetylation of **37** with few equivalents of acetylating reagent is low yielding and non-specific, but a viable possibility. The uptake of hydrophilic glycans could also be increased by electroporation or transfection reagents.

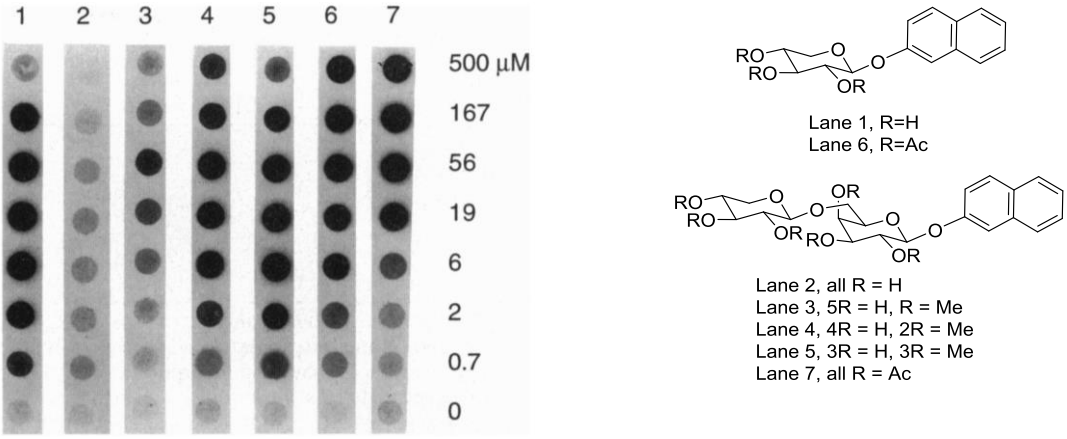

Figure 4.1: Mono- and disaccharide uptake into CHO cells depending on level of hydrophobicity. Secondary readout for glycoside uptake based on inhibition effect of naphthol-glycosides.

Since the copper-free *click* reaction is possible, but slow, we could envisage using copper-catalysed *click* reagents with non-permeating copper-ligand complexes to reduce cytotoxicity. Providing the azide-lipid is temporarily present at the cell surface, keeping the copper chelated at the cell surface could allow *click* reaction without toxicity. To increase azide-lipid presentation at the PM, we envisage the synthesis of 1-azidosphinganine (Figure 4.2), which could have an acyl chain profile closer to native ceramide, thus different localisation, as indicated for 1-azidophytosphingosine (AzPhy, Discussion 3.6). A zwitterionic

clickable lipid, azidoethylcholine phosphosphingosine (Figure 4.2) could show better plasma membrane (PM) localisation, as indicated by Klymchenko *et al*., where their zwitterionic fluorescent lipid localises at the PM, whereas the neutral analogue shows intracellular staining.[242] Longer acyl chain length could be achieved by upregulating CerS1-4 synthase enzymes, which produces longer chain ceramides.

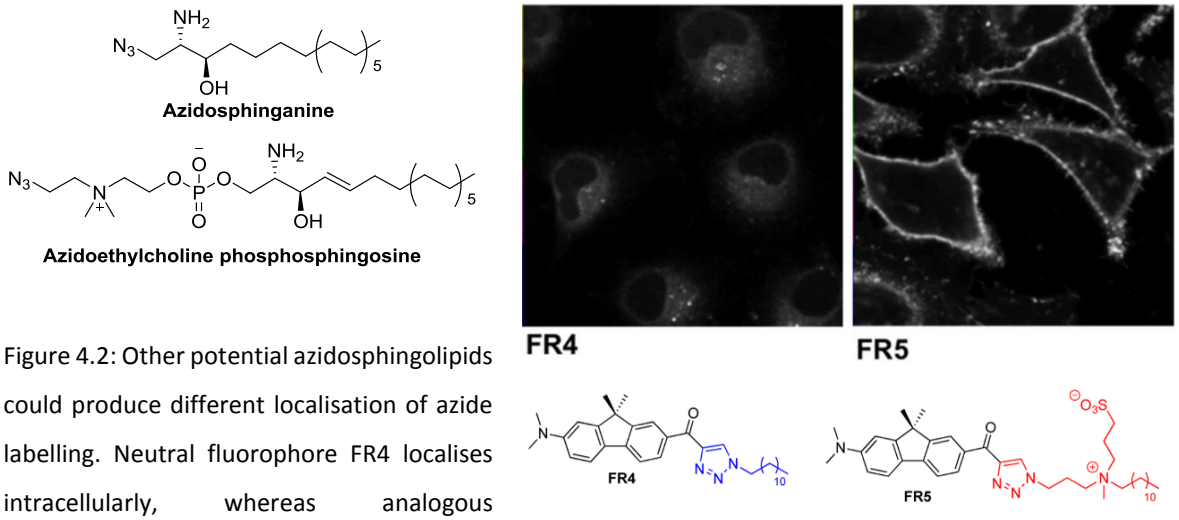

Figure 4.2: Other potential azidosphingolipids could produce different localisation of azide labelling. Neutral fluorophore FR4 localises intracellularly, whereas analogous zwitterionic FR5 localises to the PM.[242]

The suite of this project could go to investigating biological interactions of other GSLs, the strategy of the *clickable* Gb3 head group would in principle be applicable to any glycan head group. The synthetic steps required to functionalise the glycan with MFCO are as follows: hydroxyl protection, anomeric deprotection, activation, azidolysis, reduction to amine and peptide coupling with the cyclooctyne. Using this many steps is difficult to envisage for commercial oligosaccharides bought at milligram scale. Enzymatic methods, such as the use of glycosyltransferases, are ideal for direct synthesis, with retention of stereochemistry. Such methods have been applied for the synthesis of Gb3[243] and GM3.[244] We could envisage the chemoenzymatic synthesis of other glycosides from simpler functionalised starting materials, such as GM3-MFCO from lactose-MFCO with the α-2,3-sialyltransferase.

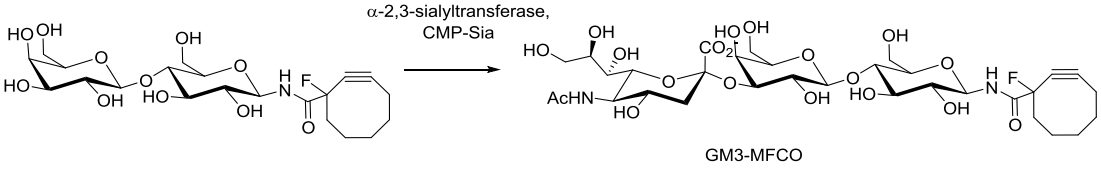

Figure 4.3: Potential enzymatic synthesis of lactose-MFCO **49** into GM3-MFCO.

If the glycoside head group can be efficiently reconstituted, one can envisage the synthetic incorporation of a crosslinking, photoactivatable group. One easy route would be to incorporate a diazirine-functionalised amino acid in the place of glycine in compound **36** (Figure 4.4). Since compound **36** has shown acceptable membrane bending properties in GUVs in complexation with STxB, we could imagine that its biological function would not be hindered, and the crosslinking group could be used to isolate interaction partners with the glycan head group of choice. To purify the lipid-protein bound complex, an additional alkyne would be required in the lipid tail to permit affinity purification.

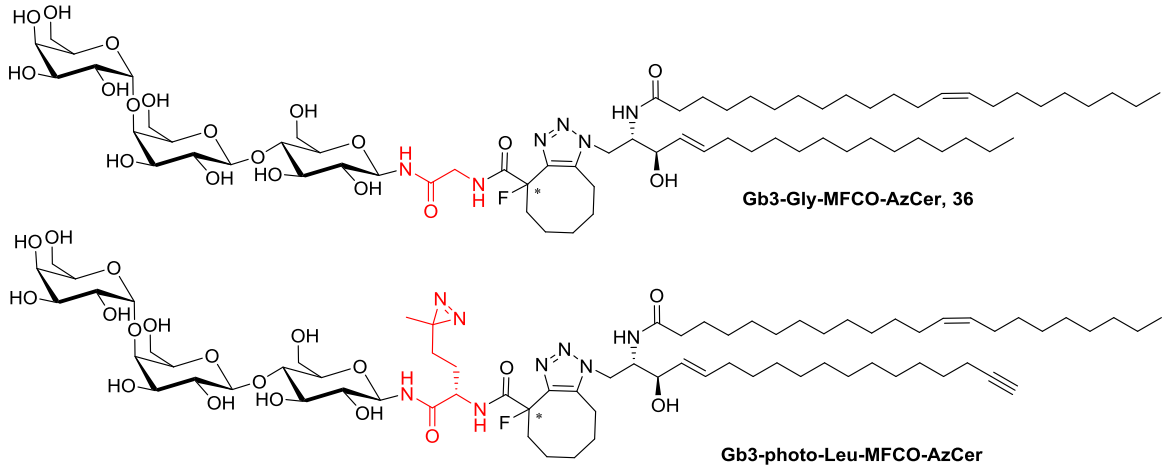

Figure 4.4: Gb3 analogue **36**, synthesised in 15 convergent steps (27 steps), and the envisageable photo-crosslinkable Gb3 analogue to study native Gb3 interaction partners.

Basic principles of organic chemistry suggest that every synthesis is feasible with the right budget and time. Now, with the developments of chemical biology and the surprising plasticity of the natural system, we can begin to believe that we can manipulate and understand each part of the cellular system. All that's needed is the right *controls*: molecules which *control* cellular function, and positive/negative *control* experiments to verify the results!

5 CONCLUSIONS

We have synthesised novel *clickable* biomolecule analogues and tested their validity in model membranes and cell culture. Two different glycan-cyclooctyne head groups, Gb3-MFCO and Gb3-Gly-MFCO, when *clicked* with 1-azidoceramide, show promising model membrane activity when bound to fluorescent STxB. This indicates that the proposed structural modification in the spacer region between glycan head and lipid tail is tolerated in biological function. The synthesis of glycan-cyclooctynes can be applied to other glycans and bioorthogonoal *click* reagents for the study of other GSLs. Similarly, the synthesis of 1-azidosphingosine and 1-azidoceramide can be extended to other azido-sphingolipid analogues for a varied metabolism profile.

We have shown efficient metabolic labelling of sphingolipids using *clickable* 1-azidosphingosine, which is rapidly incorporated into cells and metabolised into 1-azidoceramide. 1-azidoceramide localises in intracellular membranes, thus *click* reaction with non-cell-permeating reagents such as glycan-cyclooctynes is poorly efficient. 1-Azidoceramide undergoes specific and efficient bioorthogonal *click* reaction with permeable, peracetylated glycan-cyclooctynes. We have quantified this *in cellulo click* reaction by HRMS lipidomics. Endogenous deacetylation of *clicked* glycolipid analogues is inefficient in two cells lines tested. Several pathways to change the localisation of lipid or glycan parts are available, and should permit the reconstitution of a biologically functional glycolipid analogue into cells. With this technique in hand, one can envisage a precise and efficient reconstitution of long chain glycolipid analogues for the study of GL-Lect endocytosis.

6 EXPERIMENTAL

6.1 Biological validation

6.1.1 Giant unilamellar vesicle (GUV) STxB binding

1. Lipid mixture made up in prewashed glass vial and spread onto indium tin oxide (ITO) plates (2×20 µl).
2. Plates dried at 65°C for 5 min then vacuum dried for 30 min.
3. Plates separated with plastic shoots and placed inside Teflon cases. Covered with parafilm leaving a small gap. 6ml sucrose (300 mOs) added and the capsule sealed over.
4. Electrodes connected to AC (10 Hz, 1.1 V (AC) at 65°C for 2 h.
5. 8-well coverslip for imaging coated with casein (4mg/ml, 30 min)
6. GUVs cooled to rt 30 mins before use
7. 8-well coverslip washed 2x PBS
8. Wells filled with 150 ul PBS (300 mOs) and 100 ul GUV solution and mixed with pipette tip
9. Visualise GUVs
10. STxB-Alexa488 (20 or 200nM) added and mixed with pipette tip
11. Visualise tubules

		Gly (1)		Gb3-MFCO (2)		Gb3wt (3)		GSL neg	
	[Stock / mg/ml]	Molar %	Volume added	Molar %	Volume added	Molar %	Volume added	Molar %	Volume added
Cholesterol	6	30	5,6	30	5,6	30	5,6	30	5,6
DOPC	10	64.9	14,9	64.9	14,9	64.9	14,9	69.9	16
Gb3 variant	1	5	19,8	5	19	5	16,6	0	0
Liss Rhod PE	1	0.1	0,4	0.1	0,4	0.1	0,4	0.1	0,4

6.2.2 Large unilamellar vesicle (LUV) click reaction

- Lipid mixture made up with 65% DOPC, 30% cholesterol and 5% AzCer in a new glass vial
- Dry lipid solvent under stream of nitrogen
- Dry under vacuum for 1h
- Resuspend in water at 1mg/ml total lipid
- 3 vortex/freeze/thaw cycles, freezing in a EtOH/dry ice bath
- Wash extruder with water (200 nm polycarbonate filter)
- Extrude lipid solution by passing it through extruder 15 times, remembering to take final solution from opposite end to which it was injected.

Click reaction

- 50 µL of LUV solution in each reaction vial (0.049 mg/ml AzCer, 0.15 mM, 7.5 nmol per vial)
- 19 µl of 200 nM solution of Gb3-MFCO added (3.8 nmol per vial, equimolar since 50% of AzCer faces inside) and mixed with pipette tip
- Reaction left at rt for varying time points (24/6/4/3/2/1h/30min/15min/ctrl (no Gb3))
- Reaction stopped by extracting lipids with 70ul $CHCl_3$/MeOH (10:1), vortexed for 60 seconds and sample taken from aq and org layer for TLC and MS.

	mol%	µmol	µg	stock conc	vol
Total		1,2	791,0946		
AzCer	5	0,06	38,7	1	
DOPC	65	0,78	613,197	10	61,3
Chol	30	0,36	139,1976	6	23,2

6.2.3 Cellular metabolism of AzSph and click with fluorophore

- The day before, 500,000 GM95 cells/well seeded in 6-well plate (2 ml DMEM++)
- Wash 2x DMEM(++)
- Add AzSph (10 µM, 1 ml) in DMEM(++)(Penicillin/streptomycin 5%, foetal bovine serum 10%)
- Incubate 37 °C for various times
- Wash 1x PBS and 2x ammonium bicarbonate solution (150 mM) at rt
- Scratch cells in 1 mL ammonium bicarbonate solution at 4 °C (6 wells per condition)
- Centrifuge 5 min at 4700 RPM at 4 °C
- Remove supernatant
- Lipid extraction
    - Resuspend pellet in 200 µL H_2O
    - Add 1000 µL $CHCl_3$/MeOH (10 :1)
    - Vortex 75 min
    - Centrifuge quickly in small benchtop centrifuge
    - Keep supernatant
    - Dry the solvent
    - Re-suspend in 100 µL of $CHCl_3$/MeOH/H_2O (50:40:5)
- *Click* reaction (2h in Eppendorf shaker at 800 RPM, 25 °C)
    - 1 – Cell lysate/reference (150 µL; references at 50 µM, 300 µL)
    - 2 – Alexa/TAMRA (100 µM final, stock 1.25 mM)
    - 3 – Cu(I) (2 mM) ($Cu(BF_4)$) (100mM)
    - 4 – 45 µL EtOH (volume total=100ul)
- Spot supernatant mix (20 µL) on HPTLC plate (10 cm×10 cm) and dry 10 min under vacuum or with heat gun
- Elute TLC in cuvette ($CHCl_3$/MeOH/H_2O 50:40:10) and scan

6.2.4 Cytotoxicity assay

1 The day before, 50,000 cells/well seeded (200 µl in DMEM++) in a 96-well plate

2 Wash 2x DMEM(++)

3 Add compound (AzSph/AzPhy/cyclooctyne, 100 µL at descending concentrations) in DMEM(++), 3 wells per condition.

4 Incubate at 37 °C, 24 h

5 Remove medium

6 Wash cells with 200 µL virgin DMEM at 4 °C

7 Add 150 µL virgin DMEM and 20 µL MTT solution (5 $mg.mL^{-1}$ in H_2O, protected from the light)

8 Incubate for at least 3h at 37°C in the dark

9 Gently remove medium

(At this step, the plate can be conserved at 4°C to read at a later date)

10 Add 100 µL DMSO

11 Shake for 20 min

12 Read plate on spectrophotometer at 570 nm

6.2.5 Cell treatment of *click* reagents for lipidomics testing, optimised protocol

1. The day before, seed 250,000 GM95 cells/well in 6-well plate (2 ml)
2. Wash 2x DMEM (++)
3. Add AzSph/AzPhy (0.5 µM, 1 ml) in DMEM(++)
4. Incubate at 37 °C (6h to overnight)
5. Wash 2x DMEM(++)
6. Incubate w/o cyclooctyne reagent in DMEM(++) (varying time points)
7. Wash 2x with ammonium bicarbonate (150 mM) at 4°C
8. Add 1 ml ammonium bicarbonate and scratch cells at 4 °C
9. Centrifuge 5 min à 13.3K RPM à 4 °C
10. Throw away supernatant
11. Resuspend pellet in 300 µL ammonium bicarb
12. Homogenise with needle and syringe (18G, then 25G needle)
13. Take 50 µL for protein quantification (MicroBCA kit)
14. Snap freeze in N_2(l)
15. Extract cell lysate solution (200 µl, quantity adjusted with water based on protein quantification), spiked with internal standards (non-natural AzCer C22:1 and Cer C12:0)
    - Add $CHCl_3$/MeOH (2.75:1, 1 ml)
    - Shake vigorously in Eppendorf shaker for 1h
    - Centrifuge briefly and collect lower organic layer
    - Dry solvent (rotary evaporator or SpeedVac)
    - For Gb3-MFCO-AzCer extraction, a two-step extraction is used: Extract cell lysate solution (200 µl), spiked with internal standards (non-natural Gb3-MFCO-AzCer C22:1, AzCer C22:1 and Cer C12:0) first with in $CHCl_3$/MeOH (10:1, 1 ml), shaken for 2h. Organic layer collected and remaining aqueous layer extracted with $CHCl_3$/MeOH (2:1, 1 ml) as before
16. Resuspend in 100 µL of MS mix (Propanol/MeOH/ $CHCl_3$ [4:2:1] with ammonium acetate 7.5mM)
17. Direct infusion HRMS

6.2.6 Immunofluorescence test to localise *clickable* lipid

1 The previous day, spread 200,000 GM95 cells or 50,000 CHO cells/well+coverslip (in 1 ml DMEM++) in a 4-well plate with glass coverslips

2 Wash 2x with DMEM++

3 Add 500 µl AzSph in DMEM++ medium or DMEM++ medium only (control)

4 Incubate, 37°C

5 Wash 3x with DMEM++

6 Add *clickable* fluorophore (TAMRA- or Alexa-DIBO, Alexa488 alkyne) in DMEM++ and incubate **1-2h**, 37°C

7 Wash 3x with PBS++ and incubate **30 min**, rt

8 Wash 1x with PBS++

9 Add 500 µl PFA (4%) and incubate **15 min**, rt

10 Wash 3x with PBS++

11 Add NH_4Cl (50mM) and incubate **30 min**, rt

12 Wash 1x with PBS/BSA/Saponine 1X

13 Permeabilisation with PBS/BSA/Saponine 1X, rt, 30 minutes

14 Wash 1x with H_2O then add H_2O

15 Wash 3x with PBS++/1%FCS

16 Mount on a slide with Mowiol

Copper click solution (1 ml total, 0.4 mM Cu):

- 860 µL PBS
- 40 µL $CuSO_4$ 10 mM (0.4 mM final)
- 2 µL alkyne-A488 1.25 mM (2.5 µM final)
- 66 µL sodium ascorbate 150mM (10 mM final, dark - 20°C)

6.2.7 Immunofluorescence test for *clicked* glycolipid with fluorescent STxB

1 The previous day, spread 50,000 CHO cells/well+coverslip (in 1 ml DMEM++) in a 4-well plate with glass coverslips

2 Wash 2x with DMEM++

3 Add AzSph/AzPhy (0.5 µM, 500 µl) in DMEM++ medium or DMEM++ medium only

4 Incubate, 37°C

5 Wash 3x with DMEM++

6 Add Gb3-MFCO (20 µM, 500 µl), incubate 37°C

7 Wash 3x with DMEM++ at 4°C

8 Incubate at 4°C for 10 min

9 Add STxB-Cy3 in DMEM++, 4°C

10 Binding 30 min on ice, 4°C (Skip to step 19 to visualise STxB surface binding)

11 Add DMEM++ preheated to 37°C

12 Internalisation 45 min, 37°C

13 Wash 3x PBS++ (at 4°C for surface binding)

14 Fix with PFA 4% in PBS, 15 min, rt

15 Wash 1x NH_4Cl 50 mM

16 Quench with NH_4Cl 50 mM, 30 min

17 Wash 2x PBS++

18 Wash 1x H_2O then add H_2O

19 Mount on a slide with Mowiol+DAPI (Hoechst/Fluoromount 1:20000)

6.2 Chemical synthesis

General methods

All reactions were performed under argon atmosphere unless specified. Commercially available chemicals were used without further purification. Anhydrous solvents were freshly distilled before use or obtained from solvent purifier Pure SolvTM. 3Å and 4Å molecular sieves were activated immediately before reaction by a heat gun *in vacuo*. Glycosides and phytosphingosine were purchased from TCI. Other lipid starting materials were purchased from Avanti Lipids. Column chromatography (CC): silica gel 60 (0.040-0.063 mm) Merck. Analytical thin layer chromatography (TLC): Merck silica gel 60 F-254 pre-coated plates; detection by UV light (254 nm), ceric ammonium molybdate, ninhydrin, orcinol or potassium permanganate. ^{1}H NMR spectra were recorded on Bruker instruments at 300, 400 or 500 MHz. ^{13}C NMR spectra were recorded at 75, 101 or 126 MHz with complete proton decoupling. ^{31}P NMR spectra were recorded 121.4 MHz with respect to an external standard of 85% H_3PO_4, w/o proton decoupling. Chemical shifts (δ) in ppm related to protonated solvent as internal reference (^{1}H: $CHCl_3$ in $CDCl_3$, 7.26 ppm; 13C: $^{13}CDCl_3$ in $CDCl_3$, 77.0 ppm; ^{1}H: CH_3OH in CD_3OD; ^{13}C: $^{13}CD_3OD$ in CD_3OD; ^{1}H: H_2O in D_2O). Coupling constants J in Hz. Current notations are used for multiplicity (s: singlet; bs: broad singlet; d: doublet; dd: double doublet; t: triplet; q: quadruplet; m: multiplet). The assignment of ^{1}H NMR spectra was based on chemical shift correlation (DQF-COSY), whereas the assignment of ^{13}C NMR spectra were based on Carbon-Proton Heteronuclear Multiple Bond Correlation Coherence (HMBC) and Hetero Nuclear Single Quantum Coherence (HSQC). UPLC-MS analyses were obtained on an Acquity UPLC BEH C18 pre-column 2.1×5 mm and column 2.1×50 mm, 1.7 µm (Waters) coupled to a SQ Detector 2 (Waters) at a flow rate of 0.6 ml/min. High resolution mass spectra (HRMS) were obtained in-house on a Q-Exactive Orbitrap (ThermoFisher Scientific) and on a LTQ-Orbitrap (Thermo) at the Laboratoire de Spectrométrie de Masse of ICSN CNRS (Gif-sur-Yvette).

α-1-*O*-acetyl-2,3,4,6-tetra-*O*-acetyl-β-D-galactopyranosyl-(1→4)-2,3,6-tri-*O*-acetyl-D-glucopyranoside

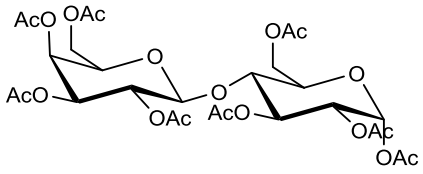

α-Lactose monohydrate (1.09 g, 3.19 mmol, 1 eq) was dissolved in a solution of acetic anhydride/pyridine (1:1) and stirred in air overnight at room temperature. The reaction mixture was extracted with CH_2Cl_2 (2×100 ml), washed with brine (200 ml), water (200 ml) and HCl (1M, 200 ml), dried ($MgSO_4$), evaporated and purified by silica column chromatography (toluene/acetone, 6:4 to 4:6) to afford peracetyl lactose (2.06 g, 95 %). R_f (toluene/acetone [1:1])=0.7; ^{1}H NMR (300 MHz, $CDCl_3$) δ 6.26 (d, *J* 3.7 Hz, 1H, 1-H_α), 5.47 (t, *J* 9.7 Hz, 1H), 5.36 (d, *J* 3.2 Hz, 1H, 1'-H_α), 5.13 (dd, *J* 10.3, 7.9 Hz, 1H), 5.01 (dd, *J* 10.3, 3.7 Hz, 1H), 4.96 (dd, *J* 10.4, 3.4 Hz, 1H), 4.49 (d, *J* 7.8 Hz, 1H), 4.45 (d, *J* 12.0 Hz, 1H), 4.16 (dd, *J* 11.0, 6.1 Hz, 2H), 4.12 – 4.07 (m, 1H), 4.07 – 3.95 (m, 1H), 3.89 (t, *J* 6.8 Hz, 1H), 3.80 (d, *J* 9.7 Hz, 1H), 2.18 (s, 3H), 2.16 (s, 3H), 2.13 (s, 3H), 2.06 (s, 6H), 2.06 (s, 3H), 2.01 (s, 3H), 1.97 (s, 3H).

2,3,4,6-tetra-*O*-acetyl-β-D-galactopyranosyl-(1→4)-2,3,6-tri-*O*-acetyl-β-D-glucopyranosyl isothiocyanate (1)[177]

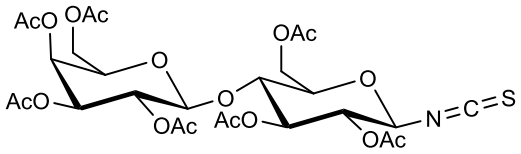

Peracetyl lactose (1.87 g, 2.56 mmol, 1 eq) and $SnCl_4$ solution (2.8 ml, 2.78 mmol, 1 eq, 1 M solution in CH_2Cl_2) were mixed in CH_2Cl_2 (17 ml), to which trimethylsilylisothiocyanate (TMSSCN, 0.43 ml, 3.06 mmol, 1.1 eq) was added dropwise at rt. The solution was stirred for 24 h, then an additional 0.25 equivalents of TMSSCN (0.1 ml, 0.69 mmol). The reaction mixture stirred for another 24h, then washed with $NaHCO_3$ (200 ml) and water (2×200 ml) and extracted with CH_2Cl_2, evaporated and purified by silica column chromatography (EtOAc/cyclohexane/CH_2Cl_2, 1:1:1) to afford **1** (0.62 g, 0.91 mmol, 33 %). R_f (EtOAc/cyclohexane [1:1])=0.4; ^{1}H NMR (300 MHz, $CDCl_3$) δ 5.35 (1H, d, $J^{4'-3'}$ 3.1 Hz, 4'-H), 5.20 (1H, t, J^{3-4} 9.2 Hz, 3-H), 5.11 (1H, dd, $J^{2'-1'}$ 10.3 Hz, $J^{2'-3'}$ 7.9 Hz, 2'-H), 5.02 (1H, m, 3'-H), 5.00 (1H, m, 2-H), 4.95 (1H, dd, J^{1-2} 10.4 Hz, J 3.3 Hz, 1-H), 4.48 (1H, d, $J^{1'-2'}$ 10.4, 1'-H), 4.48 (1H, dd, J^{6a-6b} 13.8, J^{6a-5} 2.2 Hz, 6a-H), 4.14 (1H, dd, $J^{6'a-6'b}$ 11.1, $J^{6'a-5'}$ 6.5 Hz, 6'a-H), 4.11-4.07 (2H, m, 6b-H, 6'b-H), 3.91-3.85 (1H, m, 5'-H), 3.82 (1H, dd, J^{4-5} 9.6 Hz, J^{4-3} 9.4 Hz, 4-H), 3.66 (1H, m, 5-H), 2.16, 2.14, 2.11, 2.07, 2.06, 2.05, 1.97 (21H, 7s, $COCH_3$).

***N*-1,2-dioleoyl-*sn*-glycero-3-phosphoethyl-*N'*-(2,3,4,6-tetra-*O*-acetyl-β-D-galactopyranosyl-(1→4)-2,3,6-tri-*O*-acetyl-β-D-glucopyranosyl)thiourea (2)**[177]

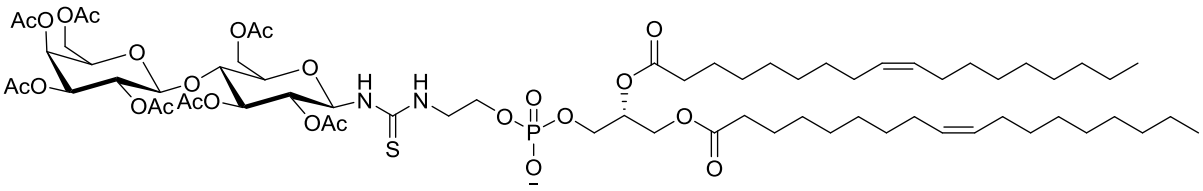

Compound **1** (10 mg, 14.8 µmol, 1 eq) and 1,2-dioleoyl-*sn*-glycero-3-phosphoethanolamine (DOPE, 11 mg, 14.8 µmol, 1 eq) were mixed in dimethylformamide (DMF, 1 ml), to which N,N-diisopropylethylamine (DIPEA, 0.1 ml, 0.57 mmol, 40 eq) was added. The solution was stirred overnight. The reaction mixture was evaporated and purified by silica column chromatography (CH_2Cl_2/MeOH [9:1]) to afford **2** (14 mg, 67 %). R_f (CH_2Cl_2/MeOH [9:1]=0.3; ^{1}H NMR (300 MHz, $CDCl_3$) δ 7.72 – 7.52 (m, 1H, NH), 5.89 (s, 1H, NH), 5.43 – 5.19 (m, 4H, HC=CH), 5.40 – 5.28 (m, 3H), 5.17 – 5.04 (m, 2H), 5.03 – 4.77 (m, 2H), 4.47 (d, *J* 28.1 Hz, 3H), 4.14 (s, 5H), 4.06 – 3.84 (m, 5H), 3.84 – 3.69 (m, 2H), 2.54 (s, 3H, OAc), 2.41 – 2.22 (m, 4H, $OCOCH_2$), 2.15 (s, 3H, OAc), 2.11 (s, 3H, OAc), 2.05 (s, 9H, OAc), 2.01 (d, *J* 5.1 Hz, 8H, C=CHC*H*$_2$), 1.97 (s, 4H), 1.58 (s, 4H, $OCOCH_2CH_2$), 1.28 (d, *J* 7.9 Hz, 40H, CH_2), 0.88 (t, *J* 6.4 Hz, 6H, CH_3).

2-(Octyloxy)-1,3,2-dioxaphospholane 2-oxide (8)[179]

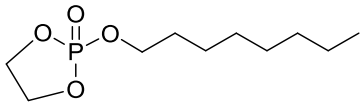

1-Octanol (285 mg, 2 mmol, 1 eq) and 2-chloro[1,3,2]dioxaphospholene-2-oxide (COP, 0.31 ml, 2 mmol, 1 eq) were dissolved in dry toluene and cooled to 0°C. Et_3N (0.36 ml, 2.6 mmol, 1.3 eq) was added dropwise and the reaction mixture stirred at 0°C for 15 minutes then at rt for 4h. The reaction mixture was filtered through Celite and washed with dry toluene. Solvent was removed under reduced pressure to afford the crude compound **8** (539 mg, 90 % pure by NMR containing Et_3NHCl). R_f (hexane/EtOAc [2:1]=0.1; ^{1}H NMR (300 MHz, $CDCl_3$) δ 4.52 – 4.26 (m, 4H), 4.14 (dd, *J* 15.2, 6.7 Hz, 2H), 1.76 – 1.64 (m, 2H), 1.45 – 1.17 (m, 10H), 0.88 (t, *J* 6.3 Hz, 3H); ^{31}P NMR (121 MHz, $CDCl_3$) δ 18.87.

Hydroxyoctyl (2-(dimethyl(prop-2-yn-1-yl)ammonio)ethyl) phosphate (9)[179]

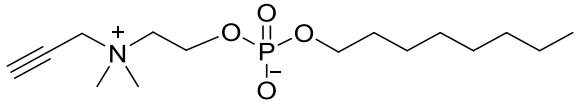

Compound **8** (284 mg, 1.2 mmol, 1 eq) was dissolved in CH_2Cl_2, to which N,N-dimethylpropargylamine (0.445 ml, 2.46 mmol, 2 eq) was added, then trimethylsilyl trifluoromethanesulfonate (TMSOTf, 0.265 ml, 2.46 mmol, 2 eq) was added dropwise. The reaction was stirred for 15 min at 0°C then at rt for 24 h. The reaction mixture was evaporated and purified by silica column chromatography ($CHCl_3$/MeOH/NH_4OH [9:1:0 to 70:30:3]) to afford **9** (129 mg, 34 % over two steps). R_f ($CHCl_3$/MeOH/NH_4OH [70:30:3])=0.2; ^{1}H NMR (300 MHz, MeOD) δ 4.46 (d, *J* 2.4 Hz, 2H, C≡CCH_2N), 4.28 (m, 2H, NCH_2CH_2OPO_3), 3.89 (q, *J* 6.5 Hz, 2H, PO_3CH_2), 3.80 – 3.71 (m, 2H, NCH_2CH_2OPO_3), 3.58 (t, *J* 2.3 Hz, 1H, C≡CH), 3.29 (s, 6H, N$(CH_3)_2$), 1.64 (dd, *J* 14.1, 6.7 Hz, 2H, PO_3CH_2CH_2), 1.48 – 1.25 (m, 10H), 0.91 (d, *J* 6.9 Hz, 3H); ^{31}P NMR (121 MHz, MeOD) δ 1.17; ^{13}C NMR (75 MHz, MeOD) δ 83.21, 72.38, 66.81, 65.24, 60.00, 56.28, 51.85, 32.98, 31.78, 30.47, 26.90, 23.70, 14.28; ESI-MS 320.4 (MH^+), 342.4 (MNH_4^+); with the major impurity formed from hydrolysis of **8** (178 mg, 58 %).

(Z)-(R)-3-((2-oxido-1,3,2-dioxaphospholan-2-yl)oxy)propane-1,2-diyl dioleate (11)[179]

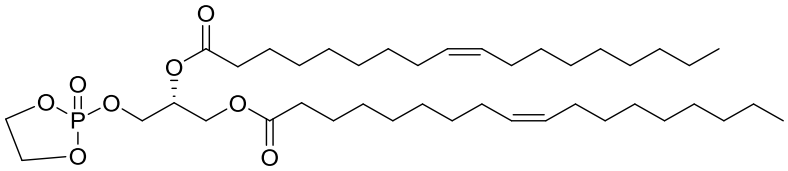

1,2-dioleoyl-*sn*-glycerol **10** (80 mg, 129 µmol, 1 eq), COP (36 µl, 386 µmol, 3 eq) and 4-dimethylaminopyridine (4-DMAP, 1.6 mg, 13 µmol, 0.1 eq) were dissolved in dry toluene and cooled to 0°C. Et_3N (540 µl, 10$_v$% in toluene, 386 µmol, 3 eq) was added dropwise and the reaction mixture stirred at 0°C for 15 minutes then at rt for 4h. The reaction mixture was filtered through Celite and washed with dry toluene. Solvent was removed under reduced pressure to afford the crude compound **11**. R_f (cyclohexane/EtOAc [3:1])=0.1; ^{1}H NMR (300 MHz, $CDCl_3$) δ 5.41 – 5.29 (m, 4H, HC=CH), 5.29 – 5.18 (m, 1H, C$H(CH_2)_2$O), 4.42 (d, *J* 10.7 Hz, 4H, P$(OCH_2)_2$), 4.35 – 4.24 (m, 2H, CH_2OPO_3), 4.16 (dd, *J* 11.9, 5.7 Hz, 2H, CH_2OCO), 2.34 (dt, *J* 11.4, 7.5 Hz, 4H, COCH_2), 2.02 (s, *J* 5.3 Hz, 8H, HC=CHCH_2), 1.61 (s, 4H, COCH_2CH_2), 1.28 (d, *J* 9.7 Hz, 40H, CH_2), 0.88 (t, *J* 6.4 Hz, 6H, CH_3); ^{31}P NMR (121 MHz) δ 18.94 (s). ESI-MS 749.9 (MNa^+), 764.5 (MK^+).

1,2-dioleate-*sn*-glyceryl-3 (2-hydroxyethyl) phosphate (5), and 1,2-dioleate-*sn*-glyceryl-3 (2-(dimethyl(prop-2-yn-1-yl) ammonio)ethyl) phosphate (12)[245]

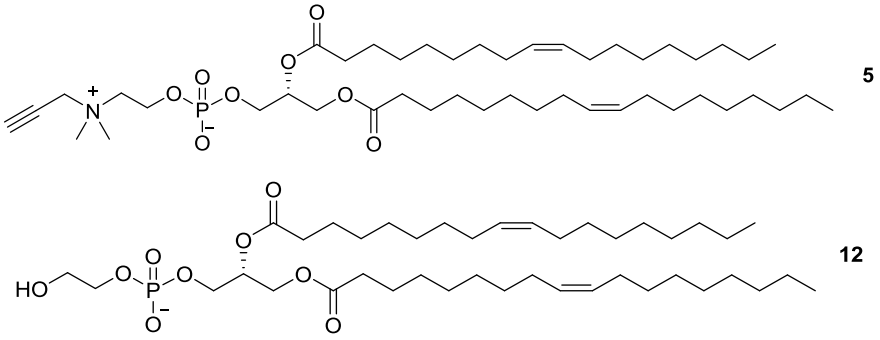

5

12

With the intention of forming compound **5**, compound **11** (284 mg, 1.2 mmol, 1 eq) was dissolved in CH_2Cl_2, to which N,N-dimethylpropargylamine (0.445 ml, 2.46 mmol, 2 eq) was added, then TMSOTf (265 µl, 2.46 mmol, 2 eq) was added dropwise. The reaction was stirred for 15 min at 0°C then at rt for 24 h. The reaction mixture was evaporated and purified by silica column chromatography ($CHCl_3$/MeOH/NH_4OH [9:1:0 to 70:30:3]) to afford the hydrolysis impurity **12** (87 mg, 91 % over two steps). R_f ($CHCl_3$/MeOH/NH_4OH [70:30:3])=0.5; ^{1}H NMR (300 MHz, MeOD) δ 5.40 – 5.28 (m, 4H, HC=CH), 5.27 – 5.19 (m, 1H, C*H*(CH_2)O), 4.31 (ddd, *J* 18.8, 12.0, 4.9 Hz, 2H, CH_2OCO), 3.99 (t, *J* 5.5 Hz, 2H, CH_2OPO_3), 3.90 (dd, *J* 11.1, 5.7 Hz, 2H, $HOCH_2CH_2OPO_3$), 3.69 (t, *J* 4.9 Hz, 2H, $HOCH_2CH_2OPO_3$), 2.32 (q, *J* 7.1 Hz, 4H, $OCOCH_2$), 2.03 (d, *J* 5.4 Hz, 8H, $HC=CHCH_2$), 1.61 (s, 4H, $OCOCH_2CH_2$), 1.46 – 1.21 (m, 40H, CH_2), 0.90 (t, *J* 6.6 Hz, 6H, CH_3); ^{32}P NMR (121 MHz, MeOD) δ 1.45; ESI-MS 744.0 (M^-).

<u>2-azidoethyl-(1,2-dioleate-*sn*-glyceryl-3)-phosphate (13)</u>[210]

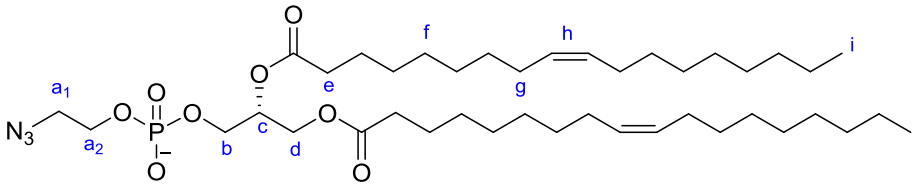

1,2-dioleoyl-*sn*-glycerol (12 mg, 20 µmol, 1 eq), COP (11 µl, 60 µmol, 3 eq) and 4-DMAP (0.25 mg, 2 µmol, cat.) were dissolved in dry toluene and cooled to 0°C. EtN_3 (8 µl, 60 µmol, 3 eq) was added dropwise and the reaction mixture stirred at 0°C for 15 minutes then at rt for 4h. The reaction mixture was filtered through Celite and washed with dry toluene. Solvent was removed under reduced pressure to afford the cyclic phosphate **11** (^{31}P NMR δ 18.92 (s)). The product was redissolved with NaN_3 (7 mg, 110 µmol, 5 eq) in DMF (1.5 ml) and heated to 80°C for 6h. The reaction mixture was dried and purified by silica column chromatography (CH_2Cl_2/MeOH [95:5 to 85:15]) to afford the compound **13** (10 mg, 65 % over two steps). R_f (CH_2Cl_2/MeOH [85:15])=0.5; ^{1}H NMR (300 MHz, $CDCl_3$) δ 6.75 – 5.21 (m, 5H, H^h, H^c), 4.44 –

3.99 (m, 6H, H^{a1}, H^{b}, H^{d}), 3.47 (s, 2H, H^{a1}), 2.32 (dd, *J* 14.1, 6.7 Hz, 4H, H^{e}), 2.01 (d, *J* 5.9 Hz, 1H, H^{g}), 1.61 (s, 4H, $H^{f'}$), 1.44 – 0.93 (m, 40H, H^{f}), 0.88 (t, *J* 6.0 Hz, 6H, H^{i}); ^{31}P NMR (121 MHz) δ -11.61 (s); ESI-MS: 769.0 (M^-).

2-azidoethyl octadecyl phosphate (14)[210]

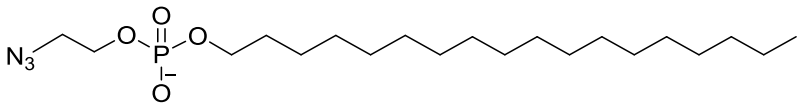

1-Octadecanol (100 mg, 370 µmol, 1 eq) was dissolved in dry toluene (3 ml), and cooled to 0°C. To this solution, COP (82 µl, 481 µmol, 1.3 eq) and EtN_3 (67 µl, 481 µmol, 1.3 eq) was added dropwise, to the apparition of white smoke. Reaction mixture stirred at 0°C for 30 minutes then at rt for 5h. The reaction mixture was filtered through Celite and washed with dry toluene (2 ml). Solvent was removed under reduced pressure to afford the crude cyclic intermediate; R_f (cyclohexane/EtOAc [2:1])=0.2; ^{1}H NMR (300 MHz, $CDCl_3$) δ 4.50 – 4.30 (m, 4 H), 4.15 (dd, *J* 15.2, 6.7 Hz, 2H), 1.77 – 1.64 (m, 2H), 1.26 (s, 30H), 0.88 (t, *J* 6.5 Hz, 3H). The solvent was evaporated from the filtered reaction material overnight. To this dried material, NaN_3 (48 mg, 740 µmol, 2 eq) and DMF (4 ml) was added and the reaction mixture was heated to 80°C. After 5h stirred, no starting material remained. The reaction was stopped and extracted with EtOAc (6×5ml) and washed with water. The organic layers were combined, dried and purified by silica column chromatography ($CHCl_3$/MeOH [93:7 to 8:2]) to afford the compound **14** (57 mg, 38 % over two steps). R_f (CH_2Cl_2/MeOH [9:1])=0.5; ^{1}H NMR (400 MHz, $CDCl_3$/MeOD/D_2O [50:25:25]) δ 3.99 (dd, *J* 10.4, 6.0 Hz, 2H, $N_3CH_2CH_2OP$), 3.87 (q, *J* 6.6 Hz, 2H, $POCH_2$), 3.45 (t, *J* 5.0 Hz, 2H, N_3CH_2), 1.67 – 1.56 (m, 2H, $POCH_2CH_2$), 1.38 – 1.17 (m, 30H), 0.86 (t, *J* 6.9 Hz, 3H, CH_3); ^{31}P NMR (121 MHz) δ 3.61 (s); ^{13}C NMR (101 MHz, MeOD) δ 66.87, 64.93, 51.98, 32.52, 31.25, 31.17, 30.28, 30.01, 29.94, 26.34, 23.25, 14.51; IR/cm^{-1}: 2915 (CH), 2849 (CH), 2109 (N_3), 1082 (P=O); ESI-MS: 418.4 (M^-).

(2*S*,3*S*,4*R*)-2-azido-1,3,4,-octadecanetriol (18)[246]

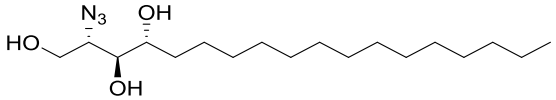

D-*Ribo*-phytosphingosine (1.04 g, 3.28 mmol, 1 eq), $CuSO_4.5H_2O$ (0.81 g, 0.315 mmol, 1 eq) and K_2CO_3 (0.76 g, 5.50 mmol, 1.7 eq) were dissolved in MeOH (20 ml). Imidazole-1-sulfonyl

azide hydrochloride (0.87 g, 4.15 mmol, 1.2 eq) was added and the solution was stirred for 24 h. The solution was filtered and the filter cake washed with CH_2Cl_2/MeOH (10:1). The mother liquor was evaporated and purified by silica column chromatography (9-20% MeOH in CH_2Cl_2) to afford the described compound **18** as a white solid (0.85 g, 2.46 mmol, 75 %). R_f (CH_2Cl_2/MeOH [10:1])=0.5; ^{1}H NMR (300 MHz, MeOD) δ 3.92 (dd, *J* 11.5, 3.4 Hz, 1H, H^{1b}), 3.75 (dd, *J* 11.6, 8.0 Hz, 1H, H^{1a}), 3.63 – 3.55 (m, 1H, H^2), 3.55 – 3.48 (m, *J* 4.4 Hz, 1H, H^3, H^4), 1.75 – 1.49 (m, 2H, CH_2), 1.29 (s, 24H), 0.90 (t, *J* 6.7 Hz, 3H).

(2*S*,3*S*,4*R*)-2-azido-1-(*tert*-butyldiphenylsilyoxy)octadecane-3,4-triol (19)[247]

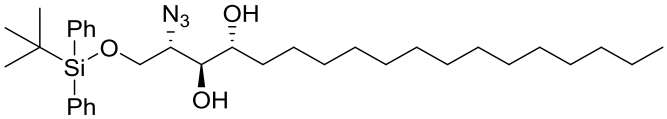

Compound **18** (0.85 g, 2.46 mmol, 1 eq), tert-butyldiphenylsilyl chloride (TBDPSCl, 0.81 g, 2.95 mmol, 1.2 eq), Et_3N (0.86 ml, 6.15 mmol, 2.5 eq) and 4-DMAP (0.015 g, 0.123 mmol, 0.05 eq) were dissolved in dry CH_2Cl_2/DMF (15/3 ml) at 0°C. The reaction mixture was stirred overnight, then diluted with EtOAc, washed with brine (2×20 ml), dried with $MgSO_4$ and purified by silica column chromatography (10-20% EtOAc in cyclohexane) to afford **19** (0.84 g, 59 %). R_f (cyclohex/EtOAc [5:1])=0.4, ^{1}H NMR (300 MHz, $CDCl_3$) δ 7.76 – 7.65 (m, 4H), 7.54 – 7.34 (m, 6H), 4.03 (dd, *J* 10.9, 4.2 Hz, 1H), 3.91 (dd, *J* 10.9, 5.7 Hz, 1H), 3.75 – 3.65 (m, 2H), 3.56 (dd, *J* 9.9, 5.5 Hz, 1H), 2.51 (d, *J* 3.4 Hz, 1H), 1.99 (d, *J* 3.6 Hz, 1H), 1.63 – 1.46 (m, 2H), 1.26 (s, 24H), 1.08 (s, 9H), 0.88 (t, *J* 6.6 Hz, 3H); ^{13}C NMR (75 MHz, $CDCl_3$) δ 136.03, 136.00, 132.93, 132.85, 130.44, 74.52, 72.74, 64.55, 63.76, 32.34, 32.23, 30.09, 29.78, 27.15, 26.07, 23.11, 19.50, 14.55.

(4S,5R)-4-((S)-1-azido-2-((tert-butyldiphenylsilyl)oxy)ethyl)-5-tridecyl-1,3,2-dioxathiolane 2,2-dioxide (20)[247]

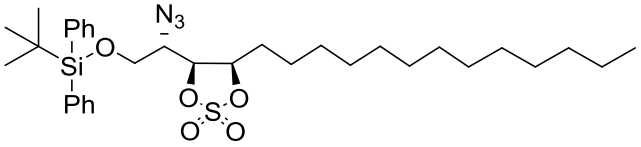

Compound **19** (0.84 g, 1.45 mmol, 1 eq) was dissolved in dry CH_2Cl_2 (8 ml), to which dry Et_3N (0.60 ml, 4.34 mmol, 3 eq) and $SOCl_2$ (0.127 ml, 1.735 mmol, 1.2 eq) were added and stirred at 0 °C. After 30 min the reaction mixture was washed with brine (2×50 ml) and extracted

with EtOAc (2×50 ml), dried ($MgSO_4$) and evaporated. The intermediate cyclic sulfite was dissolved in $CCl_4/CH_3CN/H_2O$ (12 ml, 1:1: 1) and to the solution was added $Ru(III)Cl_3$ (18 mg, 0.07 mmol, 0.05 eq) and $NaIO_4$ (0.90 g, 4.22 mmol, 3 eq). The reaction mixture was stirred for 2 h, diluted with EtOAc (30 ml), washed with sat. $NaHCO_3$ solution (2×20 ml), extracted with EtOAc, dried ($MgSO_4$), evaporated and purified by silica column chromatography (10% EtOAc in cyclohexane) to afford **20** (0.83 g, 89 %). R_f (cyclohex:EtOAc [6:1])=0.8; ^{1}H NMR (300 MHz, $CDCl_3$) δ 7.74 – 7.64 (m, 4H), 7.50 – 7.37 (m, 6H), 4.98 (ddd, *J* 10.2, 5.2, 2.6 Hz, 1H), 4.92 (dd, *J* 9.9, 5.2 Hz, 1H), 4.04 (dd, *J* 11.3, 2.4 Hz, 1H), 3.89 (dd, *J* 11.3, 5.2 Hz, 1H), 3.69 (ddd, *J* 9.7, 5.1, 2.4 Hz, 1H), 2.00 – 1.66 (m, 2H), 1.41 – 1.30 (m, 2H), 1.27 (s, 22H), 1.09 (s, 9H), 0.88 (t, *J* 6.7 Hz, 3H); ^{13}C NMR (75 MHz, $CDCl_3$) δ 135.98, 132.60, 132.36, 130.56, 128.39, 86.85, 80.26, 63.97, 59.62, 32.33, 30.06, 29.86, 29.76, 29.70, 29.36, 28.53, 27.33, 27.14, 25.59, 23.10, 19.57, 14.52.

(2*S*,3*R*)-(*E*)-2-azido-1-(*tert*-butyldiphenylsilyoxy)octadec-4-en-3-ol (21)[247]

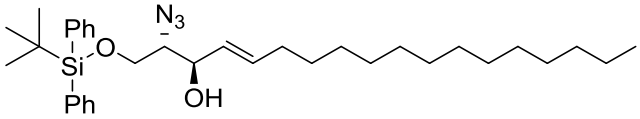

Compound **20** (772 mg, 1.20 mmol, 1 eq) was dissolved in dry toluene (8 ml), to which Bu_4NI (487 mg, 1.32 mmol, 1.1 eq) and 1,8-diazabicyclo(5.4.0)undec-7-ene (DBU, 274 mg, 1.80 mmol, 1.5 eq) was added. The reaction mixture was refluxed for 2 h, the solvent evaporated and redissolved in a solution of concentrated H_2SO_4 (0.1 ml), H_2O (0.8 ml) and tetrahydrofuran (THF, 10 ml) and stirred for a further 1 h. Purification by silica column chromatography (10% EtOAc in cyclohexane) afforded **21** (0.72 g, 60 %). R_f (cyclohex:EtOAc [10:1])=0.4; ^{1}H NMR (300 MHz, $CDCl_3$) δ 7.74 – 7.65 (m, 4H), 7.49 – 7.33 (m, 6H), 5.74 (dtd, *J* 15.5, 6.5, 0.5 Hz, 1H), 5.43 (ddt, *J* 15.4, 7.1, 0.5 Hz, 1H), 4.22 (dd, *J* 11.8, 5.4 Hz, 1H), 3.82 (dd, *J* 10.8, 6.3 Hz, 1H), 3.77 (dd, *J* 10.6, 4.6 Hz, 1H), 3.51 (dd, *J* 11.2, 4.9 Hz, 1H), 1.98 – 1.59 (m, 2H), 1.36 – 1.28 (m, 2H), 1.26 (s, 20H), 1.07 (s, 9H), 0.88 (t, *J* 6.7 Hz, 3H); ^{13}C NMR (75 MHz, $CDCl_3$) δ 135.98, 135.85, 133.15, 130.31, 128.22, 73.23, 67.28, 64.53, 32.69, 32.33, 30.08, 29.88, 29.77, 29.59, 29.35, 27.12, 23.10, 19.51, 14.53.

(2*S*,3*R*)-(*E*)-2-azido-3-*O*-benzoyl-1-O-*tert*-butyldiphenylsilyl-4-octadecene-1,3-diol (22)[248]

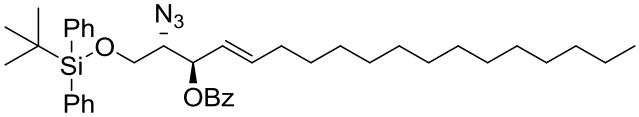

Compound **21** (1.95 g, 3.48 mmol, 1 eq) was dissolved in dry pyridine (12 ml) at 0 °C, to which BzCl (960 µl, 8.29 mmol, 2.4 eq) was added dropwise and the reaction mixture was stirred for 3 h at 0 °C to rt, quenched with H_2O (40 ml) and stirred for a further 20 min. The reaction mixture was extracted with CH_2Cl_2 (3×50 ml), washed with HCl (1 M, 100 ml), saturated $NaHCO_3$ solution (100 ml) and brine (100 ml), dried ($MgSO_4$), evaporated and purified by silica column chromatography (20 – 10% EtOAc in cyclohexane) to afford **22** (2.01 g, 87 %). R_f (cyclohex:EtOAc [10:1])=0.8; $[\alpha]^{22}_D$=-9.0° (*c* 7.0, $CHCl_3$); ^{1}H NMR (300 MHz, $CDCl_3$) δ 8.03 (d, *J* 7.5 Hz, 2H, Si(C_6H_5)$_2$), 7.73– 7.56 (5H, m, Ph), 7.50-7.30 (8H, m, Si(C_6H_5)$_2$), 5.91 (1H, ddd, $J^{5\text{-}6}$ 6.8 Hz, $J^{5\text{-}6'}$ 6.8 Hz, $J^{5\text{-}4}$ 15.2 Hz, H^5), 5.69 (1H, dd, $J^{3\text{-}4}$ 7.9, $J^{3\text{-}2}$ 4.7 Hz, H^3), 5.52 (1H, dd, $J^{4\text{-}5}$ 15.4, $J^{4\text{-}3}$ 8.0 Hz, H^4), 3.85 (1H, m, H^2), 3.75 (2H, m, H^{1a}, H^{1b}), 2.06 – 1.97 (2H, m, H^6, $H^{6'}$), 1.40 – 1.18 (22H, m, 11CH_2), 1.09 (9H, s, ^{t}Bu), 0.89 (3H, t, *J* 6.7 Hz, CH_3); ESI-HRMS: Calcd for [MNa^+] 690.4066. Found: *m/z* 690.4061.

(2*S*,3*R*)-(*E*)-2-amino-3-*O*-benzoyl-1-O-*tert*-butyldiphenylsilyl-4-octadecene-1,3-diol (23)[248,249]

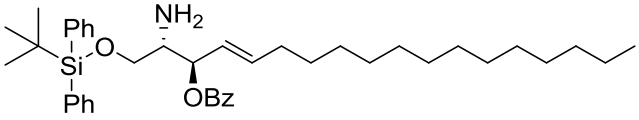

Compound **22** (685 mg, 1.03 mmol, 1 eq) was dissolved in toluene/water (20:1, 10 ml), to which PPh_3 (538 mg, 2.05 mmol, 2 eq) was added. The reaction mixture was stirred overnight, heated to 60°C for 2h until all starting material and phosphorus intermediate had disappeared from TLC. Reaction mixture was evaporated and purified by silica column chromatography (0.5 to 10% EtOAc in cyclohexane) to afford **23** (494 mg, 78 %) as a mixture of inseparable stereoisomers (2*S*,3*R*) and (2*R*,3*R*) (98:2). R_f (cyclohex:EtOAc [3:1]+1% Et_3N)=0.1; ^{1}H NMR (300 MHz, $CDCl_3$) δ 7.88 (d, *J* 7.2 Hz, 2H, Bz), 7.68 – 7.38 (m, 5H, TBDPS), 7.38 – 7.20 (m, 6H, aromatic), 7.20 – 7.10 (m, 2H, Bz), 5.90 – 5.77 (m, 1H, H^5), 5.48 – 5.34 (m, 2H, H^3, H^4), 3.72 – 3.59 (m, 2H, H^{1a}, H^{1b}), 3.10 (q, *J* 5.1 Hz, 1H, H^2), 1.97 (q, *J* 6.9 Hz, 2H, H^6), 1.29 – 1.07 (m, 22H, 11CH_2), 0.99 (s, 9H, ^{t}Bu), 0.80 (t, *J* 6.6 Hz, 3H, CH_3); ^{13}C NMR (75 MHz, $CDCl_3$) δ 165.51 (CO benzyl), 137.91 (C^5), 135.75, 135.59, 135.59, 133.38, 133.22, 133.00), 130.71, 130.27, 130.23, 129.87, 129.81, 129.75, 128.79, 128.49, 128.08, 127.90, 127.82, 127.13, 125.05 (C^4), 76.56

(C^3), 64.93 (C^1), 55.56 (C^2), 32.61 (C^6), 32.11 (C^{16}), 29.85, 29.77, 29.63, 29.55, 29.39, 29.09, 26.99 (^{t}Bu), 22.88 (^{t}Bu), 19.40 (C^{17}), 14.32 (C^{18}); ESI-MS 642.8 (MH^+), 664.8 (MNa^+), 1284.3 ($2MH^{2+}$); ESI-HRMS: Calcd for [MNa^+] 664.4161. Found: *m/z* 664.4156.

(2*S*,3*R*)-(*E*)-1-*O*-*tert*-butyldiphenylsilyl-2-(2,2-dichloroacetamido)-3-*O*-benzoyl-4-octadecene-1,3-diol (24)[250]

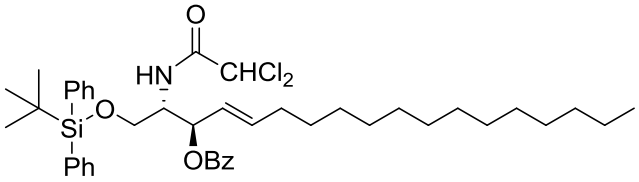

Compound **23** (970 mg, 1.51 mmol, 1 eq) was dissolved in dry CH_2Cl_2 (20 ml) and cooled to -15°C. DIPEA (385 µl, 2.26 mmol, 1.5 eq) was added dropwise, followed by dichloroacetyl chloride (182 µl, 1.89 mmol, 1.25 eq) dropwise. After 15 minutes at -10°C, the reaction was stirred 30 minutes at rt until complete conversion by TLC. The reaction was quenched with water, extracted with CH_2Cl_2, washed with brine, dried ($MgSO_4$), evaporated and purified by silica column chromatography (1 – 10% EtOAc in cyclohexane) to afford **24** (918 mg, 81 %). R_f (cyclohex:EtOAc [20:1])=0.3; $[\alpha]^{22}_D$=+20.8° (*c* 5.0, $CHCl_3$); ^{1}H NMR (300 MHz, $CDCl_3$) δ 7.95 – 7.89 (m, 2H, Bz), 7.60 – 7.45 (m, 5H, arom), 7.41 – 7.20 (m, 6H, arom), 7.12 (t, *J* 7.3 Hz, 2H, Bz), 5.94 – 5.81 (m, 1H, H^5), 5.84 (s, 1H, $CHCl_2$), 5.66 (t, $J^{3\text{-}2,\ 3\text{-}4}$ 7.5 Hz, 1H, H^3) 5.43 (dd, $J^{4\text{-}5}$ 15.4, $J^{4\text{-}3}$ 7.5 Hz, 1H, H^4), 4.27 (ddd, $J^{2\text{-}3}$ 7.2, $J^{2\text{-}1a}$3.5, $J^{2\text{-}1b}$4.0 Hz, 1H, H^2), 3.84 (dd, $J^{1a\text{-}b}$ 10.6, $J^{1a\text{-}2}$ 3.0 Hz, 1H, H^{1a}), 3.65 (dd, $J^{1a\text{-}b}$ 10.6, $J^{1b\text{-}2}$4.0 Hz, 1H, H^{1b}), 1.95 (q, $J^{6\text{-}5}$ 6.9 Hz, 2H, H^6), 1.32 – 1.09 (m, 22H), 0.99 (s, 9H), 0.81 (t, *J* 6.7 Hz, 3H); ^{13}C NMR (75 MHz, $CDCl_3$) δ 165.17 (*C*O$CHCl_2$), 163.57 (CO benzyl), 138.01 (C^5), 135.53, 135.45, 133.10, 132.34, 132.18, 130.06, 130.00, 129.88, 129.71, 128.42, 127.91, 127.79, 124.13 (C^4), 73.59 (C^3), 66.57 ($CHCl_2$), 61.72 (C^1), 53.13 (C^2), 32.37 (C^6), 31.94 (C^{16}), 29.68, 29.59, 29.47, 29.38, 29.25, 28.82, 26.77 (^{t}Bu), 22.71 (C^{17}), 19.17 (^{t}Bu), 14.16 (C^{18}); ESI-MS 752.7 (MH^+); ESI-HRMS: Calcd for [MH^+] 752.3668. Found: *m/z* 752.3663.

(2*S*,3*R*)-(*E*)-2-(2,2-dichloroacetamido)-3-*O*-benzoyl-4-octadecene-1,3-diol (25)

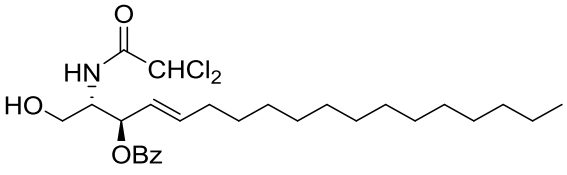

To a solution of compound **24** (888 mg, 1.18 mmol, 1 eq) in THF (20 ml), benzoic acid (187 mg, 1.53 mmol, 1.3 eq) was added and the solution cooled to 0°C. To this, tetra-n-butylammonium fluoride (TBAF, 1M solution in THF, 1.53 ml, 1.3 eq) was added dropwise over 3 minutes. The reaction was warmed to rt over 10 minutes and stirred for 4 h before complete conversion. The reaction was quenched with water (10 ml) and extracted with CH_2Cl_2 (2×10 ml), dried ($MgSO_4$), evaporated and purified by silica column chromatography (0.5 – 5% EtOH inCH_2Cl_2) to afford **25** (582 mg, 96 %). R_f (EtOH/CH_2Cl_2 [1:99])=0.2; ^{1}H NMR (300 MHz, $CDCl_3$) δ 8.04 (d, *J* 7.4 Hz, 2H, Bz), 7.53 (dt, *J* 41.5, 7.4 Hz, 3H, Bz), 7.10 (d, *J* 9.0 Hz, 1H, NH), 5.93 (s, 1H, $CHCl_2$), 5.99 – 5.81 (m, 1H, H^5), 5.68 – 5.50 (m, 2H, H^4, H^3), 4.23 (m, 1H, H^2), 3.89 – 3.57 (m, 2H, $H^{1a,b}$), 2.81 (br s, 1H, OH), 2.05 (dd, J^6 14.1, J^{6-5} 6.9 Hz, 2H, H^6), 1.48 – 1.11 (m, 22H, CH_2), 0.87 (t, *J* 6.6 Hz, 3H, CH_3); ^{13}C NMR (75 MHz, $CDCl_3$) δ 166.51 (CO benzoyl), 164.08 ($\underline{C}OCHCl_2$), 138.41 (C^5), 133.61 (Bz), 129.87 (Bz), 128.57 (Bz), 123.93 (C^4), 74.01 (C^3), 66.44 ($CHCl_2$), 60.79 (C^2), 53.78 (C^1), 32.32 (C^6), 31.93 (C^{16}), 29.67, 29.59, 29.45, 29.37, 29.24, 28.77, 22.71 (C^{17}), 14.15 (C^{18}); ESI-MS 512.4 ($M\text{-}H^-$); ESI-HRMS: Calcd for [MH^+] 514.2490. Found: *m/z* 514.2485.

(2*S*,3*R*)-(*E*)-1-((methylsulfonyl)oxy)-2-(2,2-dichloroacetamido)-3-*O*-benzoyl-4-octadecene-1,3-diol (26)

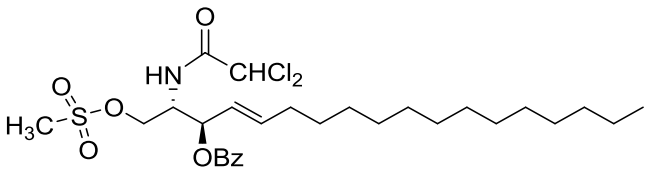

To a solution of compound **25** (510 mg, 0.99 mmol, 1 eq) in pyridine (15 ml) at -10°C, methanesulfonyl chloride (MsCl, 109 µl, 1.27 mmol, 1.4 eq) was added. The solution was warmed to rt after 5 min and stirred for 3 h before co-evaporation with toluene. The product was purified by silica column chromatography (10 – 50 % EtOAc in cyclohexane) to afford **26** (548 mg, 93 %). R_f (EtOH/CH_2Cl_2 [1:99])=0.5; ^{1}H NMR (300 MHz, $CDCl_3$) δ 8.07 – 7.99 (m, 2H), 7.60 (t, *J* 7.5 Hz, 1H), 7.47 (t, *J* 7.6 Hz, 2H), 6.93 (d, *J* 8.6 Hz, 1H, NH_2), 6.07 – 5.94 (m, 1H, H^5), 5.66 (t, J^{4-3} 7.0 Hz, 1H, H^3), 5.50 (dd, *J* 15.4, 7.4 Hz, 1H, H^4), 4.54 (m, 1H, H^2), 4.50 – 4.37 (m, 2H, $H^{1a,b}$), 3.03 (s, 3H, Ms), 2.06 (dd, J^6 14 Hz, J^5 7.0 Hz, 2H, H^6), 1.43 – 1.15 (m, 22H, CH_2), 0.87 (t, *J* 6.6 Hz, 3H, CH_3); ^{13}C NMR (75 MHz, $CDCl_3$) δ 165.31 (*C*O$CHCl_2$), 164.17 (COPh), 139.22 (C^5), 133.57 (Bz), 129.74 (Bz), 129.43 (Bz), 128.62 (Bz), 123.06 (C^4), 73.18 (C^3), 66.57 (C^1), 66.16 ($CHCl_2$), 51.67 (C^2), 37.65 (SO_2CH_3), 32.34 (C^6), 31.93 (C^{16}), 29.66, 29.57, 29.43, 29.37, 29.21,

28.71, 22.70 (C^{17}), 14.15 (C^{18}); ESI-MS 590.5 ($M\text{-}H^-$), 626.8 (MCl^-); ESI-HRMS: Calcd for [MNa^+] 614.2085. Found: *m/z* 614.2080.

(2*S*,3*R*)-(*E*)-2-(2,2-dichloroacetamido)-1-iodo-3-*O*-benzoyl-4-octadecene-3-ol (27)

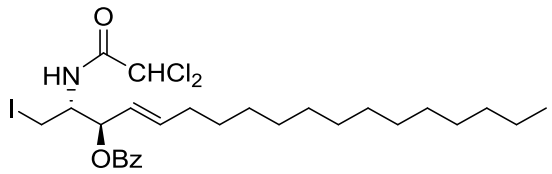

To a solution of compound **26** (62 mg, 0.11 mmol, 1 eq) in distilled acetone (1 ml), sodium iodide (146 mg, 0.30 mmol, 10 eq) was added and mixture was refluxed at 65°C for 5h. The reaction was quenched with H_2O, extracted with CH_2Cl_2, dried ($MgSO_4$) and evaporated. The product was purified by silica column chromatography (10 – 50 % EtOAc in cyclohexane) to afford **27** (48 mg, 76 %). R_f (EtOAc/cyclohexane [9:1])=0.7; ^{1}H NMR (300 MHz, $CDCl_3$) δ 7.97 (d, *J* 7.3 Hz, 2H), 7.53 (m, 1H), 7.39 (t, *J* 7.6 Hz, 2H), 6.60 (d, $J^{N\text{-}2}$ 9.1 Hz, 1H, NH^2), 6.02 – 5.88 (m, 1H, H1), 5.55 (t, *J* 6.9 Hz, 1H), 5.43 (dd, *J* 15.2, 7.5 Hz, 1H), 4.19 (td, *J* 11.1, 6.1 Hz, 1H), 3.35 (qd, *J* 10.8, 5.4 Hz, 1H), 1.99 (q, *J* 6.9 Hz, 1H), 1.40 – 1.04 (m, 12H), 0.81 (t, *J* 6.6 Hz, 2H); ^{13}C NMR (75 MHz, $CDCl_3$) δ 165.07 (*C*O$CHCl_2$), 163.70 (COPh), 139.19 (C^5), 133.42 (Bz), 129.75 (Bz), 129.59 (Bz), 128.55 (Bz),122.82 (C^4), 75.43 (C^3), 66.29 ($CHCl_2$), 52.36 (C^2), 32.40 (C^6), 31.94 (C^{16}), 29.67, 29.58, 29.43, 29.38, 29.21, 28.73, 22.72 (C^{17}), 14.16 (C^{18}), 5.17 (C^1); ESI-MS 641.5 (MNH_4^+); ESI-HRMS: Calcd for [MNa^+] 646.1327. Found: *m/z* 646.1322.

(2*S*,3*R*)-(*E*)- 1-azido-2-(2,2-dichloroacetamido)-3-*O*-benzoyl-4-octadecene-3-ol (28)

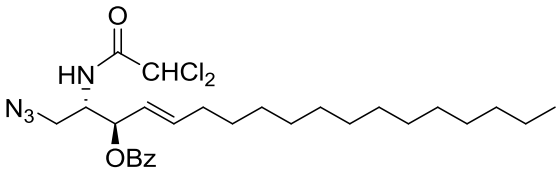

To a solution of compound **27** (380 mg, 0.61 mmol, 1 eq) in DMF (2.5 ml), sodium azide (396 mg, 6.1 mmol, 10 eq) was added and the mixture stirred for 14 h. The reaction was quenched with H_2O and extracted with EtOAc, washed with brine, dried ($MgSO_4$) and evaporated. The product was purified by silica column chromatography (4 to 5 % EtOAc in cyclohexane) to afford **28** (316 mg, 97 %). R_f (EtOAc/cyclohexane [9:1])=0.6; $[\alpha]^{22}_D$=+11.7 (c 10.0, $CHCl_3$); ^{1}H NMR (300 MHz, $CDCl_3$) δ 8.04 (d, *J* 7.3 Hz, 2H, Bz), 7.60 (t, *J* 7.4 Hz, 1H, Bz), 7.45 (m, 1H, Bz), 6.83 (d, $J^{N\text{-}2}$ 9.0 Hz, 1H, NH), 6.04 – 5.92 (m, 1H, H^5), 5.61 (t, $J^{3\text{-}4,\,3\text{-}2}$ 6.8 Hz, 1H,

H^3), 5.49 (dd, J^{4-5} 15.3, J^{4-3} 7.4 Hz, 1H, H^4), 4.41 (m, 1H, H^2), 3.70 – 3.54 (m, 2H, $H^{1a,b}$), 2.06 (dd, J^{6-5} 6.9 Hz, $J^{6-6'}$ 14 Hz, 2H, H^6), 1.43 – 1.19 (m, 12H, CH_2), 0.87 (t, *J* 6.6 Hz, 3H, CH_3). ^{13}C NMR (75 MHz, $CDCl_3$) δ 165.37 (COPh), 163.97 (*C*O$CHCl_2$), 138.70 (C^5), 133.48 (Bz), 129.76 (Bz), 129.55 (Bz), 128.57 (Bz), 123.22 (C^4), 73.93 (C^3), 66.25 ($CHCl_2$), 51.92 (C^2), 50.58 (C^1), 32.37 (C^6), 31.94 (C^{16}), 29.67, 29.59, 29.44, 29.38, 29.21, 28.76, 22.72 (C^{17}), 14.16 (C^{18}). IR, v 3292 (NH), 2923 (C-H), 2853 (C=C), 2103 (N_3), 1721, 1679, 1262, 710 cm^{-1}; ESI-MS 561.5 (MNa^+), 537.5 ($M\text{-}H^-$); ESI-HRMS: Calcd for [MNa^+] 561.2375. Found: *m/z* 561.2370.

(*2S,3R*)-(E)-2-amino-1-azido-4-octadecen-3-ol (1-azidosphingosine) (17)[184]

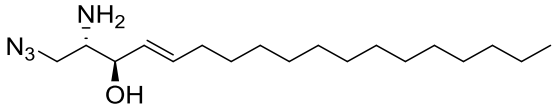

Compound **28** (30 mg, 0.056 mmol, 1 eq) was stirred in a solution of KOH (0.5M) in H_2O/MeOH (3:7) at 40°C for 4 h. The reaction mixture was evaporated and the product was purified by silica column chromatography (cyclohexane/EtOAc/NH_4OH [97:3:0.3]) to afford **17** (11 mg, 61 %). R_f (cyclohexane/EtOAc/NH_4OH [97:3:0.3])=0.3; $[\alpha]^{22}_D$=+9.8 (c 0.5, MeOH); ^{1}H NMR (300 MHz, $CDCl_3$) δ 5.87 – 5.68 (m, 1H, H^5), 5.43 (dd, J^{4-5} 15.4, J4-3 7.2 Hz, 1H, H^4), 4.00 (t, $J^{3-4,\ 3-2}$ 6.1 Hz, 1H, H^3), 3.48 (dd, J^{1a-b} 12.2 Hz, J^{1-2} 3.9 Hz, 1H, H^{1a}), 3.32 (dd, J^{1a-b} 12.1, 7.6 Hz, 1H, H^{1b}), 2.95 (bs, 1H, H^2), 2.06 (q, *J* 6.9 Hz, 2H, H^6), 1.61 (bs, 2H, NH_2), 1.44 – 1.11 (m, 23H, CH_2), 1.06 (bs, 1H, OH), 0.87 (t, *J* 6.5 Hz, 3H, CH_3); ^{13}C NMR (75 MHz, $CDCl_3$) δ 135.53 (C^5), 128.24 (C^4), 74.22 (C^3), 54.93 (C^2), 54.26 (C^1), 32.38 (C^6), 31.93 (C^{16}), 29.68, 29.62, 29.48, 29.37, 29.23, 29.11, 22.71 (C^{17}), 14.15 (C^{18}); IR v 3354 (NH), 3287 (NH), 3154 (OH, C=C-H), 2916 (C-H), 2848 (C-H), 2133 (N_3); ESI-MS 5325.5 (MH^+), 307.4 ($MH\text{-}H_2O^+$); ESI-HRMS: Calcd for [MH^+] 325.2967. Found: *m/z* 325.2962.

1-azidoceramide (C22:1) (30)[209]

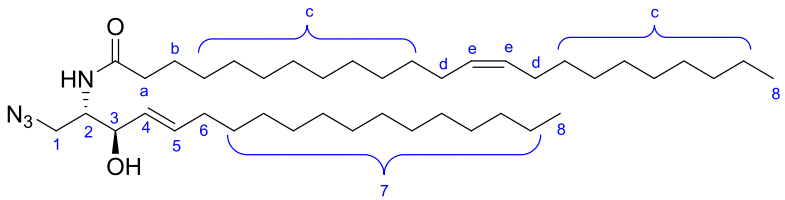

Compound **17** (3×1.67 mg, 15.5 µmol, 1 eq) was mixed in 3 separate Eppendorf tubes with erucic acid (3×2 mg, 5.9 µmol, 1.2 eq) in a phosphate buffer solution (pH 7.4, NaH_2PO_4 (0.1M),

Na_2HPO_4 (0.1M), H_3PO_4 (0.1M)) with 0.4% Triton X-100 detergent. To this, SCDase enzyme (10 µl, 50 mU) was added to each Eppendorf, and the mixture was shaken at 37°C overnight. The reaction mixture was lyophilised and purified by silica column chromatography (0.4% NH_4OH in CH_2Cl_2) to afford **30** (6.3 mg, 64%). R_f (CH_2Cl_2/MeOH [95:5])=0.8; $[\alpha]^{22}{}_D$=+1.6 (c 0.5, $CHCl_3$); ^{1}H NMR (400 MHz, $CDCl_3$) δ 5.82 (d, J^{NH-2} 8.0 Hz, 1H, NH), 5.76 (dd, J^{5-4} 15.0, J^{5-6} 7.0 Hz, 1H, H^5), 5.46 (dd, J^{4-5} 15.4, J^{4-3} 6.6 Hz, 1H, H^4), 5.35 (t, J^{e-d} 4.7 Hz, 2H, H^e), 4.18 (q, $J^{3-4,\ 3-2}$ 5.6 Hz, 1H, H^3), 4.05 (td, J^{2-1} 8.9, J^{2-3} 4.9 Hz, 1H, H^2), 3.58 (ddd, J^{1a-b} 16.5, J^{1a-2}12.6, J^{1b-2} 4.5 Hz, 2H, H^{1a}, H^{1b}), 2.40 (d, J^{OH-1} 5.6 Hz, 1H, OH), 2.20 (t, J^{a-b} 7.5 Hz, 2H, H^a), 2.12 – 1.95 (m, 6H, H^6, H^d), 1.69 – 1.57 (m, 2H, H^b), 1.26 (s, 44H, H^7, H^c), 0.88 (t, *J* 6.8 Hz, 6H, H^8); ^{13}C NMR (101 MHz, $CDCl_3$) δ 173.48 (NHCO), 135.05 (C^5), 130.00 (C^e), 128.52 (C^4), 73.51 (C^3), 52.79 (C^2), 50.96 (C^1), 36.91 (C^a), 32.35 (C^6), 32.01, 29.87, 29.78, 29.72, 29.66, 29.59, 29.45, 29.42, 29.36, 29.31, 29.18, 27.30, 25.75 (C^b), 22.78 ($\underline{C}H_2CH_3$), 14.21 (C^8); ESI-HRMS: Calcd for [MH^+] 645.6046. Found: *m/z* 645.6041.

(S)-4-((R,E)-1-hydroxyhexadec-2-en-1-yl)oxazolidin-2-one (29)

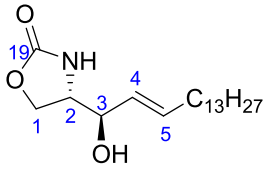

R_f (cyclohexane/EtOAc/NH_4OH [97:3:0.3])=0.3; ^{1}H NMR (300 MHz, $CDCl_3$) δ 5.79 (dt, J^{4-5} 15.4 Hz, J^{5-6} 6.7 Hz, 1H, H^5), 5.34 (dd, J^{4-5} 15.4 Hz, J^{4-3} 7.5 Hz, 1H, H^4), 5.07 (bs, 1H, NH), 4.38 (t, $J^{1a-b,\ 1a-2}$ 8.8 Hz, 1H, H^{1a}), 4.25 (dd, J^{1a-b} 8.9, J^{1b-2} 5.0 Hz, 1H, H^{1b}), 3.99 (t, $J^{3-2,\ 3-4}$ 6.6 Hz, 1H, H^3), 3.76 (dt, J^{2-1a} 8.6, $J^{2-1b,\ 2-3}$ 5.4 Hz, 1H, H^2), 2.00 (q, *J* 6.8 Hz, 2H, H^6), 1.59 (bs, 1H, OH), 1.39 – 1.25 (m, 2H, CH_2), 1.19 (s, 20H, CH_2), 0.81 (t, *J* 6.7 Hz, 3H, CH_3); ^{13}C NMR (75 MHz, $CDCl_3$) δ 159.69 (C^{19}), 137.30 (C^5), 126.69 (C^4), 73.93 (C^3), 66.70 (C^1), 55.99 (C^2), 32.33 (C^6), 31.91 (C^7), 29.56, 29.43, 29.34, 29.19, 28.95, 22.67 (C^{17}), 14.09 (C^{18}). ; IR/cm^{-1}: 3286 (OH), 2917 (CH), 2849 (CH), 16832 (C=O); ESI-MS: 326.7 [MH^+], 343.5 [MNH_4^+], 348.5 [MNa^+], 324.5 [$M\text{-}H^-$]

(2*S*,3*S*,4*R*)-2-(*N*-2,2-dichloroacetamido)-1,3,4,-octadecanetriol (32)

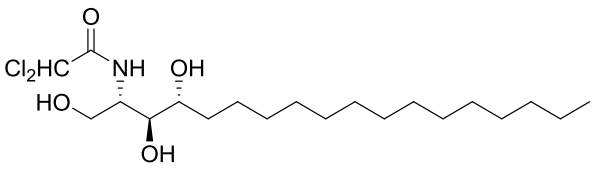

Phytosphingosine (1.1 g, 3.46 mmol, 1 eq) was suspended in THF (40 ml), to which DIPEA (0.8 ml, 4.34 mmol, 1.3 eq) was added and the mixture was cooled to -10°C. Dichloroacetyl chloride (367 µl, 3.82 mmol, 1.1 eq) was added dropwise and the reaction was warmed to rt after 15 min, then stirred at rt for 3h, evaporated and purified by silica column chromatography (2.5 to 7% MeOH in CH_2Cl_2) to afford **32** as a white crystalline solid (1.41 g, 81 %). R_f (MeOH/CH_2Cl_2 [5:95]) =0.3; $[\alpha]^{22}_D$=+7.9 (c 3.3, $CHCl_3$/MeOH [1:1]); ^{1}H NMR (500 MHz, $CDCl_3$) δ 7.60 (d, *J* 8.4 Hz, 1H, NH), 5.97 (s, 1H, $CHCl_2$), 4.07 (dt, *J* 5.0, 3.2 Hz, 1H, H^2), 3.84 (dd, *J* 11.6, 3.4 Hz, 1H, H^{1a}), 3.70 (dd, *J* 11.6, 5.4 Hz, 1H, H^{1b}), 3.64 – 3.55 (m, 2H, H^4, H^3), 1.68 – 1.35 (m, 4H, H^5, H^6), 1.35 – 1.13 (m, 22H), 0.84 (t, *J* 7.0 Hz, 3H); ^{13}C NMR (126 MHz, $CDCl_3$) δ 164.56, 75.08 (C^3), 72.59 (C^4), 66.33 ($CHCl_2$), 60.57 (C^1), 52.30 (C^2), 32.86 (C^5), 31.89 (C^6), 29.66, 29.62, 29.33, 25.80, 22.66, 14.07; ESI-HRMS: Calcd for [MH^+] 428.2329. Found: *m/z* 428.2332.

(2*S*,3*S*,4*R*)-1-azido-2-(*N*-2,2-dichloroacetamido)-3,4,-octadecanediol (3)

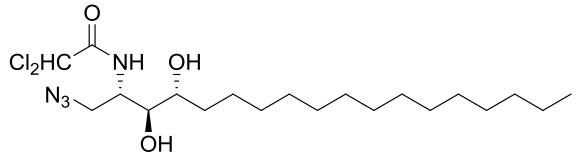

N-Protected phytosphingosine **32** (50 mg, 0.117 mmol, 1 eq) and NaN_3 (76 mg, 1.17 mmol, 10 eq) were suspended in DMF (1 ml), to which PPh_3 (61 mg, 0.23 mmol, 2 eq) and then CBr_4 (77 mg, 0.23 mmol, 2 eq) in DMF (0.5 ml) was added and the mixture stirred at rt overnight. The reaction was quenched with MeOH, evaporated, diluted with CH_2Cl_2, washed with H_2O, and purified by silica column chromatography (10 to 25% EtOAc in n-hexane) to afford **33** as a crystalline white solid (16 mg, 31 %). R_f (EtOAc/n-hexane [4:6]) =0.7; $[\alpha]^{22}_D$=+14.3 (c 0.7, $CHCl_3$/MeOH [9:1]); ^{1}H NMR (500 MHz, $CDCl_3$) δ 7.10 (d, *J* 8.5 Hz, 1H, NH), 5.97 (s, 1H, $CHCl_2$), 4.23 (td, *J* 8.9, 4.6 Hz, 1H, H^2), 3.84 (dd, *J* 12.7, 4.8 Hz, 1H, H^{1a}), 3.74 – 3.66 (m, 3H, H^{1b}, H^3, H^4), 1.75 – 1.42 (m, 4H, H^5, H^6), 1.42 – 1.19 (m, 22H), 0.90 (t, *J* 6.9 Hz, 3H); ^{13}C NMR (101 MHz, $CDCl_3$) δ 164.22, 74.35 (C^3 or C^4), 72.82 (C^3 or C^4), 66.27 ($CHCl_2$), 51.01 (C^1), 50.65 (C^2), 32.74 (C^5), 31.93 (C^6), 29.69, 29.59, 29.56, 29.52, 29.37, 25.68, 22.70, 14.14; ESI-HRMS: Calcd for [MH^+] 453.2394. Found: *m/z* 453.2395.

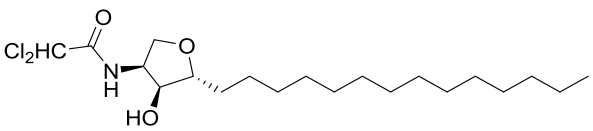

N-Protected 2-epi-Jaspine B **34**,[190] a cyclisation side product, was also purified (18 mg, 38%). R_f (EtOAc/n-hexane [4:6]) =0.8; ^{1}H NMR (500 MHz, DMSO) δ 8.37 (d, *J* 7.2 Hz, 1H, NH), 6.63 (s, 1H, $CHCl_2$), 5.58 (d, *J* 4.9 Hz, 1H, OH), 4.14 – 4.06 (m, 1H, H^2), 3.98 (dd, *J* 8.5, 6.9 Hz, 1H, H^{1a}), 3.81 (dd, *J* 11.0, 5.1 Hz, 1H, H^3), 3.60 – 3.54 (m, 1H, H^4), 3.41 – 3.36 (m, 1H, H^{1b}), 1.75 – 1.33 (m, 4H, H^5, H^6), 1.24 (s, Hz, 22H), 0.86 (t, *J* 6.9 Hz, 3H); ^{13}C NMR (126 MHz, DMSO) δ 164.07, 84.66 (C4), 73.53 (C3), 69.89 (C1), 66.99 ($CHCl_2$), 52.39 (C2), 33.52, 31.77, 29.53, 29.49, 29.19, 25.87, 22.57, 14.41; UPLC-MS (gradient 90-100% CH_3CN/H_2O, 4 min, ESI) rt=3.42; [M-H$^-$] 408.

(2*S*,3*S*,4*R*)-1-azido-2-amino-3,4,-octadecanediol (31)

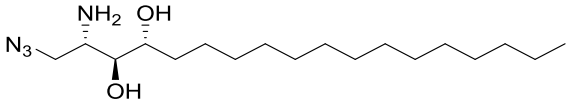

Compound **33** (23 mg, 49 µmol) was solubilised in MeOH (900 µl) and KOH (2M aqueous solution, 300 µl, 0.5M final) was added and the solution was stirred at 40°C for 6h, then rt overnight. The reaction mixture was neutralised (HCl, 2M), dried and purified by silica column chromatography (CH_2Cl_2/MeOH/NH_4OH [96:4:0.4]) to afford **31** as a crystalline white solid (9 mg, 53 %). R_f (CH_2Cl_2/MeOH/NH_4OH [95:5:0.5])=0.1; $[\alpha]^{22}_D$=+1.0 (c 0.1, MeOH); ^{1}H NMR (500 MHz, $CDCl_3$) δ 3.69 (td, *J* 8.2, 2.6 Hz, 1H, H^4), 3.62 (qd, *J* 12.2, 4.9 Hz, 2H, $H^{1a,b}$), 3.37 (t, *J* 6.9 Hz, 1H, H^3), 3.09 (s, 1H, H^2), 2.29 (s, 4H, NH, OH), 1.74 – 1.34 (m, 4H, H^5, H^6), 1.28 (s, 22H), 0.90 (t, *J* 6.9 Hz, 3H); ^{13}C NMR (126 MHz, $CDCl_3$) δ 74.26 (C4), 74.08 (C3), 55.44 (C1), 54.32 (C2), 33.15, 31.93, 29.76, 29.69, 29.37, 25.27, 22.70, 14.13; ESI-HRMS: Calcd for [MH$^+$] 343.3068. Found: *m/z* 343.3066.

(2,3,4,6-tetra-*O*-benzyl-α-D-galactopyranosyl)-(1→4)-(2,3,6-tri-*O*-benzyl-β-D-galactopyranosyl)-(1→4)-p-methoxyphenyl-2,3,6-tri-*O*-benzyl-β-D-glucopyranoside (41)[35]

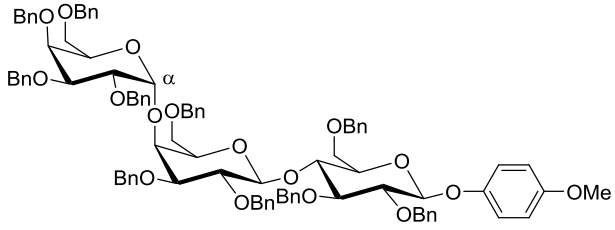

Phenyl-2,3,4,6-tetra-*O*-benzyl-1-thio-β-D-galactopyranoside **39** (1.2 g, 1.89 mmol, 1.2 eq) and 4-methoxyphenyl-4-*O*-(2,3,6-Tri-*O*-benzyl-β-D-galactopyranosyl)-2,3,6-tri-*O*-benzyl-β-D-glucopyranoside **40** (1.56 mg, 1.58 mmol, 1 eq) were dissolved in CH_2Cl_2/Et_2O (45 ml, 1:2) with

4 Å molecular sieves in a dry, inert atmosphere at -55°C. To the solution, N-iodosuccinimide (NIS, 425 mg, 1.89 mmol, 1 eq) was added, followed by TMSOTf (68 µl, 0.38 mmol, 0.2 eq) dropwise and the reaction mixture was stirred for 2 h. The reaction mixture was neutralised with Et_3N (0.2 ml) and stirred for a further 1 h, then diluted with CH_2Cl_2, washed with aqueous sodium thiosulfate solution (10 %, 2×50 ml) and brine (2×50 ml), dried ($MgSO_4$), evaporated to a crude mixture of isomers (6:1 α/β), which is purified by silica column chromatography (1.25 to 2% acetone in toluene) to afford triose **6** (1.62 g, 75 %). R_f (toluene/acetone [19:1])=0.2; $[\alpha]^{22}_D$=+20.0 (c 13.0, $CHCl_3$); ^{1}H NMR (300 MHz, $CDCl_3$) δ 7.47 – 7.12 (m, 50H), 6.92 (dd, *J* 69.7, 9.1 Hz, 4H), 5.17 – 5.05 (m, 2H), 5.03 – 4.89 (m, 2H), 4.89 – 4.85 (m, 2H), 4.84 – 4.74 (m, 6H), 4.58 – 4.45 (m, 6H), 4.42 – 4.17 (m, 6H), 4.14 – 4.09 (m, 2H), 4.07 (s, 2H), 4.04 – 3.94 (m, 2H), 3.83 (s, 2H), 3.79 (s, 3H, OCH_3), 3.72 – 3.62 (m, 3H), 3.52 (t, *J* 8.7 Hz, 3H), 3.37 (t, *J* 8.3 Hz, 2H), 3.18 (dd, *J* 8.3, 4.7 Hz, 1H); ^{13}C NMR (75 MHz, $CDCl_3$) δ 129.48, 128.93, 128.81, 128.72, 128.70, 128.67, 128.64, 128.60, 128.58, 128.57, 128.54, 128.28, 128.08, 128.03, 127.98, 127.93, 127.87, 127.84, 127.80, 127.60, 127.55, 125.74, 118.85, 114.87, 103.41 (α), 103.13 (β), 101.24 (β), 83.08, 82.10, 81.90, 79.85, 77.67, 75.80, 75.70, 75.66, 75.62, 75.43, 75.32, 75.15, 74.16, 73.71, 73.61, 73.46, 72.83, 72.50, 69.85, 68.20, 68.08, 56.05; ESI-HRMS: Calcd for $[MNa]^+$ 1533.7702; found 1533.6707.

(2,3,4,6-tetra-*O*-acetyl-α-D-galactopyranosyl)-(1→4)-(2,3,6-tri-*O*-acetyl-β-D-galactopyranosyl)-(1→4)-p-methoxyphenyl-2,3,6-tri-*O*-acetyl-β-D-glucopyranoside (42a)[35]

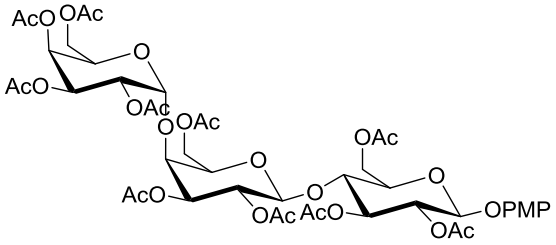

Compound **41** (1.02 g, 0.673 mmol) was dissolved in acetic acid (20 ml) and Pd/C (10_{wt}%, 400 mg) was added. Dihydrogen gas was bubbled through the solution then the reaction mixture was stirred for 1 hour in a dihydrogen atmosphere at rt for 1 h, then at 80°C for 2 h. The reaction mixture was filtered through Celite and washed with methanol and evaporated to obtain a white powder. The crude debenzylated triose-MP was solubilised in acetic anhydride/pyridine (1:2) and stirred overnight. The reaction mixture was diluted with CH_2Cl_2, washed with HCl (1M, 3×150ml), dried ($MgSO_4$), evaporated and purified by silica column

chromatography (toluene/acetone [5:1] to afford **42** (234 mg, 37 %). R_f (toluene/acetone [4:1])=0.3; $[\alpha]^{22}_D$=+34.4 (c 1.0, $CHCl_3$); ^{1}H NMR (300 MHz, $CDCl_3$) δ 6.87 (dd, *J* 37.7, 9.0 Hz, 4H, OPMP), 5.59 (d, *J* 2.3 Hz, 1H, H_{1a}), 5.40 (dd, *J* 11.0, 3.2 Hz, 1H), 5.27 (t, *J* 8.9 Hz, 1H), 5.22 – 5.05 (m, 3H), 5.03 – 4.86 (m, *J* 16.0, 5.5 Hz, 1H), 4.74 (dd, *J* 10.8, 2.0 Hz, 1H), 4.60 – 4.37 (m, 4H), 4.23 – 4.05 (m, 4H), 4.02 (s, 1H), 3.89 (t, *J* 9.2 Hz, 1H), 3.81 – 3.71 (m, 3H, OPMP), 2.19 – 2.01 (m, *J* 9.8, 6.5 Hz, 27H), 1.99 (s, 1H); ^{13}C NMR (75 MHz, $CDCl_3$) δ 155.2, 151.6, 139.0, 138.9, 138.7, 138.5, 138.4, 138.0, 137.8, 129.0, 128.5, 128.3, 128.2, 128.1, 127.8, 127.6, 127.5, 127.4, 127.1, 125.9, 118.4 (2C), 114.4 (2C), 102.9, 102.7, 100.7, 82.6, 81.7, 81.5, 79.4, 77.2, 75.3, 75.1, 75.0, 74.8, 73.7, 73.2, 73.0, 72.4, 72.1, 69.4, 68.3, 67.8, 67.7, 55.6; ESI-HRMS: Calcd for $[MNa]^+$ 1053.3063. Found: *m/z* 1053.3071.

(2,3,4,6-tetra-*O*-acetyl-α-D-galactopyranosyl)-(1→4)-(2,3,6-tri-*O*-acetyl-β-D-galactopyranosyl)-(1→4)-2,3,6-tri-*O*-acetyl-β-D-glucopyranoside (42b)[35]

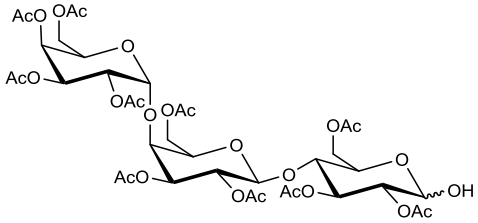

Compound **42a** (45 mg, 43.7µmol) was dissolved in CH_3CN/H_2O (4:1) and cooled to 0°C, to which ceric (IV) ammonium nitrate (CAN) was added. The reaction was stirred for 4h, the solvent evaporated and purified by silica column chromatography (0.8 to 3% $EtOH/CH_2Cl_2$) to afford **42b** (35 mg, 86 %, α:β (1:2)). R_f (toluene/acetone [7:3])=0.2; ^{1}H NMR (300 MHz, $CDCl_3$) δ 5.57 (bs, 1H, $H^{1''}$), 5.42 – 5.31 (m, 2H), 5.36 (s, 1H), 5.30 – 5.02 (m, 3H), 4.97 (d, *J* = 2.4 Hz, 1H), 4.82 (dd, *J* = 10.3, 3.3 Hz, 1H), 4.78 – 4.65 (m, 2H), 4.61 – 4.31 (m, 5H), 4.25 – 4.03 (m, 5H), 4.00 (s, 1H), 3.74 (dd, *J* = 16.0, 8.6 Hz, 3H), 3.46 (bs, 1H, OH), 2.11 (s, 6H), 2.07 (s, 9H), 2.05 (s, 9H), 2.03 (s, 3H), 1.97 (s, 3H); ^{13}C NMR (75 MHz, $CDCl_3$) δ 170.76, 170.62, 170.53, 170.44, 170.15, 169.55, 168.92, 168.87, 101.02 ($H^{1''}$), 99.56 ($H^{1'}$), 95.17 ($H^{1\alpha}$), 90.13 ($H^{1\beta}$), 73.48, 72.88, 72.42, 71.78, 71.29, 69.78, 69.00, 68.89, 68.15, 67.89, 67.11, 67.04, 62.05, 61.34, 60.26, 20.97, 20.95, 20.91, 20.80, 20.76, 20.71, 20.68, 20.63, 20.56.

(2,3,4,6-tetra-*O*-acetyl-α-D-galactopyranosyl)-(1→4)-(2,3,6-tri-*O*-acetyl-β-D-galactopyranosyl)-(1→4)-1-azido-2,3,6-tetra-*O*-acetyl-β-D-glucopyranoside (43)[185]

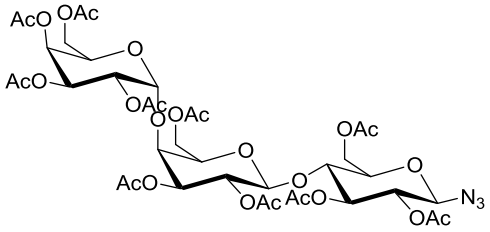

The peracetylated globoside **42c** (400 mg, 0.41 mmol) and $SnCl_4$ (1.0 ml, 1M in CH_2Cl_2) were dissolved in anhydrous CH_2Cl_2 (5 ml) and stirred at RT. After 5 min, $TMSN_3$ (50 µl, 0.50 mmol) was added, and the reaction mixture was stirred at rt for 48h. The resulting solution was washed with $NaHCO_3$ and extracted with CH_2Cl_2. The organic phase was washed with water, dried over $MgSO_4$, and concentrated in vacuum. The crude product was purified by flash chromatography on silica gel (cyclohexane/EtOAc, 85/15) to afford **43** (217 mg, 56%) as colourless foam. R_f (EtOAc/cyclohexane [75:25])=0.7; $[\alpha]^{22}_D$=+38.0 (c 3.0, $CHCl_3$); ^{1}H NMR (300 MHz, $CDCl_3$) δ 5.57 (d, J^{4-3} 2.3 Hz, 1H, $H^{4''}$), 5.37 (dd, J^{3-2} 11.0, J^{3-4} 3.2 Hz, 1H, $H^{3''}$), 5.20 (t, $J^{3-2,\ 3-4}$ 7.6 Hz, 1H, H^3), 5.17 (dd, J^{2-3} 11.0, J^{2-1} 3.6 Hz, 1H, $H^{2''}$), 5.09 (dd, J^{2-3} 10.7, J^{2-1} 7.8 Hz, 1H, $H^{2'}$), 4.97 (d, J^{1-2} 3.4 Hz, 1H, $H^{1''}$), 4.84 (t, $J^{2-3,\ 2-1}$ 9.0 Hz, 1H, H^2), 4.72 (dd, J^{3-2} 10.8, J^{3-4} 2.1 Hz, 1H, $H^{3'}$), 4.63 (d, J^{1-2} 8.7 Hz, 1H, H^1), 4.57 – 4.33 (m, 4H, $H^{1'}$, $H^{5''}$, H^{6a}, $H^{6'a}$), 4.21 – 4.03 (m, 4H, H^6, $H^{6''a,b}$, $H^{5'}$), 4.00 (s, 1H, $H^{4'}$), 3.92 – 3.62 (m, 3H, H^4, H^5, $H^{6'}$), 2.11 (s, 6H), 2.07 (s, 6H), 2.05 (s, 9H), 2.04 (s, 3H), 1.99 (s, 3H), 1.97 (s, 3H); ^{13}C NMR (75 MHz, $CDCl_3$) δ 170.62, 170.44, 170.41, 170.39, 170.33, 170.04, 169.53, 169.49, 168.84, 101.10 ($C^{1'}$), 99.64 ($C^{1''}$), 87.67 (C^1), 76.91 ($C^{4'}$), 75.95 (C^4), 74.76 (C^5), 72.82 (C^3), 72.74 ($C^{3'}$), 71.94 ($C^{5'}$), 71.10 (C^2), 68.97 ($C^{2''}$), 68.86 ($C^{2'}$), 67.91 ($C^{4''}$), 67.19 ($C^{5''}$), 67.06 ($C^{3''}$), 61.93 ($C^{6'}$), 61.35 (C^6), 60.27 ($C^{6''}$), 20.89, 20.76, 20.68, 20.63, 20.60, 20.56, 20.47; ESI-HRMS: Calcd for [MNa^+] 972.2709. Found: *m/z* 972.2704.

(2,3,4,6-tetra-*O*-acetyl-α-D-galactopyranosyl)-(1→4)-(2,3,6-tri-*O*-acetyl-β-D-galactopyranosyl)-(1→4)-1-amino-2,3,6-tetra-*O*-acetyl-β-D-glucopyranoside (44)

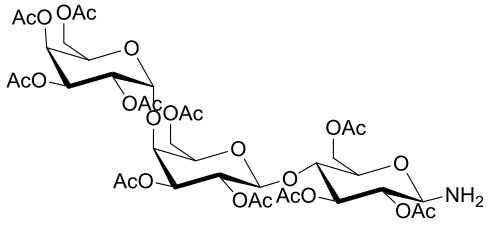

Compound **43** (63 mg, 66.3 µmol) was dissolved in EtOAc (1 ml), to which Pd/C (10%, 7 mg) was added and dihydrogen gas was bubbled through the solution for 10 min. The reaction was stirred in H_2 atmosphere for 3h, filtered through Celite and evaporated to afford amine

44 as white crystalline solid (60 mg, 98%). R_f (EtOAc/cyclohexane/Et_3N [75:25:1])=0.4; ^{1}H NMR (300 MHz, $CDCl_3$) δ 5.58 (d, J^{4-3} 2.2 Hz, 1H, $H^{4''}$), 5.39 (dd, J^{3-2} 11.0, J^{3-4} 3.1 Hz, 1H, $H^{3''}$), 5.31 – 5.03 (m, 3H, H^3, $H^{2''}$, $H^{2'}$), 4.98 (d, *J* 3.3 Hz, 1H, $H^{1''}$), 4.88 – 4.64 (m, 2H, H^2, $H^{3'}$), 4.61 – 4.31 (m, 4H, $H^{1'}$, $H^{5''}$, $2H^6$), 4.31 – 3.91 (m, 6H, H^1, $H^{5'}$, $4H^6$), 3.91 – 3.48 (m, 3H, H^4, $H^{4'}$, H^5), 2.12 (s, 6H), 2.07 (s, 6H), 2.05 (s, 9H), 2.03 (s, 6H), 1.97 (s, 3H); ^{13}C NMR (75 MHz, $CDCl_3$) δ 170.66, 170.52, 170.47, 170.43, 170.05, 169.48, 168.84, 101.07 ($C^{1'}$), 99.59 ($C^{1''}$), 84.61 (C^1), 76.80, 73.63, 73.27, 72.86, 72.60, 71.86, 69.04, 68.91, 67.93, 67.17, 67.07, 62.57, 61.38, 60.36, 60.29, 21.02, 20.91, 20.88, 20.83, 20.70, 20.65, 20.61, 20.56 (s), 20.50; ESI-HRMS: Calcd for [MH^+] 924.2985. Found: *m/z* 924.2979.

1-Fluorocyclooct-2-yne-1-carboxylic acid (MFCO) (45)[148]

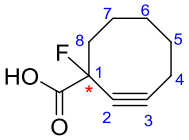

Stable intermediate **58** (Scheme 2.1.3.7) (20 mg, 0.11 mmol, 1 eq) was solublised in THF (1 ml), to which LiOH (5 mg, solution in 0.5 ml H_2O) was added. The reaction was stirred for 30 min, extracted with H_2O (3 ml) and CH_2Cl_2 (2×3 ml), neutralised with HCl (2M) and extracted with CH_2Cl_2 (4×3 ml), dried ($MgSO_4$) and evaporated to afford **45** as a clear oil (18 mg, 98%). R_f (EtOAc/cyclohexane/AcOH [50:50:1])=0.2; ^{1}H NMR (300 MHz, $CDCl_3$) δ 8.71 (bs, 1H, COOH), 3.85 (s, 3H, OCH_3), 2.42-2.22 (m, 4H), 2,10-1,82 (m, 4H), 1,75 (m, 1H), 1,49 (m, 1H); ^{13}C NMR (75 MHz, $CDCl_3$) δ 173.1 (COOH), 109.7 (C^3), 92.0 (d, *J* 195 Hz, C^1), 87.0 (C^2), 47.0 (C^8), 34.2 (C^7), 29.6 (C^6), 26.1 (C^5), 21.0 (C^4). ESI-MS 169 [M^-].

***N*-((2,3,4,6-tetra-*O*-acetyl-α-D-galactopyranosyl)-(1→4)-(2,3,6-tri-*O*-acetyl-β-D-galactopyranosyl)-(1→4)-2,3,6-tri-*O*-acetyl-β-D-glucopyranosyl)-1-fluorocyclooct-2-yne-1-carboxamide (47)**

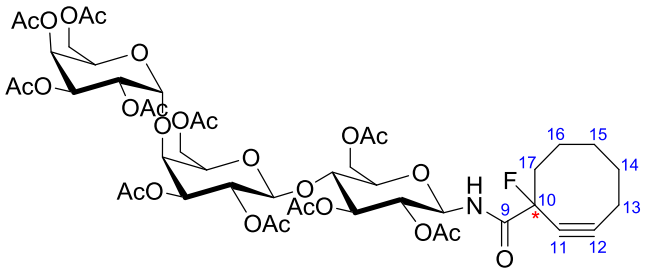

1-fluorocyclooct-2-yne-1-carboxylic acid (MFCO) **45** (72 mg, 0.42 mmol, 1 eq) was dissolved in CH_2Cl_2 (3 ml) and cooled to 0°C. DIPEA (96 µl, 0.55 mmol, 1.3 eq) was added and stirred for 5 min. Pentafluorophenyl trifluoroacetate (PFP-TFA, 80 µl, 0.50 mmol, 1.2 eq) was added dropwise and the solution was stirred overnight. The reaction was dried and purified by flash column chromatography (EtOAc/cyclohexane [7:3]) to obtain the activated MFCO-PFP ester. The pre-dried amine compound **44** was dissolved in CH_2Cl_2 (5 ml), and reacted with MFCO-PFP ester (0.42 mmol, 1 eq), with DIPEA (41 µl, 0.235 mmol, 1 eq). After overnight stirring, 1-ethyl-3-(3-dimethymainopropyl)carbodiimide (EDC, 71 µl, 0.40 mmol, 1.1 eq) was added until only trace amounts of amine material were left. The reaction mixture was dried in vacuum and purified directly by flash chromatography on silica gel (cyclohexane/EtOAc, 85:15) to afford peracetyl trisaccharide-MFCO **47** as a racemic mixture (218 mg, 78%) as colourless foam. ^{1}H NMR (300 MHz, $CDCl_3$) δ 7.02 – 6.91 (m, 1H, NH), 5.59 (d, *J* 2.5 Hz, 1H), 5.40 (dd, *J* 11.1, 3.3 Hz, 1H), 5.36 – 5.25 (m, 1H), 5.18 (dd, *J* 11.1, 3.3 Hz, 2H), 5.09 (dd, *J* 10.8, 7.6 Hz, 1H), 4.98 (d, *J* 3.7 Hz, 1H), 4.89 (td, *J* 9.5, 3.4 Hz, 1H), 4.71 (d, *J* 10.9 Hz, 1H), 4.54 – 4.37 (m, 4H), 4.23 – 4.05 (m, 4H), 4.02 (s, 1H), 3.90 – 3.61 (m, 4H), 2.43 – 2.16 (m, 4H), 2.13 (s, 6H), 2.09 (s, 6H), 2.06 (s, 9H), 2.04 (s, 3H), 2.02 (s, 3H), 1.98 (s, 3H), 1.96 – 1.74 (m, 4H), 1.68 (m, 1H), 1.45 (m, 1H); ^{13}C NMR (75 MHz, $CDCl_3$) δ 171.40, 171.21, 171.12, 170.96, 170.90, 170.85, 170.81, 170.49, 169.78 (d, *J* 18.5 Hz, NHCO), 169.19, 169.17, 110.49 (dd, *JC-F* 29.4, 10.5 Hz, C12), 101.26 (C1''), 99.98 (C1'), 94.41 (dd, *JC-F* 187.5, 23.9 Hz, C10), 86.73 (dd, *J* 31.9, 27.3 Hz, C11), 78.49 (d, *J* 13.4 Hz, C1), 77.67, 77.32, 76.35, 75.08, 73.24, 72.74, 72.26, 71.33, 71.21, 69.31, 69.24, 68.27, 67.55, 67.37, 62.43, 62.37, 61.84, 60.61, 46.44 (dd, *J* 49.4, 24.4 Hz, C17), 34.12 (C16), 29.18 (C15), 25.86 (C14), 21.85 (C13), 21.34, 21.30, 21.16, 21.08, 21.05, 21.00, 20.96, 20.92; ^{19}F NMR (282 MHz, $CDCl_3$) δ -146.95, -147.44; ESI-HRMS: Calcd for [MH^+] 1076.3622. Found: *m/z* 1076.3617.

<u>*N*-(α-D-galactopyranosyl-(1→4)-β-D-galactopyranosyl-(1→4)-β-D-glucopyranosyl)-1-fluoro-cyclooct-2-yne-1-carboxamide (37)</u>

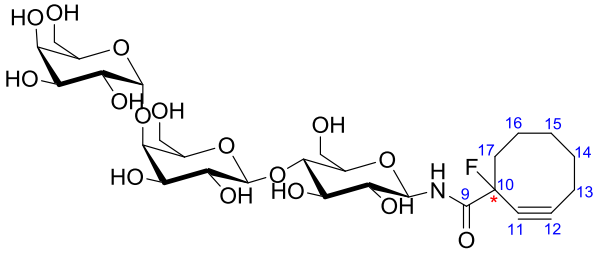

Compound **47** (24 mg, 22.3 µmol, 1 eq) was dissolved in dry MeOH (1.6 ml) and CH_3ONa (0.5 M solution in MeOH, 0.45 ml, 0.223 mmol, 10 eq) was added. The reaction was stirred overnight, quenched with Dowex50WX8-200, filtered, evaporated and purified by reverse phase C18 silica column chromatography (10 to 20% MeOH in H_2O) to obtain the *clickable* trisaccharide **37** (8 mg, 56 %) as a pure crystalline solid. R_f (^{n}BuOH/EtOH/H_2O [2:2:1])=0.5; ^{1}H NMR (400 MHz, MeOD) δ 4.96 – 4.91 (m, 2H, H^1, $H^{1'}$), 4.59 (bs, 1H, NH), 4.47 – 4.37 (m, 1H), 4.27 (t, $J^{5\text{-}6}$ 6.4 Hz, 1H), 3.99 (s, 1H), 3.94 – 3.82 (m, 5H), 3.81 (d, *J* 3.6 Hz, 1H), 3.79 (d, *J* 3.0 Hz, 1H), 3.77 – 3.63 (m, 3H), 3.63 – 3.51 (m, 4H), 3.51 – 3.41 (m, 2H), 2.43 – 2.20 (m, 4H), 2.19 – 1.78 (m, 4H), 1.75 – 1.58 (m, 1H), 1.58 – 1.37 (m, 1H). ^{13}C NMR (101 MHz, MeOD) δ 172.04 (d, *J* 25.8 Hz, C^9), 110.20 (d, *J* 10.3 Hz, C^{12}), 105.32 ($C^{1''}$), 102.65 ($C^{1'}$), 95.23 (dd, *J* 187.6, 18.6 Hz, C^{10}), 88.13 (d, *J* 31.7 Hz, C^{11}), 81.15 (d, *J* 5.6 Hz, C^1), 80.42, 79.71, 78.36, 77.27, 76.55, 74.61, 73.20, 72.80, 72.65, 71.28, 71.03, 70.54, 62.65, 61.58, 61.49, 47.59 (d, *J* 24.8 Hz, C^{17}), 34.96 (C^{16}), 30.11 (C^{15}), 26.72 (C^{14}), 21.01 (C^{13}). ^{19}F NMR (282 MHz, MeOD) δ -149.05, -149.18. ESI-HRMS: Calcd for [MH^+] 656.2566. Found: *m/z* 656.2560.

<u>*N*-(2,3,4,6-tetra-*O*-acetyl-β-D-galactopyranosyl-(1→4)-2,3,6-tri-*O*-acetyl-β-D-glucopyranosyl) 1-fluoro-cyclooct-2-yne-1-carboxamide (53)</u>

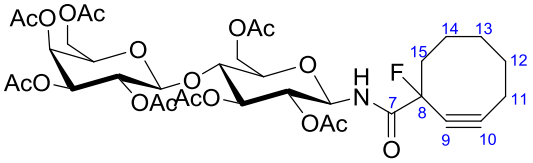

To a solution of MFCO **45** (18 mg, 106 µmol, 1 eq), the heptaacetyl-lactose-β-NH_2 **52** (85 mg, 120 µmol, 1.1 eq) and hydroxybenzotriazole (HOBt, 19 mg, 127 µmol, 1.2 eq) in CH_2Cl_2 (1 ml) at 0°C, N,N'-dicyclohexylcarbodiimide (DCC, 44 mg, 212 µmol, 2 eq) was added at the reaction mixture was warmed to rt after 10 min, and stirred overnight. The crude reaction mixture (α/β≈1:11) was evaporated and purified by silica column chromatography (40 to 90 % EtOAc in cyclohexane) containing some dicyclohexylurea impurity. This was removed by precipitation in Et_2O to afford **53** (52 mg (β), 62 %). R_f (EtOAc/cyclcohexane [1:1])=0.4. ^{1}H NMR (500 MHz, $CDCl_3$) δ 6.94 (ddd, *J* 26.6, 9.4, 4.8 Hz, 1H, NH), 5.35 (d, *J* 3.1 Hz, 1H, $H^{4'}$), 5.31 (td, *J* 9.2 Hz, 3.9 Hz, H^3), 5.17 (qd, *J* 9.5 Hz, 1.2 Hz, 1H, H^1), 5.11 (dd, *J* 10.4, 7.9 Hz, 1H, $H^{2'}$), 4.94 (dd, *J* 10.4, 3.5 Hz, 1H, $H^{3'}$), 4.88 (td, *J* 9.5, 6.9 Hz, 1H, H^2), 4.46 (dd, *J* 7.8, 1.1 Hz, 1H, $H^{1'}$), 4.41-4.45 (m, 1H, H^6), 4.10-4.17 (m, 2H, H^6, $H^{6'}$), 4.08 (dd, *J* 11.1, 7.2 Hz, 1H, $H^{6'}$), 3.87 (t, *J* 6.8 Hz, 1H, $H^{5'}$), 3.78 (td, *J* 8.8 Hz, 2.3 Hz, 1H, H^4), 3.73 (dt, *J* 10.0, 2.2 Hz, 1H, H^5), 2.47 – 2.16 (m, 4H, H^{11},

H^{15}), 2.16 (s, 3H), 2.13 (d, *J* 5.9 Hz, 3H), 2.07 (s, 3H), 2.06 (s, 3H), 2.05 (d, *J* 1.6 Hz, 3H), 2.05 (d, *J* 2.4 Hz, 3H), 1.96 (s, 3H), 1.96 (s, 3H), 1.96 – 1.79 (m, 4H, H^{12}, H^{14}), 1.74 – 1.56 (m, 1H, H^{13}), 1.48 – 1.34 (m, 1H, H^{13}). ^{13}C NMR (126 MHz, $CDCl_3$) δ 170.95, 170.76, 170.38, 170.33, 170.16, 170.09, 169.37, 168.98, 110.12 (dd, *J* 48.1, 10.4 Hz, C^{10}), 100.90 ($C^{1'}$), 94.04 (dd, *J* 187.4, 34.4 Hz, C^8), 86.51 (d, *J* 45.5 Hz, C^9), 78.16 (d, *J* 20.1 Hz, C^1), 75.91 (C^4), 74.74 (C^5), 72.17 (C^3), 71.01 ($C^{3'}$), 70.94 (C^2), 70.78 ($C^{5'}$), 69.00 ($C^{2'}$), 66.63 ($C^{4'}$), 61.87 (d, *J* 8.2 Hz, C^6), 60.90 ($C^{6'}$), 46.06 (dd, *J* 75.5, 24.7 Hz, C^{15}), 33.78 (d, *J* 6.5 Hz, C^{14}), 28.83 (C^{13}), 25.43 (C^{12}), 20.90, 20.75, 20.67, 20.64, 20.56, 20.53. ^{19}F NMR (471 MHz, $CDCl_3$) δ -146.44, -146.95. ESI-HRMS: Calcd for [MH^+] 788.2777. Found: *m/z* 788.2772.

<u>*N*-β-D-galactopyranosyl-(1→4)-β-D-glucopyranosyl) 1-fluoro- cyclooct-2-yne-1-carboxamide (49)</u>

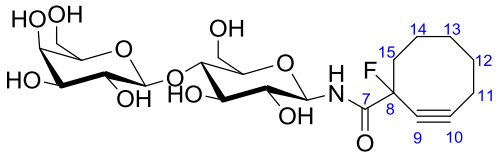

To a solution of the protected lactose **53** (48 mg, 63 µmol, 1 eq) in dry MeOH (1.5 ml), CH_3ONa (1.27 ml, 0.63 mmol, 10 eq, 0.5 M solution in MeOH) was added. The reaction was stirred for 30 minutes and filtered through a pad of Dowex 50WX8 (previously protonated HCl, 0.1M). The crude mixture was evaporated and purified by reverse phase C18 silica column chromatography (10-20% CH_3CN/H_2O) to obtain *clickable* lactose **49** (21 mg, 71 %). R_f (^{t}BuOH/EtOH/H_2O [2:2:1])=0.7. ^{1}H NMR (500 MHz, MeOD) δ 4.96 (dd, J^{1-2} 9.0, J^{1-N} 3.0 Hz, 1H, H^1), 4.39 (d, *J* 7.6 Hz, 1H, $H^{1'}$), 3.91 – 3.86 (m, *J* 2.6 Hz, 3H), 3.91 – 3.81 (m, 3H), 3.81 – 3.75 (m, 1H), 3.72 (dd, *J* 11.5, 4.3 Hz, 1H, $H^{6'}$), 3.68 – 3.54 (m, 4H), 3.54 – 3.44 (m, 3H), 2.44 – 2.26 (m, 4H), 2.16 – 1.79 (m, 4H), 1.77 – 1.59 (m, 1H), 1.54 – 1.39 (m, 1H). ^{13}C NMR (126 MHz, MeOD) δ 170.62 (dd, J^{C-F} 25.8, 5.8 Hz, C7), 108.82 (C10), 103.67 (C1'), 93.84 (dd, J^{C-F} 187.6, 23.7 Hz, C8), 86.75 (d, *J* 29.7 Hz, C9), 79.78 (d, *J* 7.3 Hz, C1), 78.65, 76.98 (d, *J* 4.0 Hz, C2), 75.89, 75.71, 73.38, 71.72, 71.15, 68.91, 61.14, 60.21, 46.21 (d, *J* 24.8 Hz, C15), 33.57 (C14), 28.73 (C13), 25.33 (C12), 19.63 (C11). ^{19}F NMR (471 MHz, MeOD) δ -148.56 (d, *J* 63.4 Hz). ESI-HRMS: Calcd for [MH^+] 494.2038. Found: *m/z* 494.2032

<u>*N*-Glycine-1-fluoro-cyclooct-2-yne-1-carboxamide (46)</u>[148]

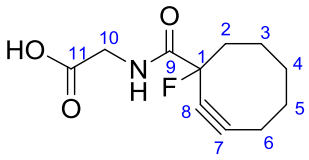

To a solution of MFCO **45** (43 mg, 0.25 mmol, 1 eq) and DIPEA (66 µl, 0.38 mmol, 1.5 eq) in CH_2Cl_2 (2 ml) at 0°C, PFP-TFA (52 µl, 0.30 mmol, 1.2 eq) was added dropwise. The reaction mixture was stirred for 3h until complete activation of the carboxylic acid. The solvent was evaporated and DMF (1 ml) was added, followed by DIPEA (66 µl, 0.38 mmol, 1.5 eq), then *O*-^{t}Bu-glycine (63 mg, 0.38 mmol, 1.2 eq). The reaction was stirred overnight, diluted with CH_2Cl_2, evaporated and extracted in EtOAc, washed with water. The partially protected material is fully deprotected in a solution of trifluoroacetic acid (TFA)/triisopropylsilane (TIS)/CH_2Cl_2 (5:5:90) for 4h, then dried and purified by silica column chromatography (EtOAc/cyclohexane/formic acid [25:75:0.5 to 30:70:0.5] to afford **46** as a racemic mixture (34 mg, 59 %). R_f (EtOAc/cyclohexane/AcOH [50:50:0.5])=0.2. ^{1}H NMR (500 MHz, $CDCl_3$) δ 8.84 (bs, 1H, COOH), 6.90 (d, *J* 3.9 Hz, 1H, NH), 4.12 (qd, *J* 18.6, 5.3 Hz, 2H, H^{10}), 2.46 – 2.24 (m, 4H, H^{2}, H^{6}), 2.10 – 1.79 (m, 4H, H^{3}, H^{5}), 1.74 – 1.61 (m, 1H, H^{4}), 1.44 (m, 1H, H^{4}). ^{13}C NMR (126 MHz, $CDCl_3$) δ 173.32 (C11), 169.29 (d, J^{C-F} 25.1 Hz, C^{9}), 110.15 (d, J^{C-F} 10.4 Hz, C^{3}), 94.35 (d, J^{C-F} 186.7 Hz, C^{1}), 86.69 (d, J^{C-F} 31.8 Hz, C^{2}), 46.46 (d, J^{C-F} 24.5 Hz, C^{8}), 41.17 (C^{10}), 33.92 (C^{7}), 28.95 (C^{6}), 25.64 (C^{5}), 20.67 (C^{4}). ^{19}F NMR (282 MHz, $CDCl_3$) δ -146.70 (s). ESI-HRMS: Calcd for [MH^{+}] 228.1036. Found: *m/z* 228.1030.

<u>*N*-(2,3,4,6-tetra-*O*-acetyl-β-D-galactopyranosyl-(1→4)-2,3,6-tri-*O*-acetyl-β-D-glucopyranosyl)-*N'*-glycine-1-fluoro-cyclooct-2-yne-1-carboxamide (54)</u>

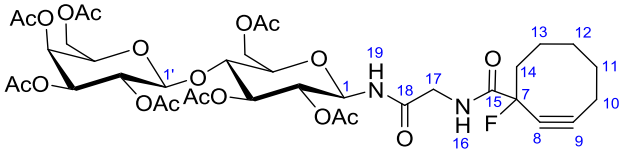

Compound **46** (6 mg, 26 µmol, 1 eq), heptaacetyl-lactose-β-NH_2 **52** (17 mg, 31 µmol, 1 eq), HOBt (6 mg, 40 µmol, 1.3 eq) and DCC (19 mg, 77 µmol, 3 eq) were stirred in dry DMF (1 ml) for 3h at 30°C. The crude reaction mixture was evaporated and purified by silica column chromatography (40 to 80 % EtOAc in cyclohexane) containing some dicyclohexylurea impurity. This was removed by precipitation in Et_2O to afford **54** (4.5 mg, 50 %). R_f (EtOAc/cyclcohexane [3:1])=0.4. ^{1}H NMR (400 MHz, $CDCl_3$) δ 6.91 (s, 1H, NH), 6.59 (dd, *J* 9.0, 4.4 Hz, 1H, NH), 5.35 (d, *J* 3.0 Hz, 1H, H^{4}), 5.30 (t, *J* 9.0 Hz, 1H), 5.18 (t, *J* 9.3 Hz, 1H), 5.10 (dd,

J 10.3, 7.9 Hz, 1H), 4.94 (dd, *J* 10.4, 3.4 Hz, 1H, H^{1}), 4.84 (t, *J* 9.6 Hz, 1H), 4.46 (d, *J* 7.9 Hz, 1H, $H^{1'}$), 4.43 (d, *J* 11.5 Hz, 1H), 4.18 – 3.98 (m, 4H), 3.98 – 3.82 (m, 3H), 3.81 – 3.69 (m, 2H), 2.49 – 2.24 (m, 4H, H^{10}, H^{14}), 2.15 (s, 3H), 2.12 (s, 3H), 2.07 (s, 3H), 2.05 (s, 3H), 2.04 (s, 3H), 2.04 (s, 3H), 1.96 (s, 3H), 1.93 – 1.63 (m, 4H, H^{11}, H^{13}), 1.21 – 1.02 (m, 2H, H^{12}). ^{13}C NMR (101 MHz, $CDCl_3$) δ 171.47, 171.42, 170.43, 170.40, 170.22, 170.15, 169.39, 169.05, 168.56, 109.94 (d, J^{C-F} 10.5 Hz, C^{9}), 101.01 ($C^{1'}$), 94.36 (d, J^{C-F} 186.2 Hz, C^{7}), 86.88 (d, *J* 31.6 Hz, C^{1}), 78.25, 75.9, 74.64, 72.25 (d, *J* 4.3 Hz), 70.96 (d, *J* 23.0 Hz, C^{8}), 69.09, 66.71, 61.95, 60.96, 46.37 (d, J^{C-F} 20.2 Hz, C^{15}), 43.13 (C^{17}), 33.98 (d, *J* 12.3 Hz, C^{13}), 28.98 (C^{12}), 25.66 (C^{11}), 20.96 (C^{10}), 20.82, 20.73, 20.59. ^{19}F NMR (282 MHz, $CDCl_3$) δ -146.42 (d, *J* 16.2 Hz). UPLC-MS (gradient 80-90% CH_3CN /H_2O, 4 min, ESI) rt=1.14 min; 843 (M^-), 846 (MH^+).

<u>*N*-β-D-galactopyranosyl-(1→4)-1-azido-β-D-glucopyranosyl-*N'*-glycine-1-fluoro-cyclooct-2-yne-1-carboxamide (50)</u>

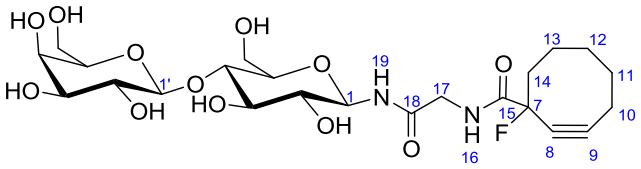

To a solution of the protected lactose **54** (5 mg, 6 µmol, 1 eq) in dry MeOH (470 µl), CH_3ONa (118 µl, 0.63 mmol, 10 eq, 0.5M solution in MeOH) was added. The reaction was stirred for 1h and filtered through a pad of Dowex 50WX8 (previously protonated HCl, 0.1M). The crude mixture was evaporated and purified by reverse phase C18 silica column chromatography (0 to 50% CH_3CN/H_2O) to obtain compound **50** (2 mg, 62 %). R_f(^{t}BuOH/EtOH/H_2O [2:2:1])=0.8. ^{1}H NMR (300 MHz, D_2O) δ 5.09 (d, *J* 9.0 Hz, 1H), 4.52 (d, *J* 7.7 Hz, 1H), 4.11 (s, 2H), 4.06 – 3.93 (m, 2H), 3.93 – 3.67 (m, 8H), 3.66 – 3.46 (m, 2H), 2.56 – 2.20 (m, 4H, H10, H^{14}), 2.20 – 1.82 (m, 4H, H^{11}, H^{13}), 1.82 – 1.58 (m, 1H, H^{12}), 1.59 – 1.38 (m, 1H, H^{12}). ^{19}F NMR (282 MHz, D_2O) δ -146.19 (d, *J* 6.2 Hz). UPLC-MS (gradient 80-90% CH_3CN/H_2O, 4 min, ESI) rt=0.27 min; 573 (MNa^+).

<u>*N*-((2,3,4,6-tetra-*O*-acetyl-α-D-galactopyranosyl)-(1→4)-(2,3,6-tri-*O*-acetyl-β-D-galactopyranosyl)-(1→4)-(2,3,6-tri-*O*-acetyl-β-D-glucopyranosyl))-*N'*-glycine-1-fluoro-cyclooct-2-yne-1-carboxamide (48)</u>

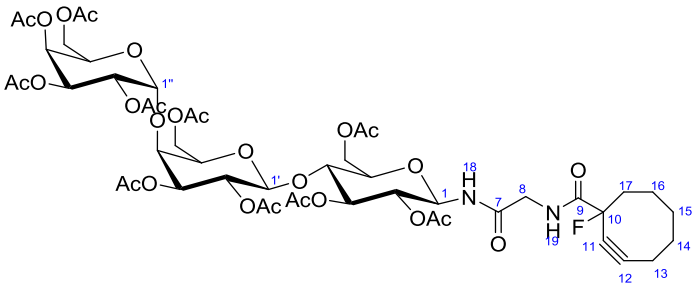

To a solution of amine **44** (21 mg, 23 µmol, 1 eq), carboxylic acid **46** (8 mg, 34 µmol, 1.5 eq) and HOBt (4 mg, 27 µmol, 1.2 eq) in CH_2Cl_2 (1 ml) at 0°C, DCC (9.5 mg, 46 µmol, 2 eq) was added at the reaction mixture was warmed to rt after 10 min, and stirred for 2h before complete formation of crude product (α/β≈1:11). The reaction mixture was evaporated and purified by silica column chromatography (50 to 90 % EtOAc in cyclohexane) to afford **48** (19 mg (β), 74 %). R_f (EtOAc/cyclcohexane [3:1]) =0.3. ^{1}H NMR (500 MHz, $CDCl_3$) δ 6.95 (bs, 1H, NH^{18}), 6.67 (d, *J* 6.1 Hz, 1H, NH^{19}), 5.58 (d, *J* 2.0 Hz, 1H), 5.39 (dd, *J* 11.0, 3.1 Hz, 1H), 5.28 (t, *J* 8.8 Hz, 1H), 5.18 (m, 2H, incl. H^1), 5.09 (dd, *J* 10.5, 7.9 Hz, 1H), 4.98 (d, *J* 3.3 Hz, 1H, $H^{1''}$), 4.85 (t, *J* 9.5 Hz, 1H), 4.71 (dd, *J* 10.8, 1.9 Hz, 1H), 4.48 (d, *J* 7.7 Hz, 1H, $H^{1'}$), 4.47 – 4.38 (m, 3H), 4.23 – 4.04 (m, 5H, incl. CH_2 gly), 4.04 – 3.93 (m, 2H), 3.93 – 3.84 (m, 1H), 3.82 – 3.70 (m, 3H), 2.49 – 2.24 (m, 4H, H^{13}, H^{17}), 2.12 (s, 3H, Ac), 2.10 (s, 3H, Ac), 2.08 (s, 3H, Ac), 2.07 (m, 3H), 2.06 (s, 3H, Ac), 2.05 (s, 6H, Ac), 2.04 (s, 3H, Ac), 2.03 (s, 3H, Ac), 1.97 (s, 3H, Ac), 1.95 – 1.76 (m, 4H, H14, H^{16}), 1.63 – 1.55 (m, 1H, H^{15}), 1.53 – 1.44 (m, 1H, H^{15}). ^{13}C NMR (126 MHz, $CDCl_3$) δ 171.49, 171.43, 170.80, 170.63, 170.57, 170.53, 170.51, 170.16, 169.59, 169.32, 169.12, 168.87, 168.60, 109.92 (d, $J^{12\text{-}F}$ 10.4 Hz, C^{12}), 100.97 ($C^{1'}$), 99.68 ($C^{1''}$), 94.36 (d, $J^{10\text{-}F}$ 186.6 Hz, C^{10}), 86.90 (d, $J^{11\text{-}F}$ 31.5 Hz, C^{11}), 78.20 (C^1), 76.07, 74.63, 72.94, 72.54, 72.49, 72.01, 70.88, 69.06, 68.99, 68.02, 67.30, 67.10, 62.12, 61.54, 60.37, 46.39 (d, $J^{17\text{-}F}$ 18.8 Hz, C^{17}), 43.10 (C^8), 33.92 (C^{16}), 28.98 (C^{15}), 25.02 (C^{14}), 21.03, 20.98, 20.83, 20.76, 20.74, 20.69, 20.60. UPLC-MS (gradient 5-100% CH_3CN/H_2O, 4 min, ESI) rt=1.13; 1132 (M^-), 1134 (MH^+). ESI-HRMS: Calcd for [MH^+] 1133.3837. Found: *m/z* 1133.3831.

<u>*N*-(α-D-galactopyranosyl-(1→4)-β-D-galactopyranosyl-(1→4)-β-D-glucopyranosyl)-*N'*-glycine-1-fluoro-cyclooct-2-yne-1-carboxamide (38)</u>

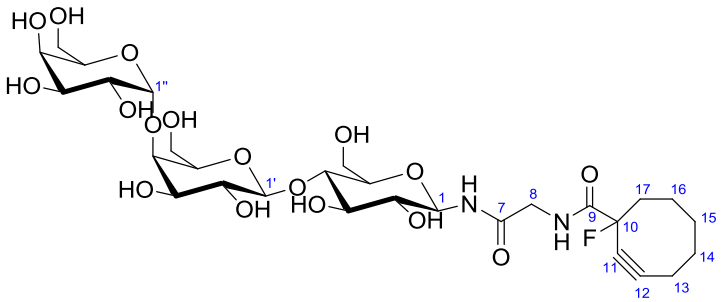

To a solution of compound **48** (18.5 mg, 16.3 µmol, 1 eq) in MeOH (400 µl), CH_3ONa (436 µl, 0.5M solution in MeOH, 13 eq) was added dropwise. The reaction was stirred for 45 min at rt, before filtering through acidified Dowex 50WX-800 and washing with MeOH at 4°C to reduce side reactions. The crude mixture was purified by reverse-phase silica column chromatography (H_2O/MeOH [100:0 to 0:100) to afford **38** (11 mg, 95 %). R_f (^{n}BuOH/EtOH/H_2O [2:2:1])=0.5. ^{1}H NMR (500 MHz, MeOD) δ 4.95 (d, *J* 3.7 Hz, 1H, $H^{1''}$), 4.93 (d, *J* 9.2 Hz, 1H, H^1), 4.42 (d, *J* 6.1 Hz, 1H, $H^{1'}$), 4.26 (t, *J* 6.2 Hz, 1H), 3.98 (s, 1H), 3.97 – 3.89 (m, 3H, incl. CH_2 gly), 3.89 – 3.82 (m, 4H), 3.82 – 3.71 (m, 3H), 3.69 (dd, *J* 10.7, 5.3 Hz, 2H), 3.62 – 3.51 (m, 4H), 3.47 (dd, J^{3-4} 6.1, J^{3-2} 2.9 Hz, 1H, H^3), 3.34 (dd, J^{2-1} 8.9, J^{2-3} 2.6 Hz, 1H, H^2), 2.40 – 2.26 (m, 4H), 2.13 – 1.83 (m, 4H), 1.74 – 1.62 (m, 1H), 1.53 – 1.42 (m, 1H). ^{13}C NMR (126 MHz, MeOD) δ 170.34 (C^7), 170.11 (d, J^{9-F} 25.5 Hz, C^9), 109.00 (d, J^{12-F} 10.2 Hz, C^{12}), 104.06 ($C^{1'}$), 101.36 ($C^{1''}$), 93.83 (d, J^{10-F} 189.7 Hz, C^{10}), 86.80 (d, J^{11-F} 31.8 Hz, C^{11}), 79.66 (C^1), 79.38, 78.41, 76.83, 75.98, 75.25, 73.32, 72.40, 71.50, 71.35, 69.97, 69.72, 69.24, 61.35, 60.41, 60.19, 46.41 (d, J^{17-F} 24.8 Hz, C^{17}), 41.92 (C^8), 33.67 (C^{16}), 28.84 (C^{15}), 25.42 (C^{14}), 19.72 (C^{13}). ^{19}F NMR (471 MHz, MeOD) δ -148.36. ESI-HRMS: Calcd for [MH^+] 713.2781. Found: *m/z* 713.2775.

1-((2*S*,3*R*,*E*)-2-((*Z*)-docos-13-enamido)-3-hydroxyoctadec-4-en-1-yl)-4-fluoro-*N*-(4-*O*-(4-*O*-α-D-galactopyranosyl-(1→4)-β-D-galactopyranosyl-(1→4)-β-D-galactopyranosyl)-5,6,7,8,9-decahydro-1H-cycloocta[d][1,2,3]triazole-4-carboxamide (35)

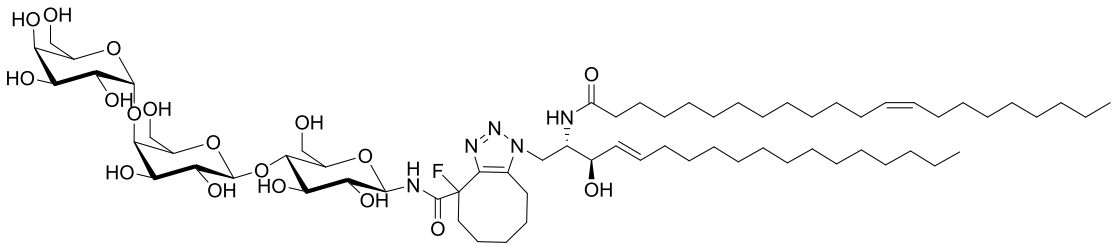

Gb3-MFCO **37** (1mg, 1.53 µmol) and 1-azidoceramide **30** (1 mg, 1.55 µmol) were stirred in MeOH/CH_2Cl_2 (3:1) for 6h. The solvent was evaporated and the racemic product (*R/S*) was purified by reverse phase silica column chromatography (20 to 100% MeOH in H_2O) to obtain pure clicked **35** (1.6 mg, 80%). R_f (^{n}BuOH/EtOH/H_2O [4:2:1])=0.6. ^{1}H NMR (400 MHz, MeOD) δ 5.83 – 5.68 (m, 1H), 5.56 – 5.40 (m, 1H), 5.40 – 5.29 (m, 2H), 4.99 (d, *J* 8.9 Hz, 1H), 4.97 – 4.95 (m, 1H), 4.50 – 4.38 (m, *J* 9.3, 6.4 Hz, 1H), 4.27 (t, *J* 6.3 Hz, 1H), 3.99 (s, 1H), 3.92 (d, *J* 2.6 Hz, 1H), 3.91 – 3.41 (m, 19H), 2.21 – 2.13 (m, *J* 8.1 Hz, 2H), 2.12 – 1.97 (m, 10H), 1.92 – 1.43 (m, 6H), 1.28 (s, 44H), 0.90 (t, *J* 6.8 Hz, 6H). ^{19}F NMR (376 MHz, MeOD) δ -148.51, -149.89. ESI-HRMS: Calcd for [MH$^+$] 1300.8534. Found: *m/z* 1300.8529.

1-((2*S*,3*R*,*E*)-2-((*Z*)-docos-13-enamido)-3-hydroxyoctadec-4-en-1-yl)-*N*'-glycine-4-fluoro-*N*-(4-*O*-(4-*O*-α-D-galactopyranosyl-β-D-galactopyranosyl)-D-glucopyranosyl)-5,6,7,8,9-decahydro-1H-cycloocta[d][1,2,3]triazole-4-carboxamide (36)

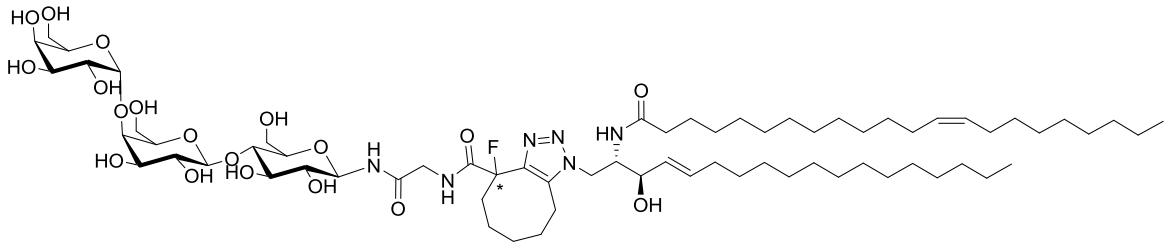

Gb3-Gly-MFCO **38** (1.4 mg, 2 µmol) and 1-azidoceramide **30** (1.3 mg, 2 µmol) were stirred in MeOH/CH_2Cl_2 (8:1) for 4h. The solvent was evaporated and the racemic product (*R/S*) was purified by reverse phase silica column chromatography (5 to 100% MeOH in H_2O) to obtain pure *clicked* **36** (1.1 mg, 41%). R_f (^{n}BuOH/EtOH/H_2O [4:2:1])=0.7. ^{1}H NMR (300 MHz, MeOD) δ 5.80 – 5.64 (m, 1H, $H^{5,AzCer}$), 5.46 (s, 1H, $H^{4,AzCer}$), 5.34 (t, *J* 4.8 Hz, 2H, $H^{e,AzCer}$), 5.00 – 4.89 (m, 2H, $H^{1,Gb3}$, $H^{1,Gb3}$), 4.57 – 4.39 (m, 3H, $H^{1,Gb3}$, $H^{3,AzCer}$, $H^{2,AzCer}$), 4.30 – 3.40 (m, 22H), 2.19 (t, *J* 7.5 Hz, 2H, $H^{a,AzCer}$), 2.12 – 1.96 (m, 10H, $H^{6,d,AzCer}$, $H^{a,e,MFCO}$), 1.94 – 1.41 (m, 6H, $H^{b,AzCer}$, $H^{b,d,MFCO}$), 1.29 (s, 44H), 0.90 (t, *J* 6.5 Hz, 6H). ^{19}F NMR (376 MHz, MeOD) δ -148.51, -149.89. ESI-HRMS: Calcd for [MH$^+$] 1357.8749. Found: *m/z* 1357.8754.

1-((2*S*,3*R*,*E*)-2-((*Z*)-docos-13-enamido)-3-hydroxyoctadec-4-en-1-yl)-4-fluoro-*N*-((2,3,4,6-tetra-*O*-acetyl-α-D-galactopyranosyl)-(1→4)-(2,3,6-tri-*O*-acetyl-β-D-galactopyranosyl)-(1→4)-(2,3,6-tri-*O*-acetyl-β-D-glucopyranosyl)-5,6,7,8,9-decahydro-1H-cycloocta[d][1,2,3]triazole-4-carboxamide (69)

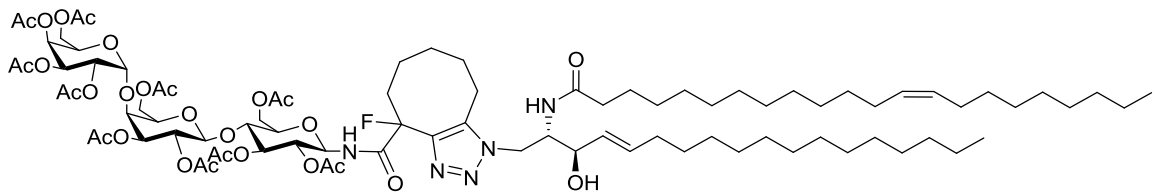

Peracteyl Gb3-MFCO **47** (0.8 mg, 0.7 µmol) and 1-azidoceramide **30** (0.5 mg, 0.78 µmol) were stirred in CH_2Cl_2 for 48h. The solvent was evaporated and the racemic product (*R/S*) was purified by silica column chromatography (0 to 2.5% MeOH in CH_2Cl_2) to obtain the isomeric *clicked* **69** (1 mg, 94%) and 1-*N*-MFCO-Gb3 (0.1 mg) recuperated. R_f (2.5% MeOH/CH_2Cl_2)=0.3. ESI-HRMS: Calcd for $[M+H^+]^+$ 1720.9585, $[M+H^+ + NH4^+]^{+2}$ 869.4962. Found: *m/z* 1720.9589 and 869.4965.

***N*-2-hydroxyethyl-1-fluoro-cyclooct-2-yne-1-carboxamide (59)**

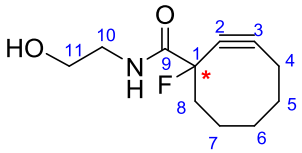

Stable intermediate **58** (Scheme 2.1.3.7) (9 mg, 49 µmol, 1 eq) was dissolved in THF (240 µl) and cooled to 0°C, to which freshly distilled ethanolamine in solution with THF (50 µl, 1:3) was added dropwise. The reaction mixture was stirred for 4h, evaporated and purified by silica column chromatography (EtOAc/cyclohexane [1:1]) to afford **59** as a racemic mixture (3 mg, 29%) R_f (EtOAc)=0.5. ^{1}H NMR (300 MHz, $CDCl_3$) δ 6.80 (s, 1H, OH), 3.77 (t, *J* 4.9 Hz, 2H, H^{11}), 3.48 (dd, *J* 10.1, 5.2 Hz, 2H, H10), 2.52 – 2.18 (m, 4H, H^6, H^2), 2.18 – 1.77 (m, 4H, H^3, H^5), 1.78 – 1.57 (m, 1H, H^4), 1.56 – 1.37 (m, 1H, H^4). ^{13}C NMR (101 MHz, $CDCl_3$) δ 169.56 (d, *J* 24.2 Hz, C^9), 109.68 (d, *J* 10.5 Hz, C^3), 94.57 (d, *J* 186.6 Hz, C^1), 87.11 (d, *J* 31.8 Hz, C^2), 62.05 (C^{11}), 46.48 (d, *J* 24.5 Hz, C^8), 42.39 (C^{10}), 33.93 (C^7), 28.95 (C^6), 25.71 (C^5), 20.67 (C^4). ^{19}F NMR (376 MHz, $CDCl_3$) δ -146.53. UPLC-MS (gradient 5-100% CH_3CN/H_2O, 4 min, ESI) rt=1.75; 214 $[MH^+]$.

β-1-*O*-trichloroacetamidate-2,3,4,6-tetra-*O*-acetyl-(1→4)-β-D-galactopyranosyl-2,3,6-tri-*O*-acetyl-β-D-glucopyranose (65)

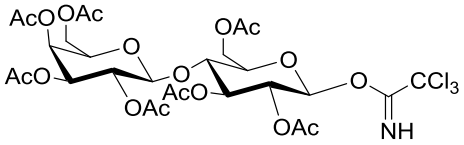

To a solution of peracetyl lactose (2×100 mg, 0.157 mmol, 1 eq) in CH_2Cl_2 (1 ml) was added trichloroacetonitrile (Cl_3CCN, 258 µl, 2.56 mmol, 20 eq) and DBU (65 µl, 0.384 mmol, 2.5 eq). The reaction was stirred overnight, evaporated and by silica column chromatography (12%-14% acetone in toluene + 0.5% Et_3N) to afford **65** (100 mg (1:3 α/β), 41% %). R_f (acetone/toluene/Et_3N [20:80:0.5])=0.4. ^{1}H NMR (300 MHz, $CDCl_3$) δ 8.65 (s, 1H, NH), 6.48 (d, *J* 3.7 Hz, 1H, H^1), 5.55 (t, $J^{3-2,\ 3-4}$ 9.7 Hz, 1H, H^3), 5.35 (d, J^{4-3} 3.0 Hz, 1H, $H^{4'}$), 5.12 (dd, J^{2-3} 10.3, J^{2-1} 7.9 Hz, 1H, $H^{2'}$), 5.05 (dd, J^{2-3} 10.1, J^{2-1} 3.8 Hz, 1H, H^2), 4.95 (dd, J^{3-2} 10.3, J^{3-4} 3.3 Hz, 2H, $H^{3'}$), 4.57 – 4.40 (m, 2H, $H^{1'}$, H^6), 4.20 – 4.02 (m, 4H, H^5, H^6, $2H^{6'}$), 3.92 – 3.77 (m, 2H, H^4, $H^{5'}$), 2.15 (s, 3H), 2.10 (s, 3H), 2.06 (s, 6H), 2.03 (s, 3H), 2.00 (s, 3H), 1.96 (s, 3H). ^{13}C NMR (75 MHz, $CDCl_3$) δ 170.27, 170.18, 170.08, 170.01, 169.29, 169.01, 160.98 (C=NH), 101.20 ($C^{1'}$), 92.91 (C^1), 90.70 (CCl_3), 75.89 (C^4), 71.12 ($C^{3'}$), 70.93 (C^5), 70.73 ($C^{5'}$), 69.97 (C^2), 69.58 (C^3), 69.16 ($C^{2'}$), 66.61 ($C^{4'}$), 61.51 (C^6), 60.78 ($C^{6'}$), 20.83, 20.76, 20.60, 20.46, 20.42. ν/cm^{-1} 3311 (NH), 1744 (C=O), 1676 (C=N), 1368 (C-H), 1213 (C-O), 1044 (C-O), 732 (C-Cl). ESI-HRMS: Calcd for [MNH_4^+] 797.1336. Found 797.1334.

(1*R*,8*S*,9*S*)-Bicyclo[6.1.0]non-4-yn-9-yl-methyl-2,3,4,6-tetra-*O*-acetyl-(1→4)-β-D-galactopyranosyl-2,3,6-tri-*O*-acetyl-β-D-glucopyranoside (66)

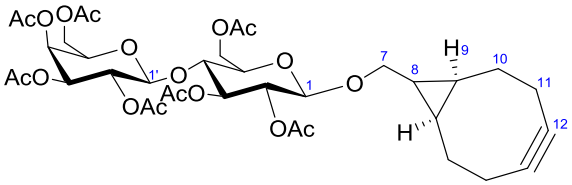

To a solution of trichloroacetamidate **65** (95 mg, 0.122 mmol, 1 eq) and (1*R*,8*S*,9*s*)-bicyclo[6.1.0]non-4-yn-9-ylmethanol (BCN, 22 mg, 0.146 mmol, 1.2 eq) with activated molecular sieves (4Å) in freshly distilled CH_2Cl_2 (2 ml), after cooling to -25°C, TMSOTf (11 µl, 61 µmol, 0.5 eq) was added. The reaction was stirred at for 4h and quenched with Et_3N, evaporated and purified by silica column chromatography (10 % acetone in toluene) to afford **66** (32 mg (β pure), 34 %). R_f (acetone/toluene [3:7]) =0.6. ^{1}H NMR (500 MHz, $CDCl_3$) δ 5.34 (d, J^{4-3} 3.3 Hz, 1H, $H^{4'}$), 5.19 (t, $J^{3-4,3-2}$ 9.3 Hz, 1H, H^3), 5.10 (dd, J^{2-3} 10.3 Hz, J^{2-1} 7.9 Hz, 1H, $H^{2'}$), 4.95 (dd, J^{3-2} 10.4 Hz, J^{3-4} 3.4 Hz, 1H, $H^{3'}$), 4.88 (dd, J^{2-3} 9.5 Hz, J^{2-1} 8.1 Hz, 1H, H^2), 4.53 – 4.45 (m, 3H, H^1, $H^{1'}$, H^6), 4.17 – 4.02 (m, 3H, H^6, $H^{6'}$), 3.92 (dd, J^{7a-7b} 10.6, J^{7-8} 7.3 Hz, 1H, H^{7a}), 3.86 (t, *J* 6.9 Hz, 1H, $H^{5'}$), 3.78 (t, *J* 9.5 Hz, 1H, H^4), 3.60 – 3.57 (m, 1H, H^5), 3.54 (dd, J^{7a-7b} 10.6, J^{7-8} 8.6 Hz, 1H, H^{7b}), 2.35 – 2.15 (m, 6H, H^{10}, H^{11}), 2.14 (s, 3H), 2.10 (s, 3H), 2.05 (s, 3H), 2.04 (s,

6H), 2.02 (s, 3H), 1.96 (s, 3H), 1.57 – 1.39 (m, 2H, H^{10}), 1.35 – 1.21 (m, 1H, H^{8}), 0.96 – 0.83 (m, 2H, H^{9}). ^{13}C NMR (126 MHz, $CDCl_3$) δ 170.37, 170.16, 170.09, 169.84, 169.59, 169.11, 101.13 ($C^{1\beta}$), 99.90 ($C^{1'\beta}$), 98.92 (C^{12a}), 98.71 (C^{12b}), 76.37 (C^{4}), 72.93 (C^{3}), 72.58 (C^{5}), 71.78 (C^{2}), 70.99 ($C^{3'}$), 70.68 ($C^{5'}$), 69.13 ($C^{2'}$), 66.97 (C^{7}), 66.59 ($C^{4'}$), 61.99 (C^{6}), 60.77 ($C^{6'}$), 29.17 (C^{10a}), 29.10 (C^{10b}), 21.42 (C^{11}), 20.87, 20.83, 20.75, 20.65, 20.52, 20.01, 19.93 (C^{9}), 18.06 (C^{8}). ESI-HRMS: Calcd for [MNH_4^+] 786.3179. Found: *m/z* 768.3173.

β-1-*O*-trichloroacetamido-2,3,4,6-tetra-O-acetyl-(1→4)-β-D-galactopyranosyl-2,3,6-tri-O-acetyl-β-D-glucopyranose (67)

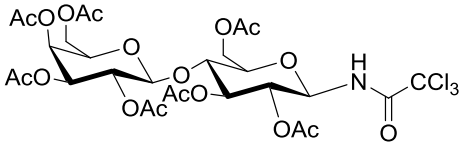

Amide decomposition impurity **67** (15 mg, 16%) closely followed **66** in chromatography purification. (R_f (acetone/toluene [3:7]) =0.5. ^{1}H NMR (500 MHz, $CDCl_3$) δ 8.44 (s, 1H, NH), 6.48 (d, J^{1-2} 3.7 Hz, 1H, H^{1}), 5.56 (t, $J^{3-2,\ 3-4}$ 9.8 Hz, 1H, H^{3}), 5.27 (d, J^{4-3} 2.7 Hz, 1H, $H^{4'}$), 5.05 (dd, J^{2-3} 10.4, J^{2-1} 7.9 Hz, 1H, $H^{2'}$), 5.00 (dd, J^{2-3} 10.3, J^{2-1} 3.8 Hz, 1H, H^{2}), 4.88 (dd, *J* 10.4, 3.4 Hz, 1H, $H^{3'}$), 4.40 (d, J^{2-1} 7.9 Hz, 2H, $H^{1'}$), 4.36 (m, 1H, H^{6}), 4.12 – 4.03 (m, 3H, H^{6}, $2H^{6'}$, H^{5}), 4.03 – 3.92 (m, 2H, H^{4}, $H^{5'}$), 3.84 – 3.73 (m, 3H), 2.08 (s, 3H), 2.06 (s, 3H), 2.05 (s, 3H), 1.98 (s, 3H), 1.96 (s, 3H), 1.95 (s, 3H), 1.88 (s, 3H). ^{13}C NMR (126 MHz, $CDCl_3$) δ 170.43, 170.38, 170.27, 170.17, 169.21, 169.15, 168.85, 101.26 ($C^{1'}$), 90.54 (CCl_3), 87.61 (C^{1}), 75.88, 73.85, 71.12, 70.80, 70.78, 69.35, 69.21, 66.66, 61.63, 60.88, 20.96, 20.77, 20.61. UPLC-MS (gradient 90-100% CH_3CN/H_2O, 4 min, ESI) rt=1.14; 780 [MH^+].

(1*R*,8*S*,9*S*)-Bicyclo[6.1.0]non-4-yn-9-methyl-(1→4)-β-D-galactopyranosyl-β-D-glucopyranoside (63)

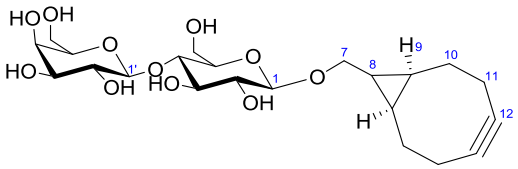

Peracteyl lactose-1-*O*-bicyclo[6.1.0]nonyne **66** (29 mg, 38 µmol) was solubilised in dry MeOH (1 ml) and CH_3ONa (530 µl, 0.5M in MeOH) was added dropwise. The reaction was stirred for 1h30 before Dowex H+ was added, the reaction mixture filtered, concentrated and purified

by reverse phase column chromatography to afford **63** (3 mg, 17 %). R_f (^{n}BuOH/EtOH/H_2O [2:2:1])=0.7. ^{1}H NMR (500 MHz, MeOD) δ 4.36 (d, J^{1-2} 7.6 Hz, 1H, $H^{1'}$), 4.32 (d, J^{1-2} 7.8 Hz, 1H, H^1), 4.00 (dd, J^{7a-b} 10.6, J^{7-8} 7.4 Hz, 1H, H^{7a}), 3.90 (dd, J^6 12.1, J^{6-5} 2.5 Hz, 1H, H^6), 3.83 (dd, J^6 12.1, J^{6-5} 4.4 Hz, 1H, H^6), 3.81 (dd, J^{4-3} 3.2, J^{4-5} 0.8 Hz, 1H, $H^{4'}$), 3.78 (dd, $J^{6'}$ 11.4, J^{6-5} 7.5 Hz, 1H, $H^{6'}$), 3.70 (dd, $J^{6'}$ 11.5, J^{6-5} 4.6 Hz, 1H, $H^{6'}$), 3.66 (dd, J^{7a-b} 10.6, J^{7-8} 8.0 Hz, 1H, H^{7b}), 3.61 – 3.50 (m, 4H, $H^{5'}$, H^4, $H^{2'}$, H^3), 3.48 (dd, J^{3-2} 9.8, J^{3-4} 3.3 Hz, 1H, $H^{3'}$), 3.40 (ddd, J^{4-5} 9.4, $^{5-6}$ 4.3, $^{5-6}$2.6 Hz, 1H, H^5), 3.25 (dd, J^{2-3} 8.9, J^{2-1} 7.9 Hz, 1H, H^2), 2.30 – 2.20 (m, 4H, H^{10}, H^{11}), 2.20 – 2.11 (m, 2H, H^{11}), 1.69 – 1.54 (m, 2H, H^{10}), 1.37 (ddd, *J* 16.9, 9.1, 7.8 Hz, 1H, H^8), 0.98 – 0.86 (m, 2H, H^9). ^{13}C NMR (126 MHz, MeOD) δ 105.11 ($C^{1'}$), 103.85 (C^1), 99.59 (C^{12}), 80.74 (C^4), 77.10 ($C^{5'}$), 76.51 (C^5 or C^3), 76.46 (C^5 or C^3), 74.83 (C^2 or $C^{3'}$), 74.80 (C^2 or $C^{3'}$), 72.57 ($C^{2'}$), 70.31 ($C^{4'}$), 67.77 (C^7), 62.50 (C^6), 62.00 ($C^{6'}$), 30.26 (C^{10}), 30.14 (C^{10}), 21.96 (C^{11}), 21.24 (C^9), 21.11 (C^9), 19.52 (C^8). UPLC-MS (gradient 5-100% CH_3CN/H_2O, 4 min, ESI) rt=1.55; 473 [M^-], 519 [M+FA-H^-], 475 [MH^+]. ESI-HRMS: Calcd for [MNa^+] 497.1993. Found: *m/z* 497.1995.

7 BIBLIOGRAPHY

1. Heuser, J. E. & Anderson, R. G. W. Hypertonic media inhibit receptor-mediated endocytosis by blocking clathrin-coated pit formation. *J. Cell Biol.* **108,** 389–400 (1989).
2. McMahon, H. T. & Boucrot, E. Molecular mechanism and physiological functions of clathrin-mediated endocytosis. *Nat. Rev. Mol. Cell Biol.* **12,** 517–533 (2011).
3. Connerly, P. L. How Do Proteins Move Through the Golgi Apparatus? *Nat. Educ.* **3,** 60 (2010).
4. Mayor, S. & Pagano, R. E. Pathways of clathrin-independent endocytosis. *Nat. Rev. Mol. Cell Biol.* 603–612 (2007).
5. Mayor, S., Parton, R. G. & Donaldson, J. G. Clathrin-independent pathways of endocytosis. *Cold Spring Harb. Perspect. Biol.* **6,** 1–20 (2014).
6. Echarri, A. & Del Pozo, M. A. Caveolae. *Curr. Biol.* **22,** 114–116 (2012).
7. Sonnino, S. & Prinetti, A. Sphingolipids and membrane environments for caveolin. *FEBS Lett.* **583,** 597–606 (2009).
8. Johannes, L., Parton, R. G., Bassereau, P. & Mayor, S. Building endocytic pits without clathrin. *Nat. Rev. Mol. Cell Biol.* **16,** 311–321 (2015).
9. Howes, M. T., Mayor, S. & Parton, R. G. Molecules, mechanisms, and cellular roles of clathrin-independent endocytosis. *Curr. Opin. Cell Biol.* **22,** 519–527 (2010).
10. Hinze, C. & Boucrot, E. Local actin polymerization during endocytic carrier formation. *Biochem. Soc. Trans.* **167,** 1–12 (2018).
11. Ewers, H. & Helenius, A. Lipid-Mediated Endocytosis. *Cold Spring Harb. Perspect. Biol.* **3,** 4721–4721 (2011).
12. Johannes, L. & Römer, W. Shiga toxins - from cell biology to biomedical applications. *Nat. Rev. Microbiol.* **8,** 105–116 (2010).
13. Cheng, Z.-J. *et al.* Distinct Mechanisms of Clathrin-independent Endocytosis Have Unique Sphingolipid Requirements. *Mol. Biol. Cell* **17,** 3197–3210 (2006).
14. Ferreira, A. P. A. & Boucrot, E. Mechanisms of Carrier Formation during Clathrin-Independent Endocytosis. *Trends Cell Biol.* **28,** 188–200 (2017).
15. Renard, H.-F. *et al.* Endophilin-A2 functions in membrane scission in clathrin-independent endocytosis. *Nature* **517,** 493–6 (2014).
16. Johannes, L., Wunder, C. & Shafaq-Zadah, M. Glycolipids and Lectins in Endocytic Uptake Processes. *J. Mol. Biol.* **428,** 4792–4818 (2016).
17. Moya, M., Dautry-Varsat, A., Goud, B., Louvard, D. & Boquet, P. Inhibition of coated pit formation in hep2 cells blocks the cytotoxicity of diphtheria toxin but not that of ricin toxin. *J. Cell Biol.* **101,** 548–559 (1985).
18. Schmid, S. L., Sorkin, A. & Zerial, M. Endocytosis: Past, Present, and Future. *Cold Spring Harb. Perspect. Biol.* **6,** 1–10 (2014).
19. Spooner, R. A. & Lord, J. M. How Ricin and Shiga Toxin Reach the Cytosol of Target Cells: Retrotranslocation from the Endoplasmis Reticulum. *Curr. Top. Microbiol. Immunol.* **357,** 19–40 (2012).
20. Bergan, J., Dyve Lingelem, A. B., Simm, R., Skotland, T. & Sandvig, K. Shiga toxins. *Toxicon* **60,** 1085–1107 (2012).
21. Pina, D. G. & Johannes, L. Cholera and Shiga toxin B-subunits: Thermodynamic and structural considerations for function and biomedical applications. *Toxicon* **45,** 389–393 (2005).
22. Merritt, E. A. *et al.* Crystal structure of cholera toxin B-pentamer bound to receptor GM1 pentasaccharide. *Protein Sci.* **3,** 166–75 (1994).

23. Pezeshkian, W. *et al.* Membrane invagination induced by Shiga toxin B-subunit: from molecular structure to tube formation. *Soft Matter* **12,** 5164–5171 (2016).

24. Pezeshkian, W. *et al.* Mechanism of Shiga Toxin Clustering on Membranes. *ACS Nano* **11,** 314–324 (2017).

25. Walde, P., Cosentino, K., Engel, H. & Stano, P. Giant Vesicles: Preparations and Applications. *ChemBioChem* **11,** 848–865 (2010).

26. Fenz, S. F. & Sengupta, K. Giant vesicles as cell models. *Integr. Biol.* **4,** 982 (2012).

27. Römer, W. *et al.* Shiga toxin induces tubular membrane invaginations for its uptake into cells. *Nature* **450,** 670–675 (2007).

28. Eierhoff, T. *et al.* A lipid zipper triggers bacterial invasion. *Proc. Natl. Acad. Sci. U. S. A.* **111,** 6–11 (2014).

29. Ewers, H. *et al.* GM1 structure determines SV40-induced membrane invagination and infection. *Nat. Cell Biol.* **12,** 11-18; sup pp 1–12 (2010).

30. Chinnapen, D. J. F. *et al.* Lipid Sorting by Ceramide Structure from Plasma Membrane to ER for the Cholera Toxin Receptor Ganglioside GM1. *Dev. Cell* **23,** 573–586 (2012).

31. Lakshminarayan, R. *et al.* Galectin-3 drives glycosphingolipid-dependent biogenesis of clathrin-independent carriers. *Nat. Cell Biol.* **16,** 595–606 (2014).

32. Johannes, L., Wunder, C. & Bassereau, P. Bending 'on the rocks'-A cocktail of biophysical modules to build endocytic pathways. *Cold Spring Harb. Perspect. Biol.* **6,** 1–18 (2014).

33. Arab, S. & Lingwood, C. A. Influence of phospholipid chain length on verotoxin/globotriaosyl ceramide binding in model membranes: Comparison of a supported bilayer film and liposomes. *Glycoconj. J.* **13,** 159–166 (1996).

34. Merrill, A. H. Sphingolipid and glycosphingolipid metabolic pathways in the era of sphingolipidomics. *Chem. Rev.* **111,** 6387–422 (2011).

35. Watkins, E. B. *et al.* Carbohydrate Conformation and Lipid Condensation in Monolayers Containing Glycosphingolipid Gb3: Influence of Acyl Chain Structure. *Biophys. J.* **107,** 1146–1155 (2014).

36. Solovyeva, V., Johannes, L. & Simonsen, A. C. Shiga toxin induces membrane reorganization and formation of long range lipid order. *Soft Matter* **11,** 186–192 (2015).

37. Simons, K. & van Meer, G. Lipid sorting in epithelial cells. *Biochemistry* **27,** 6197–6202 (1988).

38. Simons, K. & Gerl, M. J. Revitalizing membrane rafts: New tools and insights. *Nat. Rev. Mol. Cell Biol.* **11,** 688–699 (2010).

39. Lamaze, C. *et al.* Interleukin 2 receptors and detergent-resistant membrane domains define a clathrin-independent endocytic pathway. *Mol. Cell* **7,** 661–671 (2001).

40. Falguières, T. *et al.* Functionally different pools of Shiga toxin receptor, globotriaosyl ceramide, in HeLa cells. *FEBS J.* **273,** 5205–5218 (2006).

41. Kouzel, I. U. *et al.* Association of Shiga toxin glycosphingolipid receptors with membrane microdomains of toxin-sensitive lymphoid and myeloid cells. *J. Lipid Res.* **54,** 692–710 (2013).

42. Gowrishankar, K. *et al.* Active remodeling of cortical actin regulates spatiotemporal organization of cell surface molecules. *Cell* **149,** 1353–1367 (2012).

43. Sevcsik, E. & Schütz, G. J. With or without rafts? Alternative views on cell membranes. *BioEssays* **38,** 129–139 (2016).

44. Anderson, R. G. W. & Jacobson, K. Cell biology: A role for lipid shells in targeting proteins to caveolae, rafts, and other lipid domains. *Science (80-.).* **296,** 1821–1825 (2002).

45. Honigmann, A. *et al.* Scanning STED-FcS reveals spatiotemporal heterogeneity of lipid interaction in the plasma membrane of living cells. *Nat. Commun.* **5,** 1–12 (2014).

46. Eggeling, C. *et al.* Direct observation of the nanoscale dynamics of membrane lipids in a living cell. *Nature* **457,** 1159–1162 (2009).

47. Frisz, J. F. *et al.* Sphingolipid domains in the plasma membranes of fibroblasts are not enriched with cholesterol. *J. Biol. Chem.* **288,** 16855–16861 (2013).

48. Kraft, M. L. Sphingolipid Organization in the Plasma Membrane and the Mechanisms That Influence It. *Front. Cell Dev. Biol.* **4,** 1–19 (2017).

49. D'Auria, L. *et al.* Micrometric segregation of fluorescent membrane lipids: relevance for endogenous lipids and biogenesis in erythrocytes. *J. Lipid Res.* **54,** 1066–1076 (2013).

50. Wüstner, D. & Færgeman, N. J. Spatiotemporal analysis of endocytosis and membrane distribution of fluorescent sterols in living cells. *Histochem. Cell Biol.* **130,** 891–908 (2008).

51. Komura, N. *et al. Syntheses of Fluorescent Gangliosides for the Studies of Raft Domains*. *Chemical Glycobiology Part A* (2017). at <http://linkinghub.elsevier.com/retrieve/pii/S0076687917301611>

52. Suzuki, K. G. N. *et al.* Development of new ganglioside probes and unraveling of raft domain structure by single-molecule imaging. *Biochim. Biophys. Acta - Gen. Subj.* 0–1 (2017).

53. Schwarzmann, G., Arenz, C. & Sandhoff, K. Labeled chemical biology tools for investigating sphingolipid metabolism, trafficking and interaction with lipids and proteins. *Biochim. Biophys. Acta - Mol. Cell Biol. Lipids* **1841,** 1161–1173 (2014).

54. Aly, M. R. E., Rochaix, P., Amessou, M., Johannes, L. & Florent, J.-C. Synthesis of globo- and isoglobotriosides bearing a cinnamoylphenyl tag as novel electrophilic thiol-specific carbohydrate reagents. *Carbohydr. Res.* **341,** 2026–2036 (2006).

55. Polyakova, S. M. *et al.* New GM1 ganglioside derivatives for selective single and double labelling of the natural glycosphingolipid skeleton. *European J. Org. Chem.* 5162–5177 (2009).

56. Sezgin, E. *et al.* Partitioning, diffusion, and ligand binding of raft lipid analogs in model and cellular plasma membranes. *Biochim. Biophys. Acta - Biomembr.* **1818,** 1777–1784 (2012).

57. Klymchenko, A. S. & Kreder, R. Fluorescent Probes for Lipid Rafts: From Model Membranes to Living Cells. *Chem. Biol.* **21,** 97–113 (2014).

58. Safouane, M. *et al.* Lipid Cosorting Mediated by Shiga Toxin Induced Tubulation. *Traffic* **11,** 1519–1529 (2010).

59. Patalag, L. J., Sibold, J., Schütte, O. M., Steinem, C. & Werz, D. B. Gb3 Glycosphingolipids with Fluorescent Oligoene Fatty Acids: Synthesis and Phase Behavior in Model Membranes. *ChemBioChem* 1–9 (2017).

60. Schwarzmann, G. Uptake and metabolism of exogenous glycosphingolipids by cultured cells. *Semin. Cell Dev. Biol.* **12,** 163–171 (2001).

61. Pedrosa, L. R. C. *et al.* C8-glycosphingolipids preferentially insert into tumor cell membranes and promote chemotherapeutic drug uptake. *Biochim. Biophys. Acta - Biomembr.* **1848,** 1656–1670 (2015).

62. Dauner, M., Batroff, E., Bachmann, V., Hauck, C. R. & Wittmann, V. Synthetic Glycosphingolipids for Live-Cell Labeling. *Bioconjug. Chem.* acs.bioconjchem.6b00177 (2016).

63. Csiszár, A. *et al.* Novel fusogenic liposomes for fluorescent cell labeling and membrane modification. *Bioconjug. Chem.* **21,** 537–543 (2010).

64. *Matreya LLC online resource, Typical Fatty Acid Composition of Natural Lipids*. *Matreya LLC (online resource)*

65. Haicheur, N. *et al.* The B subunit of Shiga toxin coupled to full-size antigenic protein elicits humoral and cell-mediated immune responses associated with a Th1-dominant polarization. *Int. Immunol.* **15,** 1161–1171 (2003).

66. Tam, P. *et al.* Differential intracellular transport and binding of verotoxin 1 and verotoxin 2 to globotriaosylceramide-containing lipid assemblies. *J. Cell. Physiol.* **216,** 750–763 (2008).

67. Lingwood, C. a. Glycosphingolipid functions. *Cold Spring Harb. Perspect. Biol.* **3,** 1–26 (2011).

68. Lodish, H. *et al. Molecular Cell Biology*. *W. H. Freeman* (2003).

69. Hoetzl, S., Sprong, H. & van Meer, G. The way we view cellular (glyco)sphingolipids. *J. Neurochem.* **103 Suppl,** 3–13 (2007).

70. Yamashita, T. A vital role for glycosphingolipid synthesis during development and differentiaion. *Seikagaku* **96,** 9142 (1999).

71. Nishie, T. *et al.* β4-Galactosyltransferase-5 is a lactosylceramide synthase essential for mouse extra-embryonic development. *Glycobiology* **20,** 1311–1322 (2010).

72. D'Angelo, G., Capasso, S., Sticco, L. & Russo, D. Glycosphingolipids: Synthesis and functions. *FEBS J.* **280,** 6338–6353 (2013).

73. Russo, D. *et al.* Glycosphingolipid metabolic reprogramming drives neural differentiation. *EMBO J.* e97674 (2017).

74. Ho, M. Y., Yu, A. L. & Yu, J. Glycosphingolipid dynamics in human embryonic stem cell and cancer: their characterization and biomedical implications. *Glycoconj. J.* (2016).

75. Breimer, M. E., Säljö, K., Barone, A. & Teneberg, S. Glycosphingolipids of human embryonic stem cells. *Glycoconj. J.* 1–11 (2016). doi:10.1007/s10719-016-9706-y

76. Hakomori, S. Structure and function of glycosphingolipids and sphingolipids: Recollections and future trends. *Biochim. Biophys. Acta - Gen. Subj.* **1780,** 325–346 (2008).

77. Russo, D., Parashuraman, S. & D'Angelo, G. Glycosphingolipid–protein interaction in signal transduction. *Int. J. Mol. Sci.* **17,** 1–21 (2016).

78. Coskun, Ü., Grzybek, M., Drechsel, D. & Simons, K. Regulation of human EGF receptor by lipids. *Proc. Natl. Acad. Sci.* **108,** 9044–9048 (2011).

79. Simons, K. & Sampaio, J. L. Membrane organization and lipid rafts. *Cold Spring Harb Perspect Biol* **3,** a004697 (2011).

80. Sampaio, J. L. *et al.* Membrane lipidome of an epithelial cell line. *Proc. Natl. Acad. Sci. U. S. A.* **108,** 1903–7 (2011).

81. Ejsing, C. S. *et al.* Global analysis of the yeast lipidome by quantitative shotgun mass spectrometry. *Proc. Natl. Acad. Sci. {U.S.A.}* **106,** 2136–2141 (2009).

82. D'Angelo, G. *et al.* Vesicular and non-vesicular transport feed distinct glycosylation pathways in the Golgi. *Nature* **501,** 116–20 (2013).

83. Levy, M. & Futerman, A. H. Mammalian ceramide synthases. *IUBMB Life* **62,** 347–56 (2010).

84. Schulze, H. & Sandhoff, K. Lysosomal Lipid Storage Diseases. *Cold Spring Harb. Perspect. Biol.* **3,** a004804–a004804 (2011).

85. Gault, C. R., Obeid, L. M. & Hannun, Y. A. An overview of sphingolipid metabolism: From synthesis to breakdown. *Adv. Exp. Med. Biol.* **688,** 1–23 (2010).

86. Merscher, S. & Fornoni, A. Podocyte pathology and nephropathy - sphingolipids in glomerular diseases. *Front. Endocrinol. (Lausanne).* **5,** 1–11 (2014).

87. Jwa Hidari, K. I. P., Ichikawa, S., Fujita, T., Sakiyama, H. & Hirabayashi, Y. Complete removal of sphingolipids from the plasma membrane disrupts cell to substratum adhesion of mouse melanoma cells. *J. Biol. Chem.* **271,** 14636–14641 (1996).

88. Zhou, K. & Blom, T. Trafficking and functions of bioactive sphingolipids: Lessons from cells and model membranes. *Lipid Insights* **2015,** 11–20 (2015).

89. Yamaji, T. & Hanada, K. Sphingolipid Metabolism and Interorganellar Transport: Localization of Sphingolipid Enzymes and Lipid Transfer Proteins. *Traffic* **16,** 101–122 (2015).

90. Kitatani, K. *et al.* Protein kinase C-induced activation of a ceramide/protein phosphatase 1 pathway

leading to dephosphorylation of p38 MAPK. *J. Biol. Chem.* **281,** 36793–36802 (2006).

91. Kitatani, K., Idkowiak-Baldys, J. & Hannun, Y. A. The sphingolipid salvage pathway in ceramide metabolism and signaling. *Cell. Signal.* **20,** 1010–1018 (2008).

92. Futerman, A. H. & Riezman, H. The ins and outs of sphingolipid synthesis. *Trends Cell Biol.* **15,** 312–318 (2005).

93. Tanaka, K. A. K. *et al.* Membrane molecules mobile even after chemical fixation. *Nat. Methods* **7,** 865–866 (2010).

94. Takatori, S., Mesman, R. & Fujimoto, T. Microscopic methods to observe the distribution of lipids in the cellular membrane. *Biochemistry* **53,** 639–653 (2014).

95. Malhotra, R. Membrane Glycolipids: Functional Heterogeneity: A Review. *Biochem. Anal. Biochem.* **01,** 1–5 (2012).

96. Ogretmen, B. Sphingolipid metabolism in cancer signalling and therapy. *Nat. Rev. Cancer* **18,** 33–50 (2017).

97. Karve, S. S. & Weiss, A. A. Glycolipid binding preferences of shiga toxin variants. *PLoS One* **9,** (2014).

98. Luginbuehl, V., Meier, N., Kovar, K. & Rohrer, J. Intracellular drug delivery: Potential usefulness of engineered Shiga toxin subunit B for targeted cancer therapy. *Biotechnol. Adv.* 0–1 (2018).

99. Khan, I. Crisis-driven cholera resurgence switches focus to oral vaccine. *Bull. World Health Organ.* **96,** 446–447 (2018).

100. Kovbasnjuk, O. *et al.* The glycosphingolipid globotriaosylceramide in the metastatic transformation of colon cancer. *Proc. Natl. Acad. Sci. U. S. A.* **102,** 19087–19092 (2005).

101. Liang, Y.-J. *et al.* Differential expression profiles of glycosphingolipids in human breast cancer stem cells vs. cancer non-stem cells. *Proc. Natl. Acad. Sci.* **110,** 4968–4973 (2013).

102. Krengel, U. & Bousquet, P. A. Molecular recognition of gangliosides and their potential for cancer immunotherapies. *Front. Immunol.* **5,** 1–11 (2014).

103. Beck, A., Goetsch, L., Dumontet, C. & Corvaïa, N. Strategies and challenges for the next generation of antibody-drug conjugates. *Nat. Rev. Drug Discov.* **16,** 315–337 (2017).

104. El Alaoui, A. *et al.* Shiga toxin-mediated retrograde delivery of a topoisomerase I inhibitor prodrug. *Angew. Chemie - Int. Ed.* **46,** 6469–6472 (2007).

105. Johansson, D., Andersson, C., Moharer, J., Johansson, A. & Behnam-Motlagh, P. Cisplatin-induced expression of Gb3 enables verotoxin-1 treatment of cisplatin resistance in malignant pleural mesothelioma cells. *Br. J. Cancer* **102,** 383–91 (2010).

106. Bouter, A. *et al.* Intracellular trafficking of Shiga-toxin-B-subunit-functionalized spherulites. *Biol. Cell* **100,** 717–728 (2008).

107. Tyler, A. *et al.* Targeting glucosylceramide synthase induction of cell surface globotriaosylceramide (Gb3) in acquired cisplatin-resistance of lung cancer and malignant pleural mesothelioma cells. *Exp. Cell Res.* **336,** 23–32 (2015).

108. Falguières, T. *et al.* Human colorectal tumors and metastases express Gb3 and can be targeted by an intestinal pathogen-based delivery tool. *Mol. Cancer Ther.* **7,** 2498–2508 (2008).

109. Stimmer, L. *et al.* Human breast cancer and lymph node metastases express Gb3 and can be targeted by STxB- vectorized chemotherapeutic compounds. *BMC Cancer* **14,** 916 (2014).

110. Batisse, C. *et al.* A new delivery system for auristatin in STxB-drug conjugate therapy. *Eur. J. Med. Chem.* **95,** 483–491 (2015).

111. Wang, M., Wang, C., Han, R. H. & Han, X. Novel advances in shotgun lipidomics for biology and medicine. *Prog. Lipid Res.* **61,** 83–108 (2016).

112. Surma, M. A. *et al.* An automated shotgun lipidomics platform for high throughput, comprehensive, and quantitative analysis of blood plasma intact lipids. *Eur. J. Lipid Sci. Technol.* **117,** 1540–1549 (2015).

113. Patterson, D. M., Nazarova, L. A. & Prescher, J. A. Finding the Right (Bioorthogonal) Chemistry. *ACS Chem. Biol.* **9,** 592–605 (2014).

114. Baskin, J. M. *et al.* Copper-free click chemistry for dynamic in vivo imaging. *Proc. Natl. Acad. Sci. U. S. A.* **104,** 16793–16797 (2007).

115. Sletten, E. M. & Bertozzi, C. R. Bioorthogonal chemistry: Fishing for selectivity in a sea of functionality. *Angew. Chemie - Int. Ed.* **48,** 6974–6998 (2009).

116. Hang, H. C. & Bertozzi, C. R. Ketone isosteres of 2-N-acetamidosugars as substrates for metabolic cell surface engineering [7]. *J. Am. Chem. Soc.* **123,** 1242–1243 (2001).

117. Yarema, K. J., Mahal, L. K., Bruehl, R. E., Rodriguez, E. C. & Bertozzi, C. R. Metabolic delivery of ketone groups to sialic acid residues. Application to cell surface glycoform engineering. *J. Biol. Chem.* **273,** 31168–31179 (1998).

118. Jacobs, C. L. *et al.* Metabolic labeling of glycoproteins with chemical tags through unnatural sialic acid biosynthesis. *Methods Enzymol.* **327,** 260–275 (2000).

119. Saxon, E. & Bertozzi, C. R. Cell Surface Engineering by a Modified Staudinger Reaction. *Science (80-.).* **287,** 2007–2010 (2000).

120. Saxon, E. *et al.* Investigating Cellular Metabolism of Synthetic Azidosugars with the Staudinger Ligation. *J. Am. Chem. Soc.* **124,** 14893–14902 (2002).

121. Rampoldi, F., Sandhoff, R., Owen, R. W., Gröne, H.-J. & Porubsky, S. A new, robust, and nonradioactive approach for exploring N-myristoylation. *J. Lipid Res.* **53,** 2459–68 (2012).

122. Azoulay, M., Tuffin, G., Sallem, W. & Florent, J.-C. A new drug-release method using the Staudinger ligation. *Bioorganic Med. Chem. Lett.* **16,** 3147–3149 (2006).

123. Prescher, J. a & Bertozzi, C. R. Chemistry in living systems. *Nat. Chem. Biol.* **1,** 13–21 (2005).

124. Clayden, N. G., Warren, S. & Wothers, P. D. *Organic Chemistry*. (Oxford University Press, 2001).

125. Nilsson, B. L., Kiessling, L. L. & Raines, R. T. Staudinger ligation: a peptide from a thioester and azide. *Org. Lett.* **2,** 1939–1941 (2000).

126. Wang, Z.-P. A., Tian, C.-L. & Zheng, J.-S. The recent developments and applications of the traceless-Staudinger reaction in chemical biology study. *RSC Adv.* **5,** 107192–107199 (2015).

127. Prescher, J. A., Dube, D. H. & Bertozzi, C. R. Chemical remodelling of cell surfaces in living animals. *Nature* **430,** 873–878 (2004).

128. Sarkar, A. K., Fritz, T. A., Taylor, W. H. & Esko, J. D. Disaccharide uptake and priming in animal cells: inhibition of sialyl Lewis X by acetylated Gal beta 1-->4GlcNAc beta-O-naphthalenemethanol. *Proc. Natl. Acad. Sci. U. S. A.* **92,** 3323–7 (1995).

129. Whitman, C. M., Yang, F. & Kohler, J. J. Modified GM3 gangliosides produced by metabolic oligosaccharide engineering. *Bioorganic Med. Chem. Lett.* **21,** 5006–5010 (2011).

130. Luchansky, S. J. *et al.* Constructing azide-labeled cell surfaces using polysaccharide biosynthetic pathways. *Methods Enzymol.* **362,** 249–272 (2003).

131. Kolb, H. C., Finn, M. G. & Sharpless, K. B. Click Chemistry: Diverse Chemical Function from a Few Good Reactions. *Angew. Chemie - Int. Ed.* **40,** 2004–2021 (2001).

132. Huisgen, R. 1,3-Dipolar Cycloadditions. *Proc. Chem. Soc* 357–396 (1961).

133. Rostovtsev, V., Green, L., Fokin, V. V. & Sharpless, K. B. A Stepwise Huisgen Cycloaddition Process Catalyzed by Copper (I): Regioselective Ligation of Azides and Terminal Alkynes. *Angew. Chem. Int. Ed.* **41,** 2596–2599 (2002).

134. Tornøe, C. W., Christensen, C. & Meldal, M. Peptidotriazoles on solid phase: [1,2,3]-Triazoles by regiospecific copper(I)-catalyzed 1,3-dipolar cycloadditions of terminal alkynes to azides. *J. Org. Chem.* **67,** 3057–3064 (2002).

135. Huisgen, R. 1,3-Dipolar Cycloadditions; Past and Future. *Angew. Chem. Int. Ed.* **2,** 565–598 (1963).

136. Kennedy, D. C. *et al.* Cellular consequences of copper complexes used to catalyze bioorthogonal click reactions. *J. Am. Chem. Soc.* **133,** 17993–18001 (2011).

137. Hong, V., Presolski, S. I., Ma, C. & Finn, M. G. Analysis and Optimization of Copper-Catalysed Azide-Alkyne Cycloaddition for Bioconjugation. *Angew. Chem., Int. Ed. Engl.* **48,** 9879–9883 (2009).

138. Li, S. *et al.* Copper-catalyzed click reaction on/in live cells. *Chem. Sci.* **21,** 1075–1101 (2016).

139. Hong, V., Steinmetz, N. F., Manchester, M. & Finn, M. G. Labeling live cells by copper-catalyzed alkyne-azide click chemistry. *Bioconjug. Chem.* **21,** 1912–1916 (2010).

140. Li, C. *et al.* Practical labeling methodology for choline-derived lipids and applications in live cell fluorescence imaging. *Photochem. Photobiol.* **90,** 686–695 (2014).

141. Besanceney-Webler, C. *et al.* Increasing the efficacy of bioorthogonal click reactions for bioconjugation: A comparative study. *Angew. Chemie - Int. Ed.* **50,** 8051–8056 (2011).

142. Agard, N. J., Prescher, J. a & Bertozzi, C. R. A Strain-Promoted [3 + 2] Azide-Alkyne Cycloaddition for Covalent Modification of Biomolecules in Living Systems. *J. Am. Chem. Soc.* **126,** 15046–15047 (2004).

143. Dommerholt, J., Rutjes, F. P. J. T. & van Delft, F. L. Strain-Promoted 1,3-Dipolar Cycloaddition of Cycloalkynes and Organic Azides. *Top. Curr. Chem.* **374,** 1–20 (2016).

144. Dommerholt, J. *et al.* Highly accelerated inverse electron-demand cycloaddition of electron-deficient azides with aliphatic cyclooctynes. *Nat. Commun.* **5,** 1–7 (2014).

145. Codelli, J. a, Baskin, J. M., Agard, N. J. & Bertozzi, C. R. Second-Generation Difluorinated Cyclooctynes for Copper-Free Click Chemistry. *J. Am. Chem. Soc.* **130,** 11486–11493 (2008).

146. Borrmann, A. & Van Hest, J. C. M. Bioorthogonal chemistry in living organisms. *Chem. Sci.* **5,** 2123–2134 (2014).

147. McKay, C. S. & Finn, M. G. Click chemistry in complex mixtures: Bioorthogonal bioconjugation. *Chem. Biol.* **21,** 1075–1101 (2014).

148. Schultz, M. K., Parameswarappa, S. G. & Pigge, F. C. Synthesis of a DOTA-biotin conjugate for radionuclide chelation via Cu-free click chemistry. *Org. Lett.* **12,** 2398–2401 (2010).

149. McKay, C. S., Blake, J. A., Cheng, J., Danielson, D. C. & Pezacki, J. P. Strain-promoted cycloadditions of cyclic nitrones with cyclooctynes for labeling human cancer cells. *Chem. Commun.* **47,** 10040–10042 (2011).

150. Ramil, C. P. & Lin, Q. Bioorthogonal chemistry: Strategies and recent developments. *Chem. Commun.* **49,** 11007–11022 (2013).

151. Boutureira, O. & Bernardes, G. J. L. Advances in Chemical Protein Modification. *Chem. Rev.* **115,** 2174–2195 (2015).

152. Lang, K. *et al.* Genetically encoded norbornene directs site-specific cellular protein labelling via a rapid bioorthogonal reaction. *Nat. Chem.* **4,** 298–304 (2012).

153. Meyer, J. P., Adumeau, P., Lewis, J. S. & Zeglis, B. M. Click Chemistry and Radiochemistry: The First 10 Years. *Bioconjug. Chem.* **27,** 2791–2807 (2016).

154. Wang, H. *et al.* Selective in vivo metabolic cell-labeling-mediated cancer targeting. *Nat. Chem. Biol.* **13,** 415–424 (2017).

155. Jao, C. Y., Roth, M., Welti, R. & Salic, A. Metabolic labeling and direct imaging of choline phospholipids in vivo. *Proc. Natl. Acad. Sci. U. S. A.* **106,** 15332–15337 (2009).

156. Jao, C. Y., Roth, M., Welti, R. & Salic, A. Biosynthetic labeling and two-color imaging of phospholipids in cells. *ChemBioChem* **16,** 472–476 (2015).

157. Hannoush, R. N. & Sun, J. The chemical toolbox for monitoring protein fatty acylation and prenylation. *Nat. Chem. Biol.* **6,** 498–506 (2010).

158. Hang, H. C. *et al.* Chemical probes for the rapid detection of fatty-acylated proteins in mammalian cells. *J. Am. Chem. Soc.* **129,** 2744–2745 (2007).

159. Thiele, C. *et al.* Tracing fatty acid metabolism by click chemistry. *ACS Chem. Biol.* **7,** 2004–2011 (2012).

160. Kuerschner, L. & Thiele, C. Multiple bonds for the lipid interest. *Biochim. Biophys. Acta - Mol. Cell Biol. Lipids* **1841,** 1031–1037 (2014).

161. Gaebler, A. *et al.* Alkyne lipids as substrates for click chemistry-based in vitro enzymatic assays. *J. Lipid Res.* **54,** 2282–90 (2013).

162. Collenburg, L. *et al.* A Functionalized Sphingolipid Analogue for Studying Redistribution during Activation in Living T Cells. *J. Immunol.* **196,** 3951–3962 (2016).

163. Walter, T. *et al.* Incorporation and visualization of azido-functionalized N-oleoyl serinol in Jurkat cells, mouse brain astrocytes, 3T3 fibroblasts and human brain microvascular endothelial cells. *Chem. Commun.* **52,** 8612–8614 (2016).

164. Fink, J. & Seibel, J. Click reactions with functional sphingolipids. *Biol. Chem.* **0,** (2018).

165. Erdmann, R. S. *et al.* Super-Resolution Imaging of the Golgi in Live Cells with a Bioorthogonal Ceramide Probe. *Angew. Chemie - Int. Ed.* **53,** 10242–10246 (2014).

166. MacKinnon, A. L. & Taunton, J. Target Identification by Diazirine Photo-Cross-linking and Click Chemistry. *Curr. Protoc. Chem. Biol.* **1,** 55–73 (2009).

167. Yang, P. & Liu, K. Activity-based protein profiling: Recent advances in probe development and applications. *ChemBioChem* **16,** 712–724 (2015).

168. Liu, X., Dong, T., Zhou, Y., Huang, N. & Lei, X. Exploring the Binding Proteins of Glycolipids with Bifunctional Chemical Probes. *Angew. Chemie - Int. Ed.* **55,** 14330–14334 (2016).

169. Gubbens, J. *et al.* Photocrosslinking and Click Chemistry Enable the Specific Detection of Proteins Interacting with Phospholipids at the Membrane Interface. *Chem. Biol.* **16,** 3–14 (2009).

170. Haberkant, P. & Holthuis, J. C. M. Fat & fabulous: Bifunctional lipids in the spotlight. *Biochim. Biophys. Acta - Mol. Cell Biol. Lipids* **1841,** 1022–1030 (2014).

171. Hulce, J. J., Cognetta, A. B., Niphakis, M. J., Tully, S. E. & Cravatt, B. F. Proteome-wide Mapping of Cholesterol Interacting Proteins in Mammalian Cells. *Nat. Methods* **10,** 259–264 (2013).

172. Bockelmann, S. *et al.* A search for ceramide binding proteins using bifunctional lipid analogs yields CERT-related protein StarD7. *J. Lipid Res.* **59,** 515–530 (2018).

173. Pezeshkian, W. *et al.* Fluctuation-driven clustering of nanoparticles on lipid membranes. *Submitted* 1–13

174. Harrison, A. L. *et al.* A synthetic globotriaosylceramide analogue inhibits HIV-1 infection in vitro by two mechanisms. *Glycoconj. J.* **27,** 515–524 (2010).

175. Blake, D. A., Bovin, N. V, Bess, D. & Henry, S. M. FSL constructs: a simple method for modifying cell/virion surfaces with a range of biological markers without affecting their viability. *J. Vis. Exp.* 1–9 (2011).

176. Boons, G.-J. (University of Birmingham, U. *Carbohydrate Chemistry*. (Blackie A&P, 1998).

177. Kuehne, M., Gyoergydeak, Z. & Lindhorst, T. K. A simple method for the preparation of glycosyl isothiocyanates. *Synthesis (Stuttg).* 949–951 (2006).

178. Greimel, P. & Ito, Y. First synthesis of natural phosphatidyl-B-d-glucoside. *Tetrahedron Lett.* **49,** 3562–3566 (2008).

179. Sandbhor, M. S., Key, J. a., Strelkov, I. S. & Cairo, C. W. A modular synthesis of alkynyl-phosphocholine headgroups for labeling sphingomyelin and phosphatidylcholine. *J. Org. Chem.* **74,** 8669–8674 (2009).

180. Cavalli, S., Overhand, M. & Kros, A. Assembly into beta-sheet structures upon peptide-liposome conjugation through copper(I)-catalyzed [3+2] azide-alkyne cycloaddition. *Chempluschem* **79,** 564–568 (2014).

181. Kim, S., Lee, S., Lee, T., Ko, H. & Kim, D. Efficient Synthesis of D-erythro-Sphingosine and D-erythro-Azidosphingosine from D-ribo-Phytosphingosine via a Cyclic Sulfate Intermediate. *J. Org. Chem.* **71,**

8661–8664 (2006).

182. Di Benedetto, R. *et al.* Protected sphingosine from phytosphingosine as an efficient acceptor in glycosylation reaction. *Org. Lett.* **16,** 952–955 (2014).

183. Gao, Y. & Sharpless, K. B. Vicinal Diol Cyclic Sulfates: Like Epoxides Only More Reactive. *J. Am. Chem. Soc.* **110,** 7538–7539 (1988).

184. Garrido Martinez, M. New sphingolipid probes for metabolism and trafficking studies. (Thesis from Universitat de Barcelona, IQAC-CSIC, 2012).

185. Gao, H. Chemical biology approach to study toxin clustering and lipids reorganization in Shiga toxin endocytosis. (2015).

186. Kita, K., Kurita, T. & Ito, M. Characterization of the reversible nature of the reaction catalyzed by sphingolipid ceramide N-deacylase: A novel form of reverse hydrolysis reaction. *Eur. J. Biochem.* **268,** 592–602 (2001).

187. Gantner, M., Schwarzmann, G., Sandhoff, K. & Kolter, T. Partial synthesis of ganglioside and lysoganglioside lipoforms as internal standards for MS quantification. *J. Lipid Res.* **55,** 2692–2704 (2014).

188. Gouin, S. G. & Kovensky, J. Direct azidation of unprotected carbohydrates with PPh3/CBr4/NaN3. Modulation of the degree of substitution. *Tetrahedron Lett.* **48,** 2875–2879 (2007).

189. Wakiyama, Y. *et al.* Synthesis and structure-activity relationships of novel lincomycin derivatives. Part 4: Synthesis of novel lincomycin analogs modified at the 6- and 7-positions and their potent antibacterial activities. *J. Antibiot. (Tokyo).* **70,** 888–906 (2017).

190. Canals, D. *et al.* Synthesis and biological properties of Pachastrissamine (jaspine B) and diastereoisomeric jaspines. *Bioorganic Med. Chem.* **17,** 235–241 (2009).

191. Kostova, V. *et al.* Targeted Shiga toxin – drug conjugates prepared via Cu-free click chemistry. *Bioorg. Med. Chem.* **23,** 7150–7157 (2015).

192. Chang, T. C. *et al.* A photo-cleavable biotin affinity tag for the facile release of a photo-crosslinked carbohydrate-binding protein. *Bioorganic Med. Chem.* **24,** 1216–1224 (2016).

193. Ling, H. *et al.* Structure of the Shiga-like toxin I B-pentamer complexed with an analogue of its receptor Gb3. *Biochemistry* **37,** 1777–1788 (1998).

194. Carvalho, M. *et al.* Effects of diet and development on the Drosophila lipidome. *Mol. Syst. Biol.* **8,** 1–17 (2012).

195. Ogasawara, H. *et al.* Intracellular Carboxyl esterase activity is a determinant of cellular sensitivity to the antineoplastic agent KW-2189 in cell lines resistant to Cisplatin and CPT-11. *Jpn. J. Cancer Res.* **86,** 124–129 (1995).

196. Ogasawara, H. *et al.* A novel antitumor antibiotic, KW-2189 is activated by carboxyl esterase and induces DNA strand breaks in human small cell lung cancer cells. *Jpn. J. Cancer Res.* **85,** 418 (1994).

197. Sharpe, H. J., Stevens, T. J. & Munro, S. A Comprehensive Comparison of Transmembrane Domains Reveals Organelle-Specific Properties. *Cell* **142,** 158–169 (2010).

198. Li, J. *et al.* A review on phospholipids and their main applications in drug delivery systems. *Asian J. Pharm. Sci.* **10,** 81–98 (2014).

199. Korchagina, E. Y. & Henry, S. M. Synthetic Glycolipid Like Constructs as Tools for Glycobiology Research, Diagnostics, and as Potential Therapeutics. *Biochem.* **80,** (2015).

200. Korchagina, E. *et al.* Toward creating cell membrane glyco-landscapes with glycan lipid constructs. *Carbohydr. Res.* **356,** 238–246 (2012).

201. Simons, K. & Ikonen, E. Functional rafts in cell membranes. *Nature* **387,** 569–72 (1997).

202. Windschieg, B. *et al.* Lipid reorganization induced by Shiga toxin clustering on planar membranes. *PLoS One* **4,** 1–11 (2009).

203. Chai, W., Stoll, M. S., Galustian, C., Lawson, A. M. & Feizi, T. Neoglycolipid technology: deciphering information content of glycome. *Methods Enzymol.* **362,** 160–195 (2003).

204. Bock, V. D., Speijer, D., Hiemstra, H. & van Maarseveen, J. H. 1,2,3-Triazoles as peptide bond isosteres: synthesis and biological evaluation of cyclotetrapeptide mimics. *Org. Biomol. Chem.* **5,** 971–975 (2007).

205. Young, I. S. & Baran, P. S. Protecting-group-free synthesis as an opportunity for invention. *Nat. Chem.* **1,** 193–205 (2009).

206. Hörner, A., Hagendorn, T., Schepers, U. & Bräse, S. Photophysical properties and synthesis of new dye-cyclooctyne conjugates for multicolor and advanced microscopy. *Bioconjug. Chem.* **26,** 718–724 (2015).

207. Rong, L. *et al.* Long-term thiol monitoring in living cells using bioorthogonal chemistry. *Chem. Commun. (Camb).* **51,** 388–90 (2015).

208. Garrido, M., Abad, J. L., Fabriàs, G., Casas, J. & Delgado, A. Azide-tagged sphingolipids: New tools for metabolic flux analysis. *ChemBioChem* **16,** 641–650 (2015).

209. Garrido, M. *et al.* In situ synthesis of fluorescent membrane lipids (ceramides) using click chemistry. *J. Chem. Biol.* **5,** 119–123 (2012).

210. Song, Y., Yuan, W., Luo, Y. & Lu, W. A new synthetic approach to phosphatidylethanolamine. *Chinese Chem. Lett.* **23,** 154–156 (2012).

211. Lee, Y. M. *et al.* A practical and cost-effective synthesis of d-erythro-sphingosine from d-ribo-phytosphingosine via a cyclic sulfate intermediate. *Synthesis (Stuttg).* 867–872 (2011).

212. Van Den Berg, R. J. B. H. N. *et al.* A rapid and efficient synthesis of D-erythro-sphingosine from D-ribo-phytosphingosine. *European J. Org. Chem.* 6685–6689 (2011).

213. Huang, F.-T., Han, Y.-B., Feng, Y. & Yang, G.-Y. A facile method for controlling the reaction equilibrium of sphingolipid ceramide N-deacylase for lyso-glycosphingolipid production. *J. Lipid Res.* **56,** 1836–1842 (2015).

214. Ito, M., Kurita, T. & Kita, K. A novel enzyme that cleaves the N-acyl linkage of ceramides in various glycosphingolipids as well as sphingomyelin to produce their lyso forms. *J. Biol. Chem.* **270,** 24370–24374 (1995).

215. Chwalek, M., Auzély, R. & Fort, S. Synthesis and biological evaluation of multivalent carbohydrate ligands obtained by click assembly of pseudo-rotaxanes. *Org. Biomol. Chem.* **7,** 1680–1688 (2009).

216. Feldborg, L. N., Jølck, R. I. & Andresen, T. L. Quantitative evaluation of bioorthogonal chemistries for surface functionalization of nanoparticles. *Bioconjug. Chem.* **23,** 2444–2450 (2012).

217. Oude Blenke, E. *et al.* Liposome functionalization with copper-free 'click chemistry'. *J. Control. Release* **202,** 14–20 (2015).

218. Salomé, C. *et al.* Smart tools and orthogonal click-like reactions onto small unilamellar vesicles: Additional molecular data. *Chem. Phys. Lipids J.* **188,** 27–36 (2015).

219. Haberkant, P. *et al.* Bifunctional Sphingosine for Cell-Based Analysis of Protein-Sphingolipid Interactions. *ACS Chem. Biol.* **11,** doi: 10.1021/acschembio.5b00810 (2015).

220. Haberkant, P. *et al.* Protein-sphingolipid interactions within cellular membranes. *J. Lipid Res* **49,** 251–262 (2008).

221. Hofmann, K. *et al.* A novel alkyne cholesterol to trace cellular cholesterol metabolism and localization. *J. Lipid Res.* **55,** 583–91 (2014).

222. Boppana, N. B. *et al.* Ceramide synthase inhibitor fumonisin B1 inhibits apoptotic cell death in SCC17B human head and neck squamous carcinoma cells after Pc4 photosensitization. *Photochem. Photobiol. Sci.* **13,** 1621–1627 (2014).

223. Young, M. M., Kester, M. & Wang, H.-G. Sphingolipids: regulators of crosstalk between apoptosis and autophagy. *J. Lipid Res.* **54,** 5–19 (2013).

224. Woodcock, J. Sphingosine and ceramide signalling in apoptosis. *IUBMB Life (International Union*

Biochem. Mol. Biol. Life) **58,** 462–466 (2006).

225. Kan, C. C. & Kolesnick, R. N. A synthetic ceramide analog, D-threo-1-phenyl-2-decanoylamino-3-morpholino-1-propanol, selectively inhibits adherence during macrophage differentiation of human leukemia cells. *J Biol Chem* **267,** 9663–9667 (1992).

226. Sugiki, H. *et al.* C2-Ceramide induces apoptosis in a human squamous cell carcinoma cell line. *Br. J. Dermatol.* **143,** 1154–1163 (2000).

227. Desai, K. *et al.* Fumonisins and fumonisin analogs as inhibitors of ceramide synthase and inducers of apoptosis. *Biochim. Biophys. Acta - Mol. Cell Biol. Lipids* **1585,** 188–192 (2002).

228. Gerl, M. J. *et al.* Sphingosine-1-phosphate lyase deficient cells as a tool to study protein lipid interactions. *PLoS One* **11,** 1–25 (2016).

229. Hartmann, D. *et al.* Long chain ceramides and very long chain ceramides have opposite effects on human breast and colon cancer cell growth. *Int. J. Biochem. Cell Biol.* **44,** 620–628 (2012).

230. Osawa, Y. *et al.* Roles for C16-ceramide and sphingosine 1-phosphate in regulating hepatocyte apoptosis in response to tumor necrosis factor-α. *J. Biol. Chem.* **280,** 27879–27887 (2005).

231. Eto, M., Bennouna, J., Hunter, O. C., Lotze, M. T. & Amoscato, A. A. Importance of C16 ceramide accumulation during apoptosis in prostate cancer cells. *Int. J. Urol.* **13,** 148–156 (2006).

232. Hannun, Y. A. & Obeid, L. M. Sphingolipids and their metabolism in physiology and disease. *Nat. Rev. Mol. Cell Biol.* **19,** 175–191 (2018).

233. Stiban, J. & Perera, M. Very long chain ceramides interfere with C16-ceramide-induced channel formation: A plausible mechanism for regulating the initiation of intrinsic apoptosis. *Biochim. Biophys. Acta - Biomembr.* **1848,** 561–567 (2015).

234. Regina Todeschini, A. & Hakomori, S. Functional role of glycosphingolipids and gangliosides in control of cell adhesion, motility, and growth, through glycosynaptic microdomains. *Biochim. Biophys. Acta - Gen. Subj.* **1780,** 421–433 (2008).

235. Mathow, D. *et al.* Zeb1 affects epithelial cell adhesion by diverting glycosphingolipid metabolism. *EMBO Rep.* **16,** 321–331 (2015).

236. Laizure, S. C., Herring, V., Hu, Z., Witbrodt, K. & Parker, R. B. The role of human carboxylesterases in drug metabolism: have we overlooked their importance? *Pharmacotherapy.* **33,** 210–222 (2013).

237. Laughlin, S. T. & Bertozzi, C. R. Metabolic labeling of glycans with azido sugars and subsequent glycan-profiling and visualization via staudinger ligation. *Nat. Protoc.* **2,** 2930–2944 (2007).

238. Chang, P. V. *et al.* Metabolie labeling of sialic acids in living animals with alkynyl sugars. *Angew. Chemie - Int. Ed.* **48,** 4030–4033 (2009).

239. Lian, J., Nelson, R. & Lehner, R. Carboxylesterases in lipid metabolism: from mouse to human. *Protein Cell* **9,** 178–195 (2017).

240. Takumi, S. *et al.* Overexpression of carboxylesterase contributes to the attenuation of cyanotoxin microcystin-LR toxicity. *Comp. Biochem. Physiol. Part - C Toxicol. Pharmacol.* **194,** 22–27 (2017).

241. Blauvelt, M. L. *et al.* α-S-GalCer: Synthesis and evaluation for iNKT cell stimulation. *Bioorganic Med. Chem. Lett.* **18,** 6374–6376 (2008).

242. Shaya, J. *et al.* Turn-on Fluorene Push-Pull Probes with High Brightness and Photostability for Visualizing Lipid Order in Biomembranes. *ACS Chem. Biol.* **12,** 3022–3030 (2017).

243. Adlercreutz, D. *et al.* Enzymatic synthesis of Gb3 and iGb3 ceramides. *Carbohydr. Res.* **345,** 1384–1388 (2010).

244. Earle, M. a., Manku, S., Hultin, P. G., Li, H. & Palcic, M. M. Chemoenzymatic synthesis of a trimeric ganglioside GM3 analogue. *Carbohydr. Res.* **301,** 1–4 (1997).

245. Roodsari, F. S., Wu, D., Pum, G. S. & Hajdu, J. A new approach to the stereospecific synthesis of phospholipids. The use of L-glyceric acid for the preparation of diacylglycerols, phosphatidylcholines,

and related derivatives. *J. Org. Chem.* **64,** 7727–7737 (1999).

246. Goddard-Borger, E. D. & Stick, R. V. An Efficient , Inexpensive , and Shelf-Stable Diazotransfer Reagent: Imidazole-1-sulfonyl Azide Hydrochloride. *Org. Lett.* **9,** 3797–3800 (2007).

247. Kim, S., Lee, S., Lee, T., Ko, H. & Kim, D. Efficient Synthesis of D - erythro -Sphingosine and D - erythro - Azidosphingosine from D - ribo -Phytosphingosine via a Cyclic Sulfate Intermediate The synthesis of naturally occurring D - erythro -sphingosine and synthetically useful D - erythro -2-azido. *J. Org. Chem.* **71,** 8661–8664 (2006).

248. Ito, Y., Kiso, M. & Hasegawa, A. Studies on the Thioglycosides of N- Acetylneuraminic Acid. 6: Synthesis of Ganglioside GM4 Analogs. *J. Carbohydr. Chem.* **8,** 285–294 (1989).

249. Xing, G. W., Chen, L. & Liang, F. F. Facile synthesis of tumor-associated carbohydrate antigen ganglioside GM3 from sialic acid, lactose, and serine. *European J. Org. Chem.* 5963–5970 (2009).

250. Albrecht, B., Pütz, U. & Schwarzmann, G. Synthesis of fluorescent and radioactive analogues of two lactosylceramides and glucosylceramide containing β-thioglycosidic bonds that are resistant to enzymatic degradation. *Carbohydr. Res.* **276,** 289–308 (1995).